Karlsruhe Institute of Technology

Industrially Relevant Monomers:

From Fundamental Kinetics to Application in Controlled Polymerization

Zur Erlangung des akademischen Grades eines

DOKTORS DER NATURWISSENSCHAFTEN

(Dr. rer. nat.)

Fakultät für Chemie und Biowissenschaften

Karlsruher Institut für Technologie (KIT) - Universitätsbereich

genehmigte

DISSERTATION

von

Dipl. Chem. Alexander Peter Hähnel

aus

Bruchsal, Deutschland

Dekan: Prof. Dr. Peter Roesky

Referent: Prof. Dr. Christopher Barner-Kowollik

Korreferent: Priv. Doz. Dr. Andreas-Neil Unterreiner

Tag der mündlichen Prüfung: 18. Juli 2014

Alles wissenschaftliche Arbeiten ist nichts anderes,

als immer neuen Stoff in allgemeine Gesetze zu bringen.

Wilhelm von Humboldt

Briefe an eine Freundin, 7.4.1833

Wer neben den Wissenschaften noch andere Ergötzungen sucht,

muß die wahre Süßigkeit derselben noch nicht geschmeckt haben.

Gotthold Ephraim Lessing

Der junge Gelehrte 1,2 (Damis)

ABSTRACT

Detailed knowledge of the underlying kinetics and mechanisms is required for the understanding, modeling and industrial application of any polymerization technique. The availability of precision kinetic rate coefficients for elemental reactions occurring in free-radical polymerization (FRP) is not only mandatory for the industrial large scale production of polymers via FRP (via the prediction of space-time yields and numerous properties of the polymerization product), yet it also enables the targeted design of appropriate controlling agents for reversible deactivation radical polymerization (RDRP) techniques (e.g., RAFT or NMP).

The current thesis particularly aims at determining accurate propagation rate coefficients (k_p). Global trends and family type behavior for the propagation rate coefficient of (meth)acrylic monomers are identified based on an encompassing data pool of 16 newly studied monomers – mostly with industrial relevance – in combination with the already literature known data of their structural relatives. While the trends and family type behavior among the absolute k_p values are relatively clear, no unambiguous structure-property relationships can be identified with respect to the Arrhenius pre-factor, A, and the activation energy, E_a. By employing additional physicochemical polymer and monomer specific data (e.g., glass transition temperatures (T_g) and kinematic viscosities (ν)), hypotheses for the reported trends and family type behaviors are provided: (*i*) the steady increase of k_p with increasing ester side chain length for linear alkyl (meth)acrylates may tentatively be explained by a decreasing concentration of the polar ester moieties, which is resulting in a decreasing stabilization of the attacking radical in the transition state of the propagation reaction (however, further contributions to the increasing k_p may come from additional changes in the transition state and a possibly occurring pre-structuring of the reaction solution) and (*ii*) the family type behavior of the branched alkyl methacrylates can be understood by considering steric and entropic

influences. For the branched alkyl acrylates no clear trend is detectable and a family type behavior is clearly not observed in contrast to the corresponding methacrylates.

A key finding of the current thesis is the steady increase of the propagation rate coefficient, k_p, observed for the linear alkyl (meth)acrylates that scales linearly with the ester side chain length. The linear correlation of the number of carbon atoms in the ester side chain with the propagation rate at a specific temperature allows for the prediction of k_p for up to date not yet investigated linear alkyl (meth)acrylates.

The above noted insights are established by the careful construction of Arrhenius relationships of the propagation rate coefficient, k_p, for 16 acrylic and methacrylic monomers, determined via the IUPAC recommended pulsed laser polymerization – size-exclusion chromatography (PLP-SEC) method. The Mark-Houwink-Kuhn-Sakurada (MHKS) parameters for 14 of these polymers are additionally determined via multi-detector size-exclusion chromatography of narrowly distributed polymer samples obtained via fractionation, allowing for an accurate SEC calibration. Several of these monomers were additionally studied in 1 M solution in butyl acetate (BuAc) in order to underpin the trends observed in bulk. For the 2 heteroatom containing monomers for which no MHKS parameters are available and which are studied as 1 M solution in *N*,*N*-dimethylacetamide (DMAc), absolute molar mass determination is achieved via SEC coupled to on-line multi-angle laser light scattering (MALLS).

The use of laser repetition frequencies of up to 500 Hz (current state of the art) ensures the successful suppression of potential side reactions interfering with the FRP process (such as transfer to polymer) even for acrylates at elevated temperatures exceeding 50°C.

The data obtained for the heteroatom containing acrylate (i.e., HPCA, hydroxyl-*iso*-propylcarbamate acrylate) is critically compared to the literature known data sets of two structural derivatives, indicating an increase in the propagation rate coefficient with increasing ester side chain length similar to the trend observed for the linear alkyl

(meth)acrylates. Ureidoethyl methacrylate (UMA) represents the first multi heteroatom containing methacrylate to be studied via PLP-SEC, evidencing a significantly higher propagation rate coefficient compared to earlier investigated methacrylate-type monomers, yet lower than the exceptional high k_p values of hydroxyethyl methacrylate (HEMA).

Additional kinetic information regarding the free-radical polymerization behavior of both heteroatom containing monomers (i.e., HPCA and UMA) is obtained via in-situ ^{1}H-NMR experiments at elevated temperatures, allowing for an estimation of average termination rate coefficients (at low conversion) in conjunction with the determined k_p data. Furthermore, the applicability of both heteroatom containing monomers in RDRP techniques is evidenced by successfully controlling their polymerization via the reversible addition-fragmentation chain transfer (RAFT) and nitroxide-mediated polymerization (NMP) technique in a wide molecular weight range as well as via chain extension experiments.

ZUSAMMENFASSUNG

Die Voraussetzung für das Verständnis, die Beschreibung durch Modelle und die industrielle Anwendung einer jeden Polymerisationstechnik ist ein detailliertes Wissen über die ihr zu Grunde liegenden Kinetiken und Mechanismen. Die Verfügbarkeit von exakten Geschwindigkeitskoeffizienten für die Elementarreaktionen, die in der Freien Radikalischen Polymerisation (FRP) auftreten, ist nicht nur obligatorisch für die industrielle Massenproduktion von Polymeren durch die FRP (da damit die Vorhersage von Raum-Zeit Ausbeuten, Wärmeentwicklung und einer Vielzahl von Eigenschaften der Polymerisationsprodukte ermöglicht werden), sondern auch, weil sie die Auswahl adäquater Strukturen der Kontrollreagenzien für Reversible Deaktivierung Radikalische Polymerisations (RDRP) Techniken (wie z.B. RAFT oder NMP) erlaubt.

Die vorliegende Arbeit hat zum Ziel die Wachstumsgeschwindigkeitskoeffizienten (k_p) exakt zu bestimmen. Dabei wurden, auf der Grundlage einer umfassenden Datenbasis von 16 erstmalig untersuchten Monomeren – überwiegend mit industrieller Relevanz – in Kombination mit bereits in der Literatur bekannten Werten von dazu strukturell ähnlichen Monomeren, übergeordnete Trends und Familienverhalten unter den Wachstumsgeschwindigkeitskoeffizienten für ein breites Spektrum an (Meth)Acrylaten entdeckt. Während die Trends und Familienverhalten unter den absoluten k_p Werten recht eindeutig zu erkennen sind, können keine zweifelsfreien Struktur-Eigenschafts-Beziehungen mit Hilfe der Arrhenius Parameter (Vorfaktoren, A, und Aktivierungsenergien, E_a) identifiziert werden. Potentielle Erklärungen für die berichteten Trends und Familienverhalten können unter Zuhilfenahme von weiteren physikochemischen polymer- und monomerspezifischen Daten (wie z.B. Glasübergangstemperaturen (T_g) und kinematischen Viskositäten (v)) etabliert werden: (*i*) Der stetige Anstieg des k_p mit länger werdender Esterseitenkette der linearen Alkyl(meth)acrylate kann mit einer abnehmenden Stabilisierung des Radikals im Übergangs-

zustand der Wachstumsreaktion, bedingt durch eine abnehmende Konzentration an polaren Estergruppen, erklärt werden. (Weitere Beiträge zum Anstieg des k_p mögen durch zusätzliche Änderungen des Übergangszustandes und einer eventuell auftretenden Vorstrukturierung der Reaktionslösung verursacht werden.) (*ii*) Das Familienverhalten der verzweigten Alkylmethacrylate kann unter Berücksichtigung von entropischen und sterischen Einflüssen verstanden werden. Für die verzweigten Alkylacrylate kann kein eindeutiger Trend festgestellt werden, wobei jedoch ein Familienverhalten, wie es die entsprechenden Methacrylate aufzeigen, eindeutig nicht beobachtet wird.

Eine zentrale Erkenntnis der vorliegenden Arbeit ist, dass der für die linearen (Meth)Acrylate beobachtete stetige Anstieg des Wachstumsgeschwindigkeitskoeffizienten, k_p, eine lineare Abhängigkeit von der Esterseitenkettenlänge aufweist. Der lineare Zusammenhang zwischen der Anzahl der Kohlenstoffatome in der Esterseitenkette und dem Geschwindigkeitskoeffizienten bei einer gegeben Temperatur erlaubt die Vorhersage des monomerspezifischenen k_p auch für bisher noch nicht untersuchte lineare Alkyl(meth)acrylate.

Die oben genannten Erkenntnisse gründen auf der sorgfältigen Erstellung der Arrhenius Beziehungen für den Wachstumsgeschwindigkeitskoeffizienten für 16 Acrylate und Methacrylate, die mit Hilfe der Pulslaser Polymerisation – Größenausschlusschromatographie (PLP-SEC) – der von der IUPAC dafür empfohlenen Methode – bestimmt wurden. Die Mark-Houwink-Kuhn-Sakurada (MHKS) Parameter, die eine universelle Kalibrierung in der Größenausschlusschromatographie ermöglichen, wurden für 14 dieser Polymere bestimmt. Hierfür wurden engverteilte Proben, hergestellt über Fraktionierung von breitverteilten Polymeren, mit Hilfe einer mehrfach detektierenden Größenausschlusschromatographie analysiert. Mehrere dieser Monomere wurden zusätzlich in 1 M Lösung in Butylacetat (BuAc) untersucht, um die in Substanz gemessenen Wachstumsgeschwindigkeitskoeffizienten zu untermauern. Für die beiden heteroatomenthaltenden Monomere, die als 1 M Lösung in *N*,*N*-Dimethylacetamid (DMAc) untersucht wurden, sind keine MHKS Parameter zugänglich.

Die Bestimmung der absoluten molaren Masse wurde deshalb für jede Probe einzeln über Größenausschlusschromatographie gekoppelt mit Mehrwinkel Laser Lichtstreuungsdetektion (MALLS) durchgeführt.

Die Verwendung von Laserpulswiederholungsfrequenzen von bis zu 500 Hz (aktueller Stand der Technik) ermöglicht die erfolgreiche Unterdrückung von störenden Nebenreaktionen des FRP Prozesses (wie z.B. Radikalübertragung zum Polymer) auch für Acrylate bei erhöhten Temperaturen über 50°C.

Die für das heteroatomenthaltende Acrylat (Hydroxyl-*iso*-propylcarbamat Acrylat, HPCA) erhaltenen Werte werden in Bezug gesetzt zu den literaturbekannten Daten von strukturell ähnlichen Acrylaten. Dieser kritische Vergleich deutet auf einen ähnlichen Anstieg der k_p Werte mit zunehmender Esterseitenkettenlänge hin, wie er für die linearen Alkyl(meth)-acrylate beobachtet wird. Ureidoethylmethacrylat (UMA) ist das erste Methacrylat mit mehr als einem Heteroatom in der Esterseitenkette, das mit der PLP-SEC Methode untersucht wurde. UMA besitzt einen deutlich höheren Wachstumsgeschwindigkeitskoeffizienten im Vergleich zu den zuvor berichteten Methacrylaten, der jedoch niedriger ist als die außergewöhnlich hohen Werte des Hydroxyethylmethacrylats (HEMA).

Mit Hilfe von in-situ ^{1}H-NMR Experimenten bei erhöhten Temperaturen (und den zuvor bestimmten Wachstumsgeschwindigkeitskoeffizienten) wurden zusätzliche kinetische Informationen über das Verhalten in der FRP für beide heteroatomenthaltenden Monomere erlangt, die eine Abschätzung des durchschnittlichen Terminierungsgeschwindigkeits-koeffizienten (für geringe Monomerumsätze) ermöglichen. Des Weiteren konnte durch die erfolgreiche Kontrolle der Polymerisation über einen ausgedehnten Molekulargewichtsbereich und Kettenverlängerungsexperimente sowohl über die Reversible Additions-Fragmentierungs-Kettentransfer (RAFT) Polymerisation als auch über die Nitroxid Vermittelte Polymerisation (NMP) die Verwendbarkeit von beiden heteroatomenthaltenden Monomeren in RDRP Techniken bewiesen werden.

TABLE OF CONTENTS

Abstract V

Zusammenfassung VIII

Table of Contents XI

List of Figures XIV

List of Schemes XVI

List of Tables XVII

Abbreviations XIX

1 Introduction 1

1.1 Research Goal 2

1.2 Free-radical Polymerization 3

1.3 Reversible-Deactivation Radical Polymerization (RDRP) Techniques 7

1.3.1 Nitroxide-Mediated Polymerization (NMP) 8

1.3.2 Reversible Addition-Fragmentation Chain Transfer (RAFT) Polymerization 9

1.3.3 Atom Transfer Radical Polymerization (ATRP) and Single Electron Transfer – Living Radical Polymerization (SET-LRP) 12

1.4 The PLP-SEC method 15

1.4.1 Determination of Absolute Molecular Weights 18

1.4.2 Deducing Arrhenius Relationships 22

1.4.3 PLP-SEC Investigations into Aqueous Systems 25

1.5 Single Pulse – Pulsed Laser Polymerization (SP-PLP) 28

2 Alkyl (Meth)Acrylates: Global Trends for k_p? 31

2.1 Introduction 32

2.2 MHKS Parameters 37

2.3 Arrhenius Parameters 44

2.4 Trends and Family Type Behavior 53

2.4.1 Global Trends for Linear Alkyl (Meth)Acrylates 55

2.4.2 Family Type Behavior of Branched Alkyl Methacrylates 59

2.4.3 Global Trend for Branched Alkyl Acrylates? 63

2.4.4 Feasible Physicochemical Causes 68

2.4.4.1 Increasing k_p for Linear Alkyl (Meth)Acrylates 69

2.4.4.2 (Non-)Family Type Behavior for Branched Alkyl (Meth)Acrylates 75

2.5 Conclusions 80

3 Heteroatom Containing (Meth)Acrylic Monomers 83

3.1 Introduction 83

3.2 Kinetic Behavior 88

3.2.1 Arrhenius Parameters 88

3.2.2 Comparison to Related (Meth)Acrylates 90

3.3 Overall Kinetic Behavior in Free-radical Polymerization 96

3.4 Application in Reversible-Deactivation Radical Polymerization (RDRP) 101

3.5 Conclusions 114

4 Experimental Section 117

4.1 Materials 117

4.2 Pulsed Laser Polymerization Experiments 118

4.3 Fractionation of Polymer Samples via SEC 120

4.4 Characterization 120

4.4.1 Size-Exclusion Chromatography (SEC) in THF 120

4.4.2 Size-Exclusion Chromatography (SEC) in DMAc 121

4.4.3 Triple Detector Size-Exclusion Chromatography in THF 121

4.4.4 Size-Exclusion Chromatography (SEC) in DMAc – Determination of Absolute Molar Masses 122

4.4.5 Density Measurements 123

4.4.6 NMR Spectroscopy 123

4.5 Standard Procedures Applied in RDRP Techniques 124

5 Outlook 127

References 129

Appendix A: Chapter 2: Alkyl (Meth)Acrylates 137

Appendix B: Chapter 3: Heteroatom Containing (Meth)Acrylic Monomers 187

Eigenständigkeitserklärung 193

Curriculum Vitae 195

List of Publications 197

Acknowledgements 199

LIST OF FIGURES

Figure 1.1 Dependence of k_p on the concentration of MAA in aqueous phase at 25°C..... 27

Figure 2.1 Demonstration of the successful fractionation..... 38

Figure 2.2 [η] vs. M_w plots for pSA and pBeA. 40

Figure 2.3 [η] vs. M_w plots for pSMA, pBeMA, pPHMA, pTDA-MA, pTDN-MA, and pC17MA..... 41

Figure 2.4 [η] vs. M_w plots for pPHA, pINA-A, pTDA-A, pTDN-A, pC17A, and pC21A. 42

Figure 2.5 Arrhenius plots for SA and BeA. 45

Figure 2.6 Arrhenius plots for SMA and BeMA. 47

Figure 2.7 Arrhenius plots for PHMA, TDA-MA, TDN-MA, and C17MA. 48

Figure 2.8 Arrhenius plots for PHA, INA-A, and TDA-A. 49

Figure 2.9 Arrhenius plots for TDN-A, C17A, and C21A. 50

Figure 2.10 Dependence of the propagation rate coefficient, k_p, on the type of ester side chain for linear alkyl (meth)acrylates. 56

Figure 2.11 Linear correlation of the propagation rate coefficient, k_p, with the number of carbon atoms in the ester side chain for linear alkyl (meth)acrylates..... 57

Figure 2.12 Dependence of the propagation rate coefficient, k_p, on the type of ester side chain for branched alkyl methacrylates. 60

Figure 2.13 Dependence of the propagation rate coefficient, k_p, on the type of ester side chain for branched alkyl acrylates. 65

Figure 2.14 Variation of the propagation rate coefficient, k_p, in the homologous butene-type series of branched alkyl acrylates in 1 M solution in BuAc. 67

Figure 3.1 Arrhenius plots for HPCA and UMA. 90

Figure 3.2 Dependence of the propagation rate coefficient, k_p, on the type of ester side chain for acrylates. 92

Figure 3.3 Dependence of the propagation rate coefficient, k_p, on the type of ester side chain for methacrylates. 94

Figure 3.4 Kinetic analysis of FRP via ^{1}H-NMR at elevated temperatures for UMA and HPCA. 98

Figure 3.5 Exemplary SEC traces acquired via RDRP of UMA. 103

Figure 3.6 Kinetic analysis of RAFT polymerization employing UMA. 105

Figure 3.7 Kinetic analysis of NMP employing UMA. 106

Figure 3.8 Kinetic analysis of the RAFT polymerization employing HPCA. 108

Figure 3.9 Exemplary SEC traces acquired in the chain extension experiment of HPCA with methyl acrylate (MA). 110

Figure 3.10 Exemplary SEC traces acquired during the NMP of HPCA. 110

Figure 3.11 Exemplary SEC traces acquired during the NMP of HPCA and styrene. 112

Figure 3.12 Exemplary SEC traces acquired in the chain extension experiment of HPCA with butyl acrylate (BA). 114

LIST OF SCHEMES

Scheme 1.1 General mechanism of FRP. 4

Scheme 1.2 Backbiting of an acrylic macroradical. 5

Scheme 1.3 Generation and follow up reactions of a mid-chain radical. 6

Scheme 1.4 General principle of RDRP. 8

Scheme 1.5 Mechanism of RAFT polymerization. 11

Scheme 1.6 Proposed mechanisms of ATRP and SET-LRP. 13

Scheme 1.7 Photoinitiators. 16

Scheme 1.8 Association and structuring of water-soluble monomers. 26

Scheme 2.1 Monomer landscape of alkyl (meth)acrylates. 35

Scheme 3.1 Heteroatom Containing Monomer Structures. 85

Scheme 3.2 Herein employed RAFT and NMP controlling agents 102

LIST OF TABLES

Table 2.1 Monomer and polymer specific physical data of currently investigated alkyl (meth)acrylates. 40

Table 2.2 Arrhenius parameters for k_p of the herein investigated alkyl (meth)acrylates. 46

Table 2.3 Comparison of monomer and polymer melting points for the long linear alkyl (meth)acrylates. 70

Table 2.4 Arrhenius parameters of k_p for the homologous series of linear alkyl (meth)acrylates. 72

Table 2.5 Comparison of kinematic viscosities and the propagation rate coefficient at 50°C for branched alkyl acrylates. 77

Table 3.1 Monomer and polymer specific physical data of UMA and HPCA. 87

Table 3.2 Arrhenius parameters for k_p of UMA and HPCA. 89

Table 3.3 Arrhenius parameters for k_p of HPCA compared to literature data. 92

Table 3.4 Arrhenius parameters for k_p of UMA compared to literature data. 96

Table 3.5 Summary of the kinetic analysis according to Equation 3.2 for UMA and HPCA. 99

ABBREVIATIONS

abbreviation	long name	further annotation
α	MHKS parameter, exponent	
ATRP	atom transfer radical polymerization	
BA	butyl acrylate	
BeA	behenyl acrylate	mixture containing mainly 18 and 22 C-atoms in the ester side chain
BeMA	behenyl methacrylate	mixture containing mainly 18 and 22 C-atoms in the ester side chain
BMA	butyl methacrylate	
BnA	benzyl acrylate	formerly abbreviated as BzA
BnMA	benzyl methacrylate	formerly abbreviated as BzMA
BnOH	benzyl alcohol	formerly abbreviated as BzOH
BuAc	*n*-butyl acetate	
C17A	heptadecyl acrylate	isoindex 3.1
C17MA	heptadecyl methacrylate	isoindex 3.1
C21A	henicosyl acrylate	isoindex 4.2
cf.	latin: confer; compare, see also	
cHMA	*cyclo*-hexyl methacrylate	
CLD	chain length dependence	
CLDT	chain length dependent termination	
CTA	chain transfer agent	
$Đ$	dispersity	formerly: polydispersity index (*PDI*)
DA	dodecyl acrylate	
DMA	dodecyl methacrylate	
DMPA	2,2-dimethoxy-2-phenylacetophenone	photoinitiator
DSC	differential scanning calorimetry	
e.g.	latin: exempli gratia; for example	
EA	ethyl acrylate	
EHA	2-ethylhexyl acrylate	
EHMA	2-ethylhexyl methacrylate	
EMA	ethyl methacrylate	
eq.	equivalent(s)	
$[\eta]$	limiting viscosity	
FRP	free-radical polymerization	
GMA	glycidyl methacrylate	also known as oxrianyl methacrylate and epoxypropyl methacrylate
HA	hexyl acrylate	
HCPA	(hexylcarbamoyloxy)-*iso*-propyl acrylate	isomeric mixture

abbreviation	long name	further annotation
HEMA	2-hydroxyethyl methacrylate	
HPCA	hydroxyl-*iso*-propylcarbamate acrylate	isomeric mixture
HPMA	hydroxpropyl methacrylate	isomeric mixture
i.e.	latin: id est; that is	
iBMA	*iso*-butyl methacrylate	
iBoA	*iso*-bornyl acrylate	
iDeMA	*iso*-decyl methacrylate	
INA-A	*iso*-nonyl acrylate	isoindex 1.3
K	MHKS parameter, prefactor	
k_p	propagation rate coefficient	
LA	lauryl acrylate	55:45 mixture of dodecyl und tetradecyl acrylate
LASER	light amplification by stimulated emission of radiation	
LCST / UCST	lower critical solution temperature / upper critical solution temperature	
LS	light scattering	
MA	methyl acrylate	
MAA	methacrylic acid	
MALLS	multi angle LASER light scattering	
MCR	mid-chain radical	
MeHQ	methyl hydroquinone	radical stabilizer
MHKS	Mark-Houwink-Kuhn-Sakurada	cf. Equation 1.3
MMA	methyl methacrylate	
M_n	number average molecular weight	
MW	molecular weight	
M_w	weight average molecular weight	
MWD	molecular weight distribution	
NMP	nitroxide-mediated polymerization	
NMR	nuclear magnetic resonance	
pBeA	poly(behenyl acrylate)	derived from the BeA monomer
pBeMA	poly(behenyl methacrylate)	derived from the BeMA monomer
pC17A	poly(heptadecyl acrylate)	derived from the C17A monomer
pC17MA	poly(heptadecyl methacrylate)	derived from the C17MA monomer
pC21A	poly(henicosyl acrylate)	derived from the C21A monomer
PHA	2-propylheptyl acrylate	
PhCPA	(phenylcarbamoyloxy)-*iso*-propyl acrylate	isomeric mixture
PHMA	2-propylheptyl methacrylate	
pINA-A	poly(isononyl acrylate)	derived from the INA-A monomer
PLP	pulsed laser polymerization	

abbreviation	long name	further annotation
pPHA	poly(propylheptyl acrylate)	derived from the PHA monomer
pPHMA	poly(propylheptyl methacrylate)	derived from the PHMA monomer
pSA	poly(stearyl acrylate)	derived from the SA monomer
pSMA	poly(stearyl methacrylate)	derived from the SMA monomer
pTDA-A	poly(tridecyl acrylate)	derived from the TDA-A monomer
pTDA-MA	poly(tridecyl methacrylate)	derived from the TDA-MA monomer
pTDN-A	poly(tridecyl acrylate)	derived from the TDN-A monomer
pTDN-MA	poly(tridecyl methacrylate)	derived from the TDN-MA monomer
RAFT	reversible addition-fragmentation chain transfer polymerization	
RDRP	reversible deactivation radical polymerization	
RI	refractive index	
R_p	rate of polymerization	
SA	stearyl acrylate	mixture containing mainly 16 and 18 C-atoms in the ester side chain
SEC	size-exclusion chromatography	
SET-LRP	single electron transfer – living radical polymerization	
SMA	stearyl methacrylate	mixture containing mainly 16 and 18 C-atoms in the ester side chain
SP-PLP	single pulse pulsed laser polymerization	
SPR	secondary propagation radical	
tBMA	*tert*-butyl methacrylate	
TDA-A	tridecyl acrylate	isoindex 3.1, ester moiety derived via *propene* oligomerization
TDA-MA	tridecyl methacrylate	isoindex 3.1, ester moiety derived via *propene* oligomerization
TDN-A	tridecyl acrylate	isoindex 2.1, ester moiety derived via *butene* oligomerization
TDN-MA	tridecyl methacrylate	isoindex 2.1, ester moiety derived via *butene* oligomerization
T_g	glass transition temperature	
THF	tetrahydrofuran	
TS	transition state	

1 Introduction[a]

Knowledge of the kinetic parameters of fundamental chemical processes is crucial for a detailed understanding and the industrial implementation of the reaction. In polymer chemistry, it is mandatory to have an in-depth knowledge of the underlying polymerization mechanisms and kinetics in order to synthesize tailor-made polymers, suitable for the targeted application. Knowledge of temperature dependent rate data of elemental reactions constituting a polymerization process enables not only the design of appropriate controlling agents, e.g., for reversible addition-fragmentation chain transfer (RAFT) polymerization or nitroxide-mediated polymerization (NMP), yet furthermore allows predicting the important and property defining microstructure of the lateral polymer chain (short/long chain branching, tacticity, composition of (block) copolymers). In addition, the heat of reaction and space-time yields for the large scale production of polymeric materials in industry can be accessed, allowing for the design of reactors and procedures fitting the specific process demands (e.g., of stirring, cooling, residence time).

Rate coefficients, especially for the propagation and termination reactions, are highly desired key data, since they enable the determination of other, experimentally not directly accessible rate coefficients[1] as well as precise kinetic investigations via modeling of, e.g., entire (controlled / living) polymerization mechanisms such as atom transfer radical polymerization (ATRP) or single electron transfer – living radical polymerization (SET-LRP).[2-5] The detailed

[a] Parts of this chapter were adapted with permission from Haehnel, A. P.; Schneider-Baumann, M.; Hiltebrandt, K. U.; Misske, A. M.; Barner-Kowollik, C. *Macromolecules* **2013**, *46*, 15-28. and Haehnel, A. P.; Schneider-Baumann, M.; Arens, L.; Misske, A. M.; Fleischhaker, F. Y.; Barner-Kowollik, C. *Macromolecules* **2014,** DOI: 10.1021/ma500304f. Copyright (2014) American Chemical Society and Haehnel, A. P.; Stach, M.; Chovancova, A.; Rueb, J. M.; Delaittre, G.; Misske, A. M.; Lacik, I.; Barner-Kowollik, C. Polym. Chem. 2014, 5, 862-873. – The Royal Society of Chemistry.

study of free-radical polymerizations (FRP) is of paramount importance, since in each reversible deactivation radical polymerization (RDRP)[6] technique the basic reactions of the FRP are operational. In order to suppress certain non-desired reaction pathways by adjusting the basic FRP process, as much as possible needs to be known about the entire FRP process.

Due to the complexity of the radical polymerization process and the resulting complex products, access to accurate rate coefficients is of highest importance not only for academia, but also for industry.

1.1 Research Goal

The current research work is an attempt to address the above described need of fundamental rate coefficients for the FRP process. The propagation reaction is at the heart of FRP. Gaining detailed knowledge about the propagation process is thus of the highest priority. Acrylates and methacrylates are very versatile monomer families, since the associated polymers exhibit a wide field of properties as a function of the characteristics of their ester substituents. Due to their versatility and ease of accessibility, (meth)acrylates are extensively employed in academia as well as in industry. Therefore, the investigations in the current research work are concentrated on a wide range of (meth)acrylates.

The aims of the current thesis can be summarized as follows:

(i) To investigate the propagation rate coefficients of miscellaneous (meth)acrylic monomers.

(ii) To identify overarching patterns of behavior and global trends among (meth)acrylates as a function of their ester groups, possibly enabling predictions for not yet studied monomer systems.

(iii) To provide possible explanations for the existence or non-existence of global trends on the basis of further physicochemical monomer/polymer system specific data.

(iv) To deduce additional kinetic information with the aid of the previously determined propagation rate coefficients.

(v) To fine tune and apply reliable methods for the determination of absolute molecular weights, which are required for the determination of the propagation rate coefficients.

(vi) To demonstrate the principal applicability in reversible-deactivation radical polymerization (RDRP) techniques (e.g., RAFT or NMP) of novel heteroatom containing monomers.

1.2 Free-radical Polymerization

The current chapter shall outline the reaction steps occurring during a conventional free-radical polymerization (FRP), since it is – on the one hand – the basis of the pulsed laser polymerization – size-exclusion chromatography (PLP-SEC) method, which is extensively employed during the current thesis and – on the other hand –the basis for the RDRP techniques employed with the heteroatom containing monomers (cf. Chapter 3.4).

FRP is, according to Flory, a chain (growth) reaction.[7] In FRP a small concentration (conventionally about 10^{-7} mol·L^{-1}) of radicals (i.e., molecules with an unpaired electron) is reacting with monomer molecules by attacking their double bond. Thereby a new single bond and a new radical site is formed. The general mechanism of the polymerization is depicted in Scheme 1.1.[8]

FRP is initiated by the generation of radicals, R$^{\bullet}$, based on the decomposition of an initiator species, I, with another species with a (unimolecular) rate coefficient k_d and an initiator efficiency *f*. The generated radical can add to a double bond containing monomer and thereby commence macromolecular growth. The propagation of the growing radical proceeds under addition of further monomer units with the monomer specific rate coefficient k_p. In the literature, a chain length dependence of the rate coefficient is often suggested, however up to

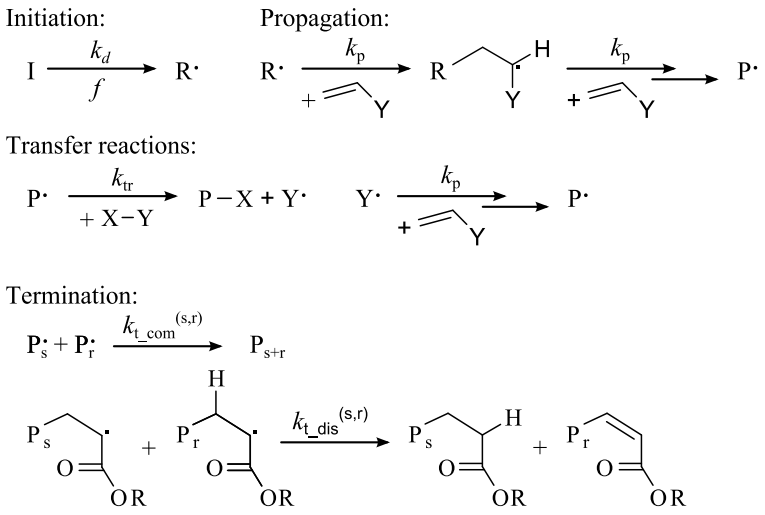

Scheme 1.1 General mechanism of FRP.
Termination via disproportionation is especially frequently occurring with methacrylic monomers. Scheme adapted from ref. 8.

date its magnitude and existence remains the subject of ongoing research.[9-10] Furthermore, the highly reactive radicals can undergo transfer reactions (with a rate coefficient k_{tr}) to low molecular weight species (e.g., monomer, solvent, transfer agent) as well as to polymeric species. The radical abstracts, for example, a proton (e.g., from a solvent or monomer molecule), becomes saturated and transfers the radical character onto the attacked molecule. Especially at high conversions (i.e., when most of the monomer is consumed) transfer to polymer chains becomes increasingly important. The probability that a proton is abstracted from a polymer molecule increases due to the rising polymer content in the reaction medium. The formed radicals are usually tertiary ones and are termed "mid-chain radicals" (MCR). As a consequence of the positive inductive effects of the substituents, tertiary radicals are more stable than secondary ones, which results, e.g., in a lower propagation rate coefficient ($k_p^{tert} < k_p^{sec}$). The reduced reactivity increases their lifetime and gives rise to further side reactions. Especially acrylates, with their secondary propagating radicals (SPR), tend to generate such MCRs via a cyclic, six-membered transition state (TS). The so called

backbiting reaction, which results in short chain branching of the polymer molecule (cf. Scheme 1.2), is a very frequently occurring intramolecular transfer to polymer reaction.[11-14]

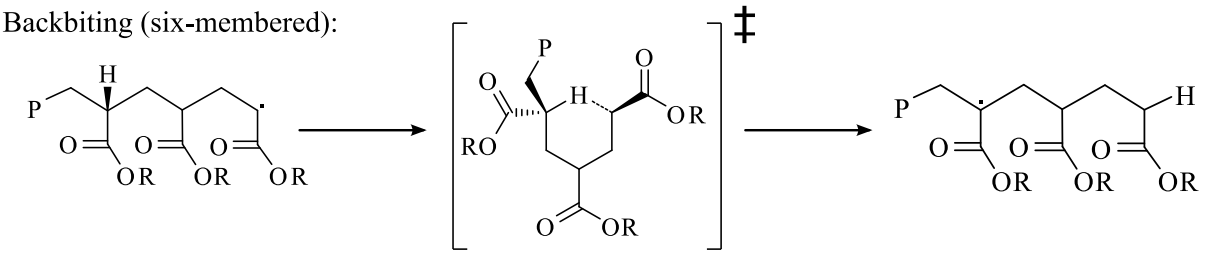

Scheme 1.2 Backbiting of an acrylic macroradical.
Scheme adapted from ref. 8.

Scheme 1.3 depicts, along with the general formation of MCRs (via backbiting as well as intra- and intermolecular transfer to polymer), several follow-up reactions which might occur.[11, 15-16] The MCR can be re-transformed into an SPR by adding a monomer unit resulting in a branching site in the macromolecule. The re-generation of SPRs can additionally occur via β-scission (or elimination), thereby also generating a double bond bearing macromonomer (cf. species b^{I} and b^{II} in Scheme 1.3), which may be incorporated into the polymerization.[17-18] The MCR can of course also undergo termination reactions resulting in 3- or 4-arm star polymers. Finally, each of the radicals, irrespective if of MCR or SPR type, is able to undergo a transfer reaction, i.e., abstracting a proton and transferring the radical site to another (small) molecule. The MCRs feature a significantly higher stability than SPRs. Interestingly the thereby prolonged lifetime is similar to that of intermediate RAFT radicals (cf. species 2 and 4 in Scheme 1.5).[11, 15, 19]

In addition to the above described MCR specific reactions, MCRs can be terminated via disproportionation as well as via recombination (cf. lower part of Scheme 1.1). Such termination reactions feature low activation energies and are diffusion controlled. Since the diffusion is strongly influenced by the size of the molecule, termination reactions exhibit a strong chain length dependence (CLD).[20-24] The termination rate coefficient decreases for the

initial 30 to 40 repeat units by approx. 1 order of magnitude (from 10^8 L·mol^{-1}·s^{-1} to 10^7 L·mol^{-1}·s^{-1})[25] and decreases additionally if the solutions viscosity is increased (e.g., at high conversions resulting in the well known Trommsdorf effect).[26] The CLD of the termination rate coefficient can be measured, e.g., by RAFT based single pulse pulsed laser polymerization (SP-PLP) or the so called RAFT-CLD-T method (cf. Chapter 1.5).[25, 27-33]

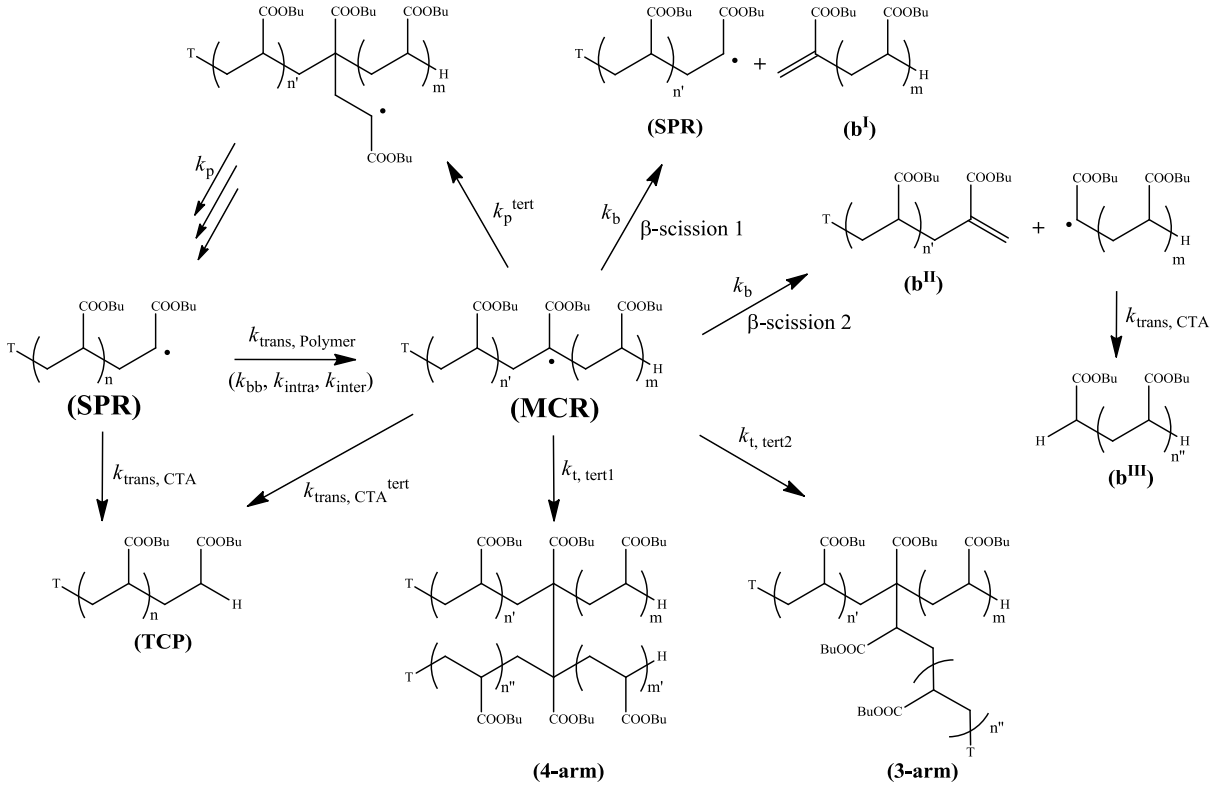

Scheme 1.3 Generation and follow up reactions of a mid-chain radical.
Scheme adapted from ref. 15.

According to theory, FRP produces polymers with a dispersity *Đ* between 1.5 when recombination and 2 when disproportionation is the only termination mode, respectively. Due to the decrease in monomer concentration, the dispersity increases with increasing conversion (as continuously lower molecular weight polymer is generated).

1.3 Reversible-Deactivation Radical Polymerization (RDRP) Techniques

RDRP techniques attempt to gain control over the FRP in order to approach the characteristics of the living anionic polymerization.[34] In 2010 the IUPAC recommended that the radical polymerization techniques such as RAFT,[35-36] NMP,[37] SET-LRP,[38] and ATRP,[39-40] which were usually termed "controlled" or "living", should be called RDRP techniques,[6] since they do not display all of the properties which must be fulfilled for a truly living process:[41]

(i) »[The] polymerization proceeds until all of the monomer has been consumed. Further addition of monomer results in continued polymerization.

(ii) The number average molecular weight, Mn (or Xn, the number average degree of polymerization), is a linear function of conversion.

(iii) The number of polymer molecules (and active centers) is a constant which is sensibly independent of conversion.

(iv) The molecular weight can be controlled by the stoichiometry of the reaction.

(v) Narrow molecular weight distribution polymers are produced.

(vi) Block copolymers can be prepared by sequential monomer addition.

(vii) Chain-end functionalized polymers can be prepared in quantitative yield.«[41]

In RDRP techniques irreversible termination is not completely suppressed, but rather a temporary deactivation of the propagating centers occurs with a high frequency (cf. Scheme 1.3). Via the reversible deactivation of the active species termination is reduced, since the main part of the macromolecules taking part in the polymerization process is stored in a stable, dormant state.[42]

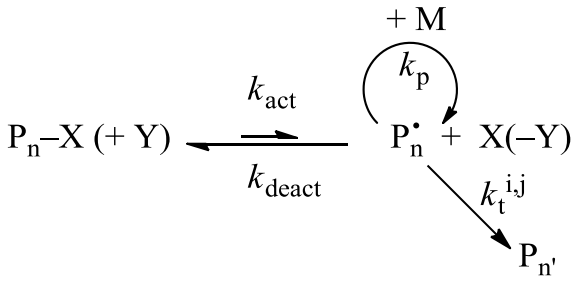

Scheme 1.4 General principle of RDRP.
The deactivation of the radical species is strongly favored compared to re-activation. In addition to propagation, the free-radical undergoes termination as in FRP.

Despite of still present termination, RDRP techniques bear the advantage that a wide variety of monomers and functional groups can be polymerized compared to truly living polymerization techniques.

In the last decade, especially the number of methacrylic and acrylic monomers, which have been investigated with respect to their kinetics and employed in reversible-deactivation radical polymerization (RDRP) methods, has significantly increased. In order to evidence the applicability of RDRP techniques towards heteroatom containing monomers (discussed in Chapter 3) NMP as well as RAFT techniques are employed to control their polymerization in the current thesis.

The subsequent chapters shall provide a fundamental overview of the mechanisms of the most common RDRP techniques, i.e., RAFT, NMP, and ATRP/SET-LRP.

1.3.1 Nitroxide-Mediated Polymerization (NMP)

In 1982 Otsu first reported a "living radical polymerization" (LRP) mediated by stable radicals (e.g., the Gomberg radical) as reversible deactivation agents.[43] In principle similar to his approach, the nitroxide-mediated polymerization (NMP) was developed.[37, 44] In NMP the radical sites are reversibly capped by a stable nitroxide moiety such as TEMPO (2,2,6,6-tetramethyl piperidin-N-oxyl), TIPNO (2,2,5-trimethyl-4-phenyl-3-azahexane-3-oxyl), or the extensively employed SG1 (also known as DEPN or BlocBuilder™, cf. Scheme 3.2 on page

102),[45-48] resulting in an alkoxyamine. In the case of NMP the species X in Scheme 1.3 is the nitroxide and species Y does not exist. If free nitroxides are employed, conventional initiators such as AIBN (azo-bis-(isobutyronitrile); cf. Scheme 1.7) are necessary in order to introduce propagating radicals into the system. However, in order to improve the control over the polymerization outcome, unimolecular thermally decomposable combinations of initiator and controlling agents such as MAMA-SG1 have been developed (cf. Scheme 3.2).[49] In order to mediate the equilibrium between capped and non-capped species via the homolytic cleavage of the alkoxyamine bond, elevated temperature of approx. 100°C are commonly necessary. Initially, the NMP method was solely applicable to styrene and its derivates, since even higher temperatures were necessary in order to cleave the TEMPO-type nitroxides. Subsequently, a wider variety of monomers (such as acrylates and methacrylates) became controllable via NMP by introducing nitroxides such as TIPNO or SG1.[37]

Via the formation of the alkoxyamines, the concentration of propagating radicals is lowered, thereby reducing the extent of undesired termination and transfer reactions, but concomitantly also reducing the overall rate of polymerization resulting in the need for longer reaction times. The nevertheless occurring termination leads to a slight excess of controlling agent (i.e. the nitroxides). Termination can be further suppressed if initially a slight excess of controlling agent is added to the system and thereby the reversible deactivation reaction is favored, according to the persistent radical effect.[50]

The disadvantages of NMP – besides the elevated temperatures – are long reaction times and a (still) limited variability of monomers that can be employed.

1.3.2 Reversible Addition-Fragmentation Chain Transfer (RAFT) Polymerization

The RAFT polymerization technique was introduced over 15 years ago by a group of Australian researchers.[51] By using dithioesters as chain transfer agents (CTA), the control

over FRP is achieved. Independently, the MADIX technique (macromolecular design by interchange of xanthates), which bases on the same mechanism, was reported by a group of French researches.[52-53] The RAFT / MADIX reaction mechanism is based on degenerative chain transfer reactions and is fundamentally different from other RDRP techniques such as NMP or ATRP / SET-LRP procedures.

Initiation, propagation as well as termination are identical to FRP. In the initial stage of a RAFT polymerization, the propagating radicals can add to the dithioester moiety (species 1 in Scheme 1.5) which is followed by a fragmentation into species 2 resulting in a (polymeric) dithioester and a new radical (R˙), which must be able to start a polymer chain. After several propagation steps the polymeric radical (P_n˙) encounters a dithioester species 3 and equilibrates via species 4. A rapid exchange of the polymeric radicals via the core equilibrium, depicted in Scheme 1.5, guarantees an equal probability for all chains to propagate, resulting in a narrow dispersity of the generated MWD. The main advantage of the RAFT technique over other RDRP procedures is the not reduced overall active radical concentration, which leads to a non-decreased overall rate of polymerization. Nevertheless, retardation (initial time span without observable conversion increase) as well as a hybrid effect (initial increase to high molecular weights of the polymer sample accompanied with elevated dispersities) are often observed.[36] The retardation might be caused by cross-termination reactions as well as by slow fragmentation of the intermediate radicals (species 2 and 4) or a combination of both.[19, 54-55] The hybrid effect, on the other side, is caused by a slowed / less favored addition of the propagating radicals to the initial dithioester species (1).

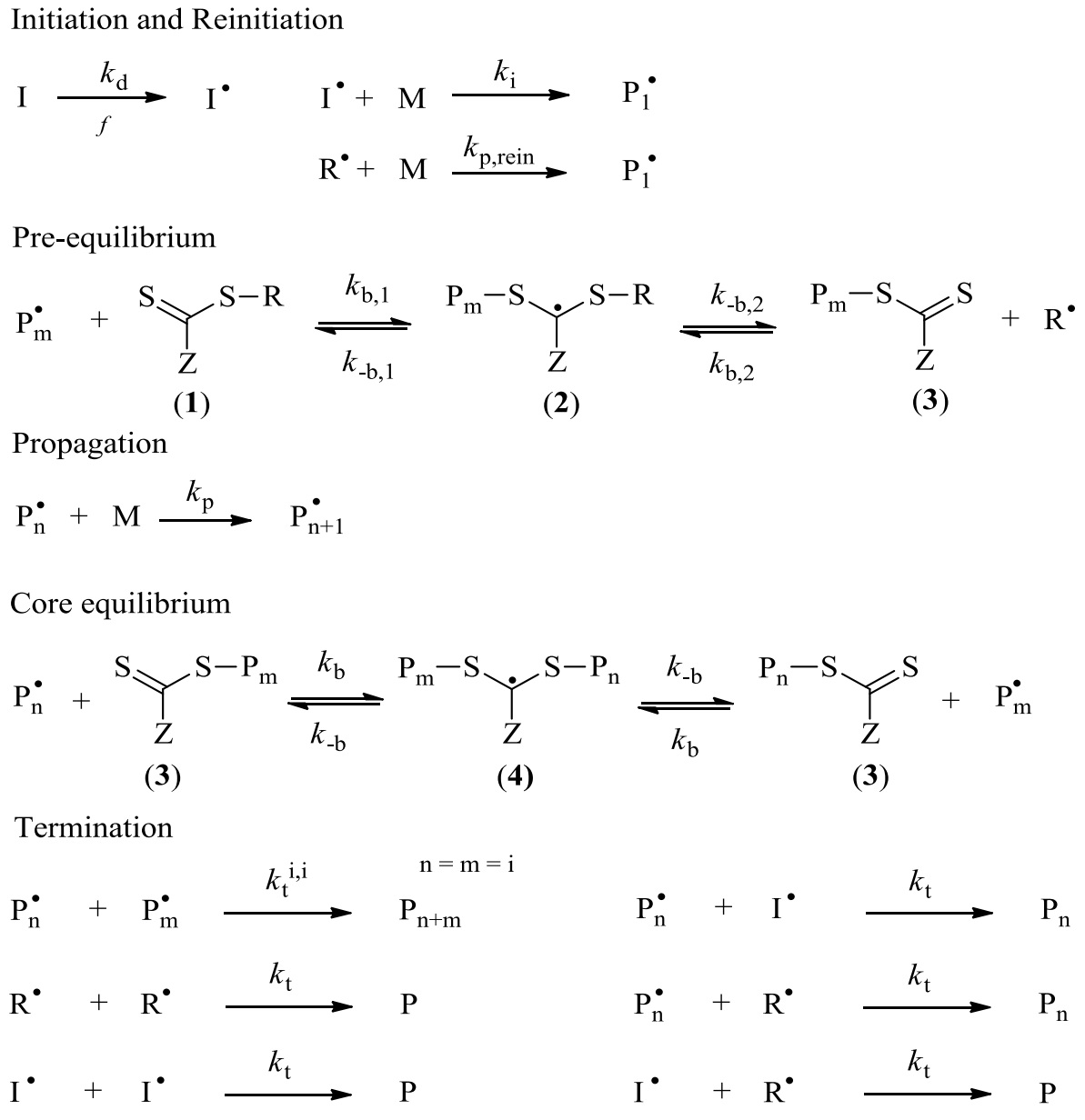

Scheme 1.5 Mechanism of RAFT polymerization.
Additional to the reactions steps of the FRP process, the RAFT specific pre-equilibrium as well as the core equilibrium are highlighted via which the control over the polymerization is achieved.

A judicious choice of a suitable RAFT agent for the desired monomer is crucial for efficiently gaining control over the RAFT polymerization.[56] Moad, Rizzardo, and Thang provide a detailed guide for choosing appropriate R and Z groups in dependence of the monomer of interest.[35] The R group needs to be able to efficiently initiate the polymerization of the monomer (usually secondary R radicals for acrylates), while being sufficiently stable to be efficiently expelled from the initial RAFT agent (tertiary R radicals for methacrylates),

whereas the Z group is responsible for an adequate stabilization of the intermediate radicals (species 2 and 4), thereby influencing the effectiveness of the exchange of the propagating chains.

Since the initiation is achieved in the same fashion as for FRP, the same mild conditions (especially low temperatures) can be employed. However, it should be noted that RAFT polymers are commonly colored (due the combination of the dithioester moiety with the respective Z group) and the temperature stability of their end groups might be reduced.[57]

1.3.3 Atom Transfer Radical Polymerization (ATRP) and Single Electron Transfer – Living Radical Polymerization (SET-LRP)

Beside NMP and RAFT there exist numerous metal mediated RDRP techniques employing, e.g., iron,[58-59] rhenium,[60-61] rhodium,[62] nickel,[63] or ruthenium[60, 64-66] and some other transition metals in an ATRP process.[67] In the last decade copper mediated techniques have attracted special attention and a vivid dispute about the underlying mechanisms of ATRP and SET-LRP is ongoing.[3, 68-73] Since these both techniques proved to be very versatile, efficient and able to allow post-polymerization modifications (via the halogen end group), their proposed mechanisms will be briefly reported herein.

ATRP was simultaneously discovered by Sawamoto[74] as well as by Matyjaszewski and coworkers[39, 75] in 1995. The group of Matyjaszewski contributed most to the development and understanding of the ATRP process.

In the same years as ATRP was reported, Percec and coworkers introduced single electron transfer – degenerative chain transfer living radical polymerization (SET-DTLRP).[76] Degenerative chain transfer (DT) means that a propagating radical abstracts an atom (typically a halide) from another polymer chain. Thus, the initial radical is reversibly deactivated by another polymer chain and the newly formed radical can propagate (in analogy to the RAFT mechanism). The SET-DTLRP can be catalyzed by various copper species in

combination with nitrogen containing ligands. By suppressing the DT, the SET-LRP technique was developed and the control over the polymerization could be improved. Scheme 1.6 highlights the mechanisms proposed for ATRP and SET-LRP.[77] In both cases a halogen containing species (initiator or chain end functionalized polymer molecule) is activated by a copper species, whose oxidation state is increased by one (ATRP: conventionally $Cu^{I}Br$ turns into $Cu^{II}Br_2$; SET-LRP: Cu^0 e.g., from copper wire or powder, turns into $Cu^{I}Br$). Thereby a carbon centered radical is generated, which can perform all reactions as in conventional FRP, i.e., propagation, transfer, and termination.

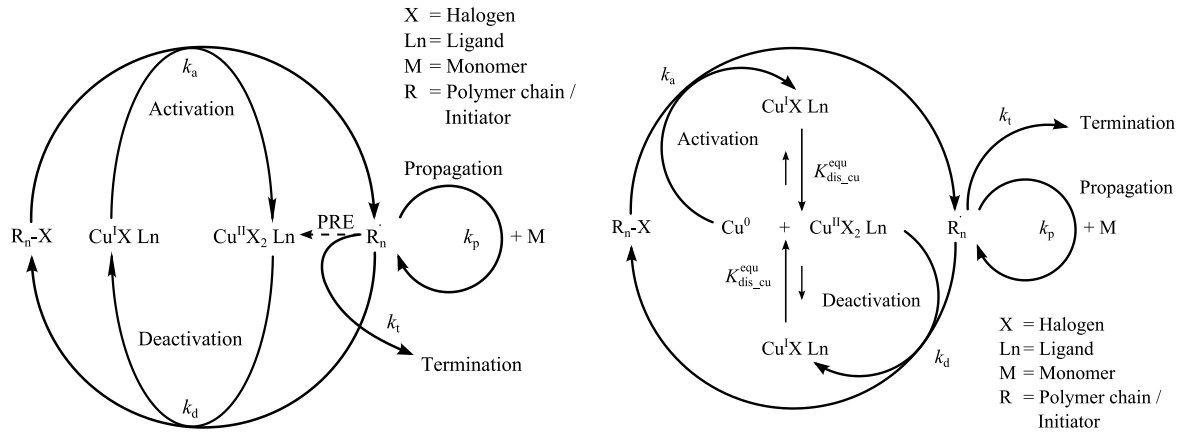

Scheme 1.6 Proposed mechanisms of ATRP and SET-LRP.
The mechanism of ATRP employing copper is highlighted on the left hand side. Via termination a slight excess of deactivating species is accumulated leading to the persistent radical effect (PRE) similar to, e.g., NMP. The SET-LRP mechanism inherently requires no PRE effect in order to efficiently gain control over the polymerization since deactivating (and activating) species are generated via disproportionation subsequent to each activation and deactivation step. Scheme adapted from ref. 77.

The radical can additionally be deactivated by $Cu^{II}Br_2$ under re-generation of a halogen containing species and reduction of the oxidation state of the copper species by one. In contrast to ATRP – where with $Cu^{I}Br$ already the activating species is regenerated – the activating and deactivating species are generated in SET-LRP via spontaneous disproportionation of Cu^{I} species into Cu^{II} and Cu^0 species. The actual catalytic species in both techniques consist of a complex containing the copper atom, a ligand (conventionally N-containing), and none, one, or two halogen atoms.[39, 75, 78-79]

An ongoing debate between Matyjaszewski and Percec has arisen about the correctness of the proposed mechanisms and the experimental conditions under which they might be active.[3, 68-73] The rate of disproportionation (which is an undesired side reaction in ATRP, yet essential in the SET-LRP mechanism) and the oxidation state of the initiating species seem to be crucial to judge which mechanism is active.[80-81] However, for both techniques almost identical experimental conditions are reported.[82-85]

Substantial efforts have been made in reducing the catalyst loadings, e.g., by using standard FRP initiators for continuous activator regeneration (ICAR-ATRP) or by using, e.g., elemental copper in activators regenerated by electron transfer (ARGET-ATRP). These two techniques are based on the reactivation of the Cu^{II} salt, which has accumulated through the irreversible termination of the propagating radicals. The initiators or metal sources are used as reducing agents to re-form the original amount of Cu^{I} activator. Furthermore, initial addition of Cu^{II} species significantly enhances the control over the polymerization and reduces the necessary overall amount of copper.[2]

In the last decade, the number of publications concerning SET-LRP and ATRP grew almost exponentially. Aside from enlarging the spectrum of monomers which could be employed,[86-92] many studies aimed to explore certain aspects of the underlying mechanism such as the influence of solvents,[81, 85, 93-96] initiator structure,[97-98] and the halogen-carbon bond dissociation[90, 99-103] as well as role of the applied ligand, [79-80, 98, 104-106] the dependence on the copper surface,[94, 107-108] the degree of disproportionation of Cu^{I} species,[80, 95, 104, 109] as well as the role of Cu^{II} deactivator.[110] Kinetic modeling studies of the entire polymerization process can also be found.[2-3, 72, 111-112]

1.4 The PLP-SEC method

After the discussion of the mechanisms of FRP as well as the RDRP techniques, the next section focuses on the herein employed method for the determination of propagation rate coefficients. The method of choice for the determination of propagation rate coefficients in free-radical polymerization is pulsed laser polymerization coupled with size-exclusion chromatography (PLP-SEC), which was initially reported by a Russian research group[113] and later on mainly developed by Olaj and co-workers.[114-116] Its theory and method are already well developed and well understood.[113, 117-118] Since 1995, the IUPAC working party "Modeling of Kinetics and Processes of Polymerization" benchmarks the propagation rate coefficients, k_p, and the associated Arrhenius parameters of various commonly employed monomer systems.[119-129] The IUPAC working party has been called into presence, since up to then a wide variety of sometimes even clearly contradictory rate coefficients, determined via various methods, were reported.[130]

A detailed description of the investigated monomer systems and trends detected among them will not be included in the current chapter. A review by Beuermann and Buback provides an encompassing picture.[117] However, a perspective of what has been achieved so far via the PLP-SEC method will be provided at the appropriate sites when comparable monomers are investigated herein, i.e., in the Introductions to Chapters 2 and 3.

The monomer under investigation is polymerized via Pulsed Laser Polymerization (PLP) with a typical photoinitiator (cf. Scheme 1.7).[128] In the current study DMPA (2,2-dimethoxy-2-phenylacetophenone) was employed. The laser pulses generate repetitively high radical concentrations which lead to a fast termination of the main part of the radical population. However, some of the radicals survive the short period directly after a laser pulse and can propagate until the next laser pulse is emitted and the radical concentration is again massively increased. Most polymer molecules, which are generated via PLP, have propagated for one

dark time period (i.e., the time span between two subsequent laser pulses) and have therefore a characteristic molecular weight, M_1, which depends on the monomer specific propagation rate coefficient. In parallel, some of the macroradicals arising from the first laser pulse survive the subsequent one(s) and propagate therefore for two (three,… *i*) dark times. Consequently, their molecular weights (M_2, M_3, M_i) should be the exact double (three times, *i*-times) of the molecular weight of the macroradicals, which were terminated after one dark time. Therefore, the ratio $(M_1 \cdot i)/M_i$ is one of the several consistency criteria that have to be fulfilled in a PLP experiment to obtain a reliable and valid propagation rate coefficient.[117]

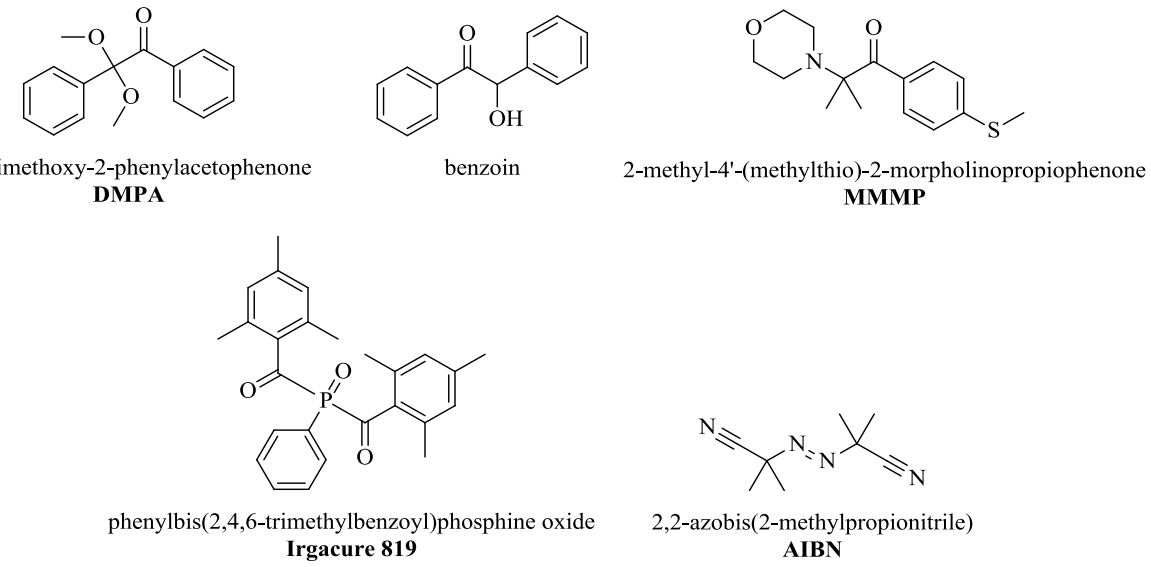

Scheme 1.7 Photoinitiators.
Exemplarily, the structure of 2,2-dimethoxy-2-phenylacetophenone (DMPA), benzoin[131], Phenyl-bis(2,4,6-trimethylbenzoyl)phosphine oxide (commerzialized as Irgacure 819),[132] MMMP[133] and AIBN[132] are depicted.

A detailed description and discussion of the consistency criteria can be found, e.g., in IUPAC benchmarking publications.[126-128] In the following, a brief list will be provided:

(i) The PLP-SEC experiment has (of course) to be reproducible within the experimental errors, as especially laser pulse profiles and the SEC evaluation might vary.

(ii) The polymerization has to be stopped at low conversions in order to not violate the boundary condition of assumed constant monomer concentration, c_M, which is necessary during the integration of underlying differential equations leading to Equation 1.1 (see below).

(iii) Higher inflection points of molecular weight distributions (MWD) should be observable or at least the deduced kp value has to be invariant towards the variation of the laser pulse frequency, thereby demonstrating that the MWD is governed by the laser pulsing.

(iv) The ratio of the propagation rate coefficient derived via the first and the second (or higher) inflection points, kp1/kp2, (equal to (M1·i)/Mi as described above) has to be as close as possible to unity. In the current study typically values between 0.95 and 1.20 are observed, whereas samples displaying values above 1.2 are usually neglected.

(v) The deduced kp values should be invariant to an alteration of the pulse repetition number (i.e., studied conversion range), pulse repetition frequency (i.e., molecular weight of the inflections), photoinitiator concentration, and laser pulse energy (both influencing the amount of photolytically generated radicals per laser pulse).

The PLP experiment results in a characteristic shape of the SEC chromatograms and the MWD of the polymer sample. Typical PLP-structures with at least two inflection points (identified by the maxima in the first derivative) are exemplarily shown in Appendix A and B for each of the currently studied monomer solution conditions (refer to e.g., Figure S1). From these maxima in the first derivative, the propagation rate coefficient can be deduced according to Equation 1.1

$$L_i = \frac{M_i}{MW_M} = i \cdot k_p \cdot c_M \cdot t_0 \qquad 1.1$$

where L_i is the degree of polymerization, M_i is molecular weight of the inflection point number i, MW_M is the molecular weight of the monomer, i is the number of the inflection point, c_M is the monomer concentration, and t_0 is the time between two subsequent laser

pulses. The monomer concentration c_M is adjusted via the temperature dependent density function, which reads:

$$\rho = \rho_0 - b \cdot T \qquad 1.2$$

where ρ_0 is the density at 0°C and b is the slope of the linear fit of the density values determined for various temperatures T (given in [°C]; ρ_0 and b are both stated, e.g., in Table 2.1 for the studied monomer systems).

However, in Equation 1.1 solely i and t_0 are known / determinable. Via a PLP-SEC experiment merely the product of the propagation rate coefficient and the monomer concentration, $k_p \cdot c_M$, is measureable. In the past, an ongoing discussion has arisen regarding the assumption that the monomer concentration, effective at the radical site (which is c_M^{local}), might differ from the overall, macroscopic monomer concentration of the solution (which is $c_M^{overall}$).[122, 134-139]

1.4.1 Determination of Absolute Molecular Weights

For the calculation of the propagation rate coefficients, the absolute molecular weight values at the inflection points are required. In addition to the direct determination of the absolute molecular weights via, e.g., a multi angle LASER light scattering (MALLS) detector, the universal calibration method based on polymer specific Mark-Houwink-Kuhn-Sakurada (MHKS) parameters is a precise and reliable method.[140] The parameters K and α allow for the calculation of the molecular weight, M, of a polymer sample from its experimentally determined intrinsic viscosity $[\eta]$ according to Equation 1.3:

$$[\eta] = K \cdot M^{\alpha} \qquad 1.3$$

According to the Equation 1.3, where $[\eta]$ represents the limiting intrinsic viscosity and M represents the molecular weight of the sample, the slope of the $[\eta]$ vs. M_w plots (cf. Figure 2.2 to Figure 2.4; following page 40) corresponds to the exponent α and the y-intercept

corresponds to the prefactor *K*. MHKS parameters are generally applicable, especially if they are determined for a wide molecular weight range.

The method of determination and application of the MHKS parameters in the PLP-SEC method bears some advantages over a direct measurement of each sample with a light scattering detector or analysis with a multi detector SEC set-up. The main disadvantage of direct analysis, e.g., with a MALLS detector is that it is beset with a high uncertainty for particles / macromolecules smaller than approx. 30000 to 50000 $g \cdot mol^{-1}$. Especially if the macromolecules do not scatter light very well – as it is the case for many of the currently investigated polymers with alkyl ester side chains – the uncertainty of a direct measurement of the PLP samples in the relevant molecular weight range is high. The uncertainty of the MALLS signal is additionally increased if low concentrations are employed, as it is necessarily the case in a high resolution SEC-setup with three columns. Consequently, for a reliable MALLS evaluation the PLP conditions would have to be modified in such a way that the molecular weight of the first inflection point is clearly above 50000 $g \cdot mol^{-1}$, thereby giving rise to, e.g., acrylate specific problems related to backbiting and a possible loss of the PLP structure in the MWD.

Thus, it seems preferable – wherever possible – to determine the MHKS parameters of all PLP generated polymers, as no MHKS parameters for these species – and certainly not synthesized under PLP conditions – can be found in the literature.[b] For this purpose – as it is the case for the herein studied alkyl (meth)acrylates – broadly distributed PLP-generated polymers can be fractionated via a SEC column to obtain narrowly distributed polymer samples, which are subsequently analyzed via a triple detection SEC (refractive index (RI),

[b] From the currently investigated monomer/polymer systems solely for poly(stearyl methacrylate) (pSMA) MHKS parameters were available in the literature prior to this study.[141] However, it was necessary to determine the MHKS parameters for pSMA again, since the literature values correspond to pure C18 ester side chains, whereas herein a commercially available C16/C18 mixture was employed. This difference is also reflected in the parameters: K = 14.62 (Lit.: 8.95)$\cdot 10^{-3}$ $mL \cdot g^{-1}$ and α = 0.620 (Lit.: 0.67).

light scattering (LS, i.e., in the current study MALLS), and viscosimetry (Visco) detectors) for the determination of the absolute weight average molecular weight, M_W, as well as the limiting viscosity $[\eta]$.[142] With the aid of the obtained MHKS parameters the determination of the absolute molecular weight of various PLP polymer samples can be performed according to the universal calibration method against narrowly distributed poly(styrene) polymer standards.[143-145] The universal calibration is based on the principle of SEC, i.e., separation of the molecules solely based on their hydrodynamic volume via elution in a matrix of porous material (e.g., poly(styrene) crosslinked with divinylbenzene to microspheres featuring pores in the range of nanometers). A separation according to the chemical nature of the molecules, i.e., via enthalpic interactions with the column material (which is the basic principle of high-pressure liquid chromatography (HPLC)), has to be explicitly avoided. In agreement with the SEC principle, varying polymers passing the column (containing the stationary phase, i.e., the porous material) after the same elution volume (of solvent, also referred to as mobile phase) share the same hydrodynamic volume. The hydrodynamic volume, V_h, (defined as the volume of a hypothetical hard sphere, exhibiting the same diffusion properties as the investigated macromolecule in solution, further described by the Stokes-Einstein relation) can be related to the product of the intrinsic viscosity $[\eta]$ and the molecular weight M_w.[144, 146-149]

Consequently, polymers eluting at the same retention time share the same $[\eta]$. Since the molecular weight of, e.g., poly(styrene) samples can be determined via other methods (mass spectrometry, light scattering, NMR, …) and since their MHKS parameters are known (i.e., determined via, e.g., triple detector SEC) they can be employed as calibration standards for conventional and universal calibration. If additionally the MHKS parameters of the samples' polymer type are known, absolute molecular weight are accessible via Equation 1.3.

The universally calibrated chromatograms obtained in the current study are computationally smoothed and their first derivative is employed to determine the molecular weights of the inflection points, M_i. The pulse repetition rate in the current study was – whenever possible –

modified for each temperature in such a way that the molecular weight of the first inflection point, M_1, is in the range between approx. 10000 to 40000 g·mol^{-1}. If the inflection points for every sample are in a similar molecular weight region (i.e., the corresponding macromolecules elute after comparable times in the SEC system), the experimental errors (especially SEC errors) have a similar extent for all samples and therefore the comparability of the PLP-SEC results among each other is enhanced.

Since polymers generated via PLP were used to obtain the narrowly distributed samples, the microstructure of the polymers is arguably the same as the one of the analyzed polymer samples employed for the determination of the Arrhenius parameters. Especially in the case of the poly(acrylates), the microstructures would differ significantly if narrowly distributed samples were used from, e.g., thermal or controlled polymerization processes. Their microstructure is very dependent on the degree of transfer to polymer caused by acrylate typical backbiting and follow-up reactions which are discussed in detail in Chapter 1.2.[11, 150]

As noted above, not for every monomer system the MHKS parameters are accessible. Both in Chapter 3 discussed heteroatom containing (meth)acrylates are examples of such systems. The viscosity of the solvent DMAc is quite high, which leads to severe difficulties for the application of an on-line viscosimeter detector (high initial pressure of the pure solvent, low signal to noise ratios, need for elevated temperatures and high concentrations). Therefore, these monomer systems were analyzed at the Polymer Institute of the Slovak Academy of Scienes (Bratislava) with an on-line SEC-MALLS set-up. Such a procedure of determining the absolute MWD of each individual PLP sample directly is more elaborate and difficult. In order to obtain a high signal-to-noise ratio in the light-scattering detector, several pulse repetition rates were employed for each temperature in order to fine-tune the temperature-specific optimum PLP conditions. The accuracy of the SEC calibration via the MALLS detector is mainly dependent on the high-molar-mass fraction within the polymer sample. High-molar-mass fractions originate during the PLP experiment for two reasons: (*i*) a low

pulse repetition rate and (*ii*) the ever-present uncontrolled free-radical polymerization background. To a limited extent, non-PLP-based polymerization can occur during sample preparation and the sample work-up until an additional inhibitor (e.g., methyl hydroquinone (MeHQ)) is added. Such a background polymerization is often undesired as it reduces the monomer concentration without generating polymer with a chain length that was regulated by the repetitive laser pulses. A (significantly) reduced monomer concentration violates the necessary assumption in Equation 1.1 that the actual monomer concentration, c_M, is equal to the initial one.

In the case of the direct SEC-MALLS evaluation, however, the background polymerization is – to a certain extent – helpful to ensure an accurate SEC calibration. The inflection points of the SEC distribution, which determine the value of the propagation rate coefficient, are usually in the range between 10000 and 60000 g·mol^{-1}, whereas the high-molar-mass fraction of the polymer sample – responsible for a valid SEC-MALLS evaluation that can be extrapolated into the low molar mass region – is commonly well above 100000 g·mol^{-1}. It has to be noted that the accuracy of the light-scattering detector is significantly decreased for macromolecules smaller than approx. 30000 g·mol^{-1}. In order to fulfill all consistency criteria of the PLP-SEC method, the PLP conditions therefore have to be tuned in such a way as to strike a balance between a valid SEC-MALLS analysis, not too low molar masses of the inflection points (for the MALLS detector), not too high molar masses of the inflection points, i.e., not too low pulse repetition rates (in order to avoid affection via mid-chain radicals (e.g., via backbiting)), the occurrence of higher inflection points, and a limitation of the overall polymerization to low conversion.

1.4.2 Deducing Arrhenius Relationships

The molecular weights of the inflection points, M_i, can – once they are reliably determined – subsequently be used to calculate the propagation rate coefficients according to Equation 1.1.

The k_p values, determined via the above described method, obey (usually / ideally) the Arrhenius equation:

$$k_p = A \cdot e^{-\frac{E_a}{R \cdot T}} \qquad 1.4$$

The Arrhenius parameters are available via a linear fit of a $\ln(k_p / [L \cdot mol^{-1} \cdot s^{-1}])$ vs. T^{-1} plot. During the evaluation procedure the various consistency criteria for a reliable determination of k_p have to be fulfilled (described above in the list on page 16). In the current thesis, the influence of the degree of conversion is checked by applying different pulse numbers for the same combination of temperature and laser pulse frequency. The number of laser pulse repetitions must be sufficiently low so that the observed scattering between samples produced with different pulse repetition numbers is in the same range as the scattering observed within multiple injections of the same sample into the SEC system. Therefore, in the current research work no correlation between fluctuations in k_p and the corresponding pulse repetition numbers, which are proportional to conversion, could be identified. In the case of BeMA, for example, even samples with 15000 pulses could be incorporated into the Arrhenius evaluation, since they are – surprisingly – in perfect agreement with the conventionally applied lower pulse numbers of 150 and 300 repetitions. Nevertheless, in order to not violate the assumption of an (ideally) infinitesimally low conversion, equal to a constant c_M, the sample polymerized with the lowest pulse repetition number should be taken into account for the calculation of the Arrhenius plot, which provides a valid PLP-structure in the SEC chromatogram with a good signal to noise ratio in the first derivative and a good agreement of $k_{p,1}$ and $k_{p,2}$. In several samples of the current investigations (especially of linear methacrylates) even $k_{p,5}$ could be determined and was found to be still in reasonable agreement with $k_{p,1}$ (e.g., $k_{p,1}/k_{p,5} = 1.07$). In the Arrhenius plots at least two representative data points were selected for each temperature, corresponding to a higher and a lower frequency. In cases where this was not possible – as no valid samples with different

frequencies are available (i.e., for the acrylates, especially at elevated temperatures) – a second, valid sample with a higher pulse repetition number was implemented into the Arrhenius plot.

The acrylate typical transfer to polymer events generate relatively stable tertiary radicals (mid-chain radicals, MCR), which propagate substantially slower than the secondary acrylic radicals (cf. Chapter 1.2).[11] MCR have to be avoided by employing the highest pulse repetition rates in order to determine solely the k_p of secondary propagating radicals (SPR), k_p^{sec}. However, above 50°C to 80°C (varying with the monomer) the (currently employed maximum) laser pulsing frequency of 500 Hz is no longer sufficient to prevent the appearance of the MCRs and the k_p value determined via the PLP-SEC experiment is a composite of secondary and tertiary propagation rate coefficients. Such composite k_p values, usually accompanied with significant deviations of $k_{p,1}/k_{p,2}$ from unity, should principally not be incorporated into the determination of Arrhenius parameters for k_p.

In order to assess the remaining consistency criteria, the laser pulse energy as well as the initial photoinitiator concentration was varied in the current study from 2 to 5 mJ·pulse^{-1} and from 1 to 15 mmol·L^{-1}, respectively.

As described above, the Arrhenius parameters are available via linear fits to a $\ln(k_p / [L \cdot mol^{-1} \cdot s^{-1}])$ vs. T^{-1} plot. However, via a simple arithmetic averaging procedure the experimental errors and the possibly differing number of data points at the miscellaneous temperatures might significantly distort the thereof deduced Arrhenius parameters. Furthermore, the half logarithmic nature of the Arrhenius plot results in an underestimation of the experimental errors at elevated temperatures, which are corresponding with higher rate coefficients than lower temperatures. Thus, van Herk and co-workers established the program CONTOUR (current version CONTOUR V2.0.2), which employs a sophisticated mathematical procedure, in order to determine the Arrhenius parameters via a nonlinear fit of the Arrhenius equation.[151-152] Based on the large set of experimentally available PLP-SEC

sample data, the error ranges were assumed to be approx. 10% for methacrylates and 15% in the case of the acrylates, respectively. The minimization procedure employs constant errors for each data point as estimated absolute error ranges. The data points reported herein can be adequately fitted with 95% probability for each monomer system. The stated error ranges are the boundary values of the 95% joint confidence intervals and, consequently, they are not symmetric (cf. Table 2.2, page 46). The Arrhenius parameters stated in the current thesis are the most probable values and are in the center of the symmetric joint confidence contours of 75%, 90%, and 95% probability.

1.4.3 PLP-SEC Investigations into Aqueous Systems

In contrast to the organic (solvent / bulk) systems to which is contributed in the current study and which will therefore be discussed in detail at the appropriate sites when comparable systems are studied herein, a short summary of the insights gained for aqueous systems will be given in the following section.

In the last two decades a variety of water-soluble monomers have been investigated with respect to their Arrhenius data via the PLP-SEC method: *N*-vinylformamide (NVF),[153-154] *N*-vinylpyrrolidone (NVP),[155] acrylamide (AAm),[156] *N*-isopropyl acrylamide (NIPAAM),[157] as well as methacrylic acid (MAA) and acrylic acid (AA).[136, 158-160] In contrast to the monomer systems soluble in organic media, the aqueous monomer solutions exhibit pronounced solvent effects which are based on hydrogen bonds as well as strong changes in the dipolar or electrostatic interactions or even in hydrophobicity of generated polymers. The alterations in the interactions result in changes of the polarity, thermodynamics as well as stabilization of the radical site. Such changes are not only caused by changes of the ratio of water to monomer in the reaction solution, but also vary with monomer conversion.[159, 161] Aqueous systems exhibit apparently a significantly more complicated polymerization behavior than the monomer systems in organic solutions. The polymerization rate is enhanced

via association and structuring of the monomer molecules in solution according to Scheme 1.8.

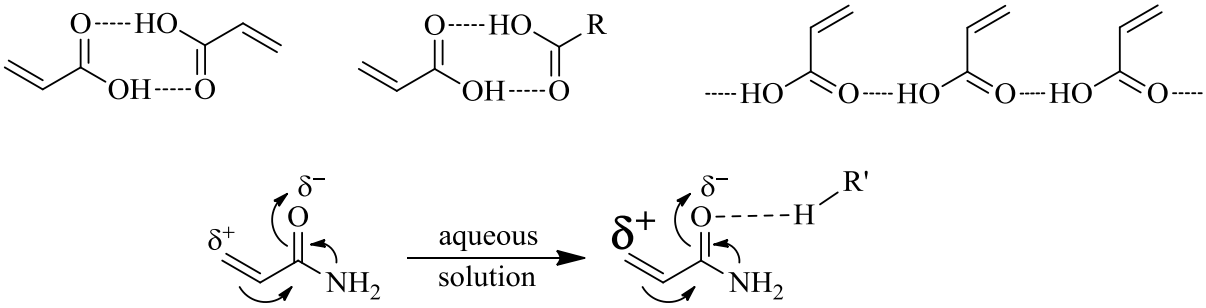

Scheme 1.8 Association and structuring of water-soluble monomers.
Acrylic acid is highlighted as exemplary monomer able to form hydrogen bonds, leading to a pre-structuring of the polymerization mixture. The dipole moment of the vinylic double bond is increased via hydrogen bonds to the carbonyl oxygen, resulting in an enhanced reactivity of the monomer in propagation, exemplary highlighted for acrylamide. The bent arrows symbolize the shift of electron density. Scheme adapted from ref. 162.

Initially, it was believed that also changes in the local monomer concentrations, c_M^{local}, might be responsible for the observed alterations in k_p. However, when studies covering the entire concentration range from bulk to high dilutions of MAA,[159-160] NIPAAM[157] as well as AA[136, 163] were reported, it became clear that real kinetic influences must be operational: The 10-fold increased k_p values observed in highly diluted conditions compared to bulk are too significant to be effects of an increased local monomer concentration. In fact, when going from high dilutions to bulk the k_p value seems to feature an exponential decay, as can be exemplarily be seen by inspection of Figure 1.1 highlighting the situation for MAA at 25°C.

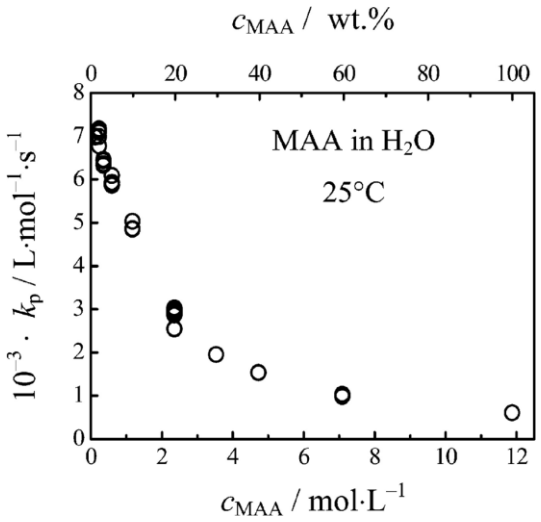

Figure 1.1 Dependence of k_p on the concentration of MAA in aqueous phase at 25°C.
The determined values of the propagation rate coefficient exhibit a decrease similar to an exponential decay with increasing concentration of methacrylic acid (MAA). Reprinted with permission from ref. 159: Beuermann, S.; Buback, M.; Hesse, P.; Lacík, I. *Macromolecules* **2005,** *39*, 184-193. Copyright 2005 American Chemical Society.

Since the alterations of k_p are accompanied with variations in the Arrhenius frequency factor, however not in the activation energies, the currently proposed explanation is based on the changes in the transition state (TS.) With increasing monomer content, internal rotations of the TS become hindered, leading to a reduced rate of propagation. The behavior of MAA depicted in Figure 1.1 was detected via two different approaches of the SEC analysis: Kuchta *et al.*[160] esterified the via PLP generated polymer samples in order to transfer the water-soluble pMAA into pMMA, which can be analyzed via standard organic SEC systems. Beuermann *et al.* [159] instead analyzed their pMAA samples directly via SEC in aqueous phase. Based on the perfect agreement in the k_p behavior of both analysis approaches, their reliability was underpinned and the data were employed for an IUPAC benchmark activity.[164] Further investigations addressed the k_p dependence of (meth)acrylic acids on the ionization in terms of the pH value or the ionic strength. The degree of ionization, α, appears to influence the pre-exponential factor, *A*, as well as the activation energies, E_a. Consequently, the propagation rate coefficient is in such aqueous systems a function of the monomer concentration as well as of the degree of ionization.[137, 165-166] Consequently, the consideration

of the ionization of AA as well as MAA complicates – beside the experimental challenges of analyzing the obtained samples – the understanding of the already complex kinetic situation in the aqueous systems. The general findings detected for AA and MAA are analogously found for NVP[167] and NVF.[154]

The availability of precise propagation rate coefficient data for water-soluble monomer systems opened access to a precise investigation of their termination kinetics. Exemplary work was here executed for MAA,[168] thereby enabling also the realistic modeling of the entire polymerization process in aqueous media.[169] The understanding of the polymerization kinetics of water-soluble monomer systems was mainly driven by Beuermann, Buback, Lacík, Hutchinson, and their coworkers.

1.5 Single Pulse – Pulsed Laser Polymerization (SP-PLP)

In order to obtain an encompassing picture of the polymerization behavior, an accurate determination of the propagation rate coefficient is only the first step. Of comparable high importance as the propagation reaction is the frequency at which the termination reaction takes place, since it limits the life time of a radical and thereby determines in cooperation with k_p how fast the polymerization proceeds and what molecular weights are obtained.

The SP-PLP method offers the necessary access to the reliable determination of the termination rate coefficient, k_t. A single laser pulse is employed to initiate the polymerization and its progress is monitored via on-line infrared or near-infrared spectroscopy. Thereby time resolutions in the range of microseconds are necessary in order to monitor the time dependent consumption of monomer. The recorded conversion vs. time profiles provide – via fitting according to the underlying kinetic equations – the ratio of termination to propagation rate coefficients, k_p / k_t, which, under employment of precise monomer specific k_p values (determined via the PLP-SEC method), yields the monomer specific k_t values over an extended range of monomer conversion.[170]

The best SP-PLP results are obtained if the monomer features a low termination rate coefficient value and a high propagation rate coefficient. Via a fast propagation a higher monomer conversion is achieved per pulse and thereby the data quality and the signal to noise ratio is increased. For monomers which feature low k_p values, such as methyl methacrylate (MMA) or styrene, the conversion vs. time profiles of several pulses (up to 10^2) need to be co-added in order to obtain evaluable data.[171]

Under ideal conditions a single laser pulse generates a narrowly distributed population of propagating radicals, whose degree of polymerization is linearly increasing with time, until transfer reaction (especially to monomer) become effective. Consequently, the SP-PLP methods principally provide also access to the important information on the chain length dependence (CLD) of the termination rate coefficient. However, for a standard SP-PLP experiment, k_t (and k_p) is assumed to feature no chain length dependence, although this is obviously not correct.[117, 172] Therefore the obtained termination rate coefficients should be denoted as $<k_t>$. As mentioned above, the radical chain length increases linearly with time, what implies that the termination rate coefficient $k_t(i,i)$ determined at a specific time after the laser pulse refers to two radicals of approx. the same chain length i. The chain length dependence of the termination rate coefficient is commonly expressed via a power law according to Equation 1.5, where i and j represent the chain lengths of the terminating polymer species.[25]

$$k_t(i,j) = k_t(1,1) \cdot (i \cdot j)^{\frac{-\alpha}{2}} \rightarrow k_t(i) = k_t(1,1) \cdot (i)^{-\alpha} \qquad 1.5$$

Under the approximation that both terminating species have the same degree of polymerization, as it can be justified in the case of a narrowly distributed polymer sample, Equation 1.5 can be simplified to the expression on the right. A further technique providing access to the CLD termination information is the RAFT-CLD-T method (RAFT chain length dependent termination), which will not be explained in detail herein.[21-23] However, “it should

be noted that [this equation] represents an approximation of the chain length dependence of k_t because closer inspection of experimental k_t data as well as theoretical predictions suggests that α is chain length dependent itself. Thus, α is usually reported for certain chain length regimes, in which a significant change of its value is not expected within the accuracy of the individual method."[25]

Employing the SP-PLP method, two regimes with a "constant" exponent α can be detected, i.e., for $0 < i < 30$ (corresponding to α_1) and for $i > 50$ (corresponding to α_2). It should be noted that the initial $k_t(1,1)$, α_1, and α_2 change slightly with the assumed monomer reaction order, which is unity if no transfer reactions are occurring and which increases if transfer reactions are occurring.

For more details on the SP-PLP method and the kinetic information which can be deduced from it, the reader is referred to the literature.[20-23, 27, 117, 168, 173-176]

2 Alkyl (Meth)Acrylates: Global Trends for k_p?[c]

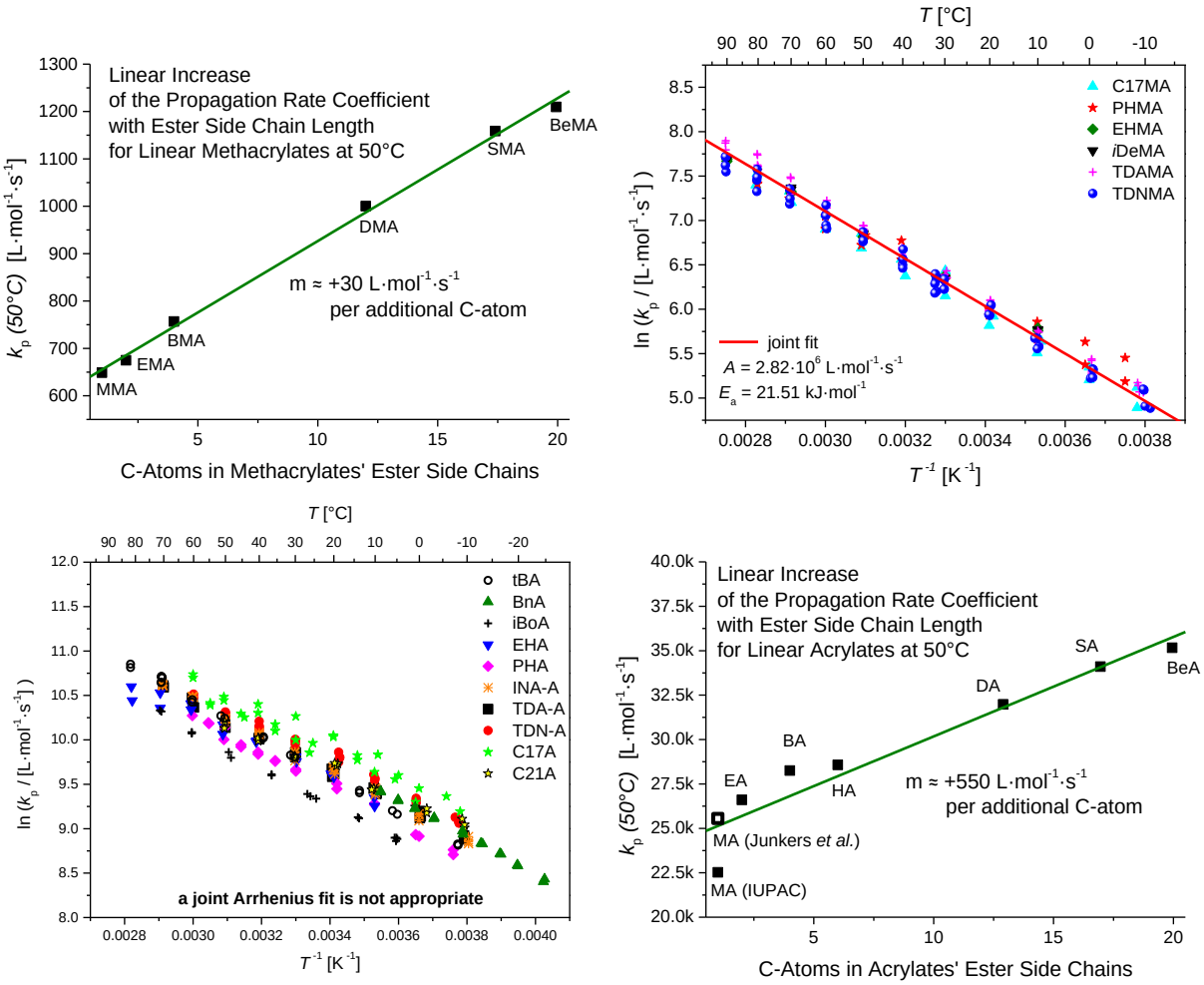

[c] Parts of this chapter were reproduced with permission from Haehnel, A. P.; Schneider-Baumann, M.; Hiltebrandt, K. U.; Misske, A. M.; Barner-Kowollik, C. *Macromolecules* **2013**, *46*, 15-28. and Haehnel, A. P.; Schneider-Baumann, M.; Arens, L.; Misske, A. M.; Fleischhaker, F. Y.; Barner-Kowollik, C. *Macromolecules* **2014,** DOI: 10.1021/ma500304f. Copyright (2014) American Chemical Society.

2.1 Introduction

The current chapter aims at studying trends and family type behavior of the propagation rate coefficient as a function of the composition and steric demand of the ester group in an extended bibliotheca of alkyl (meth)acrylates. The knowledge of the monomer specific propagation rate coefficients has for a long time been a desire in polymer chemistry and several methods were developed in order to determine it.[130] However, the deduced k_p values and the associated error ranges (up to more than 50%) have been very dependent on the employed determination method and were sometimes clearly contradictory to each other. Only with the introduction of the PLP-SEC method a sufficiently accurate and reliable method was established for the determination of propagation rate coefficients. The obtained k_p values are in agreement with several other techniques, but the major advantage of the PLP-SEC method is that it provides a variety of self-consistency criteria – even within a single experiment. In the 1990s the laser pulse repetition frequency was limited to rates not exceeding 100 Hz which allowed for the determination of k_p for relatively slowly propagating monomers such as styrene or methyl methacrylate.[127-128] For faster propagating radicals – such as the acrylates – the determination was only executable at very low temperatures.[121] The failure of the k_p determination at elevated temperatures for acrylates is related to their typical transfer reactions, which cannot sufficiently be suppressed at low pulse repetition rates (cf. Chapter 1.2). With the advent of high frequency laser set-ups the benchmark values of the Arrhenius parameters initially obtained in the low temperature region could be confirmed also for elevated temperatures exceeding ambient conditions.[177] Furthermore, several studies into the copolymerization behavior and the solvent dependence were performed; it is however beyond the scope of the current chapter to discuss the thereof gained insights, since the current thesis focuses on homopolymerizations.

In the past, a selection of acrylates and methacrylates with varying alkyl ester groups was investigated. Based on their propagation rate coefficients, two main trends were described in previous publications:

(i) An increase of the propagation rate coefficients, k_p, at 50°C for linear methacrylates when going from MMA to DMA by a factor of 1.5[126, 178-179] and for linear acrylates when going from MA to DA by a factor of 1.4,[117] respectively, and

(ii) a family type behavior for methacrylates with cyclic ester side chains such as glycidyl methacrylate (GMA, i.e., oxiranylmethyl methacrylate), *cyclo*-hexyl methacrylate (*c*HMA), *iso*-bornyl methacrylate (*i*BoMA), and benzyl methacrylate (BnMA, formerly abbreviated as BzMA).[125, 129]

The latter family type behavior may be described by a "best linear fit" for the combined propagation rate coefficient data of these three monomers.[129] In the current chapter, it will be explored if these two trends are also observed when the topology of the alkyl ester side chains is significantly altered and if similar trends or family type behavior are detectable for branched (meth)acrylates.

The monomer structures of alkyl (meth)acrylates – which have been investigated via PLP-SEC thus far – are depicted in Scheme 2.1, where the monomers investigated in the current thesis are highlighted in bold inside black boxes. To date, the Arrhenius parameters of k_p for the following linear acrylates have been reported: methyl acrylate (MA),[180] ethyl acrylate (EA),[181] butyl acrylate (BA),[177] hexyl acrylate (HA),[181] dodecyl acrylate (DA),[182] stearyl acrylate (SA),[183] and behenyl acrylate (BeA).[183] In the homologous series of linear methacrylates methyl methacrylate (MMA),[126] ethyl methacrylate (EMA),[126] butyl methacrylate (BMA),[126] dodecyl methacrylate (DMA),[126] stearyl methacrylate (SMA),[134] and behenyl methacrylate (BeMA)[134] were investigated via the PLP-SEC method. In both linear series, acrylic and methacrylic, the monomers featuring the largest moieties, i.e., a stearyl or a

behenyl ester function, are investigated in the course of the current research work. As branched alkyl methacrylates *iso*-butyl methacrylate (*i*BMA),[178] *tert*-butyl methacrylate (*t*BMA),[184-185] *iso*-decyl methacrylate (*i*DeMA),[178] 2-ethylhexyl methacrylate (EHMA)[178] as well as a group of cyclic methacrylates (cyclohexyl methacrylate (*c*HMA), benzyl methacrylate (BnMA, formerly abbreviated as BzMA), and glycidyl methacrylate (GMA)[129]) were previously reported. This series is extended herein by propylheptyl methacrylate (PHMA),[134] two variants of tridecyl methacrylate (TDN-MA, isoindex 2.6, and TDA-MA, isoindex 2.2)[183] with differing degrees of branching in their ester side chains as well as heptadecyl methacrylate (C17MA, isoindex 3.1).[134] The latter 3 monomers are isomeric mixtures since the corresponding alcohols (employed in the esterification reaction) are derived from oligomerization of *n*-butene (or propene in the case of TDA-MA) with subsequent hydroformylation and reduction to the homologous alcohol. Prior to the current study, the number of branched acrylates for which accurate k_p values were known was limited to 4 monomers being *tert*-butyl acrylate (*t*BA),[124] 2-ethylhexyl acrylate (EHA),[186] as well as *iso*-bornyl acrylate (*i*BoA),[124] and benzyl acrylate (BnA, formerly abbreviated as BzA).[181] The current study adds to the family of branched acrylates additional 6 monomers, i.e., 2-propylheptyl acrylate (PHA), *iso*-nonyl acrylate (INA-A, isoindex 1.3), tridecyl acrylate (TDN-A, isoindex 2.1), tridecyl acrylate (TDA-A, isoindex 3.1), heptadecyl acrylate (C17A, isoindex 3.1) as well as henicosyl acrylate (C21A, isoindex 4.2). The latter 5 branched acrylates (all except PHA) and the branched methacrylate C17MA are isomeric mixtures synthesized via the analogous procedure as noted above for TDN-MA (TDA-A features the same ester moiety as TDA-MA, which is derived from propene instead of butene). Propylheptyl acrylate and methacrylate are isomeric mixtures consisting of approx. 93% of the depicted 2-propylheptyl ester. The residual isomeric ester groups are 2-propyl-4-methylhexyl (approx. 2.9%), 2-propyl-5-methylhexyl (approx. 3.9%), and 2-*iso*-propylheptyl (approx. 0.2%).

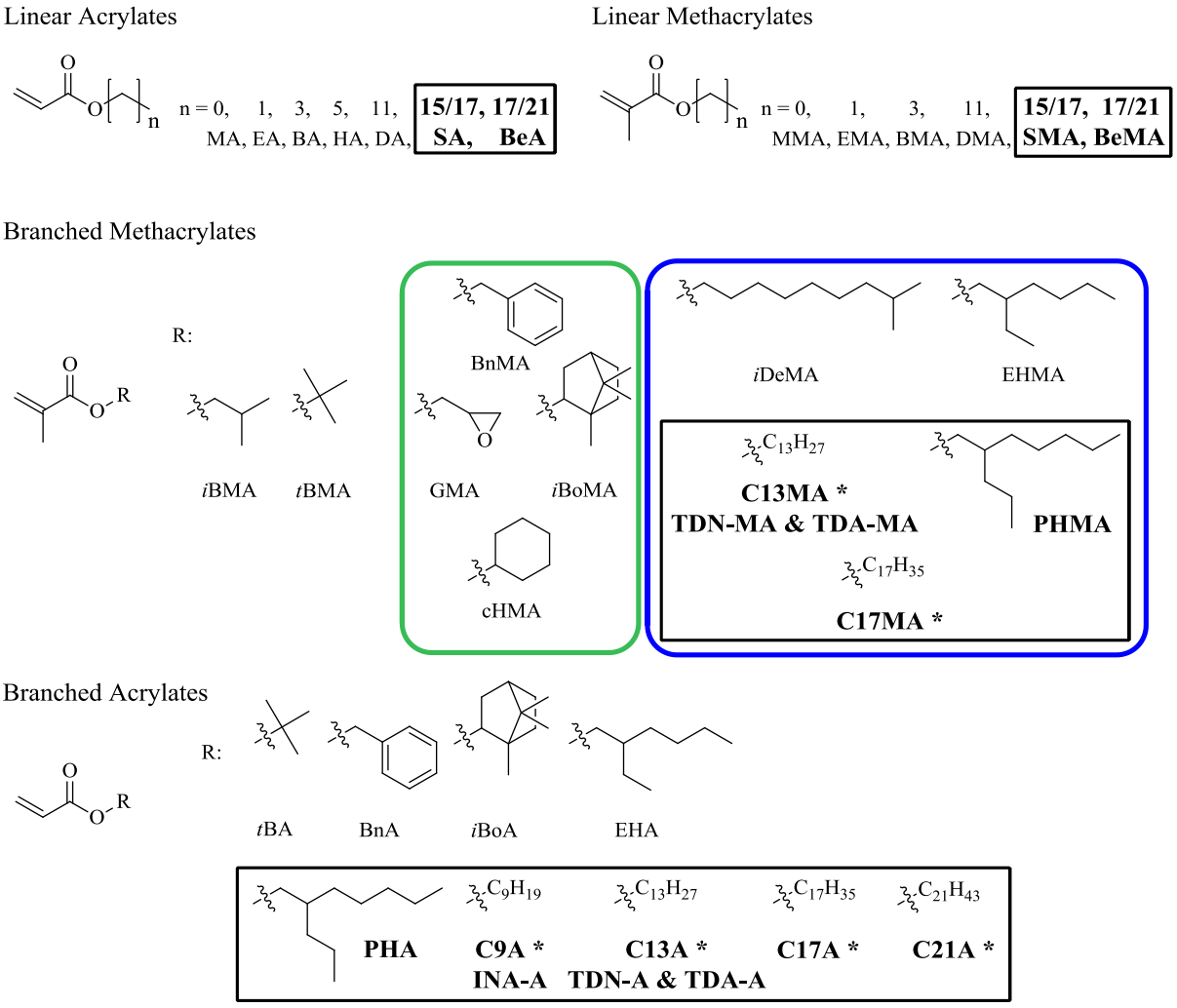

Scheme 2.1 Monomer landscape of alkyl (meth)acrylates.
Structures of the alkyl monomers investigated in the thesis are shown in angular boxes and printed in bold, whereas previously literature known monomers are printed regularly. The monomers are divided in four categories: **(*i*)** linear acrylates: methyl acrylate (MA), ethyl acrylate (EA), butyl acrylate (BA), hexyl acrylate (HA), dodecyl acrylate (DA),[a] **stearyl acrylate (SA), behenyl acrylate (BeA)**; **(*ii*)** linear methacrylates: methyl methacrylate (MMA), ethyl methacrylate (EMA), butyl methacrylate (BMA), dodecyl methacrylate (DMA), **stearyl methacrylate (SMA)**, **behenyl methacrylate (BeMA)**; **(*iii*)** branched methacrylates: *iso*-butyl methacrylate (*i*BMA), *tert*-butyl methacrylate (*t*BMA), *cyclo*-hexyl methacrylate (*c*HMA), benzyl methacrylate (BnMA),[b] glycidyl methacrylate (GMA), *iso*-bornyl methacrylate (*i*BoMA), *iso*-decyl methacrylate (*i*DeMA), ethylhexyl methacrylate (EHMA), **propylheptyl methacrylate (PHMA)**, **tridecyl methacrylates (TDN-MA and TDA-MA)**, **heptadecyl methacrylate (C17MA)**, **(*iv*)** branched acrylates: *tert*-butyl acrylate (*t*BA), benzyl acrylate (BnA),[b] *iso*-bornyl acrylate (*i*BoA), ethylhexyl acrylate (EHA), **propylheptyl acrylate (PHA)**, ***iso*-nonyl acrylate (INA-A)**, **tridecyl acrylates (TDN-A and TDA-A)**, **heptadecyl acrylate (C17A)**, **henicosyl acrylate (C21A)**. The alcohols, employed in the esterification to synthesize the highly branched monomers (marked with an asterisk), i.e., INA-A, TDN-A, C17A, C21A as well as TDN-MA and C17MA, are synthesized via oligomerization of *n*-butene with subsequent hydroformylation and reduction to the homologous alcohol. The highly branched monomers TDA-MA and TDA-A are obtained via the esterification utilizing alcohols synthesized via the analogous procedure employing propene instead of *n*-butene. The green and blue round edged boxes group monomers exhibiting family type behavior.

[a] It should be noted that the monomer reported in literature as dodecyl acrylate (DA) is in fact in most of the studies lauryl acrylate (LA), which is a 55:45 mixture of dodecyl (C12) and tetradecyl (C14) acrylate. LA was choosen since it was available in a significantly higher purity (>99%) than dodecyl acrylate (90%, technical grade). Currently, LA is no longer commercially available.

[b] For benzyl acrylate and benzyl methacrylate the abbreviation BzA and BzMA, respectively, is often employed in the literature instead of BnA and BnMA, which is misleading since Bz typically denotes a benzoyl moiety (C(=O)Ph) instead of a benzyl moiety (CH_2Ph).

With the 14 newly investigated monomers the current chapters aims at validating

(i) if the trend of increasing k_p of (meth)acrylates with increasing linear ester side chain length persists towards longer ester side chains (with the aid of SMA and BeMA as well as SA and BeA),

(ii) if a family type behavior of k_p for branched methacrylates is detectable among the sterically demanding ester side chain monomers or if they can be incorporated into the family type behavior of the cyclic methacrylates reported so far (with the aid of PHMA, TDN-MA, TDA-MA, and C17MA), and

(iii) if a similar family type behavior of k_p can be identified for branched acrylates as for branched methacrylates (with the aid of PHA, INA-A, TDN-A, TDA-A, C17A, and C21A).

In addition to answering these primary scientific questions, the present chapter significantly enhances the number of PLP-SEC studied monomers and provides a profound data base for future IUPAC benchmarking activities.

Several of the acrylic monomers, i.e., SA, BeA, INA-A, TDA-A, TDN-A, C17A, and C21A as well as the methacrylates SMA and BeMA are additionally investigated in 1 M solution in butyl acetate (BuAc). Due to the high melting point of SA and BeA, the temperature range which is accessible for their investigation is relatively narrow (approx. 30 K). Thus, an investigation in solution (featuring melting points of approx. 20 K lower than the monomers in bulk) is desirable, allowing for the determination of Arrhenius parameters with a higher reliability, since they are based on a wider temperature range. Furthermore, the solution data of the 4 linear monomers will reveal if the high k_p values observed in bulk are confirmed, thereby evidencing if they are monomer specific features or if another causality is potentially active.

Furthermore, the investigation of the branched acrylates of the butene-type series, i.e., INA-A, TDN-A, C17A, and C21A, (their ester side chains are constituted of 2, 3, 4, and 5 former butene moieties, which were oligomerized) in 1 M solution in BuAc might allow for the identification of possible trends within this monomer family. In addition, it can be tested if the behavior observed within data obtained in bulk is analogously reflected in 1 M solution in BuAc. Finally, the investigation of TDA-A in 1 M solution allows for the comparison of both tridecyl acrylate species, which differ solely in their degree of branching in the ester side chain.

2.2 MHKS Parameters

As described in Chapter 1.3, the determination of reliable k_p values requires access to absolute molecular weights of the inflection points. In order to ensure a valid SEC calibration, the Mark-Houwink-Kuhn-Sakurada (MHKS) parameters for the above mentioned alkyl (meth)acrylates are determined and subsequently employed in the evaluation of the SEC chromatograms according to the universal calibration method (cf. page 20 in Chapter 1.3).

In order to determine the MHKS parameters, broadly distributed polymer samples are fractionated via an (preparative) SEC column. The broadly distributed polymers are obtained via combining and purification (via precipitation in (ice-cold) methanol, hexane, or diethyl ether or via dialysis versus butyl acetate or tetrahydrofuran) of several PLP generated samples, stemming from the investigation of the propagation rate coefficient or newly polymerized samples under analogous experimental conditions. The microstructure of the polymer chains (with respect to existence and extend of long / short chain branching) is consequently the same as for the polymer samples incorporated into the Arrhenius parameter evaluation. The success of the fractionation is exemplarily demonstrated for poly(behenyl methacrylate) (pBeMA) in Figure 2.1 and – additionally – exemplary triple detector SEC traces are shown for each monomer in Appendix A (cf. Figure S19 to Figure S22). The

dispersity values, $Đ$, of the obtained fractions typically range between 1.05 and 1.25, yet also displays values above 1.5 in the case of some acrylates.

The thereby obtained narrowly distributed polymer samples are analyzed multiple times via a triple detection SEC set-up employing THF as solvent at 35°C. In the following, the [η] vs. M_w plots for each of the studied alkyl monomers are highlighted. The thereof derived MHKS parameters are collated in Table 2.1 along with additional monomer and polymer specific data. The glass transition temperatures have been critically evaluated in a recent publication by establishing general structure-property relationships.[187] The refractive index increments,

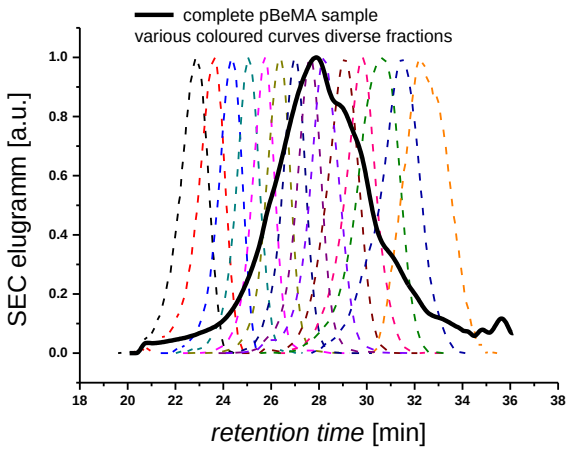

Figure 2.1 Demonstration of the successful fractionation.
The black, bold, and solid line corresponds to the complete pBeMA ($Đ$ = 13.35) polymer sample, which was used for the fractionation. This pBeMA polymer was obtained via combination and joint purification of numerous samples which were generated under various PLP conditions. The variously colored dashed lines correspond to the individual fractions obtained via a SEC fractionation as described in Chapter 4.3. The dispersity indexes of the obtained fractions range between 1.05 and 1.25. The individual fractions are subsequently analyzed via triple detector SEC in order to determine the MHKS parameters. Reprinted with permission from ref. 134. Copyright 2013 American Chemical Society.

dn/dc, have been derived via the RI detector signal of the triple detection SEC measurements employing the exactly known concentration of the purified polymer samples. The temperature dependent density functions are employed to deduce the precise monomer concentration at the relevant temperatures. The glass transition temperatures and/or melting points are determined via differential scanning calorimetry (DSC) and are employed to underpin the observed trends

among the propagation rate coefficients, since they allow obtaining insights regarding the structuring motives in bulk polymer samples, which might similarly be active in bulk monomer solutions (cf. discussion on page 70). The [η] vs. M_w plots (depicted in Figure 2.2 to Figure 2.4) feature a clearly linear behavior over a wide molecular weight range (from approx. 50000 g·mol^{-1} up to approx. $7 \cdot 10^6$ g·mol^{-1}; cf. Table S24 to Table S26 in the Appendix A). As explained in Chapter 1.3, the slope of the [η] vs. M_w plots correspond to the exponent α and the y-intercept corresponds to the prefactor K. The data points of samples with low molecular weights (below ~50000 g·mol^{-1}) were neglected if they did not support the global trend of the higher molecular weight fractions, since such low molecular weight samples often display high experimental errors (e.g., major changes on the analysis may result due to minor changes to the integration borders) and significant scattering within multiple injections of the same polymer sample (cf. discussion about MALLS analysis in Chapter 1.4.1). For several monomers remarkably high molecular weight fractions well above $2 \cdot 10^6$ g·mol^{-1} (up to $6.6 \cdot 10^6$g·mol^{-1} for pINA-A) were obtained (see Table S24 to Table S26 in the Appendix A, which summarize for each monomer the weight average molecular weight values, M_W, and the related intrinsic viscosities, [η], of the samples incorporated in the MHKS determination). A broad molecular weight range, especially if including such high molecular weights, significantly enhances the reliability of the obtained MHKS parameters and allows for a reliable extrapolation into the lower molecular weight range (i.e., below the lowest incorporated molecular weights of approx. 50000 g·mol^{-1}.

Monomer		MW g·mol^{-1}	ρ_0 g·mL^{-1}	b g·mL^{-1}·°C^{-1}	dn/dc mL·g^{-1}	K [a] cm^3·g^{-1}	α [a] –	T_g °C
SA	bulk	346.55	0.88408	$7.2497\cdot10^{-4}$	0.063	$7.28\cdot10^3$	0.703	37[b,c]
	1 M in BuAc		0.89405	$9.0817\cdot10^{-4}$				
BeA	bulk	370.57	0.88401	$7.0452\cdot10^{-4}$	0.072	$7.08\cdot10^3$	0.708	-92 51[b]
	1 M in BuAc		0.89141	$8.8263\cdot10^{-4}$				
SMA	bulk	330.15	0.88227	$7.1395\cdot10^{-4}$	0.071	$14.62\cdot10^3$	0.620	30[b,c]
	1 M in BuAc		0.89220	$9.0210\cdot10^{-4}$				
BeMA	bulk	366.26	0.88321	$7.4087\cdot10^{-4}$	0.065	$21.00\cdot10^3$	0.595	45[b,c]
	1 M in BuAc		0.89223	$8.8718\cdot10^{-4}$				
PHMA	bulk	226.36	0.89225	$7.9634\cdot10^{-4}$	0.079	$8.88\cdot10^3$	0.682	-14
TDA-MA	bulk	268.43	0.90437	$7.6073\cdot10^{-4}$	0.077	$12.96\cdot10^3$	0.624	-33 -31[187]
	1 M in BuAc		0.90233	$9.5034\cdot10^{-4}$				
TDN-MA	bulk	268.43	0.89263	$7.5291\cdot10^{-4}$	0.086	$4.68\cdot10^3$	0.745	-57
	1 M in BuAc		0.89865	$9.4940\cdot10^{-4}$				
C17MA	bulk	324.54	0.89082	$7.2027\cdot10^{-4}$	0.078	$5.26\cdot10^3$	0.697	-51
PHA	bulk	212.33	0.88913	$5.0772\cdot10^{-4}$	0.069	$5.55\cdot10^3$	0.743	-69
INA-A	bulk	198.3	0.89982	$8.2439\cdot10^{-4}$	0.061	$8.36\cdot10^3$	0.707	-68[187]
	1 M in BuAc		0.90159	$9.8790\cdot10^{-4}$				
TDA-A	bulk	254.41	0.89842	$7.6423\cdot10^{-4}$	0.066	$7.88\cdot10^3$	0.692	-55[187]
	1 M in BuAc		0.90070	$9.5521\cdot10^{-4}$				
TDN-A	bulk	254.41	0.89479	$7.6200\cdot10^{-4}$	0.066	$3.65\cdot10^3$	0.760	-69
	1 M in BuAc		0.89957	$9.5381\cdot10^{-4}$				
C17A [d]	bulk	310.51	0.89286	$7.2577\cdot10^{-4}$	0.071	$2.60\cdot10^3$	0.762	-72[134] -64[187]
	1 M in BuAc		0.89799	$9.2113\cdot10^{-4}$				
C21A	bulk	366.62	0.89396	$7.0311\cdot10^{-4}$	0.076	$4.81\cdot10^3$	0.715	-65[187]
	1 M in BuAc		0.89792	$8.9060\cdot10^{-4}$				

Table 2.1 Monomer and polymer specific physical data of currently investigated alkyl (meth)acrylates. In addition to the molecular weight (MW) and the parameters of the temperature dependent densities (ρ_0, b), the change of the refractive index over the change of the concentration (dn/dc) and the Mark-Houwink-Kuhn-Sakurada parameters (K, α) are stated. The temperature dependent densities of TDA-MA and TDN-MA in 1 M solution in BuAc are included for the sake of completeness. The glass transition temperatures, T_g, are determined via differential scanning calorimetry (DSC) (cf. Figure S24 to Figure S28) or collected from the noted reference. [a] at 35°C in tetrahydrofuran (THF); [b] melting point; [c] no T_g detectable between -150°C and 125°C.

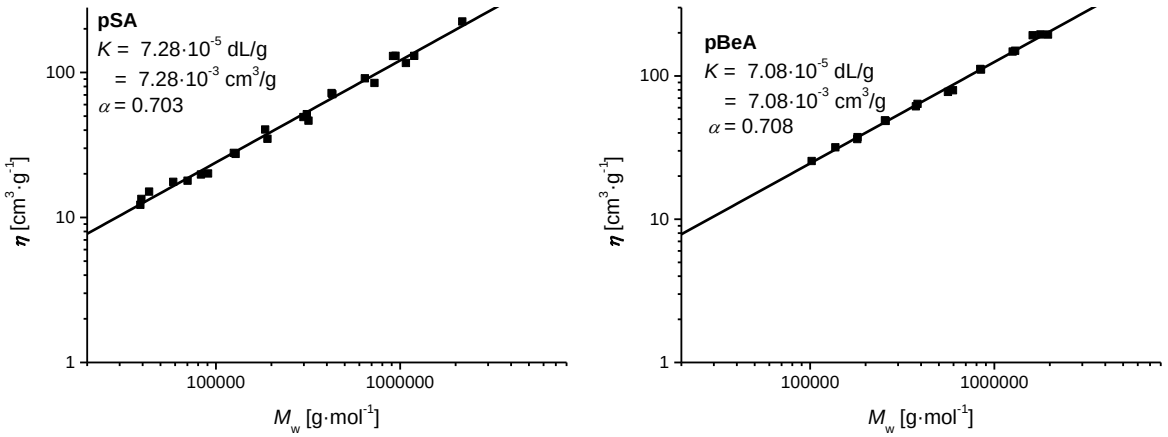

Figure 2.2 [η] vs. M_w plots for pSA and pBeA.
[η] vs. M_w plots with linear fits for the determination of the MHKS parameters at 35°C in tetrahydrofuran (THF) of poly(stearyl acrylate) (pSA) and poly(behenyl acrylate) (pBeA). The monomer structures are shown in Scheme 2.1 and the MHKS parameters are collated in Table 2.1. Adapted with permission from ref. 183. Copyright 2013 American Chemical Society.

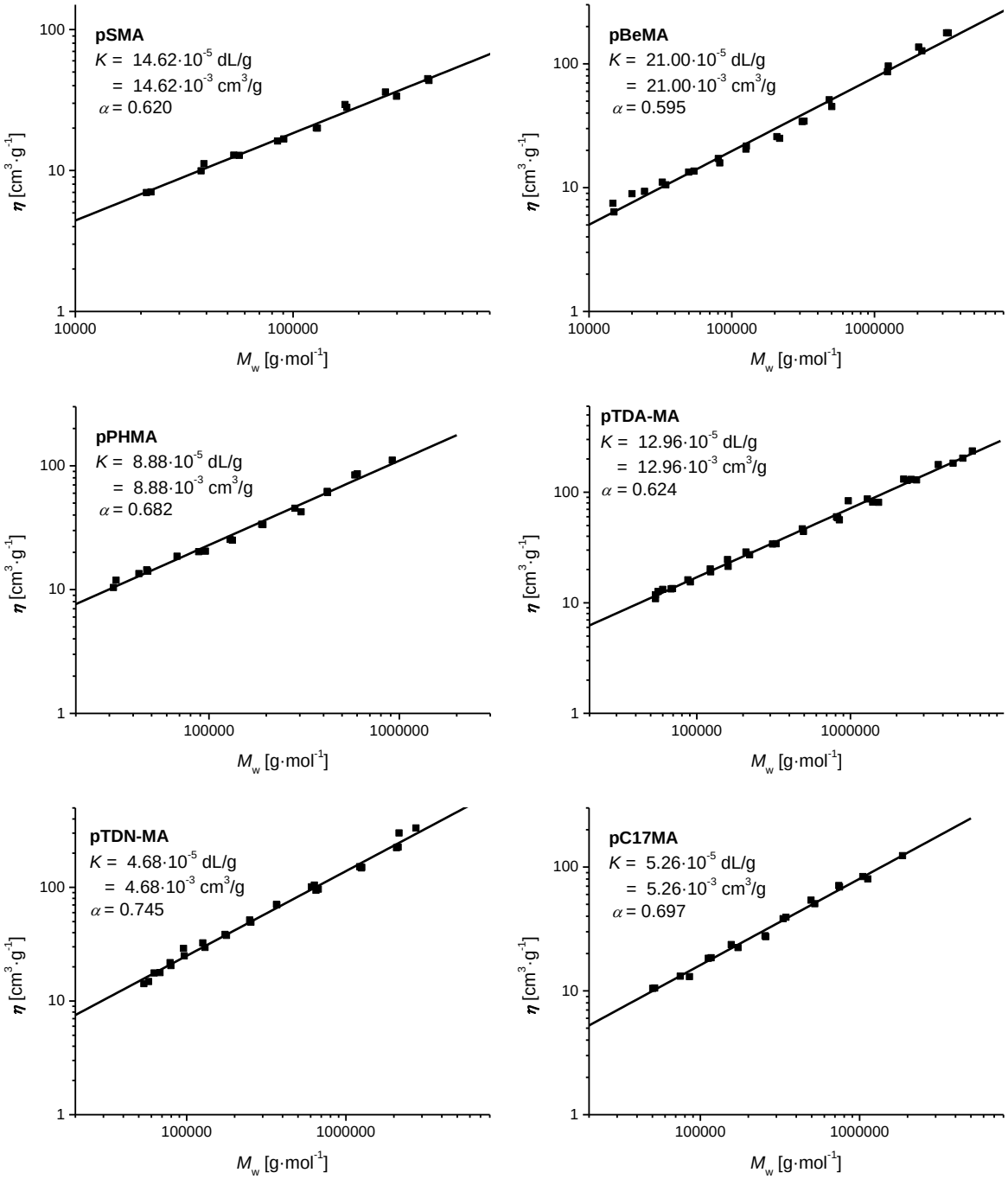

Figure 2.3 [η] vs. M_w plots for pSMA, pBeMA, pPHMA, pTDA-MA, pTDN-MA, and pC17MA.
[η] vs. M_w plots with linear fits for the determination of the MHKS parameters at 35°C in tetrahydrofuran (THF) of poly(stearyl methacrylate) (pSMA), poly(behenyl methacrylate) (pBeMA), poly(propylheptyl methacrylate) (pPHMA), both poly(tridecyl methacrylate)s (i.e., pTDA-MA and pTDN-MA), and poly(heptadecyl methacrylate) (pC17MA). The monomer structures are shown in Scheme 2.1 and the MHKS parameters are collated in Table 2.1. Adapted with permission from ref. 134 and 183. Copyright 2013 American Chemical Society.

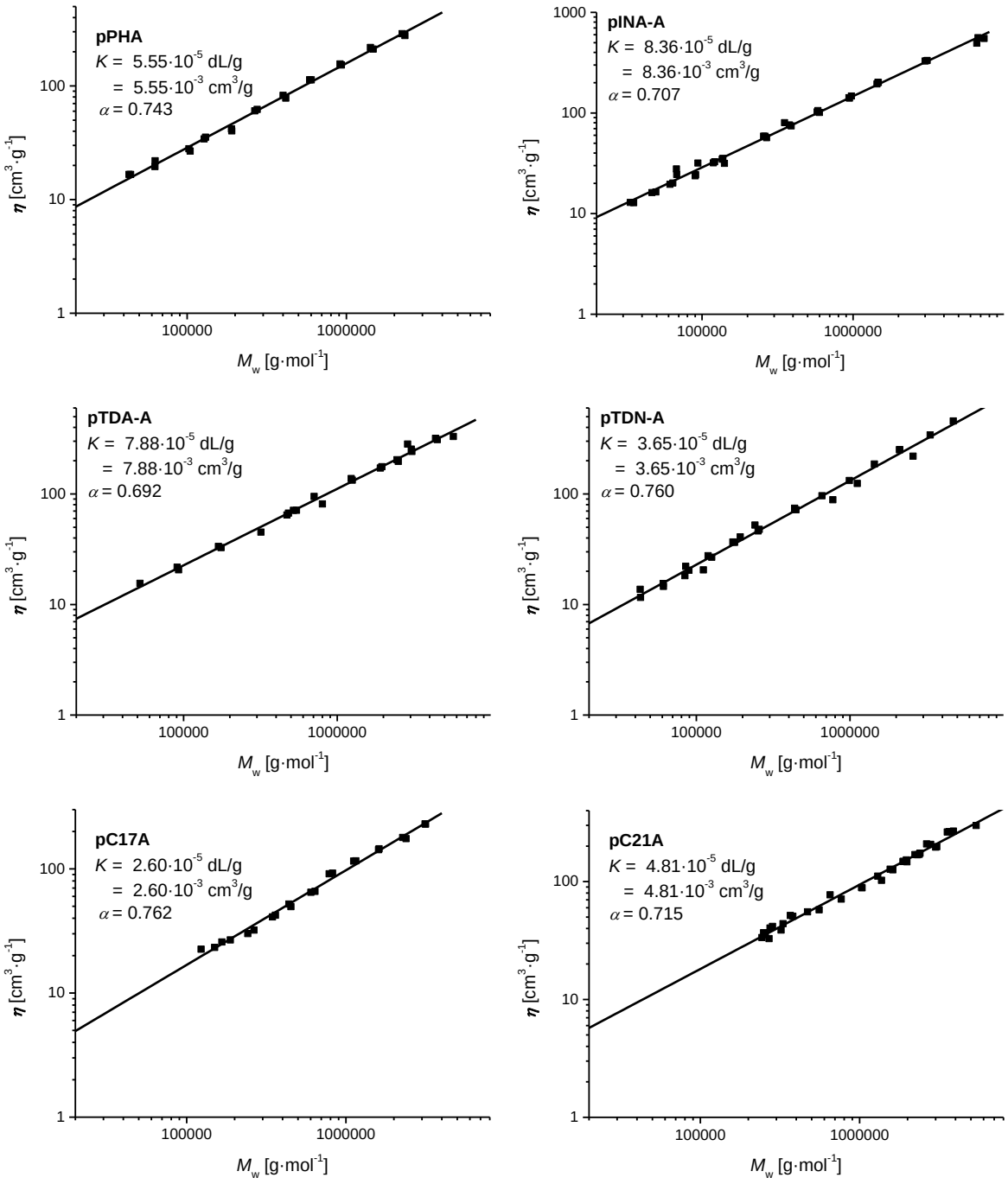

Figure 2.4 [η] vs. M_w plots for pPHA, pINA-A, pTDA-A, pTDN-A, pC17A, and pC21A.
[η] vs. M_w plots with linear fits for the determination of the MHKS parameters at 35°C in tetrahydrofuran (THF) of poly(propylheptyl acrylate) (pPHA), poly(isononyl acrylate) (pINA-A), both poly(tridecyl acrylate)s (i.e., pTDA-A and pTDN-A), poly(heptadecyl acrylate) (pC17A), and poly(henicosyl acrylate) (pC21A). The monomer structures are shown in Scheme 2.1 and the MHKS parameters are collated in Table 2.1. Adapted with permission from ref. 134 and 183. Copyright 2013 American Chemical Society.

As mentioned in a previous study,[124] it is in principle possible to obtain an [η] vs. M_w plot for each sample analyzed with a triple detector SEC set-up, since [η] can be determined for each elution increment. However, this analysis method would be much more susceptible to experimental errors arising from the determination of the sample concentration and slight fluctuations in the chromatograms as well as being limited using a small molecular weight (MW) range. In contrast, the application of a large number of average values, obtained from the narrowly distributed polymer samples, is more robust.

To date there are many different sets (based on polymers prepared by various polymerization techniques and at variable reaction conditions, e.g., temperature, solvent, and initiator as well as methods of measurement) of MHKS parameters for various polymers available.[130] As noted above, the polymerization technique can have a strong influence on the microstructure of the polymer backbone (especially for poly(acrylates)).[11, 158, 188] The microstructure influences the hydrodynamic volume and, consequently, also their elution behavior during the SEC experiment.[189] In the available sets of MHKS parameters no clear trends can be assigned. Therefore, it is very crucial to evaluate the SEC trace with the correct MHKS parameters, which are polymer specific (and dependent on experimental conditions such as solvent and temperature), in order to obtain correct molecular weight distributions (MWD). For SMA, MHKS parameters of $K = 8.95 \cdot 10^{-3}$ cm$^3 \cdot$g^{-1} and $\alpha = 0.67$ were published in the early 1980s.[141, 144] However, the monomer compositions and polymerization technique are different: Xu *et al*. employed SMA with pure octadecanyl ester side chains polymerized via free-radical solution polymerization at 50°C.[144] Although the polymerization technique should not have a strong influence on the microstructure of methacrylates, since the probability of transfer to polymer during polymerization is negligible, the currently determined MHKS parameters are clearly different: $K = 14.62 \cdot 10^{-3}$ cm$^3 \cdot$g^{-1} and $\alpha = 0.62$. Beside the applied polymerization technique to generate the polymer, the different monomer composition (pure C18 vs. a 0.3/0.7 mixture of C16 and C18 ester side chains) is likely the main reason for the

differences between the two MHKS parameter sets. Concerning all other polymers (beside SMA), which are investigated in the current study, i.e., pSA, pBeA, pBeMA, pPHMA, pTDA-MA, pTDN-MA, pC17MA, pPHA, pINA-A, pTDA-A, pTDN-A, pC17A, and pC21A, no MHKS parameter sets were previously published in the literature.

Although the MHKS parameters show a correlation with the stiffness / flexibility of the polymer molecules (in the specific solvent at the specific temperature) which are influenced by the monomer structures, no direct correlation between the monomer structure and the parameter values can be identified. Unfortunately, no general structure-property relationships can be established for the numerous MHKS parameters that have been reported up to date, since they depend additionally, e.g., on the solvent, temperature, chain length, microstructure, and conversion.[130]

2.3 Arrhenius Parameters

Having the correct polymer specific MHKS parameters at hand, it is possible to deduce valid propagation rate coefficients k_p from the SEC chromatograms obtained from polymer samples synthesized during a PLP experiment. The deduced k_p values can be presented in the form of Arrhenius plots, i.e., $\ln(k_p / [\mathrm{L \cdot mol^{-1} \cdot s^{-1}}])$ vs. T^{-1}. Before progressing to a detailed discussion of each investigated monomer within its corresponding family, the obtained Arrhenius relationships for each system will be reviewed.

Figure 2.5 depicts the Arrhenius relations of the linear acrylates (i.e., SA and BeA) in bulk as well as in 1 molar solution in BuAc, whereas Figure 2.6 displays the analogous graphs for the linear methacrylates (i.e., SMA and BeMA). The Arrhenius plots of the branched methacrylates in bulk are collated in Figure 2.7. Figure 2.8 and Figure 2.9, finally, highlight the Arrhenius relations of the branched acrylates in bulk and in 1 molar solution in BuAc (except PHA, which is solely investigated in bulk). The specific sample details corresponding to each data point in the Arrhenius graphs are stated in the Appendix A in Table S1 to

Table S23. The resulting Arrhenius parameters are collated in Table 2.2 together with the related error margins and the corresponding temperature range considered in the Arrhenius analysis. Table 2.2 additionally collates the value of the propagation rate coefficient at 50°C, enabling a coherent comparison of the propagation rate coefficients.

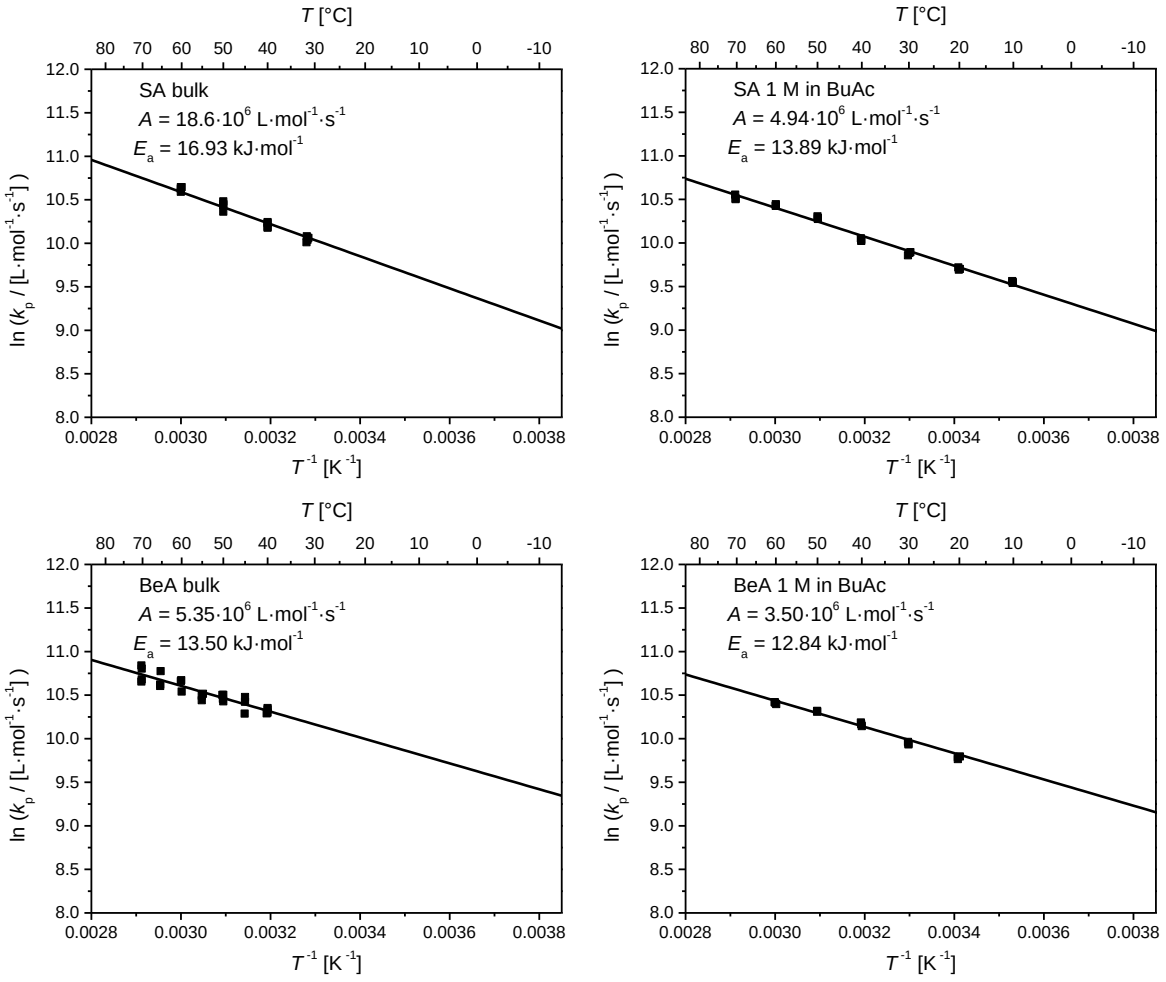

Figure 2.5 Arrhenius plots for SA and BeA.
$\ln(k_p$ / [L·mol^{-1}·s^{-1}]) vs. T^{-1} plots with linear fits for the determination of the Arrhenius parameters in bulk and in 1 M solution in BuAc for SA and Be. The associated monomer structures are shown in Scheme 2.1. The resulting Arrhenius parameters are collated in Table 2.2 jointly with the associated error margins. Adapted with permission from ref. 134 and 183. Copyright 2013 American Chemical Society.

Monomer		A	±	E_a	±	$k_p^{50°C}$	θ interval
		$L \cdot mol^{-1} \cdot s^{-1}$		$kJ \cdot mol^{-1}$		$L \cdot mol^{-1} \cdot s^{-1}$	°C
SA	bulk	$18.60 \cdot 10^6$	$-7.23 \cdot 10^6$ $6.04 \cdot 10^6$	16.93	-1.85 2.72	34000	31 to 60
	1 M in BuAc	$4.94 \cdot 10^6$	$-1.31 \cdot 10^5$ $3.86 \cdot 10^6$	13.89	-1.26 1.27	28000	10 to 70
BeA	bulk	$5.35 \cdot 10^6$	$-2.21 \cdot 10^5$ $4.75 \cdot 10^6$	13.02	-2.28 4.07	35000	40 to 70
	1 M in BuAc	$3.50 \cdot 10^6$	$-1.15 \cdot 10^6$ $3.71 \cdot 10^6$	12.84	-1.40 1.48	29500	20 to 60
SMA	bulk	$3.45 \cdot 10^6$	$-1.17 \cdot 10^6$ $4.46 \cdot 10^6$	21.49	-1.59 1.90	1160	31 to 102
	1 M in BuAc	$3.25 \cdot 10^6$	$-9.93 \cdot 10^5$ $4.76 \cdot 10^6$	22.10	-1.32 1.97	870	1 to 92
BeMA	bulk	$2.51 \cdot 10^6$	$-7.98 \cdot 10^5$ $3.06 \cdot 10^6$	20.52	-1.43 1.85	1210	35 to 107
	1 M in BuAc	$3.47 \cdot 10^6$	$-1.16 \cdot 10^6$ $3.40 \cdot 10^6$	22.10	-1.60 1.58	930	20 to 100
PHMA	bulk	$2.83 \cdot 10^6$	$-8.23 \cdot 10^5$ $3.15 \cdot 10^6$	21.72	-1.20 1.64	870	-9 to 80
TDA-MA	bulk	$3.81 \cdot 10^6$	$-1.45 \cdot 10^6$ $1.35 \cdot 10^7$	22.11	-1.99 3.03	1000	-10 to 90
TDN-MA	bulk	$2.03 \cdot 10^6$	$-1.45 \cdot 10^6$ $7.86 \cdot 10^6$	20.73	-2.29 3.13	900	-11 to 90
C17MA	bulk	$2.04 \cdot 10^6$	$-6.63 \cdot 10^5$ $1.71 \cdot 10^6$	20.72	-1.42 1.38	910	-7 to 80
family type behavior of branched alkyl methacrylates in bulk		$2.82 \cdot 10^6$	$-1.61 \cdot 10^6$ $2.25 \cdot 10^7$	21.51	-2.76 3.75	950	-11 to 90
PHA	bulk	$10.50 \cdot 10^6$	$-4.20 \cdot 10^6$ $2.81 \cdot 10^7$	16.41	-1.99 2.42	23400	-7 to 60
INA-A	bulk	$13.50 \cdot 10^6$	$-3.35 \cdot 10^6$ $6.22 \cdot 10^6$	16.54	-0.91 0.87	28500	-10 to 70
	1 M in BuAc	$16.60 \cdot 10^6$	$-6.41 \cdot 10^5$ $3.99 \cdot 10^6$	17.63	-1.93 2.31	23500	-10 to 70
TDA-A	bulk	$10.50 \cdot 10^6$	$-3.10 \cdot 10^6$ $9.45 \cdot 10^6$	15.98	-1.10 1.44	27500	-10 to 70
	1 M in BuAc	$9.63 \cdot 10^6$	$-2.71 \cdot 10^5$ $9.28 \cdot 10^6$	16.18	-1.02 1.33	23500	-10 to 70
TDN-A	bulk	$5.71 \cdot 10^6$	$-1.57 \cdot 10^6$ $5.08 \cdot 10^6$	14.08	-1.02 1.33	30000	-8 to 60
	1 M in BuAc	$15.9 \cdot 10^6$	$-6.69 \cdot 10^5$ $6.18 \cdot 10^7$	17.52	-2.19 2.90	23500	-10 to 70
C17A	bulk	$8.15 \cdot 10^6$	$-2.83 \cdot 10^6$ $1.03 \cdot 10^7$	14.66	-1.49 1.66	34800	-8 to 60
	1 M in BuAc	$6.24 \cdot 10^6$	$-2.55 \cdot 10^5$ $1.42 \cdot 10^6$	14.73	-2.12 2.29	26000	-12 to 70
C21A	bulk	$3.22 \cdot 10^6$	$-9.94 \cdot 10^5$ $2.89 \cdot 10^6$	12.99	-1.16 1.30	25500	-10 to 50
	1 M in BuAc	$8.16 \cdot 10^6$	$-3.18 \cdot 10^5$ $1.74 \cdot 10^7$	16.50	-1.98 2.24	23400	-9 to 70

Table 2.2 Arrhenius parameters for k_p of the herein investigated alkyl (meth)acrylates.
Arrhenius parameters with error margins of the 95% joint confidence intervals, values for the propagation rate coefficient at 50°C, k_p(50°C), and temperature intervals considered in the Arrhenius fit.

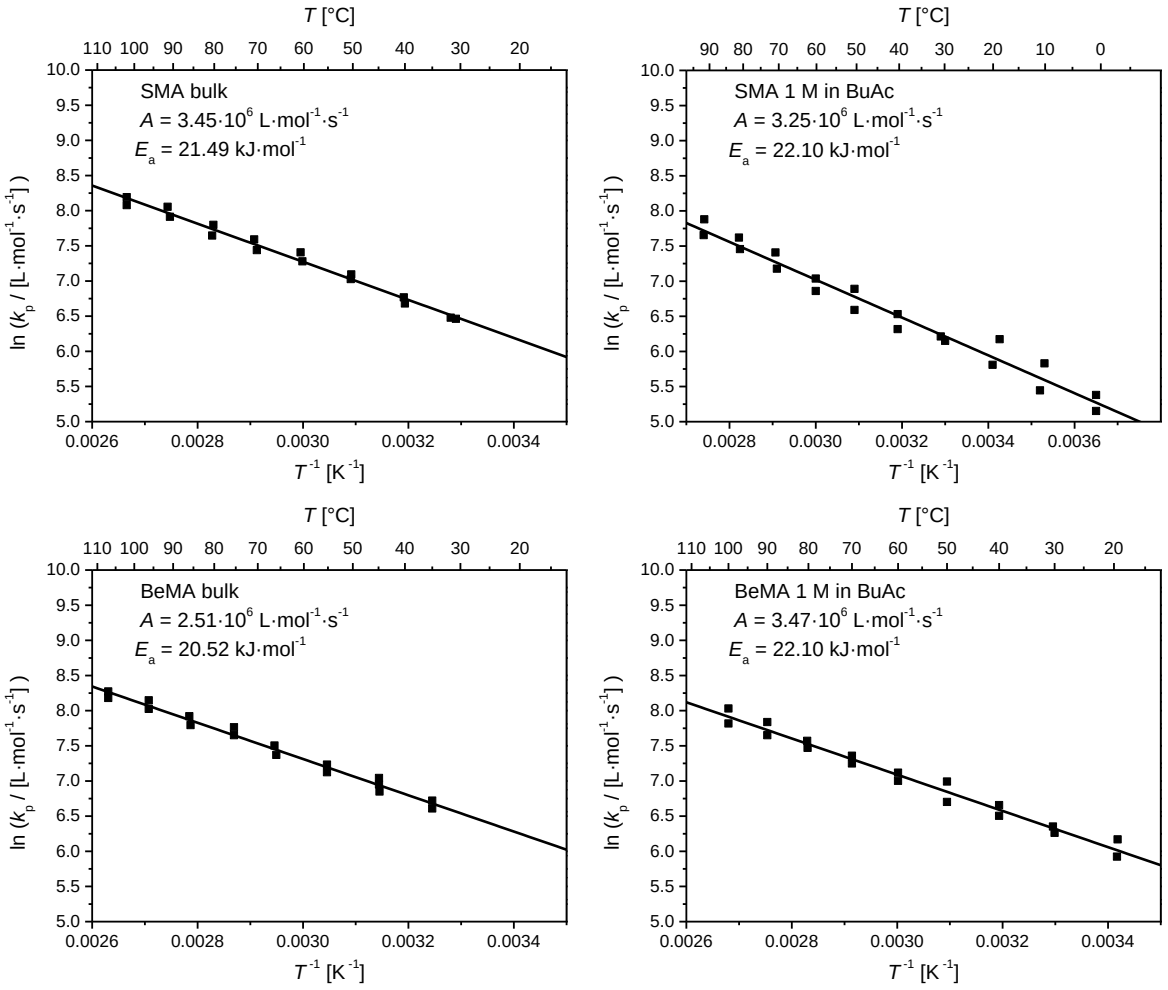

Figure 2.6 Arrhenius plots for SMA and BeMA.
$\ln(k_p / [L \cdot mol^{-1} \cdot s^{-1}])$ vs. T^{-1} plots with linear fits for the determination of the Arrhenius parameters in bulk and in 1 M solution in BuAc for SMA and BeMA. The associated monomer structures are shown in Scheme 2.1. The resulting Arrhenius parameters are collated in Table 2.2 jointly with the associated error margins. Adapted with permission from ref. 134 and 183. Copyright 2013 American Chemical Society.

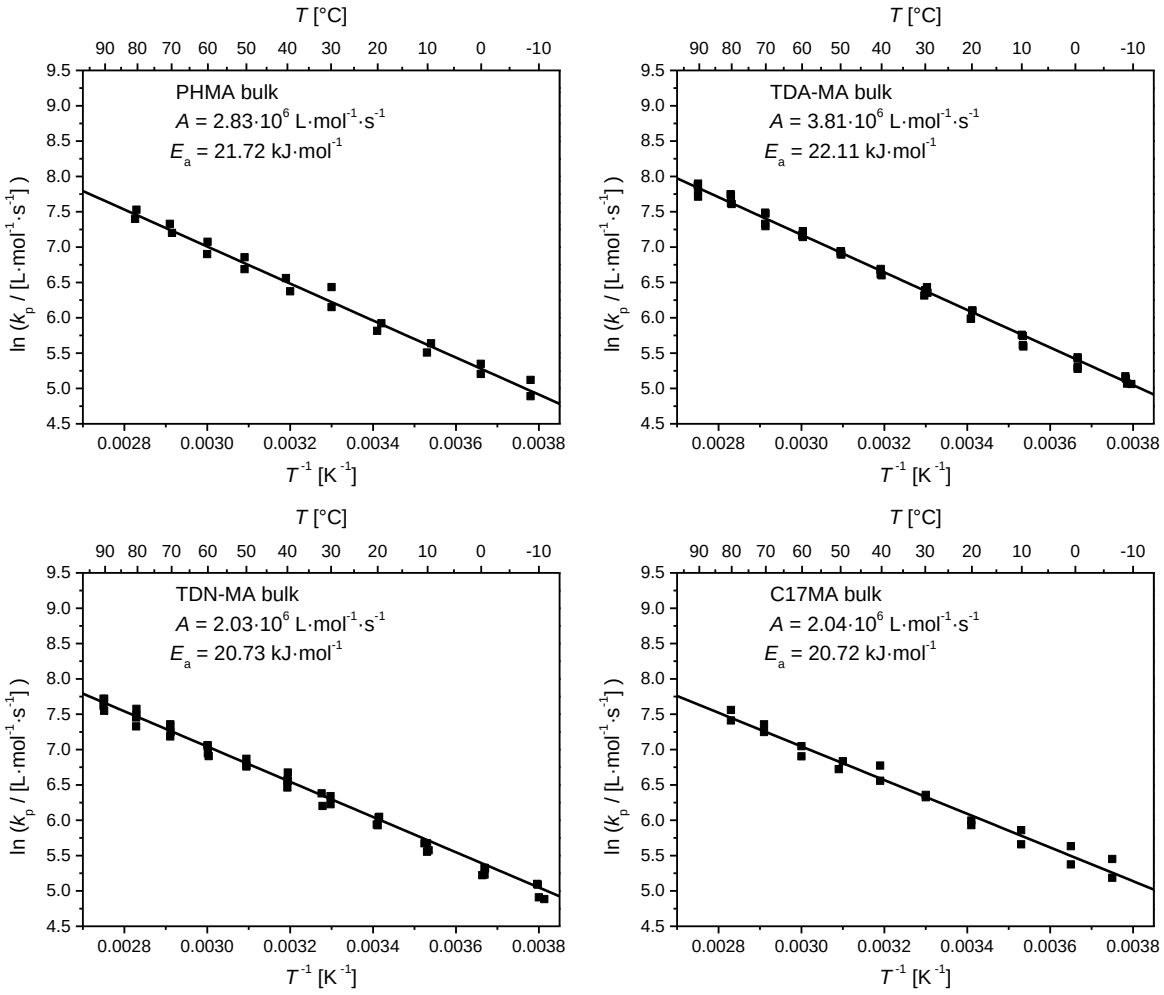

Figure 2.7 Arrhenius plots for PHMA, TDA-MA, TDN-MA, and C17MA.
$\ln(k_p / [\mathrm{L \cdot mol^{-1} \cdot s^{-1}}])$ vs. T^{-1} plots with linear fits for the determination of the Arrhenius parameters in bulk for PHMA, TDA-MA, TDN-MA, and C17MA. The associated monomer structures are shown in Scheme 2.1. The resulting Arrhenius parameters are collated in Table 2.2 jointly with the associated error margins. Adapted with permission from ref. 134 and 183. Copyright 2013 American Chemical Society.

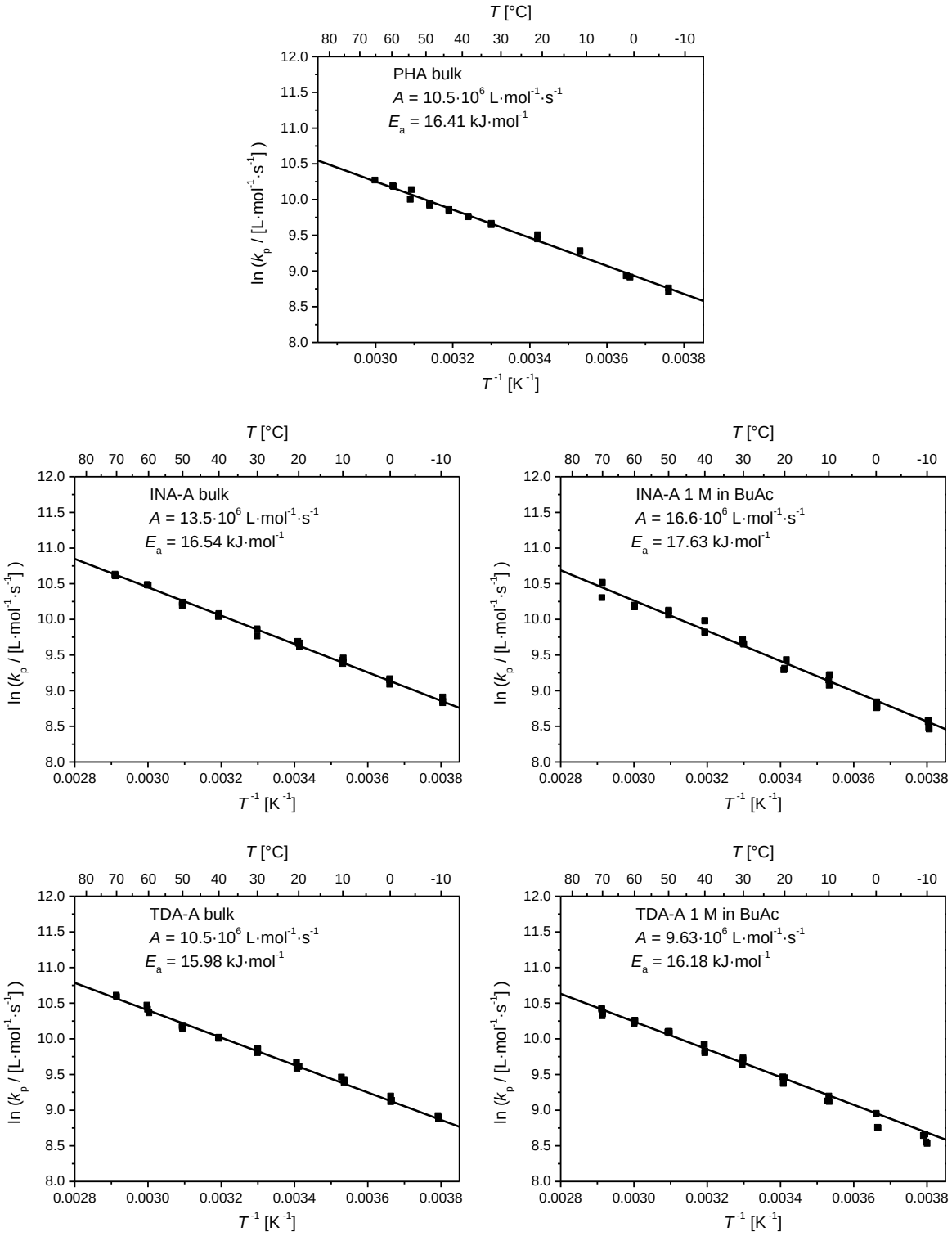

Figure 2.8 Arrhenius plots for PHA, INA-A, and TDA-A.
$\ln(k_p / [L \cdot mol^{-1} \cdot s^{-1}])$ vs. T^{-1} plots with linear fits for the determination of the Arrhenius parameters in bulk and in 1 M solution in BuAc for PHA, INA-A, and TDA-A (PHA was not investigated in 1 M solution in BuAc). The associated monomer structures are shown in Scheme 2.1. The resulting Arrhenius parameters are collated in Table 2.2 jointly with the associated error margins. Adapted with permission from ref. 134 and 183. Copyright 2013 American Chemical Society.

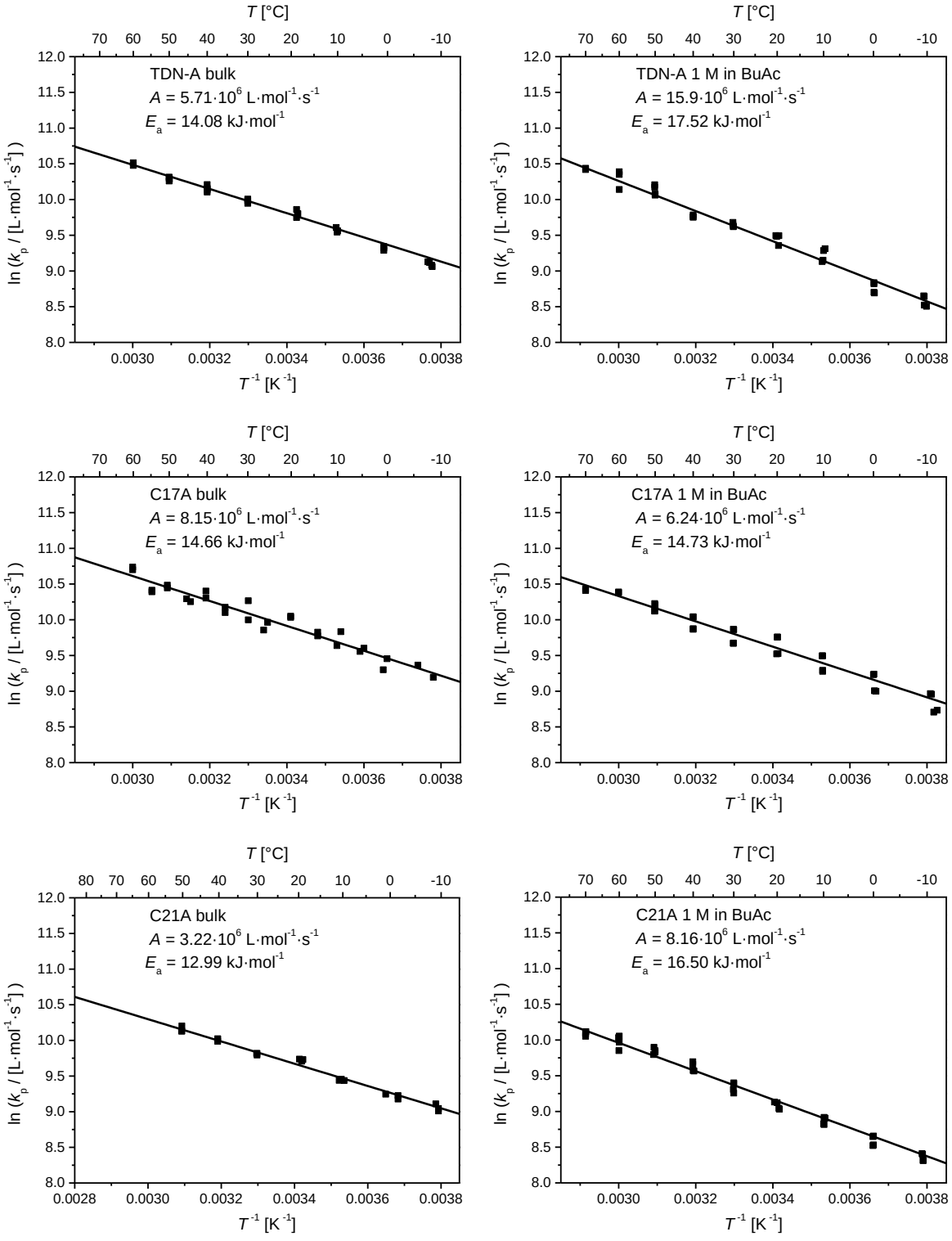

Figure 2.9 Arrhenius plots for TDN-A, C17A, and C21A.
$\ln(k_p / [L \cdot mol^{-1} \cdot s^{-1}])$ vs. T^{-1} plots with linear fits for the determination of the Arrhenius parameters in bulk and in 1 M solution in BuAc for TDN-A, C17A, and C21A. The associated monomer structures are shown in Scheme 2.1. The resulting Arrhenius parameters are collated in Table 2.2 jointly with the associated error margins. Adapted with permission from ref. 134 and 183. Copyright 2013 American Chemical Society.

Inspection of the obtained Arrhenius relationships demonstrates that the k_p values for all monomers and solvent conditions feature a strictly linear behavior over the entire investigated temperature range. In none of the 23 Arrhenius plots a deviation from linearity was observed in the studied temperature range under the applied PLP conditions (combination of pulse repetition frequency, pulse repetition number, and sample temperature).[190] If the temperature range for the acrylic monomers (such as e.g., SA, PHA, or C17A) is extended to higher temperatures (above 60°C), a deviation to lower $\ln(k_p/L\cdot mol^{-1}\cdot s^{-1})$ values is observed. However, such a deviation is simultaneously accompanied by a loss of the PLP structure in the SEC chromatogram, i.e., no clear second inflection point (corresponding to a second maximum in the derivative of the SEC chromatogram) is observed, yet rather shoulders on the high molecular weight side of the first maximum or merely just one maximum in the derivative of the SEC chromatogram. This acrylate typical behavior in the high temperature region – also reflected in a significant deviation of k_{p1}/k_{p2} from unity – is due to the increasing occurrence of transfer to polymer reactions (such as backbiting) and the consequently increasing influence of the propagation rate coefficient of the mid-chain radicals (MCR), k_p^{MCR}.[1, 11, 188, 191] For a detailed mechanistic description of the side reactions operational in acrylate FRP refer to Chapter 1.2. A possible method to compensate for the loss of the PLP-structure in the SEC chromatograms is the application of an even higher pulse repetition rate. Unfortunately, laser systems with pulse repetition rates exceeding 500 Hz are just becoming available at the wavelength of 351 nm.[192-193] Likewise, a possible chain length dependence (CLD) of the propagation reaction for macroradicals consisting of only a few monomer units is not reflected in the current data.[9] Such a CLD would result in higher $\ln(k_p/L\cdot mol^{-1}\cdot s^{-1})$ values especially in the low temperature region. However, since the pulse repetition rate was appropriately lowered when going to lower reaction temperatures to maintain a molecular weight of the first inflection point of at least 10000 $g\cdot mol^{-1}$ (corresponding to at least 30

repeating units), such a deviation from linearity to higher $\ln(k_p/L \cdot mol^{-1} \cdot s^{-1})$ values is not observed in the current study.

The scattering of the data points is small and within the typically observed range of the corresponding monomer family. For methacrylates a very narrow scattering range is observed, whereas acrylic monomers display a slightly more pronounced scattering.[117, 122, 181] The scattering correlates with the typical error margins of approx. 1 $kJ \cdot mol^{-1}$ for the methacrylates' activation energies and approx. 2 $kJ \cdot mol^{-1}$ for the activation energies of the acrylates. Due to the extrapolated nature of the linear Arrhenius fits, the uncertainty in the frequency factor is also higher for the acrylic monomers than for the methacrylic ones. The difference in the data scattering between the acrylic and methacrylic monomer families is also reflected in the corresponding error ranges, collated in Table 2.2, which are calculated via the program CONTOUR V2.0.2 by van Herk[151-152] jointly with the Arrhenius parameters. The average error per data point usually ranges between 3.5% (in the case of PHA) and 9%, which is lower than the initially assumed error range for the respective monomer type (except the data of SMA in 1 molar solution, which feature approx. 17% average error).

The temperature ranges considered for SA and BeA in bulk are – as already mentioned – relatively narrow (approx. 30 K) due to their high melting points (approx. 30°C for SA and 40°C for BeA, respectively). In order to validate and confirm the determined high k_p values of SA and BeA, they were additionally investigated in 1 M solution in BuAc. The BuAc solutions feature lower melting points (approx. 10 and 20°C, respectively) and thus allow for a wider temperature range for the determination of the Arrhenius parameters, resulting in a higher reliability. The elevated k_p values of SA and BeA are confirmed, since their 1 M solution data feature significantly higher k_p values (which are – as usual – slightly below the corresponding bulk values) than the short acrylates such as MA in bulk.

As stated in Chapter 1.3, k_p values featuring k_{p1}/k_{p2} ratios higher than 1.2 should principally not be incorporated into the determination of the associated Arrhenius parameters, since they

most probably are composite values of k_p^{sec} as well as lower k_p^{tert} values corresponding to SPRs and MCRs, respectively. However, for some monomer systems, such as e.g., SA, several PLP-SEC samples in the high temperature region (above 50°C), which are associated with k_{p1}/k_{p2} ratios higher than 1.2, are incorporated into the Arrhenius evaluation, as long as they clearly support the linear trend derived from the lower temperature region (cf. e.g., Table S1 in Appendix A). Such samples, featuring $k_{p1}/k_{p2} > 1.2$, would usually be neglected in line with the consistency criteria of the PLP-SEC method, yet the incorporation of these samples into the Arrhenius fits significantly enhances the reliability of the Arrhenius parameters by expanding the investigated temperature range. Furthermore, it should be noted that C21A is a very challenging monomer to investigate, especially in bulk. The high viscosity of C21A causes experimental difficulties during sample preparation (especially during nitrogen purging, transferring into sample vials, and filtering). In addition, a very small number of pulses has to be applied to the sample to prevent the formation of insoluble material. However, no support for the formation of a branched gel due to increased transfer to polymer (via H-abstraction within the ester side chain) was identified, since no relevant quaternary carbon atoms were observed by the combination of various ^{13}C-NMR experiments (following the method of Liang *et al.*[194] for an soluble polymer sample; the investigation of an insoluble polymer sample via solid state NMR techniques is still under investigation).

2.4 Trends and Family Type Behavior

In the subsequent section the above reported results will be discussed with respect to the literature known trends and family type behaviors, before tendering a hypothesis explaining the propagation rate coefficient behavior within the respective monomer families. Unfortunately, the comparison of the resulting Arrhenius parameters in conjunction with the literature known Arrhenius parameters of the monomers shown in Scheme 2.1 does not allow for an identification of systematic trends. The activation energies vary independently of the

length or steric demand of the ester side chain in a range of approx. 5 kJ·mol^{-1} for the linear and branched acrylates, approx. 2 kJ·mol^{-1} for the linear methacrylates and less than 2 kJ·mol^{-1} for the branched methacrylates (cf. Table 2.2). Since the frequency factor *A* is derived by extrapolation of the determined slope – which is proportional to the activation energy – the values of *A* exhibit basically the same scattering: monomers featuring a high activation energy feature a high frequency factor, too and vice versa. Hence, no systematic trends can be identified in the frequency factors as well. The frequency factors usually range in the order of 10^6 to 10^7 L·mol^{-1}·s^{-1}, whereby acrylates feature slightly elevated values than the methacrylates. For the linear alkyl methacrylates Beuermann *et al*. already conceded in 2000: "While no systematic variation of the activation energies and the pre-exponential factors may be observed within experimental uncertainty, it is definite that k_p values are enhanced with increasing size of the ester group."[126] Thus, in order to detect encompassing global trends and family type behavior, the propagation rate coefficients at different temperatures (-50°C, 0°C, 50°C, and 100°C) are plotted versus the miscellaneous monomers of the corresponding families. For the acrylic monomers the comparison at 100°C is omitted, since at such elevated temperatures no experimental data is available and a potential extrapolation is beset with a higher uncertainty than in the low temperature regime, due to the logarithmic nature of the extrapolation. Via such an analysis, the detection of trends is facilitated compared to plots containing the entire Arrhenius curves. Moreover, in such a representation it is graphically easier to arrange the monomers in a homologous series of, e.g., increasing ester side chain length. Via comparison of the monomer specific k_p values at several temperatures, it will be demonstrated that the increase of k_p with increasing length of the alkyl ester side chain even holds for the very long, linear alkyl ester side chain (meth)acrylates (i.e., SA and BeA as well as SMA and BeMA). Before proceeding with the same analysis of the branched alkyl acrylates, where a similar trend as for the linear alkyl (meth)acrylates is detected (albeit with some exceptions), the branched alkyl methacrylates

will be analyzed via the same procedure, revealing a family type behavior, in analogy to the previously reported family of some cyclic methacrylates.[125] In addition to the detailed description of the observed trends, they will be placed onto a physicochemical basis.

2.4.1 Global Trends for Linear Alkyl (Meth)Acrylates

For linear alkyl acrylates and methacrylates comparable trends of increasing propagation rate coefficients with increasing ester side chain lengths are reported.[117, 126] As Figure 2.10 demonstrates, these trends are also supported by the very long alkyl monomers carrying the linear stearyl and behenyl ester side chains.

In the homologous series from MA to EA, BA, HA, DA, SA, and BeA the value of k_p at 50°C increases by factors of 1.18, 1.25, 1.27, 1.42, 1.51, and 1.56, respectively, relative to $k_p^{50°C}$ of MA. Similarly, the k_p at 50°C increases constantly from MMA to EMA, BMA, DMA, SMA, and finally to BeMA by factors of 1.04, 1.17, 1.54, 1.75, and 1.81, respectively, relative to $k_p^{50°C}$ of MMA. Such an increase correlates with an increase of k_p by approx. 2% or 4-5% per additional CH_2 group in the ester side chain at 50°C for the linear acrylates or methacrylates, respectively. If the k_p values at 50°C are plotted as a function of the number of carbon atoms in the ester side chain, the increase can be accurately – within the associated typical error range of the monomer type – described by a linear fit as it is demonstrated in Figure 2.11. On average, the k_p value is increased by an additional CH_2 group in the ester side chain by approx. 30 $L \cdot mol^{-1} \cdot s^{-1}$ for methacrylates and by 550 $L \cdot mol^{-1} \cdot s^{-1}$ for acrylates.

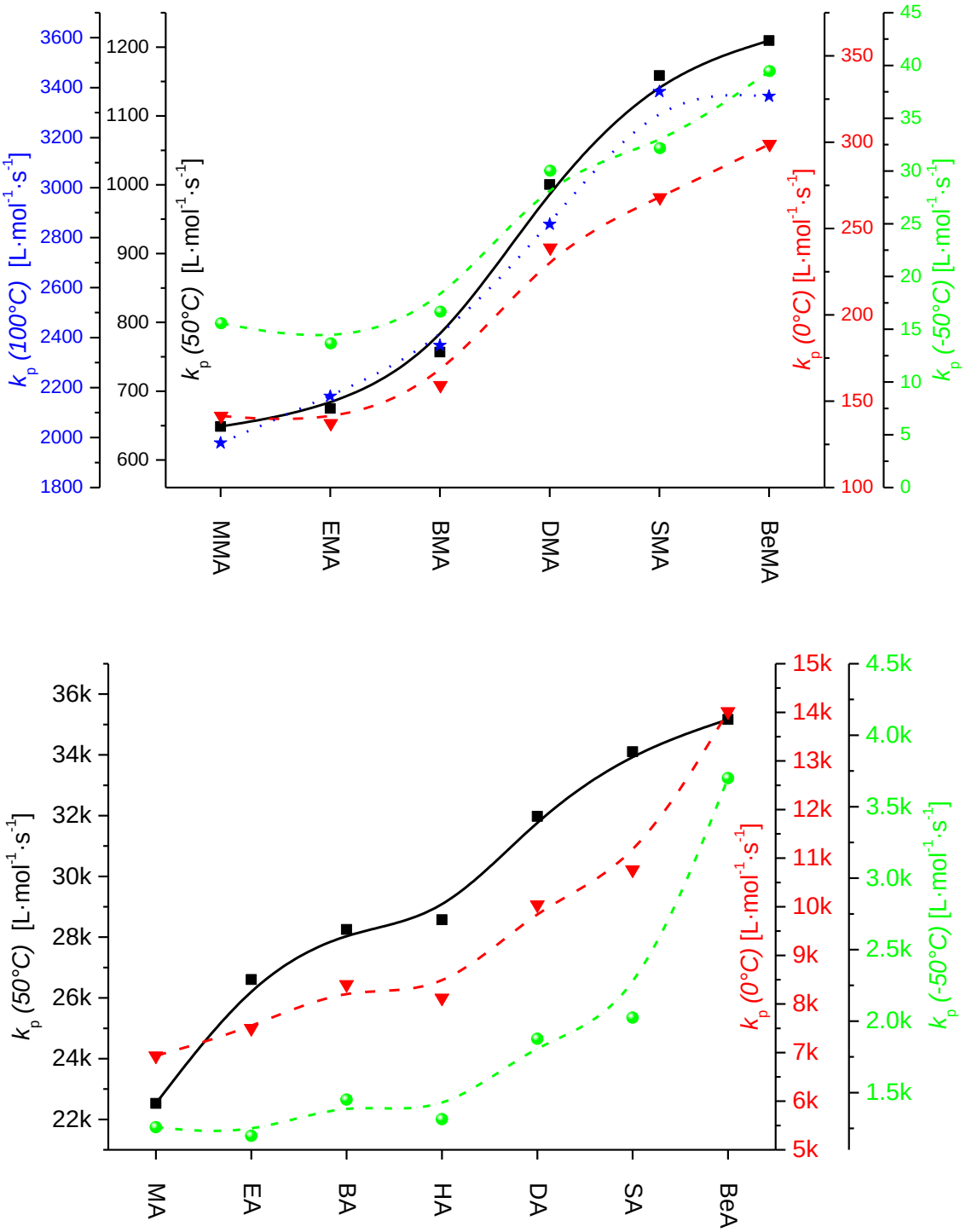

Figure 2.10 Dependence of the propagation rate coefficient, k_p, on the type of ester side chain for linear alkyl (meth)acrylates.
Propagation rate coefficients, k_p, at different temperatures (left outer scale = blue dotted line = k_p(100°C) (omitted for acrylates); left inner scale = black solid line = k_p(50°C); right inner scale = red dashed line = k_p(0°C); right outer scale = green dotdashed line = k_p(-50°C)) for acrylates and for methacrylates. Monomers are displayed in the order of increasing linear ester side chain length: **Methacrylates (upper part):** Methyl methacrylate (MMA),[126] ethyl methacrylate (EMA),[126] butyl methacrylate (BMA),[126] lauryl methacrylate (DMA),[126] stearyl methacrylate (SMA), behenyl methacrylate (BeMA); **Acrylates (lower part):** Methyl acrylate (MA),[180] ethyl acrylate (EA),[181] butyl acrylate (BA),[177] hexyl acrylate (HA),[181] lauryl acrylate (DA),[182] stearyl acrylate (SA), behenyl acrylate (BeA). Adapted with permission from ref. 134 and 183. Copyright 2013 American Chemical Society.

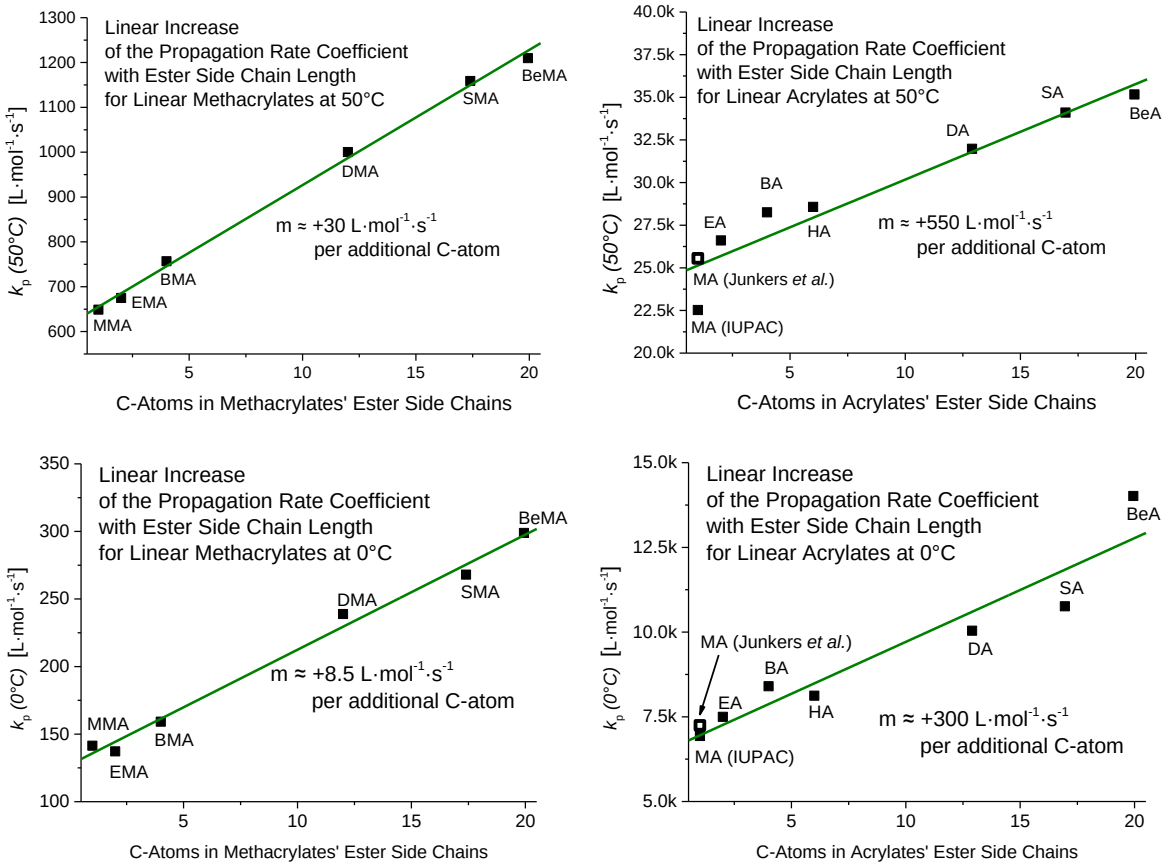

Figure 2.11 Linear correlation of the propagation rate coefficient, k_p, with the number of carbon atoms in the ester side chain for linear alkyl (meth)acrylates.
Linear fit of the propagation rate coefficient at 50°C and 0°C with increasing ester side chain length. Monomers are plotted according to their number of carbon atoms in the ester side chain. **Methacrylates (left hand side):** Average values for SMA (17.40) and BeMA (19.94).**Acrylates (right hand side):** Average values for DA (12.90), SA (16.95), and BeA (19.95). Additionally, the k_p values of MA deduced from the Arrhenius parameters reported by Junkers *et al.*[186] are depicted as hollow square (cf. discussion in the text). Adapted with permission from ref. 134 and 183. Copyright 2013 American Chemical Society.

The IUPAC subcommittee on *Modeling of Polymerization Kinetics and Processes* recently benchmarked the k_p values of MA.[180] The latest k_p data set, which was available before the IUPAC benchmarking activity, reported a k_p at 50°C for MA, which is 3000 L·mol^{-1}·s^{-1} higher than the currently employed one (depicted additionally in the lower part of Figure 2.10 as hollow square for clarification).[186] This is noteworthy, as the value lies somewhat above the green line of the linear fit depicted in the lower part of Figure 2.10, thus an incorporation of this data point instead of the IUPAC benchmark value would result in a much smoother linear fit with lower data scattering. Note that the data set represented by the hollow square is

in fact incorporated into the IUPAC benchmark data set for MA. It may well be possible that there exists a stronger increase in the propagation rate coefficient when going from a methyl to an ethyl ester group than for the higher homologues. The comparison of both MA values (IUPAC benchmark and hollow square) may further be indicative for the error margin related to the data points. Figure 2.11 additionally highlights the linear correlation of the propagation rate coefficient with the number of carbon atoms in the ester side chain at 0°C. In the case of the methacrylates, again a lower scattering of the k_p values around the linear fit is observed than for the acrylates resulting in an increase per additional CH_2 group in the ester side chain by approx. 8.5 $L \cdot mol^{-1} \cdot s^{-1}$. In the case of the acrylates at 0°C, the k_p values increase per additional CH_2 group in the ester side chain by approx. 300 $L \cdot mol^{-1} \cdot s^{-1}$. Both k_p values of MA, i.e., the one deduced from the IUPAC benchmarking report and the one reported by Junkers *et al.*, display a much lower scattering at 0°C than at 50°C. However, at 0°C especially the k_p values corresponding to long linear alkyl acrylates (i.e. DA, SA, and BeA) exhibit stronger deviations from the linear fit as they do at 50°C. The error associated with the slope of the corresponding linear fits is approx. 10% in all 4 cases displayed in Figure 2.11 (i.e. at 50°C as well as 0°C for acrylates as well as for methacrylates) and thereby similar to the error range associated with each individual data point incorporated into the linear fits. At the temperatures of -50°C and 100°C, similar increases are observed as highlighted above for the 50°C and the 0°C cases, as can be recognized by inspection of Figure 2.10. For -50°C only extrapolated values are available, since the lowest measured data points are typically in the range of -5°C to -10°C (except for the benchmarking report of MA). Consequently, the $k_p^{-50°C}$ data set is beset with an elevated uncertainty.

In summary, at both temperatures highlighted in Figure 2.11 (i.e., 50°C and 0°C) a clear linear correlation of the propagation rate coefficient with the number of carbon atoms in the ester side chain is detected. This realization is a central contribution of the current chapter to the overall knowledge of the propagation behavior of (meth)acrylates. Furthermore, the linear

correlation even allows for predictions of the k_p values for up to date not yet investigated linear alkyl (meth)acrylates (such as e.g. hexyl methacrylate or octyl acrylate).

2.4.2 Family Type Behavior of Branched Alkyl Methacrylates

After the analysis of linear (meth)acrylates, the following section addresses the branched methacrylates via an in-depth discussion of their family type behavior. Figure 2.12 (upper part) depicts the propagation rate coefficients for the branched methacrylates in the same analysis as provided above for the linear (meth)acrylates. The relatively small methacrylates *i*BMA and *t*BMA feature distinctly lower k_p values over the entire temperature range than all other reported branched methacrylates as the inspection of the upper part in Figure 2.12 clarifies. In 2003, Beuermann and co-workers proposed to describe all available k_p values of methacrylates with a cyclic ester group (i.e., *iso*-bornyl, *cyclo*-hexyl, benzyl, and glycidyl methacrylate; the latter one is also often denoted as oxiranylmethyl methacrylate, OMA) by one single best Arrhenius fit.[125, 129] The joint Arrhenius parameters of this monomer family read $A = 4.24 \cdot 10^6$ L·mol^{-1}·s^{-1} and $E_a = 20.96$ kJ·mol^{-1}, which were employed to calculate the k_p values depicted in Figure 2.12. In addition, the other 6 branched and sterically demanding methacrylates (i.e., the previously reported iDeMA and EHMA as well as the in the cause of the current thesis investigated PHMA, TDA-MA, TDN-MA, and C17MA) display only a negligible variation of k_p over the entire temperature range from -50°C to 100°C. Solely TDA-MA exhibits a minor deviation to higher values (at elevated temperatures above 50°C), which is however still within the error range. Therefore, it seems reasonable to describe them – in analogy to the best fit for the cyclic methacrylates by Beuermann *et al.*[125] – by a joint Arrhenius fit. Especially the lower part in Figure 2.12, displaying the joint plot of all published data points of these 6 monomers, evidences that deviations among the k_p values of the miscellaneous branched alkyl methacrylates are well within the experimental error range and that all the data points of the branched alkyl methacrylates can be adequately described by

a joint Arrhenius fit. The corresponding Arrhenius parameters are collated in Table 2.2. Since the number of published data points varies for each monomer, the individual monomers do not contribute equally to the joint fit. However, since they seem to feature a family behavior and all k_p values are in a narrow range for each temperature, the weighting of the individual monomers should be not decisive for the outcome of the joint fit. As assumed above for the individual methacrylates, an error of 10% in the k_p value is assumed for each data point for the joint fit.

➔

Figure 2.12 Dependence of the propagation rate coefficient, k_p, on the type of ester side chain for branched alkyl methacrylates.
Upper part: Dependence of the propagation rate coefficient, k_p, on the type of ester side chain for branched alkyl methacrylates at different temperatures (left outer scale = blue dotted line = k_p(100°C); left inner scale = black solid line = k_p(50°C); right inner scale = red dashed line = k_p(0°C); right outer scale = green dotdashed line = k_p(-50°C)). Monomers are displayed in the order of approximated increasing steric demand of their ester side chain: *iso*-Butyl methacrylate (*i*BMA),[178] *tert*-butyl methacrylate (*t*BMA),[184] joint fit cyclic methacrylates: i.e., for *iso*-bornyl methacrylate (*i*BoMA), *cyclo*-hexyl methacrylate (*c*HMA), benzyl methacrylate (BnMA), and glycidyl methacrylate (GMA),[125] *iso*-decyl methacrylate (*i*DeMA),[178] ethylhexyl methacrylate (EHMA),[178] propylheptyl methacrylate (PHMA),[134] tridecyl methacrylate (TDN-MA and TDA-MA), and heptadecyl methacrylate (C17MA). **Lower part:** Combined Arrhenius plot for the family of branched alkyl methacrylates with joint linear Arrhenius fit of the propagation rate coefficient. Adapted with permission from ref. 134 and 183. Copyright 2013 American Chemical Society.

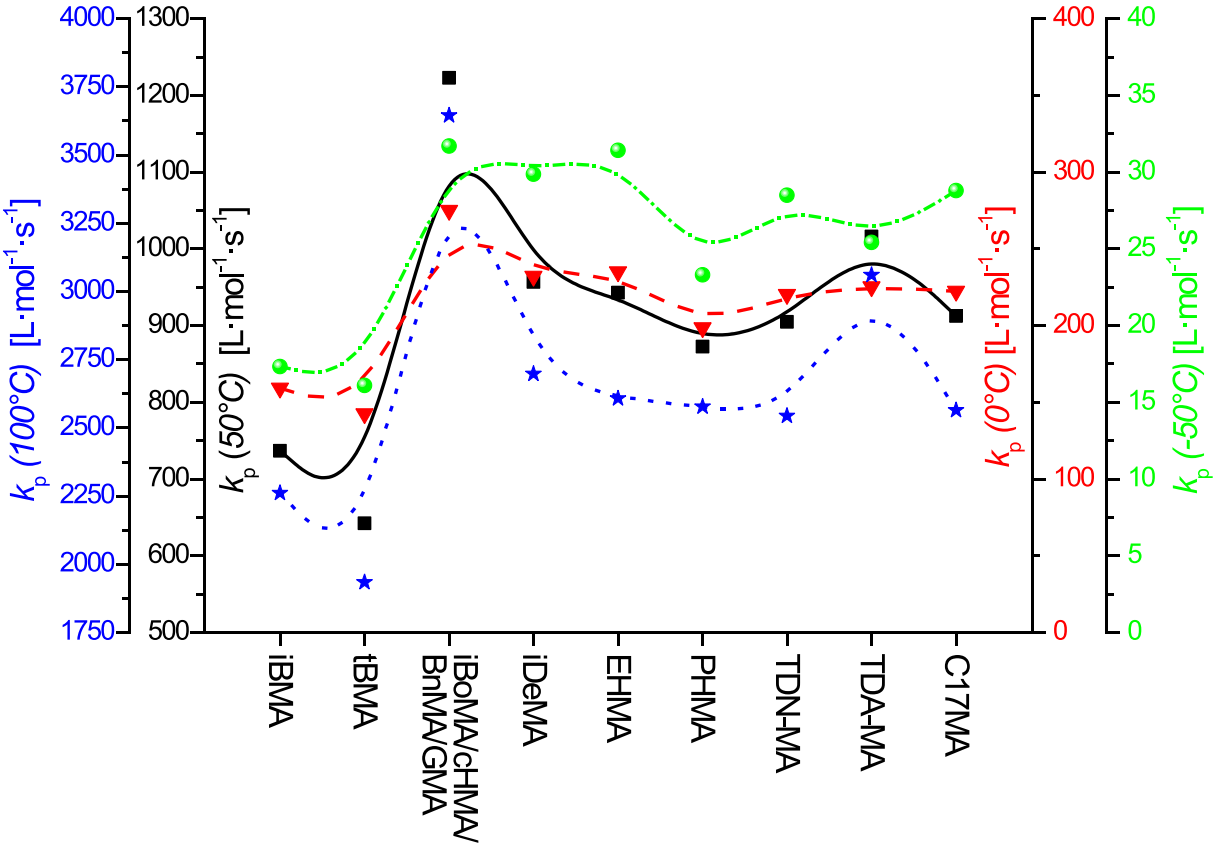
k_p (100°C) [L·mol^{-1}·s^{-1}]
k_p (50°C) [L·mol^{-1}·s^{-1}]
k_p (0°C) [L·mol^{-1}·s^{-1}]
k_p (-50°C) [L·mol^{-1}·s^{-1}]
iBMA
tBMA
iBoMA/cHMA/ BnMA/GMA
iDeMA
EHMA
PHMA
TDN-MA
TDA-MA
C17MA

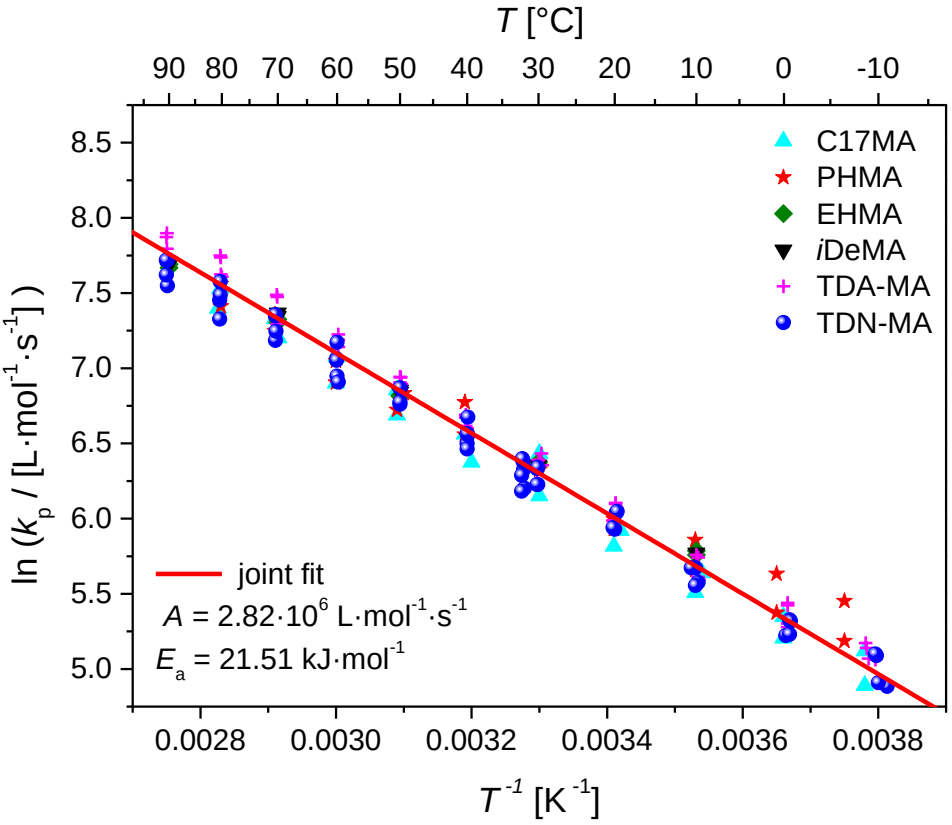
T [°C]
ln (k_p / [L·mol^{-1}·s^{-1}])
T^{-1} [K^{-1}]
C17MA
PHMA
EHMA
iDeMA
TDA-MA
TDN-MA
joint fit
A = 2.82·10^6 L·mol^{-1}·s^{-1}
E_a = 21.51 kJ·mol^{-1}

For the 6 branched methacrylates no increase / no strong variation of k_p is observable with an theoretical exchange of the ester side chain. Nevertheless, a difference in the absolute k_p values to the previously described family type behavior of GMA, *c*HMA, *i*BoMA, and BnMA is noticeable.[129] This previously in the literature described set of monomers (GMA, *c*HMA, *i*BoMA, and BnMA) features slightly elevated k_p values for all temperatures compared to the set of EHMA, PHMA, TDA-MA, TDN-MA, C17MA, and *i*DeMA (e.g., $k_p^{50°C}$: ~1250 $L \cdot mol^{-1} \cdot s^{-1}$ vs. ~950 $L \cdot mol^{-1} \cdot s^{-1}$). However, it should be noted that Beuermann *et al.* introduced GMA, BnMA, *c*HMA exhibiting a family type behavior in an initial publication. In a second contribution Beuermann and co-workers incorporated *iso*-bornyl methacrylate (*i*BoMA) into the family of the cyclic methacrylates, although it does not completely fit to the other 3 monomers. *i*BoMA features in the low temperature region (0°C and -50°C) k_p values similar to the herein introduced set of branched methacrylates, whereas the k_p values in the high temperature region (100°C and 50°C) fit to the set of cyclic methacrylates introduced by Beuermann and co-workers. *i*BMA and *t*BMA feature – as mentioned above – significantly lower k_p values over the entire temperature range and fit neither to one of the two groups. It is very noteworthy that the position of the branching point (e.g., in α-position to the ester functionality for *i*BoMA and *c*HMA or in β-position for EHMA and PHMA or even in positions far away from the ester functionality as for *i*DeMA) is not decisive for the absolute values of the propagation rate coefficients.

As noted above, the propagation rate coefficients of *i*BMA and *t*BMA exhibit a very similar behavior over the entire temperature range, too. However, it is proposed to describe them not yet as a family in its own, since it would be premature to introduce a family type behavior encompassing a data set consisting of solely two species.

2.4.3 Global Trend for Branched Alkyl Acrylates?

Finally, the analogous analysis of the derived propagation rate coefficient data for the branched alkyl acrylates is carried out. The acrylate specific problems, such as an influence on the PLP-SEC experiment by, e.g., transfer to polymer reactions (backbiting, cf. Chapter 1.2), need for high pulse repetition rates, the effect of the microstructure on the SEC analysis, and the thereof resulting increased error range compared to the methacrylates have already been addressed in the previous chapters of the current thesis, yet they are re-mentioned here to be aware of them.

In Figure 2.13 (upper part), the k_p values of the miscellaneous branched alkyl acrylates are plotted for three temperatures (i.e., -50°C, 0°C, and 50°C). The monomers are sorted in the most likely order of increasing steric demand of their ester side chain, where PHA and TDA-A are assigned a higher steric demand than EHA and TDN-A, respectively, since their ester side chains contain more carbon atoms (propylheptyl vs. ethylhexyl) or their ester side chains feature a higher degree of branching characterized by their isoindex. The corresponding TDA alcohol (isoindex: 3.1) is obtained via tetramerization of propene with subsequent hydroformylation and reduction, whereas the corresponding TDN alcohol (isoindex: 2.1) is obtained via trimerization of butene with subsequent hydroformylation and reduction.

tert-Butyl acrylate (*t*BA) features almost the same k_p values at the displayed temperatures as *n*-butyl acrylate (BA; e.g. $k_p^{50°C} \sim 28500\ L \cdot mol^{-1} \cdot s^{-1}$ and $k_p^{0°C} \sim 8500\ L \cdot mol^{-1} \cdot s^{-1}$). Benzyl acrylate (BnA) exhibits clearly elevated k_p values when compared to other acrylates with a similar number of carbon atoms in the ester side chain. Willemse *et al*. noted that the elevated k_p values are caused by "enthalpic effects […] related to the electronic interaction of the phenyl ring with the unpaired electron."[181]

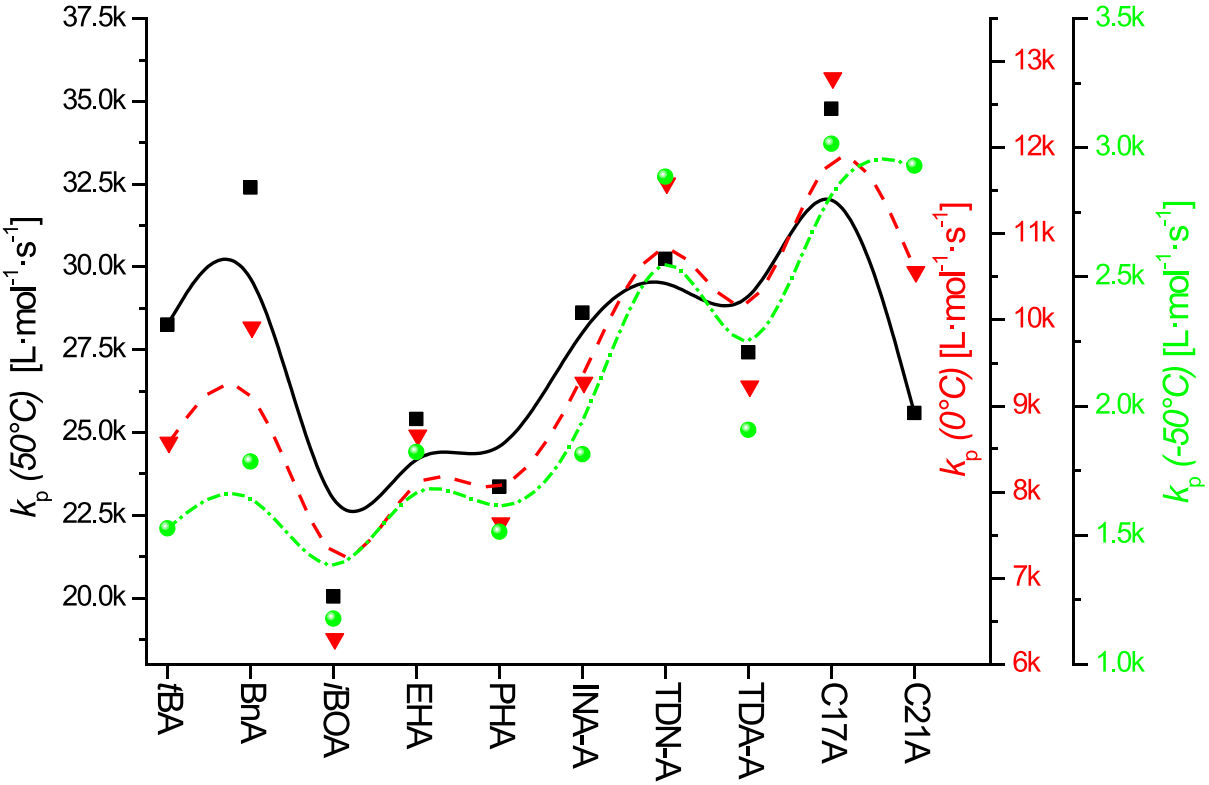
37.5k
35.0k
32.5k
30.0k
27.5k
25.0k
22.5k
20.0k
k_p (50°C) [L·mol^{-1}·s^{-1}]
13k
12k
11k
10k
9k
8k
7k
6k
k_p (0°C) [L·mol^{-1}·s^{-1}]
3.5k
3.0k
2.5k
2.0k
1.5k
1.0k
k_p (-50°C) [L·mol^{-1}·s^{-1}]
tBA
BnA
iBOA
EHA
PHA
INA-A
TDN-A
TDA-A
C17A
C21A

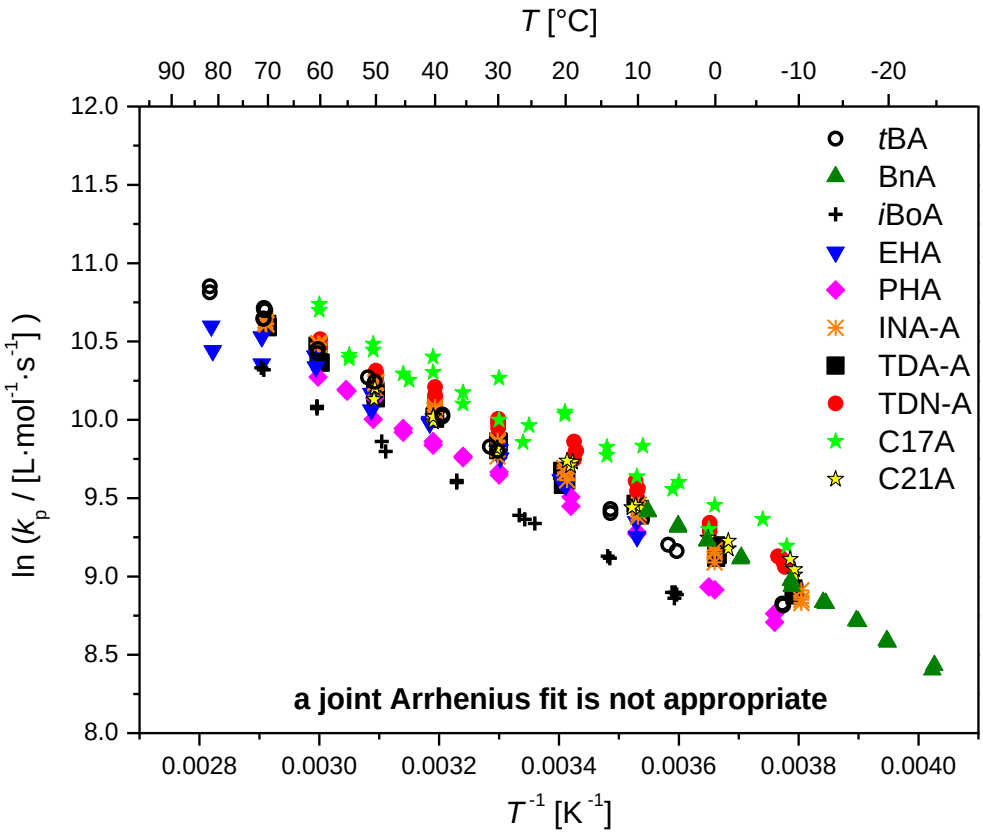
T [°C]
90 80 70 60 50 40 30 20 10 0 -10 -20
12.0
11.5
11.0
10.5
10.0
9.5
9.0
8.5
8.0
ln (k_p / [L·mol^{-1}·s^{-1}])
tBA
BnA
iBoA
EHA
PHA
INA-A
TDA-A
TDN-A
C17A
C21A
a joint Arrhenius fit is not appropriate
0.0028
0.0030
0.0032
0.0034
0.0036
0.0038
0.0040
T^{-1} [K^{-1}]

Figure 2.13 Dependence of the propagation rate coefficient, k_p, on the type of ester side chain for branched alkyl acrylates.
Upper part: Dependence of the propagation rate coefficient, k_p, on the type of ester side chain for branched alkyl acrylates at different temperatures (left scale = black solid line = k_p(50°C); right inner scale = red dashed line = k_p(0°C); right outer scale = green dotdashed line = k_p(-50°C)). Monomers are displayed in the order of approximated increasing steric demand of their ester side chain: *tert*-Butyl acrylate (*t*BA),[124] benzyl acrylate (BnA),[181] *iso*-bornyl acrylate (*i*BoA),[124] ethylhexyl acrylate (EHA),[186] propylheptyl acrylate (PHA),[134] *iso*-nonyl acrylate (INA-A), tridecyl acrylates (TDN-A and TDA-A), heptadecyl acrylate (C17A), and henicosyl acrylate (C21A). **Lower part:** Combined Arrhenius plot for the branched alkyl acrylates. A joint linear Arrhenius fit of the propagation rate coefficient is clearly not appropriate, in contrast to the branched alkyl methacrylates (cf. Figure 2.12). Reprinted with permission from ref. 183. Copyright 2013 American Chemical Society.

Inspection of the upper part of Figure 2.13 indicates that the branched alkyl acrylates do not feature a similar family type behavior of k_p as described above for the branched alkyl methacrylates. For clarification of the discrepancies between branched alkyl acrylates and methacrylates, the lower part of Figure 2.13 is presented, which collates all available k_p data for branched alkyl acrylates (for a straightforward comparison the scale entails 4 logarithmic units just as the lower part of Figure 2.12). A joint Arrhenius fit is not appropriate as the differences are clearly larger than the related experimental errors (e.g., at 0°C PHA ~7250 $L \cdot mol^{-1} \cdot s^{-1}$ vs. C17A 11750 $L \cdot mol^{-1} \cdot s^{-1}$). Furthermore, inspection of Figure 2.13 demonstrates that for the branched alkyl acrylates the same strict trend of increasing k_p with increasing ester side chain length (or number of carbon atoms in the ester side chain) does not apply as described above for the linear alkyl (meth)acrylates. Instead, the branching of the ester side chain appears to play an important role. For example, *i*BoA and PHA with 10 carbon atoms in the ester side chain feature significantly lower k_p values over the entire depicted temperature range than EHA with 8 or INA-A with 9 carbon atoms (note that *i*BoA was studied in 50 vol% toluene solution).[124] Moreover, TDA-A, also featuring 13 carbon atoms as TDN-A, yet with a higher isoindex (3.1 instead of 2.1), displays again lower k_p values compared to TDN-A over the entire investigated temperature range. Nevertheless, a tendency to a slight increase in k_p with increasing steric demand of the ester side chain and increasing alkyl moiety is noticeable. A closer inspection of the upper part in Figure 2.13 reveals an increase

of k_p within the homologous butene-type series of monomers, which feature an ester side chain derived from the oligomerization of *n*-butene, i.e., from INA-A via TDN-A to C17A. However, the largest monomer in the butene-type series, i.e., C21A (derived from pentamerization of *n*-butene with subsequent hydroformylation and reduction), clearly departs from the trend of increasing k_p with growing ester side chain, featuring lower k_p values. Especially in the high temperature region close to 50°C, C21A exhibits k_p values even lower than INA-A (cf. lower part of Figure 2.13), which is due to a significantly lower activation energy (cf. Table 2.2). Nevertheless, a clear increase from EHA and PHA, which have very similar k_p values within the error margins, to TDN-A or C17A is observable.

Perhaps in the future the detection of a clearer trend or concept of influence on k_p by the ester side chain will be possible if more branched acrylate type monomers are investigated with the PLP-SEC method. Maybe also an increased accuracy of the determination of k_p for acrylic monomers, especially via higher pulse repetition rates, may enable the detection of global trends among the branched alkyl acrylates. However, based on the already available data, it is clearly noticeable that for the branched acrylates not the same family type behaviors are observable as in the case of the branched methacrylates (especially differences between EHA/PHA vs. C17A or TDA-A vs. TDN-A).

In order to provide an encompassing and more detailed analysis of the propagation behavior of the branched alkyl acrylates, the homologous butene-type series was additionally investigated in 1 molar solution in BuAc. BuAc is very often used for such studies, since it mimics butyl acrylate without the ability to polymerize and features similar polarity and viscosity than many alkyl acrylates. Figure 2.14 presents the synopsis of the 1 M solution and the bulk data obtained for the branched alkyl acrylates in the previously employed analysis of k_p at three different temperatures. The respective y-scales are the same in both plots, which facilitates a straightforward comparison.

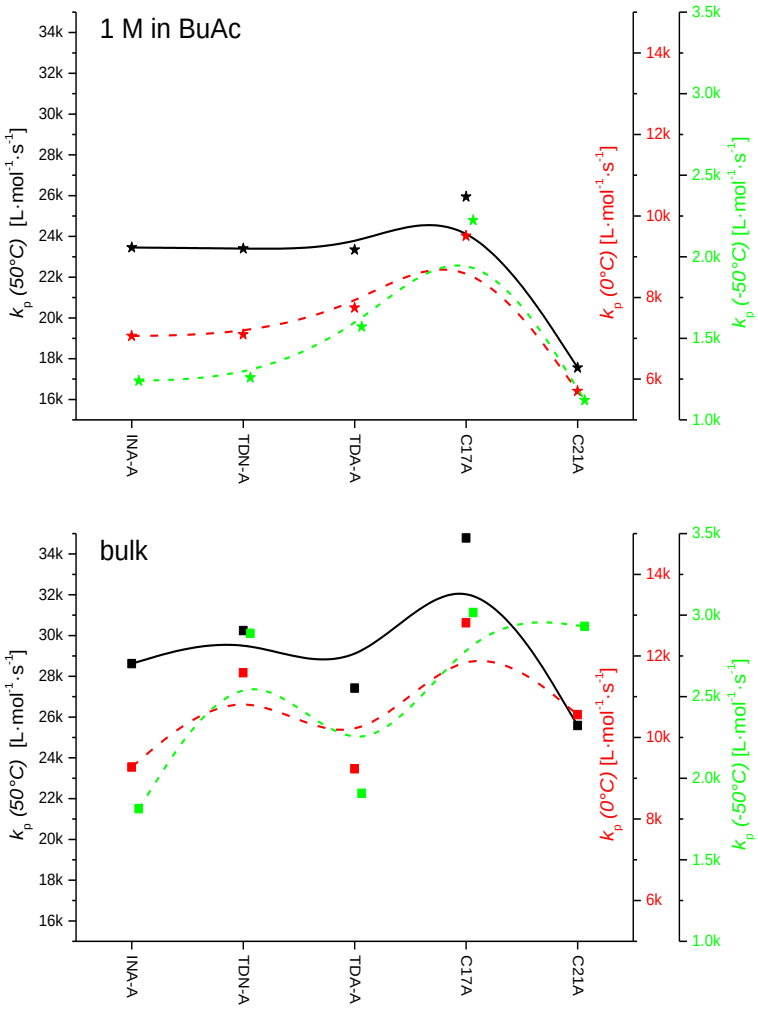

Figure 2.14 Variation of the propagation rate coefficient, k_p, in the homologous butene-type series of branched alkyl acrylates in 1 M solution in BuAc.
Dependence of the propagation rate coefficient, k_p, on the type of ester side chain for branched alkyl acrylates of the homologous butene-type series at different temperatures (left scale = black solid line = k_p(50°C); right inner scale = red dashed line = k_p(0°C); right outer scale = green dotdashed line = k_p(-50°C)) in 1 molar solution in BuAc. Monomers are displayed in the order of increasing steric demand of their ester side chain: *iso*-Nonyl A acrylate (INA-A), tridecyl N acrylate (TDN-A), tridecyl A acrylate (TDA-A), heptadecyl methacrylate (C17A), and henicosyl acrylate (C21A). **Upper part:** 1 M solution in BuAc (stars). **Lower part:** Bulk (squares, depicted again to enable direct comparison). The scales corresponding to the various temperatures are the same as in the upper part. Adapted with permission from ref. 183. Copyright 2013 American Chemical Society.

Figure 2.14 clearly demonstrates that the k_p value slightly decreases when the concentration is altered from bulk to 1 M solution in BuAc. A similar decrease is observed for the linear alkyl (meth)acrylates (cf. k_p values at 50°C in Table 2.2). A more detailed study into the solvent dependence of linear acrylates (bulk vs. BuAc vs. toluene solution), also addressing some effects proposed in a review by Buback,[123] is currently underway. The comparison of the upper and lower part in Figure 2.14 demonstrates that the branched alkyl acrylates in BuAc

solution do not exhibit a similar dependence of k_p on the ester side chain as in bulk. Especially, the k_p decrease from TDN-A to TDA-A in bulk is changed into a slight increase in solution. C21A features again distinctly lower k_p values over the entire temperature range than the other branched acrylates, just as in bulk. Remarkably, there are almost no differences between INA-A, TDN-A, and TDA-A in 1 M solution in BuAc; solely in comparison to C17A and C21A a distinct difference is detectable, which is clearly outside the experimental error range. The solution data do not exhibit a steady increase in the butene-type series (i.e., INA-A, TDN-A, C17A, C21A), which might suggest an analogous trend as for the linear alkyl (meth)acrylates. Unfortunately, the study of the branched alkyl acrylates in 1 M solution in BuAc does not allow for a detection of a clear trend or a family type behavior.

2.4.4 Feasible Physicochemical Causes

A detailed analysis of experimental data to arrive at fundamental principles and overarching trends allowing for predictions is the basis of science. In other words, precise observations have to be turned into a theoretical framework whenever possible.

The following chapter attempts to provide a rationale for the above indentified trends on the basis of additional monomer and polymer specific physicochemical properties in combination with reaction kinetic considerations.

A summary of the above identified trends reads as follows:

(i) for linear alkyl acrylates and methacrylates:

$\boldsymbol{k_p}$ **increases** steadily **with** increasing ester side chain length (**number of carbon atoms**)

(ii) for branched alkyl methacrylates and cyclic methacrylates:

$\boldsymbol{k_p}$ is **not** decisively **influenced by the specific structure** of the ester side chain within the described families

(iii) for branched alkyl acrylates:

no clear trend can be identified – clearly **no family type behavior** – a tendency to increasing k_p values with growing ester side chains might be argued.

The difference in the reactivity of the monomers is most probably not based on electronic differences within the double bond or the corresponding radicals, since the varying alkyl groups are electronically separated from the reactive region (radical or double bond) by the ester moiety and the differences in the +I-effect (positive inductive effect) between, e.g., a butyl, behenyl, tridecyl, or henicosyl moiety is likely negligible.

2.4.4.1 Increasing k_p for Linear Alkyl (Meth)Acrylates

However, a possible explanation for the increase of k_p with the increasing ester side chain length might be the following one: The polar ester moiety stabilizes the attacking (propagating) radical which is in the transition state (TS) particularly delocalized. An increasing alkyl content, due to an increasing ester side chain length, leads to a reduction of this stabilization, since the concentration of the ester moieties is lowered (close to 10 $mol \cdot L^{-1}$ in the case of MA vs. less than 3 $mol \cdot L^{-1}$ for BeA). Consequently, the radicals tend to react with the double bond in another monomer unit more readily, since a repulsive potential energy surface facilitates leaving the TS in the direction of the product radical. Accordingly, the k_p increase of the linear alkyl acrylates and methacrylates may be understood. The branched alkyl acrylates exhibit approximately a similar increase; however, there are some exceptions from a steady increase. The family type behavior of the branched methacrylates cannot be explained by the above stated rationale.

An alternative explanation for such an increase in k_p (as described as point (*i*) in the list above) may be a pre-structuring of the reaction solution, since the long linear alkyl side chains are strongly non-polar and tend to align with each other in such a way that the methacrylic ester groups are in close proximity. Such a stacking may result in propagation of closely

associated monomer units, altering the local monomer concentration and leading to an apparently higher k_p value: The longer the ester side chain, the more pronounced the pre-structuring and the faster the radical propagation. The potential pre-structuring of the monomer species is supported by the observation that for the long linear ester side chain polymers (i.e., pSMA, pBeMA, pSA, and pBeA) melting points are detectable (cf. Table 2.3), which are very close to the melting points of the related monomer species, whereas no glass transition temperatures are detectable in the range between -150°C and 125°C (except for pBeA). The corresponding DSC curves of the polymers are depicted in the Appendix A in Figure S25 and Figure S26.

Monomer system	T_m of monomer [a] °C	T_m of polymer °C	T_g of polymer °C
SA	25	37	– [b]
BeA	>30	51	-92
SMA	19	30	– [b]
BeMA	28-33	45	– [b]

Table 2.3 Comparison of monomer and polymer melting points for the long linear alkyl (meth)acrylates.
Additionally, the glass transition temperature of pBeA is stated for completeness.
[a] according to product information provided by BASF;
[b] no glass transition temperature detectable between -150°C and 125°C.

The detection of melting points instead of glass transition temperatures suggests that the long linear alkyl ester side chains dominate the crystallization behavior of the polymer species and the influence of the polymer backbone on the crystallization is negligible. Smaller ester side chain monomers come increasingly under the influence of the methacrylate type backbone. A similar process may thus be operational in structuring the monomers in solution. The above described observations suggest that the very long linear alkyl ester side chains tend to crystallize more efficiently than the polymer backbones, hence the side chains are overcompensating the influence of the polymer backbone observed with smaller ester side chain monomers. Consequently, the ester side chains are the structuring motive in the solid state as well as in solution and not the polymer backbones. Thus, the effective monomer

concentration in close proximity of the radical sites, c_M^{local}, may be higher than the overall monomer concentration of the sample, $c_M^{overall}$. The hitherto open question regarding the existence of significant differences between c_M^{local} and $c_M^{overall}$ arises from the fact that in Equation 1.1 the c_M^{local} is required as an input parameter (yet merely $c_M^{overall}$ is available). Thus, Equation 1.1 may suffer from the fact that only the product of $k_p \cdot c_M^{local}$ can be determined (cf. Chapter 1.3).

An alternative explanation for the increase of the k_p values in the homologous series from methyl to behenyl (meth)acrylate may be based on intermolecular interactions between the TS structures and the monomer environment. As noted in ref. 159, for a polar monomer especially the rotational motion barrier in the TS should decrease if the environment of the TS is becoming more polar, as it is the case for methacrylic acid (MAA) in aqueous solution. In the currently investigated homologous series of linear alkyl (meth)acrylates, however, the polarity is constantly decreasing when going from M(M)A to Be(M)A due to the increasing alkyl ester side chain length. Since all monomers were studied in bulk, the TS is constantly subjected to a more non-polar environment. However, ref. 159 notes that the increase of k_p with the amount of water for MAA is solely associated with an increase in the frequency factor *A*. As inspection of Table 2.4 demonstrates, such a constant and strong increase of *A* is not observed in the current homologous series.

Especially the pronounced decreases of the frequency factor *A* from BMA to DMA and from SMA to BeMA (each by approximately one third) do not support the theory of reduced rotational barriers in the TS of the propagation step (cf. Table 2.4). The acrylic monomers exhibit a similar decrease in *A* from EA to BA and from HA to DA/SA to BeA (i.e., with increasing ester side chain length). A theoretical ab-initio calculation study reported that the hydrogen-bonding type interactions, which are dominating the TS in the gas phase for methyl acrylate (MA) and vinyl acetate (VAc), are effectively disrupted by solvent effects if bulk

Monomer	A	E_a	$k_p^{50°C}$
	$L \cdot mol^{-1} \cdot s^{-1}$	$kJ \cdot mol^{-1}$	$L \cdot mol^{-1} \cdot s^{-1}$
MA[180]	$14.10 \cdot 10^6$	17.3	22500
EA[181]	$26.90 \cdot 10^6$	18.6	26500
BA[177]	$21.30 \cdot 10^6$	17.8	28000
HA[181]	$27.50 \cdot 10^6$	18.5	28500
DA[182]	$17.90 \cdot 10^6$	17.0	32000
SA[183]	$18.60 \cdot 10^6$	16.9	34000
BeA[183]	$5.35 \cdot 10^6$	13.5	35000
MMA[126]	$2.67 \cdot 10^6$	22.4	650
EMA[126]	$4.06 \cdot 10^6$	23.4	670
BMA[126]	$3.78 \cdot 10^6$	22.9	760
DMA[126]	$2.50 \cdot 10^6$	21.0	1000
SMA[134]	$3.45 \cdot 10^6$	21.5	1120
BeMA[134]	$2.51 \cdot 10^6$	20.5	1170

Table 2.4 Arrhenius parameters of k_p for the homologous series of linear alkyl (meth)acrylates.
The values for S(M)A and Be(M)A are determined in the current study; the values for M(M)A, E(M)A, B(M)A, HA, and D(M)A are adapted from the stated references.

monomer solutions are investigated.[195] However, for a non-esterified monomer such as MAA the hydrogen-bonding interactions are likely to be much stronger due to the availability of protons with a higher acidity and therefore the solvent effects may not dominate over the hydrogen-bonding interactions. Consequently, it is reasonable that the experimental results for MAA differ from the behavior observed herein for (meth)acrylic ester monomers. Nevertheless, as stated in ref. 159, "longer alkyl groups are capable of more effectively shielding the polar interactions of the carbonyl groups, thereby reducing rotational barriers for the relevant motions of the TS structure for (meth)acrylate propagation." Instead of an approximate increase in the frequency factor A with increasing ester chain length, a tendency of decreasing activation energies E_a is observed at least in the homologous series from E(M)A to Be(M)A. Yet, the currently available set of data demonstrates that alterations of interactions in the TS are not the only effect influencing the propagation rate coefficients and the related Arrhenius parameters of the linear alkyl (meth)acrylates.

In order to further validate and to perform an in-depth analysis of the observed high k_p values of SA and BeA as well as SMA and BeMA, it appeared mandatory to assess if similarly high

propagation rate coefficients are found in diluted solution PLP-SEC experiments. Therefore, PLP-SEC experiments employing 1 molar solutions of Be(M)A and S(M)A in BuAc were performed (cf. Figure 2.6 lower part) in addition to the bulk experiments. The employed solvent BuAc is similar to *n*-propyl acetate, which is a reported *θ*-solvent for SMA.[141] It is reasonable to assume that if the alkyl ester side chain in the monomer unit is elongated, the alkyl ester side chain in the solvent molecules is elongated as well in order to maintain the *θ*-solvent feature. BuAc consequently may be almost a *θ*-solvent for BeMA as well as for SMA. In *θ*-solvents the interactions between the polymer molecules (intra- and intermolecular) are equal to the interactions between the polymer molecules and the solvent. Consequently, the solvent itself should exhibit no effects on the reactivity of the macroradicals and the conformational behavior of polymer molecules. The changes in the reactivity should therefore only be caused by the lowered monomer concentration and not by altered chemical properties of the reacting species.

Moreover, the PLP-SEC experiments in solution allow the determination of k_p values in a wider temperature range, especially below the melting points of the monomers. In the case of the acrylic monomers – as already noted above – this is very desirable as the expanded temperature range significantly enhances the reliability of the determined Arrhenius parameters. Furthermore, the data can be applied to evidence if the k_p values determined in bulk enable a reliable extrapolation to lower temperatures. Since the overall concentration is incorporated in the evaluation of k_p, the method should be independent of the actual monomer concentration. However, for several monomer and solvent combinations a variation of k_p is reported (cf. also Chapter 1.4.3).[117, 122, 159, 161, 196] In the current case, the obtained Arrhenius parameters are – in agreement with the theory – very similar to the ones obtained from the corresponding bulk solutions (cf. Table 2.2). For the methacrylic monomer systems the observed differences in the frequency factors *A* are small and negligible within the error margin. The same situation is found for BeA, whereas SA displays a strong drop in *A* in BuAc

solution compared to bulk, which is accompanied by a significant decrease in the activation energy E_a. The activation energies E_a of the other 3 monomer systems (i.e., SMA, BeMA, and BeA) are in the same range for the 1 molar solutions as in bulk. All 4 monomer systems displays similarly approx. 20% lower absolute k_p values for the 1 molar solutions than for bulk at 50°C (cf. Table 2.2). Decreases in the absolute k_p values of similar extent are observed in high pressure studies applying supercritical carbon dioxide ($scCO_2$) as solvent, which is applied in recent studies to address the solvent influence issue.[122, 197]

The PLP-SEC experiments with 1 molar solutions of S(M)A and Be(M)A clearly demonstrate that the propagation rate coefficients – which are elevated compared to the smaller homologous of, e.g., M(M)A and B(M)A – are distinct monomer specific features related to the very long linear ester side chains. As noted above, a PLP-SEC experiment in itself determines the product of the propagation rate coefficient and the monomer concentration, $k_p \cdot c_M$. The solution PLP-SEC experiments, in comparison with the bulk ones, demonstrate that the variation of the product $k_p \cdot c_M$ is proportional to the variation of the overall monomer concentration, whereas k_p is invariant to the monomer concentration. Consequently, the approximation that c_M^{local} and $c_M^{overall}$ are equal is applicable and valid. Finally, the elevated propagation rate coefficients are clearly distinct, concentration independent monomer features. If a pre-structuring of the reaction solution – as proposed for the homologous series of linear (meth)acrylates – would be occurring, the extent of the pre-structuring is changing proportionally to the alteration of the concentration. The solution PLP-SEC experiments indicate that if c_M^{local} in bulk is higher than $c_M^{overall}$ by a certain factor, then in 1 molar solution of BuAc c_M^{local} has to be also higher than $c_M^{overall}$ by a similar factor. Since it is relatively unlikely that c_M^{local} in 1 molar solution and in bulk is higher than $c_M^{overall}$ by almost the same factor, the solution experiments are in some contrast to the above described pre-structuring theory and rather support the theory that associates the changes of the propagation rate coefficient in alterations of the respective TS. However, the absolute values of the

propagation rate coefficient, which are approx. 20% lower at 50°C for 1 molar solutions of the monomers compared to the bulk solutions – mainly due to an altered activation energy – provide some scope for a variation of the above mentioned ratio of c_M^{local} to $c_M^{overall}$.

In summary, one may conclude that there appears to be not one single factor responsible for the increasing propagation rate coefficient with increasing ester side chain length for linear alkyl (meth)acrylates. Both proposed theories (i.e., a potential pre-structuring in solution or alterations in the TS, due to (de)stabilization of the radical and/or reduced rotational barriers) are supported by some experimental findings (DSC analysis resulting in melting points instead of glass transition temperatures and PLP-SEC experiments in 1 molar solution resulting in comparable k_p values as obtained from bulk experiments).

2.4.4.2 (Non-)Family Type Behavior for Branched Alkyl (Meth)Acrylates

In order to proceed with the physicochemical analysis of the observed trends, the reader's attention is drawn again to point (*ii*) of the list on page 68 (which is restated here for convenience): k_p is not decisively influenced by the specific structure of the ester side chain within the reported families of branched alkyl and cyclic methacrylates. In the case of such branched and sterically demanding ester side chains as PHMA, TDA-MA, or C17MA, a pre-structuring of the reaction solution is unlikely. On the contrary, it appears that the monomer molecules behave – in a first approximation – in solution as spherical objects. Therefore, the chemical nature of the ester side chains is not decisive for the rate of propagation, as long as it is sufficiently bulky – an observation that applies to all monomers with branched ester side chains – all except *i*BMA and *t*BMA (which itself behave very similar over the entire temperature range). The propagation rate coefficients of the sufficiently bulky monomers, i.e., the group of EHMA, PHMA, TDA-MA, TDN-MA, and C17MA as well as *i*DeMA, are almost identical for all temperatures. The observations can be summarized as follows: If the ester side chains are virtually exchanged, the propagation rate coefficients differ only slightly

as long as the two ester side chains have similar sterical demands; consequently their exact shapes and structures are not decisive for the approximate value of k_p. A tentative explanation for the observed family type behaviors (cyclic and branched methacrylates) and the differences to the linear non-branched methacrylates becomes clearer by trying to explain the behavior of the branched alkyl acrylates and their not observed family type behavior. (cf. especially page 77)

As stated in point (*iii*) in the list on page 69, no clear trend for the branched alkyl acrylates can be identified, however, a tendency to increasing k_p values with increasing number of carbon atoms in the ester side chain, in analogy to the linear (meth)acrylates, can be detected. The difference between the behavior of branched alkyl methacrylates and acrylates is most probably based on the influence of the α-methyl substituent in the methacrylates, which is missing for the acrylates. Its steric demand and positive inductive effect (+I-effect) influences the TS of the propagation reaction with respect to, e.g., rotational degrees of freedom and electronic energy levels as well as the stiffness of the polymer backbone. The latter one influences the diffusion behavior of the polymer molecules as well as of the monomer units. Furthermore, the dipole character of the ester functionality is shielded by the α-methyl substituent, which again influences the TS of the propagation reaction. The combination of these effects arising from the α-methyl substituent lead to a less pronounced influence of the branched ester side chains for the methacrylates and to a more pronounced influence of the branched ester side chains for the acrylates. In addition, it should be noted that the α-methyl substituent of the methacrylates leads to an increasing helical tendency of the lateral polymer chain if the steric demand of the ester side chain is increased.[198] For the corresponding acrylates such an increased tendency towards a helical conformation is not reported. Consequently, for acrylates fundamentally different family type behavior and trends are expectable and observed. With additional branched acrylic monomers studied via the PLP-

SEC method with respect to their propagation rate coefficient, the observed trend might become more obvious.

Although the propagation reaction is chemically controlled, a possible explanation for the complex behavior of the branched alkyl acrylates might involve their differing viscosities. It is evident that the diffusion of molecules depends on the viscosity of the reaction medium (which is bulk in the current case). Hypothetically, the normally chemically controlled propagation reaction could come under diffusion control in highly viscous media, thus decreasing k_p. However, this – unlikely – hypothesis is challenged by the inspection of Table 2.5 listing the kinematic viscosities, v, for several branched alkyl acrylates. The monomers in Table 2.5 are listed in the same order of estimated increasing steric demand as in Figure 2.13 above. If the hypothesized dependence of k_p on the kinematic viscosities, v, would be operational, then TDN-A, exhibiting a higher viscosity than TDA-A, should feature a lower propagation rate coefficient than TDA-A (in Table 2.5 exemplarily demonstrated by the $k_p^{50°C}$). However, this is not the case: TDA-A displays a significantly lower viscosity and lower propagation rate coefficient. Therefore, clearly no correlation between the rate of the propagation reaction and the viscosity of the reaction medium can be drawn.

Monomer		EHA	PHA	INA-A	TDA-A	TDN-A	C17A	C21A
isoindex	–	1	1	1.3	3.1	2.1	3.1	4.2
$k_p^{50°C}$	$[10^3\ L \cdot mol^{-1} \cdot s^{-1}]$	25.5	23.5	28.5	27.5	30.0	35.0	25.5
$v^{25°C}$	$[10^6\ mm^2 \cdot s^{-1}]$	1.8	2.7	–	5.2	16.2	10.8	23.2

Table 2.5 Comparison of kinematic viscosities and the propagation rate coefficient at 50°C for branched alkyl acrylates.
Kinematic viscosities, v, for the branched alkyl acrylates are stated in the order of estimated increasing steric demand of their ester side chains along with the isoindex and the propagation rate coefficient at 50°C. The kinematic bulk viscosities were determined with the aid of an Ubbelohde capillary viscometer.

A combination of entropic and steric effects might be the reason for the observed family type behavior of the branched alkyl methacrylates and the exceptions in the series of branched alkyl acrylates. The bulky and branched ester side chains lead to high rotational barriers due to their steric demand. In the case of the methacrylates, the rotational hindrance is

significantly more pronounced, due to the α-methyl group and its steric interactions with the ester side chain. The steric demands and rotational hindrances result in a lower entropy of the polymer chains, which is also reflected in the glass transition temperatures, T_g: Methacrylates (especially with small ester side chains) feature an approx. 80-100°C higher T_g than acrylates, since they are stiffer and feature a higher degree of order.[187] Consequently, more thermal energy is necessary to overcome their higher degree of order and to set the polymer chains in motion. The Gibbs-Helmholtz-equation describes the correlation of free Gibbs energy, enthalpy, temperature, and entropy:

$$\Delta G = \Delta H - T \cdot \Delta S \qquad 2.1$$

The Gibbs-Helmholtz-equation cannot only be employed to describe the overall reaction process. It also can be employed to describe energetic changes between the reactants and the TS, if ΔG is replaced by the Gibbs activation barrier, $\Delta G^{\ddagger}$.[199] The difference in the enthalpy, ΔH, which is mainly governed by the electronic configuration of the reactants, should be not altered significantly by the varied ester side chains as stated above. However, it is strongly altered by the α-methyl group of the methacrylates, which is one of the reasons why methacrylates propagate substantially slower than acrylates. The difference in the entropy, ΔS, however depends strongly on the specific nature of the ester side chain, since the side chain influences the rotational barriers, the stiffness, and thereby the degree of order within the polymer chain. Specific examples are the herein reported tridecyl acrylates, TDA-A and TDN-A, which differ only in the degree of branching in their ester side chains (cf. Table 2.5). TDA-A features significantly lower k_p values than TDN-A. The difference of the molecular weights of L_1 (which is the first inflection point in the derivative of the SEC chromatogram) between TDA-A and TDN-A is approx. 5000 g·mol^{-1} at 50°C (approx. 45000 vs. 50000 g·mol^{-1}; cf. Table S16 and Table S18 in the Appendix A). Such a difference of approx. 10% equals the associated error range of the corresponding SEC measurement and evaluation process. However, since the monomer specific MHKS parameters are employed, which were

determined via the same methodology for both monomers, the difference between TDA-A and TDN-A is very likely significant.[179] Since both monomers feature the same ratio of alkyl side chain to ester moieties, the above noted destabilization of the attacking radical (probably responsible for the k_p increase for linear alkyl (meth)acrylates) should not distinguish between both monomers. Thus, – since the differing viscosity is already excluded as possible cause – the lowered k_p value of TDA-A has to be the consequence of the higher steric influence of the more branched ester side chain, which is resulting in higher rotational barriers and therefore in a stronger decrease in entropy. The determined T_g values of the tridecyl (meth)acrylates underpin this notion, since TDA-A features a higher T_g than TDN-A (-55°C vs. -69°C, cf. Figure S29 and Figure S30) and TDA-MA a higher T_g than TDN-MA (-33°C vs. -57°C, cf. Figure S27 and Figure S28). The higher the stiffness / degree of order of the polymer chain, the higher the T_g, the more entropy is lost during the polymerization process and the more non-favored is / the slower proceeds the propagation reaction, since the more positive is the contribution of the entropy to the overall free reaction energy (which must be negative for a freely progressing reaction).

An additional effect causing a difference between the family type behavior of the branched methacrylates in contrast to a probable increase of k_p for the branched acrylates might be the varying relative contribution of steric influence by the ester side chains. Assuming the entropic effect of the miscellaneous branched side chains has the same magnitude for methacrylates as for acrylates, the overall extent might still be negligible in the case of the methacrylates, resulting in the family type behavior, whereas it has a relevant impact in the case of the acrylates, resulting in the increase of k_p. This fact becomes clear once the entropic and electronic contributions are quantified: Assume a small and short branched side chain influences the entropy by a factor of 2 and a very long and large side chain by a factor of 20. Their influence might then have a much stronger relative effect on acrylates than on methacrylates, since the enthalpic part to the free Gibbs energy might be 100 in the case of the

acrylates (up to 20% influence) or 1000 in the case of the methacrylates (up to 2% influence). The above consideration makes clear that even if the branched side chains would have a similar effect on methacrylates as on acrylates, it might not be detectable due to the much stronger electronic influence of the α-methyl group.

2.5 Conclusions

The steady increase of k_p with increasing ester side chain length in the homologous series of linear (meth)acrylates holds true up to very long alkyl ester side chains of more than 20 carbon atoms. For the acrylic monomers the increase of k_p per additional carbon atom is approx. 20 times higher than for the linear alkyl methacrylates (estimated slope of ~550 $L \cdot mol^{-1} \cdot s^{-1}$ vs. ~30 $L \cdot mol^{-1} \cdot s^{-1}$ at 50°C). According to these slopes, the propagation rate coefficient increases by approx. 3-4% per additional homologous CH_2 group when going from MMA to BeMA at 50°C and by approx. 2-3% when going from MA to BeA. At other temperatures (-50°C, 0°C, 100°C) a similar trend is observed. A tentative explanation for the observed increase in k_p involves the decreasing stabilization of the attacking radical in the TS by the polar ester moieties due to their decreasing concentration. An alternative reason for the observed trend may be associated with a pre-structuring of the reaction solution, a notion that is supported by the crystallization data and behavior of the higher ester side chain length (meth)acrylates. Furthermore, solution experiments of S(M)A and Be(M)A (1 molar in BuAc) demonstrate that the elevated propagation rate coefficients are distinct monomer features. However, a slight decrease in the activation energy E_a is observed, caused by approx. 20% lowered absolute k_p values, whereas the frequency factors A remain almost constant. The somewhat lowered values of the propagation rate coefficient in 1 molar solution compared to bulk do not fully support the pre-structuring theory, but appear to support the (additional) explanation, which includes changes in the TS of the propagation reaction (e.g., of the polarity, rotational degrees of freedom). In summary, it appears that no single reason alone is

responsible for the increasing propagation rate coefficients with increasing ester side chain length for linear alkyl (meth)acrylates. While the trend of increasing k_p with ester side chain length is relatively clear for each temperature, no unambiguous trend can be identified with respect to A and E_a in the homologous series, even though a tendency towards decreasing values is observed at least in the homologous series from E(M)A to Be(M)A.

The family type behavior observed for branched methacrylates entails a wide variety of sterically demanding monomers. The present data suggest that as soon as a certain sterical demand is reached, the value of k_p is almost invariant to any topological change of the ester side chain. The limiting case for these steric requirements seems to be somewhere above the spatial demands of *i*BMA and *t*BMA, yet below EHMA or *i*DeMA. According to their similar k_p behavior it is proposed to describe *i*DeMA, EHMA, PHMA, TDA-MA, TDN-MA, and C17MA as a family in its own, in addition to the previously reported family of GMA, *c*HMA, *i*BoMA, and BnMA. The family type behavior of the branched alkyl methacrylates can be understood by considering steric and entropic effects additionally to the evident enthalpic effects caused by the electronic situation of the tertiary radical site. Strong steric interactions between the α-methyl group and the branched ester side chain – irrespective the specific structure of the branched ester side chain – lead to high rotational barriers and an increased loss of entropy (compared to linear alkyl (meth)acrylates) during the propagation reaction. An analogous explanation might be applicable for the family type behavior of the cyclic methacrylates reported previously.[125]

Interestingly, in the extended family of branched acrylates (i.e., the herein reported PHA, INA-A, TDA-A, TDN-A, C17A, and C21A as well as the previously reported *t*BA, BnA, *i*BoA, and EHA) no similar family type behavior can be identified as found for the branched methacrylates. On the contrary, e.g., the propagation rate coefficient $k_p^{50°C}$ changes from EHA to PHA / C17A / C21A by a factor of 0.92 / 1.36 / 1.00, respectively. The differences between branched alkyl methacrylates and acrylates with respect to their family type behavior are most

probably based on the influences / existence of the α-methyl substituent – of course – which is resulting in differing relative contributions of the influences by the branched ester side chains to the overall free Gibbs energy of the TS. However, to date no clear trends or family type behavior can be detected for the branched acrylates and no conclusive explanation for the differences between methacrylates and acrylates can be given. The study of the branched acrylates in 1 M solution in BuAc did neither allow for the detection of a global trend in their kinetic behavior. Since no clear trends in the kinetic behavior of the branched alkyl acrylates can be identified, it is necessary to determine monomer specific Arrhenius data of k_p for each branched alkyl acrylate.

The above described global trends for the linear and branched alkyl (meth)acrylates were detected on the basis of an encompassing data set of propagation rate coefficients determined via the PLP-SEC method. The monomers were studied in bulk as well as (many of them) in 1 M solution in BuAc employing laser repetition frequencies of up to 500 Hz (especially for the acrylates). Determination of the absolute molecular weights of the polymer samples – necessary for a reliable deduction of k_p values – was achieved via the polymer specific MHKS parameters determined in the course of the current study. In addition, further monomer and polymer specific data such as changes of the refractive index with the change of the concentration, temperature dependent densities, kinematic viscosities, and glass transition temperatures are reported for the investigated monomers and employed to support the physicochemical explanations of the observed trends.

3 Heteroatom Containing (Meth)Acrylic Monomers[d]

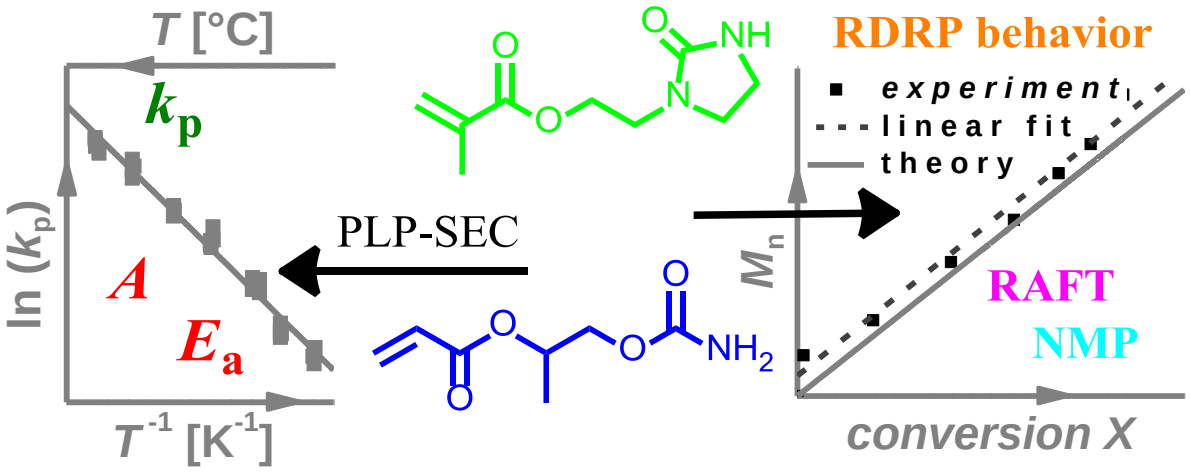

3.1 Introduction

After focusing on a wide variety of alkyl (meth)acrylates, the subsequent chapter addresses rather unusual (meth)acrylic monomers. Since the herein studied monomers feature additional functional groups in the ester side chain, their applicability in RDRP techniques will be tested in addition to an in-depth analysis of their kinetic behavior. While for the alkyl monomers discussed in Chapter 2 no extraordinary challenges for an application in RDRP techniques are to be expected, the herein reported ureidoethyl methacrylate (UMA) and hydroxy-*iso*-propylcarbamate acrylate (HPCA; structures are depicted in Scheme 3.1) present a challenge: For monomers containing amines, side reactions, e.g., with the thiocarbonyl functionality of

[d] Parts of this chapter are reproduced from ref. 200: Haehnel, A. P.; Stach, M.; Chovancova, A.; Rueb, J. M.; Delaittre, G.; Misske, A. M.; Lacik, I.; Barner-Kowollik, C. Polym. Chem. 2014, 5, 862-873. with permission of The Royal Society of Chemistry.

RAFT controlling agents, are reported[201-202] (although RAFT polymerization is possible for, e.g., acrylamide in water).[203] Furthermore such heteroatom containing ester side chains are quite similar to metal complexing ligands of such as tris(2-dimethylaminoethyl)amine (Me_6Tren) or 2,2′-bipyridin (Bipy). Such a possibly complexing nature of the monomer might interfere with, e.g., copper mediated RDRP techniques such as ATRP or SET-LRP. NMP however should principally not be negatively influenced by the present amine-based additional functional groups.

Yet, before the applicability of UMA and HPCA in RDRP techniques is discussed, their investigation is commenced with the kinetic analysis of their FRP behavior and the comparison to literature known data.

In addition to the alkyl (meth)acrylates mentioned in Chapter 2, the knowledge about the Arrhenius parameters for k_p of acrylates with heteroatom containing ester side chains is relatively limited. Prior to the current investigations the following monomers were reported: ethoxyethyl acrylate (EEA),[124] 2-(phenylcarbamoyloxy)ethyl acrylate (PhCEA),[204] 2-(phenylcarbamoyloxy)-*iso*-propyl acrylate (PhCPA),[204] 2-(hexylcarbamoyloxy)ethyl acrylate (HCEA)[204], and 2-(hexylcarbamoyl-oxy)-*iso*-propyl acrylate (HCPA).[204] The latter 4 monomers are in their solid state at standard conditions, requiring them to be studied in 1 M solutions in BuAc. The comparison of the propagation rate data of these 4 monomers revealed that extending the ethyl group to an *iso*-propyl group (i.e., when going from PhCEA to PhCPA and HCEA to HCPA) results in an significant (almost factor of 2) decrease in k_p, being still as high as the values observed for, e.g., butyl acrylate.[204] Furthermore, the authors identified a decrease in k_p by virtually exchanging the phenyl substituent by a hexyl moiety, which however is only valid for the ethyl containing monomers and not for the monomers bearing an *iso*-propyl group (cf. also Figure 3.2 below).

Furthermore, the Arrhenius parameters of monomers with hydroxyl functions in the ester side chain have been reported, i.e., 2-hydroxyethyl acrylate (HEA, not final values since an

adequate SEC calibration was not yet reported, which should however not affect the determined activation energy),[194] 2-hydroxyethyl methacrylate (HEMA)[205] as well as 2-hydroxypropyl methacrylate (HPMA).[206] It is noteworthy that all heteroatom containing acrylates except HEA (i.e., EEA, PhCEA, HCEA, PhCPA, and HCPA) feature a significantly decreased activation energy (of approx. 14 kJ·mol^{-1}) compared to alkyl acrylates (typically in the range of 17 to 19 kJ·mol^{-1}). Solely the in Chapter 2 discussed very long behenyl acrylate displays a similar low activation energy of 13.5 kJ·mol^{-1}.

currently studied monomers

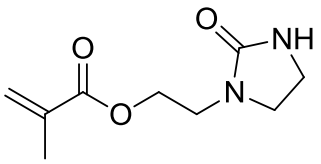

Ureidoethyl methacrylate
UMA

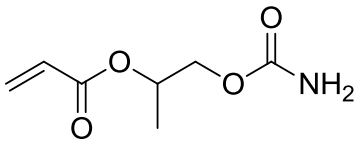

Hydroxy-*iso*-propylcarbamate acrylate
HPCA

related monomers investigated in a previous study

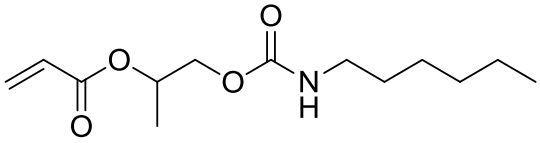

(Hexylcarbamoyloxy)-*iso*-propyl acrylate
HCPA

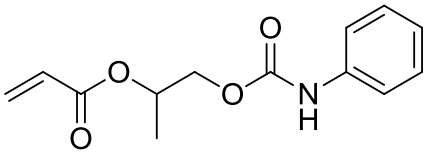

(Phenylcarbamoyloxy)-*iso*-propyl acrylate
PhCPA

Scheme 3.1 Heteroatom Containing Monomer Structures.
Structures of the monomers investigated in the current study: ureidoethyl methacrylate (UMA) and hydroxy-*iso*-propylcarbamate acrylate (HPCA). Additionally, the structures of two previously reported HPCA-related monomers are depicted: (hexylcarbamoyloxy)-*iso*-propyl acrylate (HCPA)[204] and (phenylcarbamoyloxy)-*iso*-propyl acrylate (PhCPA).[204] Please note that HPCA, PhCPA, and HCPA are isomeric structures in regard to the orientation of the *iso*-propyl unit. Reprinted from ref. 200 with permission of The Royal Society of Chemistry.

In the current chapter, the exploration of the propagation behavior is extended to unusual monomer systems by focusing the attention on the determination of the Arrhenius parameters of the propagation rate coefficient of ureidoethyl methacrylate (UMA) and hydroxy-*iso*-propylcarbamate acrylate (HPCA). Since their ester side chains contain functional groups,

which are most likely influencing their propagation behavior significantly, they were not incorporated into the discussion of the branched alkyl (meth)acrylates discussed in Chapter 2. Yet, the results of the herein newly investigated (meth)acrylates, i.e., UMA and HPCA, will be placed into context of the trends observed for alkyl (meth)acrylates. The monomer structures are depicted in Scheme 3.1 together with the structures of the two monomers closely related to HPCA, i.e., HCPA and PhCPA, which were previously studied in our laboratories via the PLP-SEC method.[204]

To the best of the candidate's knowledge, UMA is the first methacrylic monomer with a heteroatom containing ester side chain being studied via PLP-SEC (beside the above mentioned hydroxyl functional ones). The investigation of UMA will shed light on the effects which the ester side chain, with its cyclic ureido group, has on the propagation reaction and its propagation rate coefficient. In contrast to most alkyl (meth)acrylates, which are liquids at ambient conditions, the pure monomer UMA is a colorless, white powder. The properties of UMA may thus be strongly influenced by the ester side chain with its stacking features, e.g., leading to the possibility to form intermolecular hydrogen bonds. The hydrogen bonds might increase the stiffness of the lateral polymer chain or may lead to a pre-structuring of the monomers in solution. Both possible effects may have a significant influence on the diffusion behavior of the radicals and consequently alter the observed propagation rate coefficient. Consequently, significant differences compared to the common alkyl ester side chain methacrylates are expected, due to the heteroatom containing ester side chain.

The second monomer, HPCA, which is a crystalline solid, features a carbamate group, which possesses – just as the ureido functionality in UMA – the ability to form hydrogen bonds. Therefore, the above described influences on k_p may also be effective for HPCA. Furthermore, there are two structural derivatives of HPCA already reported in the literature, i.e., (hexylcarbamoyloxy)-*iso*-propyl acrylate (HCPA)[204] and (phenyl-carbamoyloxy)-*iso*-propyl acrylate (PhCPA).[204] The structural similarities can be readily recognized by

inspection of Scheme 3.1. In HCPA, one of the hydrogen atoms of the carbamate is replaced by an *n*-hexyl group and by a phenyl group in PhCPA. Among these three monomers the influence of the substituents *n*-hexyl and phenyl – as far as there is one – may be detectable. One of the most obvious impacts of the substituent is the reduced polarity of HCPA and PhCPA, which allowed for the SEC analysis of the resulting polymers in tetrahydrofuran (THF, polarity index 4.0),[207] whereas this is not possible for polyHPCA, which had instead to be analyzed by SEC in *N*,*N*-dimethylacetamide (DMAc, polarity index 6.5),[207] due to insolubility of polyHPCA in THF. Based on these differing properties of HPCA from its derivatives, pronounced differences within the corresponding propagation rate coefficients are expected.

Table 3.1 collates monomer specific data, which is necessary for the PLP-SEC evaluation, i.e., information about the temperature dependent density as well as the refractive index increment, d*n*/d*c*, as well as the molecular weight (MW). For sake of completeness the polymer specific glass transition temperatures (T_g) are also stated.

Monomer		MW g·mol^{-1}	ρ_0 g·mL^{-1}	b g·mL^{-1}·°C^{-1}	dn/dc mL·g^{-1}	T_g °C
UMA	1 M in DMAc	198.22	1.03624	0.084	0.084	74
HPCA	1 M in DMAc	173.17	0.99861	0.068	0.068	32

Table 3.1 Monomer and polymer specific physical data of UMA and HPCA.
In addition to the molecular weight (MW) and the parameters of the temperature dependent densities (ρ_0, b), the change of the refractive index over the change of the concentration (dn/dc) and glass transition temperatures, T_g, (determined via differential scanning calorimetry (DSC) (cf. Figure S34 in the Appendix B) are stated. The determination of the Mark-Houwink-Kuhn-Sakurada parameters (K, α) was not possible.

In addition to the PLP-SEC investigations, the free-radical polymerization of both monomers (UMA and HPCA) is probed via in-situ ^{1}H-NMR spectroscopy at elevated temperatures to deduce – with the aid of the determined propagation rate coefficients – estimates for the steady-state radical concentration as well as to arrive at estimates (at low conversions) for the average termination rate coefficient.

Finally, it is assessed whether the polymerization of both monomers can be controlled via RDRP processes, i.e., reversible addition-fragmentation chain transfer (RAFT) polymerization[36] and nitroxide-mediated polymerization (NMP).[37]

3.2 Kinetic Behavior

Initially, the determination of the propagation rate coefficients of the herein investigated monomers UMA and HPCA is discussed. Subsequently, the polymerization kinetics of the monomers will be analyzed in conventional free-radical polymerization, before in the next subchapter the application of UMA and HPCA in RDRP techniques will be reported along with a similar kinetic analysis as for FRP.

3.2.1 Arrhenius Parameters

The pulsed laser polymerization of both monomers was carried out in DMAc as solvent at pulsing rates of up to 500 Hz. Typically, clear inflection points were observed. PLP-SEC samples which featured only a minor inflection in the first derivative of the molar mass distribution instead of a clear second maximum were not incorporated into the determination of the Arrhenius parameters. Exemplary molar mass distributions with their corresponding first derivative are highlighted in Figure S31 and Figure S32 in the Appendix B. Typically, a third inflection point can be identified for the acrylic HPCA and a fourth inflection point for the methacrylic UMA. The detailed PLP conditions are summarized in Table S27 and Table S28 in Appendix B. With such a large set of temperature dependent propagation rate coefficient data at hand, it is possible to derive an individual Arrhenius relation for both monomers. The resulting Arrhenius parameters are collated in Table 3.2 together with the related error margins. The Arrhenius plots for UMA and HPCA polymerized in 1 M solution in *N*,*N*-dimethylacetamide (DMAc) are depicted in Figure 3.1.

Monomer		A	±	E_a	±	$k_p^{50°C}$	θ interval
		$L \cdot mol^{-1} \cdot s^{-1}$		$kJ \cdot mol^{-1}$		$L \cdot mol^{-1} \cdot s^{-1}$	°C
UMA	1 M in DMAc	$2.08 \cdot 10^6$	$-4.47 \cdot 10^5$ $9.09 \cdot 10^5$	19.89	-0.89 0.91	1270	-11 to 92
HPCA	1 M in DMAc	$3.97 \cdot 10^6$	$-1.38 \cdot 10^6$ $5.13 \cdot 10^6$	14.29	-1.44 1.63	19400	-15 to 50

Table 3.2 Arrhenius parameters for k_p of UMA and HPCA.
Arrhenius parameters with error margins of the 95% joint confidence intervals (not symmetric), values for the propagation rate coefficient at 50°C, $k_p^{50°C}$, and temperature intervals considered in the Arrhenius fit.

The Arrhenius plots exhibit a clear linear behavior in the entire studied temperature range (60 K for the acrylic and 100 K for the methacrylic monomer). For each temperature, several samples (usually 3 or 4) with varying PLP conditions were taken into account, whereby the molar mass of the first inflection point should be in the range between 10000 and 60000 $g \cdot mol^{-1}$ and at least the secondary inflection point has to be present (cf. Chapter 1.4). Thereby, the influence of the conversion and the pulse frequency on the resulting Arrhenius parameters is minimized. Furthermore, the observed scattering between different samples is in the same range as if the same sample was injected multiple times into the SEC device.

In analogy to the alkyl (meth)acrylates, the remaining consistency criteria are assessed via variation of the laser pulse energy (from 1 to 4 $mJ \cdot pulse^{-1}$) as well as the initial photoinitiator concentration (from 1 to 15 $mmol \cdot L^{-1}$). The observed errors of the activation energy are typical for these types of monomer, i.e., approx. ±1 $kJ \cdot mol^{-1}$ for methacrylates[117, 125] and approx. ±2 $kJ \cdot mol^{-1}$ for acrylates.[117, 121] HPCA features a significantly lower activation energy than UMA. The Arrhenius parameters and the error margins determined via the same procedure as for the alkyl (meth)acrylates are displayed in Table 3.2. The average error per data point is close to 11% (in the case of HPCA) and 16% (in the case of UMA).

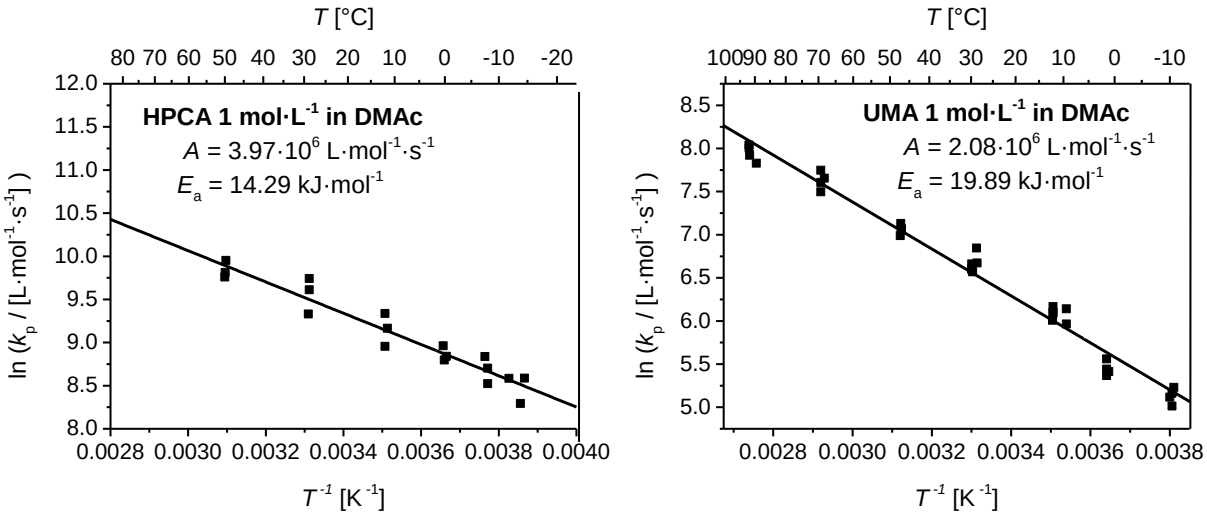

Figure 3.1 Arrhenius plots for HPCA and UMA.
ln(k_p / [L·mol^{-1}·s^{-1}]) vs. T^{-1} plots with linear fits for the determination of the Arrhenius parameters of **(left hand part)** hydroxy-*iso*-propylcarbamate acrylate (HPCA) and **(right hand part)** ureidoethyl methacrylate (UMA) in 1 M solution in *N*,*N*-dimethyl acetamide (DMAc). The associated monomer structures are depicted in Scheme 3.1. The resulting Arrhenius parameters are collated in Table 3.2 together with the related error margins. Detailed PLP conditions are summarized in Table S27 and Table S28 in the Appendix B. Adapted from ref. 200 with permission of The Royal Society of Chemistry.

3.2.2 Comparison to Related (Meth)Acrylates

In a subsequent step, the newly determined Arrhenius parameters and propagation rate coefficients are compared with literature known data in order to identify possible structure-reactivity relations with existing data sets. The discussion is commenced by comparing HCPA to its structural derivatives and will be continued afterwards with the comparison of UMA to other methacrylates. Due to the structural similarity, the Arrhenius parameters of HPCA, PhPCA, and HCPA will be compared with each other in order to establish if there is a trend observable caused by the substituent pattern of these acrylates.

During the following critical discussion, one should be aware of possibly existing influences of the monomer concentration and of the type of solvent on the propagation rate coefficient, which also introduce an uncertainty into the comparison of the Arrhenius parameters. HCPA and PhCPA, which are structurally closely related to HPCA, were polymerized in 1 M solution in BuAc and analyzed in THF, whereas HPCA had to be studied in DMAc, due to

insolubility in BuAc and THF. However, the solvent dependence might be negligible, as indicated by a study (currently in progress in our laboratories), which is comparing 1 M monomer solutions in BuAc and toluene as well as previous reports combining, e.g., the data obtained for HPMA in bulk with solutions in benzyl alcohol (BnOH) and toluene.[208] Furthermore, it should be noted that all three monomers are isomeric mixtures regarding the orientation of the isopropyl unit which connects the acrylic ester with the carbamate functionality. Scheme 3.1 (above on page 85) highlights the dominant structure for each monomer. HCPA and PhCPA were synthesized from an approx. 1:2 mol/mol (primary : secondary) mixture of the esterified alcohol, whereas HPCA consists of approx. 2:1 mol/mol (primary : secondary) mixture (both ratios were determined based on a ^{1}H-NMR analysis, cf. Figure S35 in Appendix B). Despite the reversed isomeric ratio, the three monomers HPCA, PhCPA, and HCPA are structurally very similar and comparable in terms of kinetic aspects. As will be seen below, a clear trend within the kinetic data for the three monomers can be identified by placing them in order of increasing length of their ester side chain.

Inspection of Table 3.3 (first three lines) demonstrates that the activation energy, E_a, is almost identical for all three monomers, whereas the pre-exponential factor is slightly increasing within the margins of error. However, the resulting propagation rate coefficients increase over the entire temperature range – as can be readily recognized by inspection of Figure 3.2 – uniformly by a factor of approx. 1.3 for PhCPA and of approx. 1.8 for HCPA compared to HPCA. A similar uniform increase, correlated with the length of the ester side chain, is also highlighted on the right-hand side of Figure 3.2, which shows the already known increase of k_p from methyl acrylate (MA) to butyl acrylate (BA), dodecyl acrylate (DA), and behenyl acrylate (BeA).

Monomer		MW g·mol^{-1}	A L·mol^{-1}·s^{-1}	E_a kJ·mol^{-1}	$k_p^{50°C}$ L·mol^{-1}·s^{-1}	θ interval °C
HPCA[200]	1 M in DMAc	173.17	$3.97 \cdot 10^6$	14.3	20000	-15 to 50
PhCPA[204]	1 M in BuAc	249.26	$4.9 \cdot 10^6$	14.2	25000	6 to 81
HCPA[204]	1 M in BuAc	257.33	$6.6 \cdot 10^6$	14.1	35000	3 to 72
MA[186]	bulk	86.09	$2.50 \cdot 10^7$	18.5	25500	11 to 61
BA[177]	bulk	128.17	$2.13 \cdot 10^7$	17.8	28500	-65 to 70
DA[117]	bulk	240.38	$1.79 \cdot 10^7$	17.0	32000	-3 to 30
BeA[183]	bulk	370.57	$5.35 \cdot 10^6$	13.5	35000	40 to 70

Table 3.3 Arrhenius parameters for k_p of HPCA compared to literature data.
HPCA is compared to its structural derivatives, PhCPA and HCPA, as well as to linear alkyl acrylates, i.e., methyl acrylate (MA), butyl acrylate (BA), dodecyl acrylate (DA), and behenyl acrylate (BeA) depicted also in Figure 3.2. For illustration purposes, the propagation rate coefficients at 50°C are stated alongside the molecular weight of the monomers and the temperature intervals considered in the Arrhenius fits.

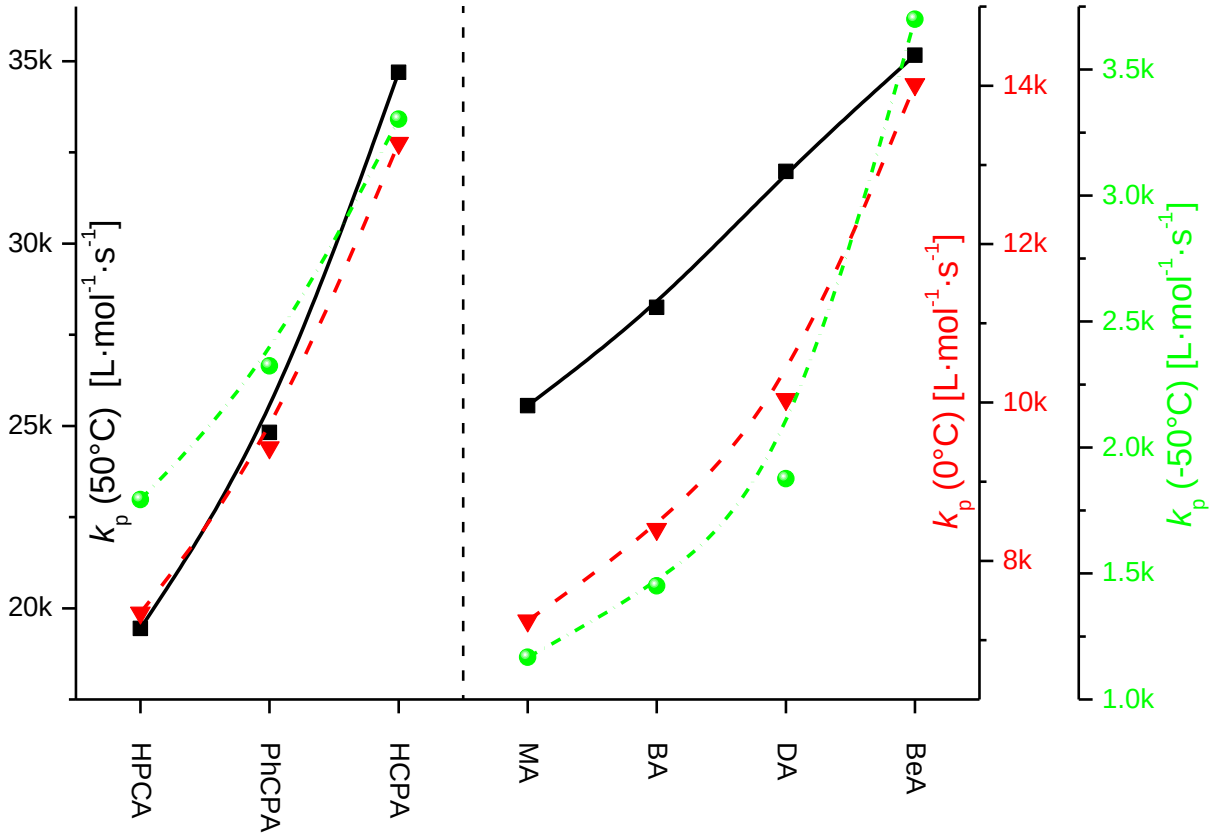

Figure 3.2 Dependence of the propagation rate coefficient, k_p, on the type of ester side chain for acrylates.
Propagation rate coefficients, k_p, at different temperatures (left scale = black solid line = k_p(50°C); right inner scale = red dashed line = k_p(0°C); right outer scale = green dotdashed line = k_p(-50°C)) for acrylates. The lines are merely for guiding the eye and are no fits. Monomers are displayed in the order of increasing linear ester side chain length on both sides of the central dashed line: **(left hand side)**: hydroxyl-*iso*-propylcarbamate acrylate (HPCA), (hexylcarbamoyloxy)-*iso*-propyl acrylate (HCPA), and (phenylcarbamoyloxy)-*iso*-propyl acrylate; **(right hand side)**: methyl acrylate (MA),[180] butyl acrylate (BA),[177] lauryl acrylate (DA),[182] behenyl acrylate (BeA).[183] The associated monomer structures of HPCA, PhCPA, and HCPA are shown in Scheme 3.1. The corresponding Arrhenius parameters and propagation rate coefficients at 50 °C, $k_p^{50\,°C}$, are collated in Table 3.3. Adapted from ref. 200 with permission of The Royal Society of Chemistry.

Inspection of Figure 3.2 evidences the pronounced increase of the propagation rate coefficient, k_p, over the entire temperature range from -50°C to 50°C, when one of the carbamate protons is substituted by a phenyl or an *n*-hexyl group, respectively, i.e., the longer and the more sterically demanding the ester side chain is. The phenyl substituent is rigid and flat, whereas the flexible and long *n*-hexyl group is sterically significantly more demanding. A comparison with the right-hand part of Figure 3.2 demonstrates that the observed increase is more pronounced as in the case of the linear alkyl acrylates. For linear alkyl acrylates, an ester side chain extension of 11 or 18 carbon atoms (i.e., when going from methyl to dodecyl or behenyl acrylate, respectively) results in an increase of k_p by factors of approx. 1.3 or 1.6 at 50°C. However, for the currently studied carbamate-containing acrylates, an ester side chain extension of solely 6 carbon atoms (when going from a hydrogen substituent in HPCA to a hexyl substituent in HCPA) results in an increase of $k_p^{50°C}$ by a factor of approx. 1.8.

When establishing a possible explanation for the behavior identified above, electronic/inductive effects of the substituents are likely less important as the substituents are very far removed from the reactive vinyl functionality (cf. also Chapter 2.4.4). This notion is additionally supported by the very similar activation energy of all three monomers (cf. Table 3.3). The differences between the three monomers HPCA, PhCPA, and HCPA seem to be mainly based on differences in the pre-exponential factor; a clear contrast to the linear alkyl acrylates, which display variations similarly in A and E_a. The pre-exponential factor is also termed frequency factor, since it is a measure for the number of molecule collisions taking place per unit of time. Consequently, the steric orientations of the monomers with a substituent at the carbamate nitrogen seem to facilitate more (reactive) collisions.[10, 123]

Next, the propagation rate data of UMA will be set into the context of other literature known methacrylates. Unfortunately, there are – to the best of the candidate's knowledge – no methacrylates reported in the literature which feature a structural similarity with UMA. Indeed, there are no PLP-SEC studies of methacrylates with heteroatom-containing ester side

chains reported beside the hydroxyl functional 2-hydroxyethyl methacrylate (HEMA)[205] and hydroxpropyl methacrylate (HPMA, isomeric mixture).[208]

In view of the lack of literature known monomers similar to UMA, the herein obtained kinetic data of UMA are placed in relationship to the data of literature known linear, branched, cyclic, and hydroxyl functional methacrylates. During the discussion of the data, it should be kept in mind that all monomers were studied in bulk except UMA, which was polymerized in 1 M solution with DMAc as the solvent, since it is a crystalline solid.

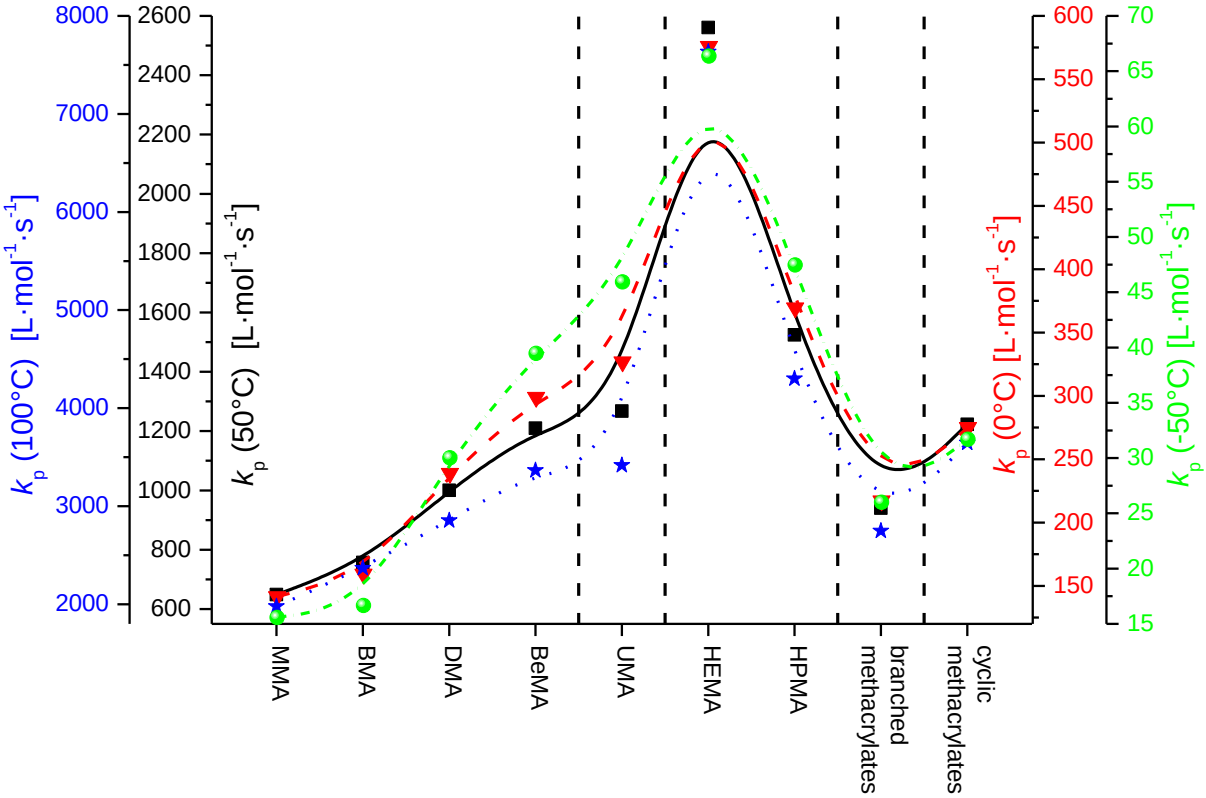

Figure 3.3 Dependence of the propagation rate coefficient, k_p, on the type of ester side chain for methacrylates.
Propagation rate coefficients, k_p, at different temperatures (left outer scale = blue dotted line = k_p(100°C); left inner scale = black solid line = k_p(50°C); right inner scale = red dashed line = k_p(0°C); right outer scale = green dotdashed line = k_p(-50°C)) for methacrylates. The vertical dashed lines group the methacrylates into: **(*i*)** linear alkyl: methyl methacrylate (MMA),[127] butyl methacrylate (BMA),[126] dodecyl methacrylate (DMA),[126] behenyl methacrylate (BeMA);[134] **(*ii*)** ureidoethyl methacrylate (UMA);[200] **(*iii*)** hydroxyl functional: 2-hydroxyethyl methacrylate (HEMA)[205] and hydroxpropyl methacrylate (HPMA, isomeric mixture);[208] **(*iv*)** branched: joint fit for EHMA, PHMA, TDA-MA, TDN-MA, C17MA, and *i*DeMA; and **(*v*)** cyclic: joint fit for *c*HMA, BzMA, *i*BoMA, and GMA.[125] The monomer structure of UMA is shown in Scheme 3.1. The corresponding Arrhenius parameters and propagation rate coefficients at 50°C, $k_p^{50°C}$, are collated in Table 3.4. Adapted from ref. 200 with permission of The Royal Society of Chemistry.

Figure 3.3 depicts (on the left-hand side until the first dashed line) the propagation rate coefficient data for some linear alkyl methacrylates. Within these data, the literature known increase of k_p with the number of carbon atoms in the ester side chain can clearly be recognized.[134] When the currently obtained propagation rate coefficient data for UMA are compared with the linear alkyl methacrylates, it would equal an ester side chain even longer than behenyl methacrylate, which itself contains on average 20 carbon atoms in its ester side chain. Next to UMA, in the center of Figure 3.3, the two hydroxyl functional methacrylates (HEMA and HPMA) are highlighted. HEMA features outstandingly high k_p values (often at least doubled) compared to all other methacrylates, which are assigned to strong hydrogen bonds among the monomer molecules, comparable to, e.g., methacrylic acid.[205, 208] HPMA displays significantly lower k_p values than HEMA, which are still somewhat elevated than those of UMA and other alkyl methacrylates. On the right-hand side of Figure 3.3, the joint Arrhenius fits of the families of cyclic and branched methacrylates are highlighted. Interestingly, each family – the four cyclic as well as the six branched methacrylates – can be best described by a distinct joint Arrhenius fit. As described in Chapter 2.4.2, such a procedure was reported in 2003 by Beuermann *et al.* for the cyclic methacrylates, i.e., *cyclo*-hexyl methacrylate (*c*HMA), benzyl methacrylate (BzMA), *iso*-bornyl methacrylate (*i*BoMA), and glycidyl methacrylate (GMA)[125] and was above also applied to the branched methacrylates, i.e., ethylhexyl methacrylate (EHMA), propylheptyl methacrylate (PHMA), two kinds of tridecyl methacrylates (TDA-MA and TDN-MA), heptadecyl methacrylate (C17MA), and *iso*-decyl methacrylate (*i*DeMA).[134, 183] However, inspection of Figure 3.3 and Table 3.4 demonstrates that UMA – which could be considered as a cyclic monomer similar to the group *c*HMA / BzMA / *i*BoMA / GMA – does clearly not fit into their family type behavior. Especially at low temperatures (i.e., 0°C and -50°C), UMA features a significantly higher propagation rate coefficient. This difference – compared to the cyclic methacrylates – is reflected by an activation energy that is 2 kJ·mol^{-1} lower (cf. Table 3.4). Within the pre-

exponential factors no clear trend is observable since all variances are within the typical error margins of $\pm 3 \cdot 10^6$ L·mol^{-1}·s^{-1}, beside HEMA, which features a significantly higher *A* value, reflecting the elevated k_p values.

Monomer		MW g·mol^{-1}	*A* L·mol^{-1}·s^{-1}	E_a kJ·mol^{-1}	$k_p^{50°C}$ L·mol^{-1}·s^{-1}	θ interval °C
MMA[127]	bulk	100.12	$2.67 \cdot 10^6$	22.36	650	-1 to 90
BMA[126]	bulk	142.20	$3.78 \cdot 10^6$	22.88	750	-20 to 90
DMA[126]	bulk	254.41	$2.50 \cdot 10^6$	21.02	1000	9 to 90
BeMA[134]	bulk	366.26	$2.51 \cdot 10^6$	20.52	1200	35 to 107
UMA[200]	1 M in DMAc	128.17	$2.08 \cdot 10^6$	19.89	1300	-11 to 92
HEMA[205]	bulk	130.14	$8.88 \cdot 10^6$	21.90	2600	-4 to 70
HPMA[208]	bulk[a]	144.17	$3.51 \cdot 10^6$	20.80	1500	-1 to 110
branched MAs	bulk	–	$2.82 \cdot 10^6$	21.52	950	-11 to 90
cyclic MAs[125]	bulk	–	$4.24 \cdot 10^6$	21.90	1200	-9 to 90

Table 3.4 Arrhenius parameters for k_p of UMA compared to literature data.
UMA[200] is compared to other (representative) methacrylates, depicted in Figure 3.3: methyl methacrylate (MMA),[127] butyl methacrylate (BMA),[126] dodecyl methacrylate (DMA),[126] behenyl methacrylate (BeMA)[134] as well as 2-hydroxyethyl methacrylate (HEMA),[205] hydroxpropyl methacrylate (HPMA, isomeric mixture),[208] branched methacrylates (i.e., EHMA, PHMA, TDA-MA, TDN-MA, C17MA, and *i*DeMA),[183] and cyclic methacrylates (i.e., *c*HMA, BzMA, *i*BoMA, and GMA).[125] For illustration purposes, the propagation rate coefficients at 50°C are stated alongside the molecular weight of the monomers and the temperature intervals considered in the Arrhenius fits.
[a] Combined fit with data of solutions in toluene and BnOH (benzyl alcohol, formerly abbreviated as BzOH); THF solutions feature lowered k_p values, which is assigned to coordination of THF to the hydroxyl moiety, thereby disrupting hydrogen bonding between the monomer molecules.

3.3 Overall Kinetic Behavior in Free-radical Polymerization

In addition to the PLP-SEC studies aiming at the determination of the Arrhenius parameters of the propagation reaction, free-radical batch solution polymerizations at 70°C were performed to examine how the differences in the k_p values of the monomers are reflected in the related conversion vs. time evolutions. Such a procedure is in analogy to previously performed studies, e.g., for the water-soluble monomers *n*-vinylpyrrolidone (NVP) and *n*-vinylformamide (NVF).[153, 209] Basic kinetics of FRP predict for an isothermal batch reactor with negligible volume contraction that the rate of polymerization, i.e., the change of the monomer concentration as a function of time, is given by Equation 3.1:

$$R_p = -\frac{d[\mathrm{M}]}{dt} = k_p \cdot [\mathrm{M}] \cdot \sqrt{\frac{f \cdot k_d\,[\mathrm{I}]}{k_t}} = k_\mathrm{p} \cdot [\mathrm{M}] \cdot [\mathrm{R}^\bullet] = k^{\mathrm{app}} \cdot [\mathrm{M}] \qquad 3.1$$

where [M] is the monomer concentration, k_p is the propagation rate coefficient, f is the initiator efficiency, k_d is the rate coefficient of the initiator decay, [I] is the initiator concentration, k_t is the overall rate coefficient of the termination reactions, [R$^\bullet$] is the radical concentration, and k^{app} is the apparent polymerization rate coefficient. When Equation 3.1 is integrated, it can readily be plotted in a half-logarithmic form according to the upper part of Equation 3.2.

$$\ln\left(\frac{[\mathrm{M}]_0}{[\mathrm{M}]}\right) = k^{app} \cdot t = k_p \cdot [\mathrm{R}^\bullet] \cdot t \qquad [R^\bullet] = \frac{k^{app}}{k_p} = \sqrt{\frac{f \cdot k_d\,[\mathrm{I}]}{k_t}} \qquad 3.2$$

When such a half-logarithmic ln([M]$_0$/[M]) vs. time plot features a linear evolution, the polymerization follows first-order kinetics with respect to the monomer concentration and the radical concentration remains constant throughout the polymerization process. Furthermore, via Equation 3.2 (lower part), the radical concentration allows access to an estimate of the overall termination rate coefficient via the initiator efficiency, *f*, initiator decay rate coefficient, k_d, and the initiator concentration, [I]. In a subsequent step, the above described procedure will be employed to obtain the apparent rate coefficient, the radical concentration, and an estimation of the average (low conversion) termination rate coefficient. The linear first-order plots corresponding to Equation 3.2 are presented in Figure 3.4 jointly with the conversion vs. time evolutions of the free-radical batch solution polymerizations at 70°C for different concentrations (0.2, 1.0, and 2.0 mol·L^{-1}) of UMA and HPCA in DMAc. Inspection of the conversion vs. time evolutions indicates that UMA polymerizes much slower than HPCA, which is in agreement with their k_p values at 70°C (which are 1950 L·mol^{-1}·s^{-1} and

26500 $L \cdot mol^{-1} \cdot s^{-1}$, respectively) – given that the (average) termination rate coefficient in both systems is of similar magnitude. Furthermore, the rate of polymerization increases with increasing monomer concentration, resulting in high conversions (e.g., above 70%) in a shorter time period. However, this effect is significantly more pronounced for HPCA than for UMA.

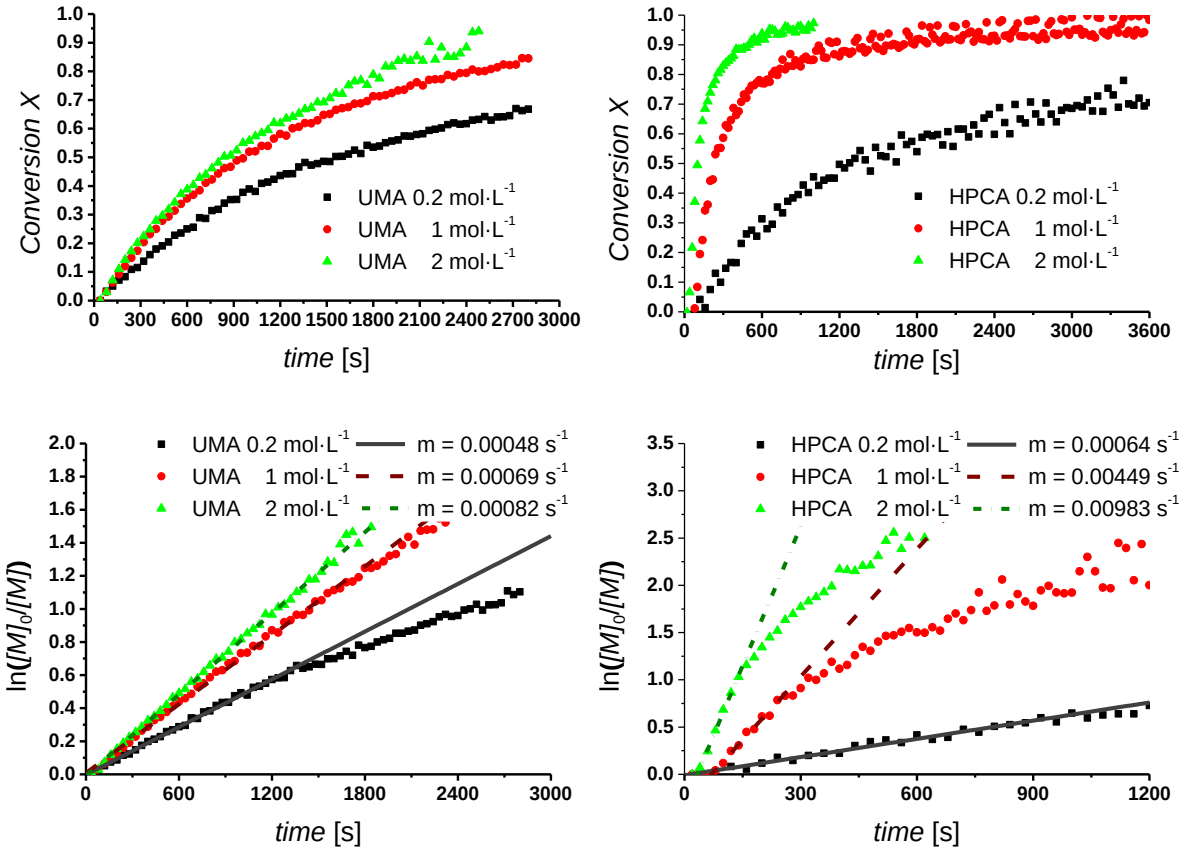

Figure 3.4 Kinetic analysis of FRP via ^{1}H-NMR at elevated temperatures for UMA and HPCA. Conversion vs. time evolutions for the FRP of UMA **(upper left)** and HPCA **(upper right)** in DMAc-d_9 solution recorded via in-situ ^{1}H-NMR spectroscopy and the corresponding linear first order analysis according to Equation 3.2 for UMA **(lower left)** and HPCA **(lower right)**. The polymerizations were executed at 70°C in DMAc-d_9 employing AIBN as initiator (12 $mmol \cdot L^{-1}$). The black squares and grey straight lines correspond to a monomer concentration of 0.2 $mol \cdot L^{-1}$, the red dots and dashed brown lines correspond to a monomer concentration of 1 $mol \cdot L^{-1}$, whereas the green triangles and dark green dotdashed lines correspond to a monomer concentration of 2 $mol \cdot L^{-1}$. The lines are linear fits of the early polymerization times (e.g., up to 150 s in the case of 2 M HPCA or up to 1800 s in the case of 1 M UMA); the corresponding slope, m, is stated in the graphs legend and is equal to the apparent polymerization rate coefficient k^{app}. The apparent polymerization rate coefficient values are summarized in Table 3.5 together with the corresponding radical concentrations and the thereof deduced estimates of the termination rate coefficients. Reprinted from ref. 200 with permission of The Royal Society of Chemistry.

Inspection of the plots according to Equation 3.2 (lower part of Figure 3.4) demonstrates that all concentrations of the methacrylate UMA fulfill the linear first-order plot up to high polymerization times, whereas this is only the case for the lowest monomer concentration (0.2 mol·L^{-1}) for the acrylic monomer HPCA. The observed deviations from linearity to lower polymerization rates are most probably caused by a decreasing radical concentration. The slope of linear fits during early polymerization times in these graphs provide access to k^{app}, [R$^{\bullet}$], and finally $\overline{k_t}$.[e] The numbers obtained by the above described kinetic analysis are collated in Table 3.5 and will be discussed in the following section.

Monomer	concentration in DMSO	[AIBN] mol·L^{-1}	k^{app} s^{-1}	[R$^{\bullet}$] mol·L^{-1}
HPCA	0.2 M	$1.20\cdot10^{-2}$	$6.40\cdot10^{-4}$	$2.42\cdot10^{-8}$
	1.0 M	$1.18\cdot10^{-2}$	$4.49\cdot10^{-3}$	$1.69\cdot10^{-7}$
	2.0 M	$1.19\cdot10^{-2}$	$9.83\cdot10^{-3}$	$3.71\cdot10^{-7}$
UMA	0.2 M	$1.17\cdot10^{-2}$	$4.80\cdot10^{-4}$	$2.46\cdot10^{-7}$
	1.0 M	$1.14\cdot10^{-2}$	$6.90\cdot10^{-4}$	$3.54\cdot10^{-7}$
	2.0 M	$1.14\cdot10^{-2}$	$8.20\cdot10^{-4}$	$4.21\cdot10^{-7}$

Monomer	$k_p^{70°C}$ L·mol^{-1}·s^{-1}	average [I] mol·L^{-1}	average [R$^{\bullet}$] mol·L^{-1}	$\overline{k_t}$ L·mol^{-1}·s^{-1}
HPCA	26500	$1.19\cdot10^{-2}$	$1.88\cdot10^{-7}$	$2.16\cdot10^{6}$
UMA	1950	$1.15\cdot10^{-2}$	$3.40\cdot10^{-7}$	$6.38\cdot10^{5}$

Table 3.5 Summary of the kinetic analysis according to Equation 3.2 for UMA and HPCA.
The apparent polymerization rate coefficient equals the slope of the linear fittings in Figure 3.4 (lower part). The radical concentration [R$^{\bullet}$] is derived with the aid of the $k_p^{70°C}$ value according to the Equation 3.2. The arithmetical averages of the initiator concentration and radical concentration were employed to calculate an estimate of the overall average termination rate coefficient $\overline{k_t}$ under the assumption of an initiator efficiency of 0.13, as recommended in Ref. 210 for systems with an elevated viscosity.

As noted above, the apparent polymerization rate coefficient can be employed to derive the active radical concentration, which is typically in the range of 10^{-7} mol·L^{-1}. The radical concentration is increasing with increasing monomer concentration as the values in Table 3.5

[e] The herein determined average termination rate coefficients are termed as $\overline{k_t}$ in order to make a distinction to the $<k_t>$ values accessible via the SP-PLP method (cf. Chapter 1.5). Both values are average values with respect to the chain length of the terminating macromolecules. However, $\overline{k_t}$ is additionally the average value over the initial conversion regime and several monomer concentrations, whereas $<k_t>$ describes the conversion and monomer concentration independent termination rate coefficient (determined in an ideally infinitesimal small conversion range).

demonstrate. The probability of a radical encountering a monomer unit increases with increasing monomer concentration, thus more radicals can be present in the polymerization mixture without undergoing termination. In order to arrive at an estimate of the overall average termination rate coefficient, the initiator concentration and the radical concentration were averaged and the resulting values used as input into Equation 3.2. As a further input parameter the initiator efficiency is required, which is typically in the range of 0.6 to 0.7 (e.g., for bulk polymerization of styrene).[211] However, for polymerization systems with elevated viscosity, such as dodecyl acrylate, the initiator efficiency is reported to be as small as 0.13 and even decreasing with increasing conversion, since the systems viscosity is further increased as the polymerization progresses.[210] The currently investigated monomer solutions in DMAc (η = 1.02 mPa·s)[212] feature a high viscosity, which is rather similar to dodecyl acrylate (studied as 1.5 M solution in toluene featuring η = 1.15 mPa·s)[20] than to styrene (η = 0.76 mPa·s).[213] Therefore, the value of f = 0.13 as reported by Charton *et al.*[210] is employed to obtain average $\bar{k}_t$ values of $2.16 \cdot 10^6$ L·mol^{-1}·s^{-1} for HPCA and $6.38 \cdot 10^5$ L·mol^{-1}·s^{-1} for UMA. The herein obtained average $\bar{k}_t$ values are distinctly lower than the typically observed termination rate coefficients for monomers such as styrene,[214] methyl acrylate,[20] or methyl methacrylate[171] (in bulk), which typically feature values in the range between 10^7 and 10^8 L·mol^{-1}·s^{-1} for the average termination rate coefficient (the corresponding unimer-unimer termination rate coefficients read for methyl acrylate (MA) $k_t^{1,1} \sim 3 \cdot 10^8$ L·mol^{-1}·s^{-1}; for butyl acrylate (BA) $k_t^{1,1} \sim 1 \cdot 10^8$ L·mol^{-1}·s^{-1} and for dodecyl acrylate (DA) $k_t^{1,1} \sim 3 \cdot 10^7$ L·mol^{-1}·s^{-1}).[20] According to the Stokes-Einstein equation and the Smoluchowski equation, the termination rate coefficient is a function of the hydrodynamic radius, r_1, and of the dynamic viscosity, η, (which should be understood as the microviscosity or solvent viscosity), i.e., $k_t^{1,1} \propto (r_1 \cdot \eta)^{-1}$.[20] The available data for termination rate coefficients confirms the expected correlation: The higher the viscosity and the higher the

hydrodynamic radius, the lower the termination rate coefficient (cf. the $k_t^{1,1}$ values stated above for MA, BA, and DA). However, having the above described findings in mind, the distinctly lower $\overline{k_t}$ values are in perfect agreement with the expectations: As stated above, the DMAc solutions of HPCA and UMA feature elevated viscosities; thus, the corresponding termination rate coefficients should be similar to that of dodecyl acrylate for instance. However, in the case of HPCA, a further contribution to the decreased $\overline{k_t}$ value has to be considered: In acrylate polymerizations the formation of mid-chain radicals (MCR) is frequently occurring and MCRs are believed to possess lower termination rate coefficients.[11] UMA features an even lower $\overline{k_t}$ value ($6.38 \cdot 10^5$ L·mol^{-1}·s^{-1}) as HPCA, a decrease which is – perhaps coincidentally – also found when going from dodecyl acrylate ($k_t^{1,1}$ ~ $3 \cdot 10^7$ L·mol^{-1}·s^{-1})[20] to dodecyl methacrylate ($k_t^{1,1}$ ~ $1 \cdot 10^7$ L·mol^{-1}·s^{-1}).[173]

In summary, the herein determined – relatively low – estimates of the average termination rate coefficients, $\overline{k_t}$, can be understood by the increased viscosity of the reaction medium for UMA and HPCA, when compared to monomers such as styrene, methyl methacrylate, or methyl acrylate.[24]

3.4 Application in Reversible-Deactivation Radical Polymerization (RDRP)

In order to obtain an all-encompassing picture of the polymerization behavior of UMA and HPCA, these monomers were additionally polymerized via RDRP techniques such as reversible addition-fragmentation chain transfer (RAFT) polymerization and nitroxide-mediated polymerization (NMP). For the RAFT polymerization of the acrylic monomer (i.e., HPCA) CPDA and DoPAT were employed as chain transfer agents, whereas CPDB features suitable R and Z groups for methacrylates and was therefore employed for UMA. In the NMP experiments for both monomers, MAMA-SG1 (also known as: MAMA-DEPN) was

employed as unimolecular initiator and controlling agent in combination with a slight excess of the controlling agent SG1 (i.e., DEPN). The structures of the employed NMP and RAFT reagents are displayed in Scheme 3.2 along with their systematic names and the monomer structures are depicted above in Scheme 3.1. It should be noted that it was in some cases not possible to re-dissolve polyUMA and polyHPCA in DMAc after precipitation (especially when the polymer samples were dried/stored over an extended time period). Such a behavior

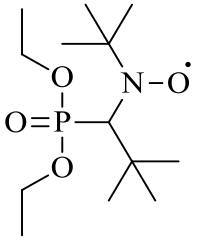

2-((*tert*-butyl(1-(diethoxyphosphoryl)-2,2-dimethylpropyl)amino)oxyl)
SG1 / DEPN

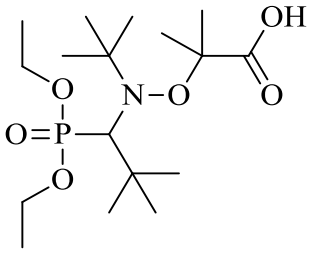

2-((*tert*-butyl(1-(diethoxyphosphoryl)-2,2-dimethylpropyl)amino)oxy)-2-methylpropanoic acid
MAMA-SG1 / MAMA-DEPN

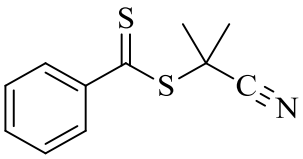

2-cyanopropan-2-yl benzodithioate
cyanopropyl dithiobenzoate
CPDB

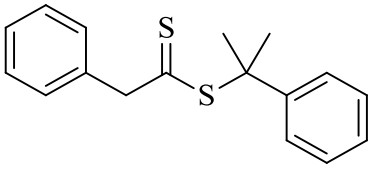

2-phenylpropan-2-yl 2-phenylethanedithioate
cumylphenyldithioacetate
CPDA

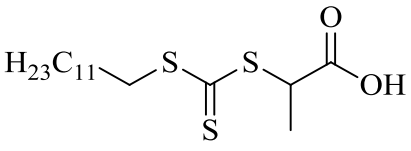

2-(dodecylthiocarbonothioylthio)propanoic acid
dodecyl *iso*-propionic acid trithiocarbonat
DoPAT

Scheme 3.2 Herein employed RAFT and NMP controlling agents.
Structures of the chain transfer agents (CTA) CPDB, CPDA, and DoPAT as well as the employed NMP reagents SG1 and MAMA-SG1 are depicted. MAMA-SG1 functions as unimolecular initiator and controlling agent. The systematic names are displayed below the corresponding structures. Reprinted from ref. 200 with permission of The Royal Society of Chemistry.

may be caused by the formation of hydrogen bonds during a possible stacking process along the lateral polymer chain that cannot be energetically re-compensated by the solvent (i.e., DMAc). Such a behavior has for instance been reported for polyNiPAAM[215] or poly(*N*,*N*-diethylacrylamide)-based polymers.[216]

Initially, the results of the RDRP experiments obtained with UMA in NMP and RAFT polymerization are discussed. Thereafter, the RDRP results acquired for HPCA as the monomer are reported. The SEC traces obtained in polymerizations targeting approx. 35000 g·mol^{-1} via NMP and RAFT are depicted in Figure 3.5. In the NMP experiment, a small amount of a comonomer, i.e., 9 mol% styrene, was employed – as it is required for an effective control in the NMP of methacrylates[217] – in order to gain/improve the control over the polymerization outcome. In the RAFT polymerization, CPDB – especially suitable for methacrylates[35] – was employed as the controlling agent. The SEC trace evolutions, obtained for both RDRP techniques, exhibit clear and uniform shifts of the molar mass distributions without developing a shoulder, neither in the high molar mass range, which would indicate a

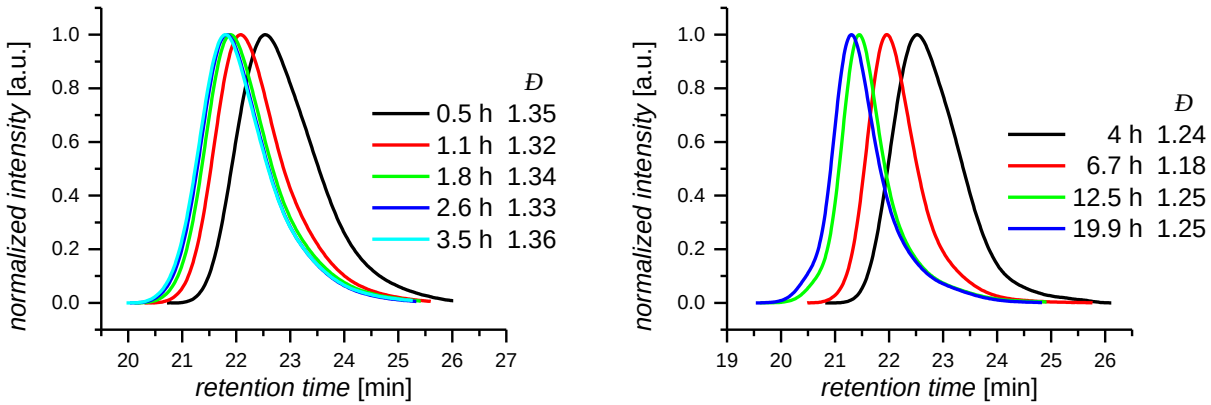

Figure 3.5 Exemplary SEC traces acquired via RDRP of UMA.
Normalized SEC traces acquired in **(left hand side)** the NMP of UMA (172 eq.) targeting a M_n of 36000 g·mol^{-1} employing MAMA-SG1 (1 eq.) as the NMP agent and a slight excess of the controlling agent SG1 (0.09 eq.) in combination with the comonomer styrene (15 eq.) at 90°C in DMAc solution (2:1 w/w) and **(right hand side)** the RAFT polymerization of UMA (172 eq.) targeting a M_n of 34000 g·mol^{-1} employing CPDB (1 eq.) as the CTA and AIBN (0.2 eq.) as initiator at 60°C in DMAc solution (2:1 w/w). The dispersity values of the polymer samples (all in the range of $Đ$ = 1.35 for NMP and $Đ$ = 1.25 for RAFT) are stated in the legend jointly with the associated polymerization times. Reprinted from ref. 200 with permission of The Royal Society of Chemistry.

significant extent of termination via recombination, nor in the low molar mass range, which would indicate a significant loss of chain end functionality. Such a uniform shifting is an important key feature of a controlled polymerization exhibiting living characteristics.

As a further demonstration of the controlled characteristics of the NMP and RAFT polymerizations employing UMA as monomer, Figure 3.6 and Figure 3.7 are highlighted. The Figures depict, beside the conversion vs. time evolutions and the corresponding kinetic analysis according to Equation 3.2, the M_n vs. conversion evolutions obtained in NMP and RAFT polymerizations targeting molar masses of approx. 5000 $g \cdot mol^{-1}$ and 35000 $g \cdot mol^{-1}$ (detailed experimental conditions are stated in the captions of Figure 3.6 and Figure 3.7). The conversion vs. time evolutions of the RAFT polymerizations (cf. Figure 3.6) feature an inhibition period before the polymerization proceeds to almost complete conversion. The kinetic analysis indicates that the polymerization follows first-order kinetics in monomer concentration and that the radical concentration remains constant by maintaining a linear characteristic up to long polymerization times, where high conversion values are reached. Correspondingly, the M_n vs. conversion evolutions feature almost exactly the same slope as the theoretical evolution, even though a small hybrid effect can be observed.[218] The controlled characteristics are further underpinned by the dispersity values of the collected samples, which are all in the range of $Đ = 1.2$. A similar situation is demonstrated by Figure 3.7 for the NMP experiments employing a small amount of styrene as comonomer. The polymerization proceeds relatively fast, yielding 75% conversion in less than 2 hours. In the kinetic analysis according to Equation 3.2, significant deviations from linearity to lower values are observed in the high conversion regime ($X \geq 75\%$). However, the M_n vs. conversion evolutions feature a clear linear behavior with only a slightly decreased slope compared to the theoretical evolution. Similar to the RAFT polymerizations, the dispersity values of the collected samples additionally underpin the controlled characteristics, featuring values of approx. $Đ = 1.35$, which are in the typically observed range for NMP experiments.[37]

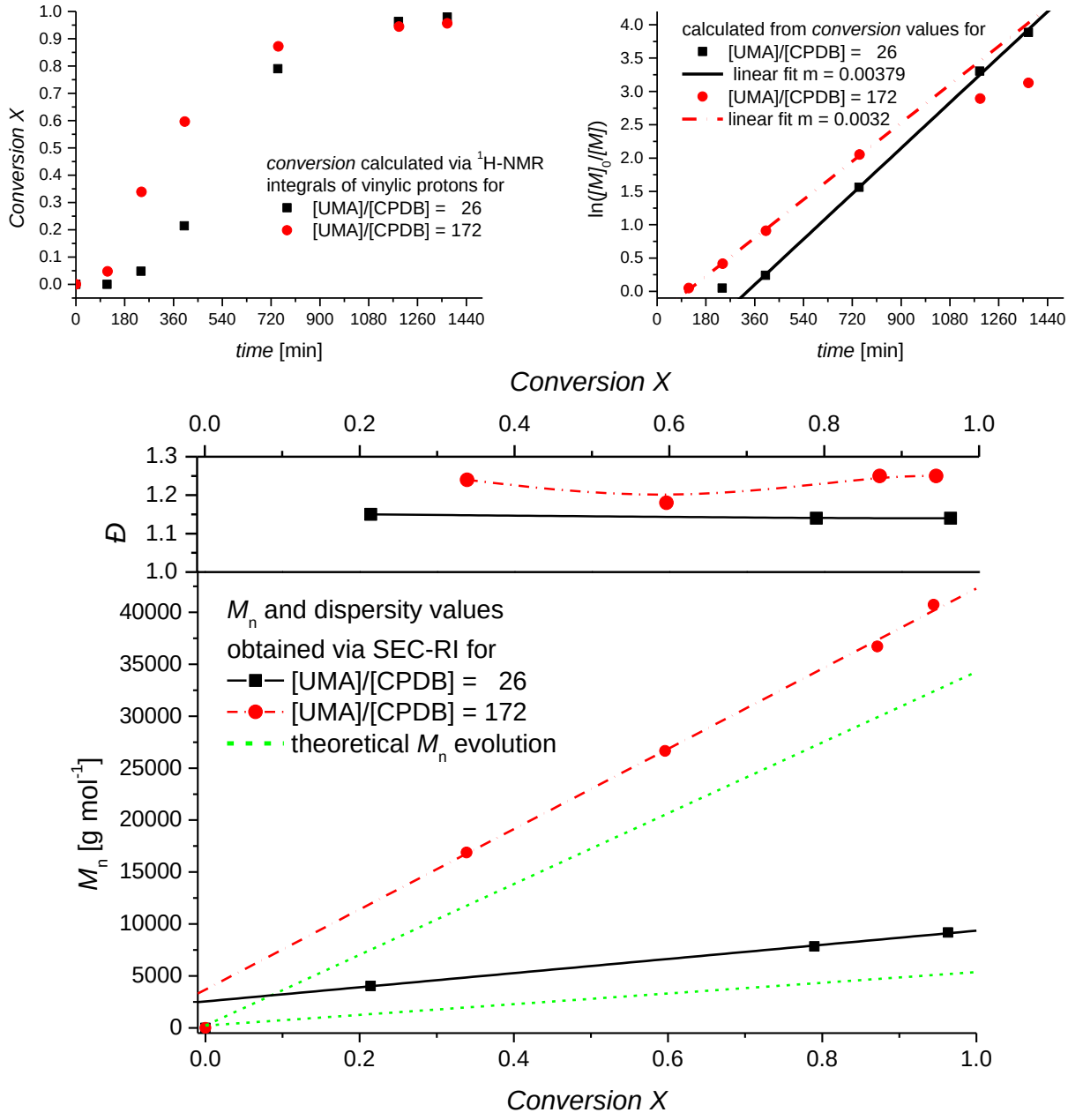

Figure 3.6 Kinetic analysis of RAFT polymerization employing UMA.
Conversion vs. time evolution determined by ^{1}H-NMR spectroscopy **(upper left hand side)** and the corresponding linear first-order plot according to Equation 3.2 **(upper right hand side)** for the RAFT polymerizations of UMA (26 eq. and 172 eq., respectively) in DMSO (2:1 w/w) at 60°C. The polymerization mixture contains AIBN (0.2 eq.) and CPDB (1 eq.) as CTA. The initial inhibition period, when no polymerization is taking place, can readily be recognized in the conversion vs. time evolution followed by ^{1}H-NMR spectroscopy. The kinetic analysis yields apparent polymerization rate coefficients of $k^{app} = 6.33 \cdot 10^{-5}$ L·mol^{-1}·s^{-1} (26 eq. UMA) and $k^{app} = 4.17 \cdot 10^{-5}$ L·mol^{-1}·s^{-1} (172 eq. UMA) corresponding to a radical concentration of $[R^{\bullet}] = 3.96 \cdot 10^{-8}$ mol·L^{-1} (26 eq. UMA) and $[R^{\bullet}] = 2.60 \cdot 10^{-8}$ mol·L^{-1} (172 eq. UMA) resulting in average overall termination rate coefficients of $\overline{k_t} = 1.28 \cdot 10^{7}$ L·mol^{-1}·s^{-1} (26 eq. UMA) and $\overline{k_t} = 4.35 \cdot 10^{6}$ L·mol^{-1}·s^{-1} (172 eq. UMA). An exemplary critical comparison of the $\overline{k_t}$ values obtained from RAFT polymerizations with the ones obtained from FRP is on page 109 for the values obtained with HPCA. Additionally, the M_n vs. conversion evolutions **(lower part)** are depicted in combination with the corresponding dispersity values. The linear fits of M_n vs. conversion evolution feature almost exactly the same slopes as their corresponding theoretical evolutions. The lines connecting the dispersity values are solely for guiding the eye; they are no fits. Reprinted from ref. 200 with permission of The Royal Society of Chemistry.

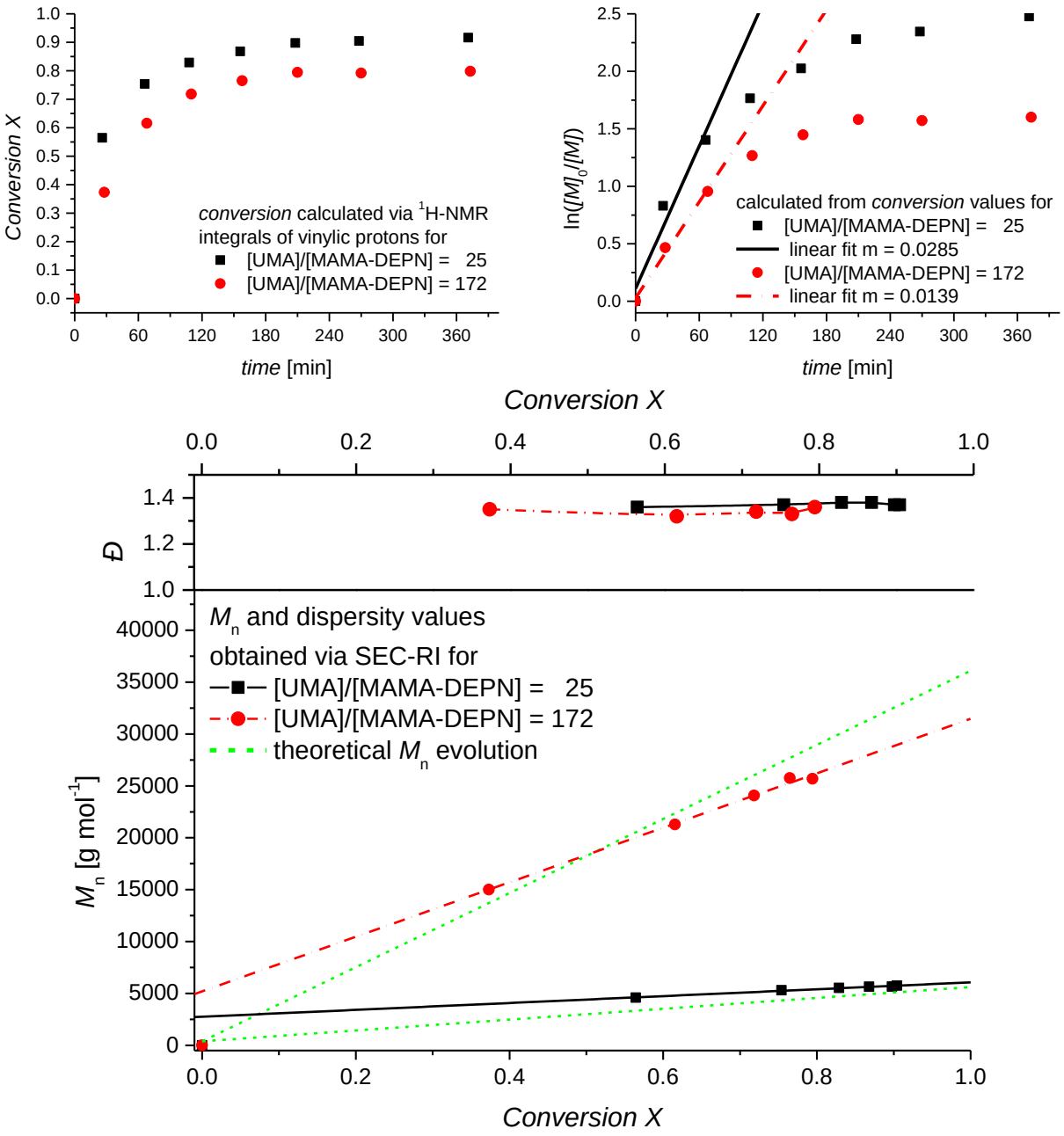

Figure 3.7 Kinetic analysis of NMP employing UMA.
Conversion vs. time evolution determined by ^{1}H-NMR spectroscopy **(upper left)** and the corresponding linear first-order plot according to Equation 3.2 **(upper right)** for the NMP experiments with UMA (25 eq. and 172 eq., respectively) in DMSO (2:1 w/w) at 90°C employing styrene (2 eq. and 15 eq., respectively) as a controlling comonomer. The polymerization mixture contains MAMA-SG1 (1 eq.) and SG1 (0.09 eq.). The kinetic analysis yields apparent polymerization rate coefficients of $k^{app} = 4.75 \cdot 10^{-4}$ L·mol^{-1}·s^{-1} (25 eq. UMA) and $k^{app} = 2.32 \cdot 10^{-4}$ L·mol^{-1}·s^{-1} (172 eq. UMA) corresponding to a radical concentration of $[R^{\bullet}] = 2.08 \cdot 10^{-8}$ mol·L^{-1} (25 eq. UMA) and $[R^{\bullet}] = 1.02 \cdot 10^{-8}$ mol·L^{-1} (172 eq. UMA) resulting in average overall termination rate coefficients of $\overline{k_t} = 2.35 \cdot 10^{8}$ L·mol^{-1}·s^{-1} (25 eq. UMA) and $\overline{k_t} = 1.47 \cdot 10^{8}$ L·mol^{-1}·s^{-1} (172 eq. UMA). An exemplary critical comparison of the $\overline{k_t}$ values obtained from RAFT polymerizations with the ones obtained from FRP is on page 109 for the values obtained with HPCA. Additionally, the M_n vs. conversion evolutions **(lower part)** are depicted in combination with the corresponding dispersity values. The linear fits of the M_n vs. conversion evolution feature slightly decreased slopes as their corresponding theoretical evolutions. The lines connecting the dispersity values are solely for guiding the eye; they are no fits. Reprinted from ref. 200 with permission of The Royal Society of Chemistry.

After the discussion of the application of UMA in RAFT and NMP, the investigation of the RDRP applicability is now proceeded for HPCA, which was also successfully polymerized via the NMP as well as the RAFT technique. In the case of HPCA, the CTAs CPDA and DoPAT were employed since they feature R and Z groups that are appropriate for an acrylate.[35] For the polymerization employing CPDA as the CTA, an almost ideal linear evolution of the M_n with conversion was observed, which is a key property of a controlled polymerization featuring living characteristics (depicted in the upper left hand part of Figure 3.8).

The M_n values were determined via the RI detector of the SEC set-up employing poly(styrene) MHKS parameters resulting in an effective calibration, since the molar mass range is too limited to be reliably determined via a MALLS detector. The corresponding SEC traces are displayed in the lower part of Figure 3.8. The conversion values were determined via integration of the resonances associated with the vinylic protons (detailed procedure and chemical shifts are stated in the Experimental Section on page 123) in the in-situ measured ^{1}H-NMR spectra (every 100 s) at the same elevated temperature (i.e., 60°C) as the corresponding batch polymerizations. The resulting conversion vs. time evolution (cf. Figure 3.8 lower part) was correlated with the M_n vs. time evolution whilst taking the differing inhibition periods into account (approx. 18 min in the case of the polymerization in the NMR spectroscope vs. approx. 23 min in the case of the batch polymerizations). The initial inhibition period, when no polymerization is taking place, can readily be recognized in the conversion vs. time evolution recorded via ^{1}H-NMR spectroscopy (cf. Figure 3.8 lower part).

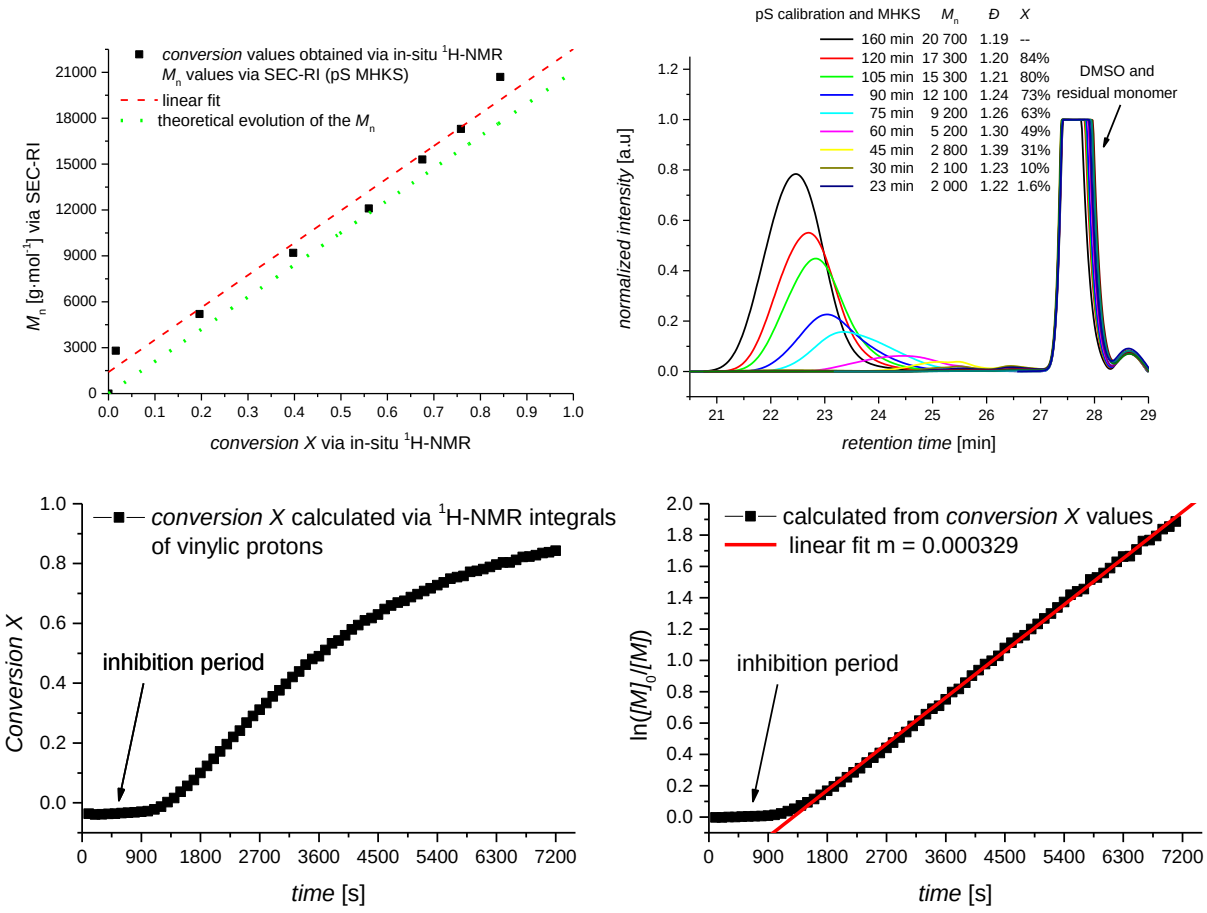

Figure 3.8 Kinetic analysis of the RAFT polymerization employing HPCA.
Upper left hand part: Evolution of the number-average molar mass, M_n, with the monomer conversion obtained from the RAFT polymerization of HPCA at 60°C in DMSO employing CPDA as CTA. The M_n values were determined via SEC-RI employing poly(styrene) MHKS parameters in the effective calibration. The conversion values were determined via integration of the resonance associated with the vinylic protons in the ^{1}H NMR spectra. A difference in the inhibition period between the polymerization in the NMR spectroscope (approx. 18 min) and the batch polymerization in the flask (approx. 23 min) was compensated. The experimental procedure is described in detail in the Experimental Section on page 123. SEC-RI traces **(upper right hand part)** and conversion vs. time evolution recorded via ^{1}H-NMR spectroscopy **(lower left hand part)** for the RAFT polymerizations of HPCA (100 eq.) in DMSO (2:1 w/w) at 60°C. The polymerization mixture contains furthermore AIBN (0.1 eq.) and CPDA (1 eq.) as CTA. The initial inhibition period, when no polymerization is taking place, can readily be recognized in the conversion vs. time evolution recorded via ^{1}H-NMR spectroscopy. Additionally, the linear first-order plot according to Equation 3.2 is depicted **(lower right hand part)**, resulting in an apparent polymerization rate coefficient $k^{app} = 3.29 \cdot 10^{-4}$ L·mol^{-1}·s^{-1} corresponding to a radical concentration of $[R^\bullet] = 1.44 \cdot 10^{-8}$ mol·L^{-1} and an average overall $\overline{k_t} = 1.82 \cdot 10^7$ L·mol^{-1}·s^{-1}. The critical comparison of the $\overline{k_t}$ values obtained from RAFT polymerization with the ones obtained from FRP is given on page 109. Reprinted from ref. 200 with permission of The Royal Society of Chemistry.

In the lower part of Figure 3.8 the kinetic analysis according to Equation 3.2 is additionally depicted resulting in an apparent polymerization rate coefficient $k^{app} = 3.29 \cdot 10^{-4}$ L·mol^{-1}·s^{-1} corresponding to a radical concentration of $[R^\bullet] = 1.44 \cdot 10^{-8}$ mol·L^{-1} and an average $\overline{k_t}$ of $1.82 \cdot 10^7$ L·mol^{-1}·s^{-1}. The radical concentration $[R^\bullet]$ (here: for RAFT at 60°C) is almost

one order of magnitude lower than in the FRP experiments described above (at 70°C) and consequently the related overall average termination rate coefficient is one order of magnitude increased compared to the FRP (cf. Table 3.5). The increased average termination rate coefficient can be understood by invoking the composite model for termination: the RAFT process limits the radical chain length to lower values (especially at low conversion), resulting in an average chain length which is smaller than the one observed during conventional FRP. In fact, this feature has been made ample use of to determine the chain length dependency of the termination rate coefficient via the RAFT chain length dependent termination (RAFT-CLD-T) method.[21-23, 27] Herein, the chain length discrepancy between the free-radical and the RAFT-mediated processes is manifested in an overall higher average $\overline{k_t}$ value. In the FRP process an approximate chain length of 300–500 repeat units (i.e., M_n of approx. 60000 to 100000 g·mol^{-1}) is reached, while the kinetic analysis of the RAFT process considered for deducing $\overline{k_t}$ spans a chain length regime from 1 to 75 repeat units (i.e., $M_n \leq 15000$ g·mol^{-1}). Based on an approximate composite model for dodecyl acrylate,[20] a reduction in chain length from 300 to 75 corresponds to a decrease in the termination rate coefficient of approx. one order of magnitude. It is important to note that the above stated rationale should not be over interpreted, as it represents an estimation of qualitative nature, yet rationalizes the obtained data.

In a next step, a chain extension experiment employing polyHPCA macromolecular CTA (macroCTA) generated via RAFT is presented to underpin the living characteristics of the RDRP (cf. Figure 3.9). The macroCTA was generated at 60°C employing DoPAT as the CTA in 30 min polymerization time resulting in a polymer featuring a number-average molar mass of M_n = 11000 g·mol^{-1} and a dispersity of $Đ$ = 1.3. The DoPAT-based polyHPCA was isolated by precipitation in water and dried. Subsequently, it was employed as a macroCTA for the polymerization of methyl acrylate (MA), yielding in a block copolymer featuring a M_n = 37500 g·mol^{-1} and a dispersity of $Đ$ = 1.3 after 1 hour polymerization time at 60°C and

M_n = 53000 g·mol^{-1} ($Đ$ = 1.5) after 3 hours. The clear shift of the molecular mass distribution can be readily recognized by inspection of Figure 3.9; merely a minor tailing on the low-molar-mass side of the block copolymer may be detected. Via the employment of CPDA (for kinetic analysis) and DoPAT (chain extension) as CTAs, it is evidenced that the polymerization of HPCA can be controlled by several standard RAFT controlling agents.

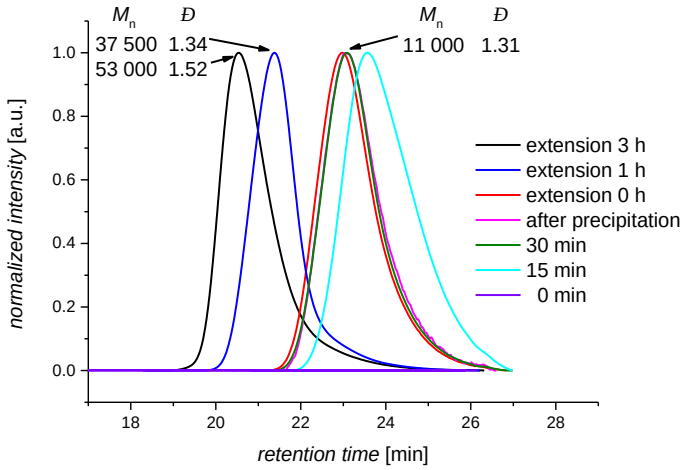

Figure 3.9 Exemplary SEC traces acquired in the chain extension experiment of HPCA with methyl acrylate (MA).
HPCA was polymerized with DoPAT as the CTA and AIBN as the initiator at 60°C in DMAc solution (2:1 w/w). The macroCTA was isolated by precipitation in water, dried, and subsequently re-dissolved in DMAc together with the new monomer MA and additional AIBN to be polymerized at 60°C. The SEC traces of the polymer after 30 min reaction time and after precipitation (i.e., the isolated macroCTA) are cloaking each other since they are virtually the same. Reprinted from ref. 200 with permission of The Royal Society of Chemistry.

➔

Figure 3.10 Exemplary SEC traces acquired during the NMP of HPCA.
A M_n of 5000 g·mol^{-1} **(upper part)**, 35000 g·mol^{-1} **(middle part)**, and 70000 g·mol^{-1} **(lower part)** is targeted by employing 31 eq. (or 203 eq. or 406 eq., respectively) HPCA with MAMA-SG1 (1 eq.) as the NMP agent and a slight excess of the controlling agent SG1 (0.085 eq.) at 110°C in DMAc solution (2:1 w/w). The dispersities of the polymer ($Đ$ > 1.5 in the middle and lower part) are stated in the legend jointly with the related polymerization time. Despite the fact that some dispersities feature values clearly above $Đ$ = 1.5, a clear and uniform shift of the polymer signal can be observed. The elevated dispersities may be associated with the evaluation of the SEC traces employing poly(styrene) MHKS in lack of pHPCA specific MHKS parameters. The traces in the upper part are normalized to their maximum peak, which is initially the monomer signal close to 28 min retention time and towards the end of the polymerization the polymer signal close to 24 min retention time, whereas the traces in the middle and lower part are normalized to their polymer peak (around 22 min retention time) in order to emphasize the decreasing monomer content. Reprinted from ref. 200 with permission of The Royal Society of Chemistry.

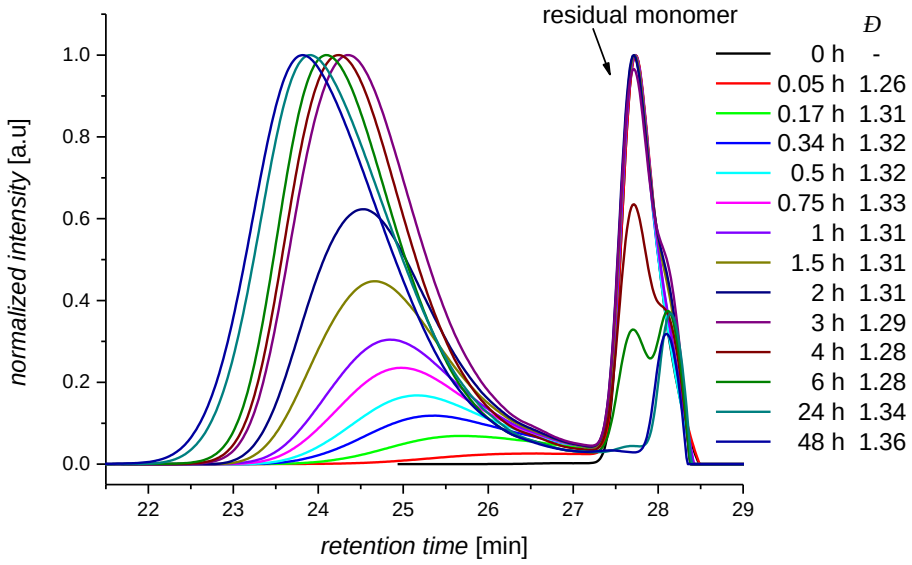
residual monomer
Đ
0 h -
0.05 h 1.26
0.17 h 1.31
0.34 h 1.32
0.5 h 1.32
0.75 h 1.33
1 h 1.31
1.5 h 1.31
2 h 1.31
3 h 1.29
4 h 1.28
6 h 1.28
24 h 1.34
48 h 1.36
normalized intensity [a.u]
retention time [min]

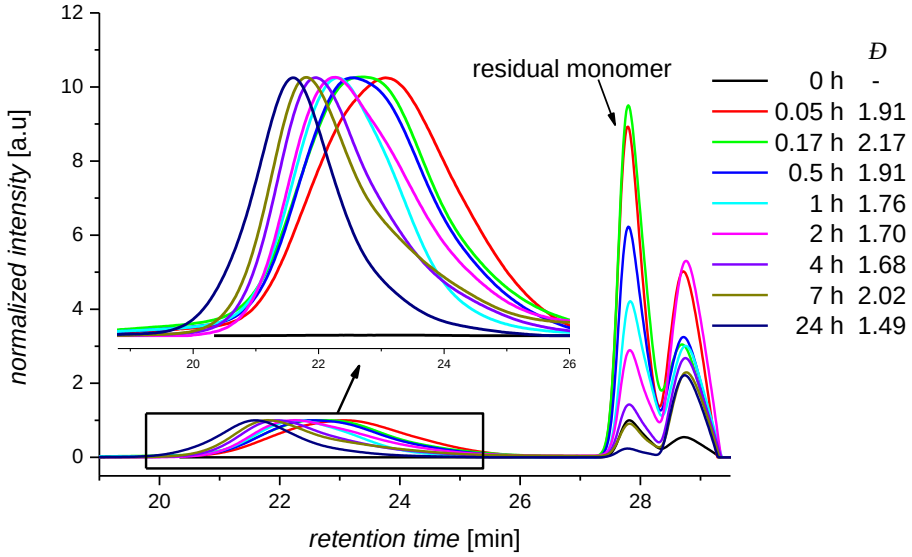
residual monomer
Đ
0 h -
0.05 h 1.91
0.17 h 2.17
0.5 h 1.91
1 h 1.76
2 h 1.70
4 h 1.68
7 h 2.02
24 h 1.49
normalized intensity [a.u]
retention time [min]

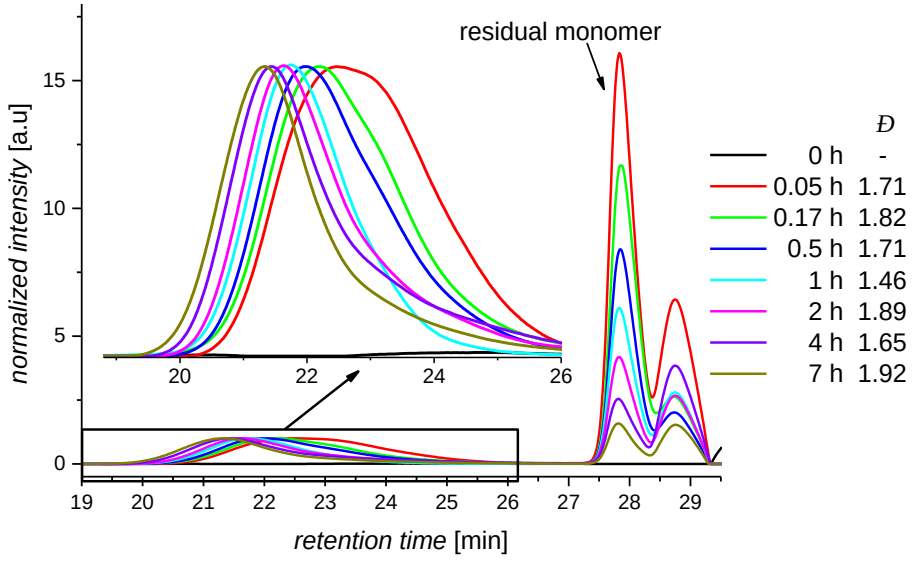
residual monomer
Đ
0 h -
0.05 h 1.71
0.17 h 1.82
0.5 h 1.71
1 h 1.46
2 h 1.89
4 h 1.65
7 h 1.92
normalized intensity [a.u]
retention time [min]

Finally, the investigation of the RDRP applicability of HPCA is concluded with its application in NMP focusing on the synthesis of HPCA homopolymers and copolymers of HPCA and styrene featuring various molar masses (approx. 5000 g·mol^{-1}, 35000 g·mol^{-1}, and 70000 g·mol^{-1}). The copolymerizations of HPCA and styrene were performed in analogy to the NMP experiments for UMA and in order to highlight the adaptability of HPCA as monomer. In order to obtain detailed information about the NMP process, samples for SEC analysis were collated after pre-defined polymerization times within short intervals. Figure 3.10 highlights the SEC traces acquired during the NMP of HPCA, targeting a M_n of 5000 g·mol^{-1} as well as 35000 g·mol^{-1} and 70000 g·mol^{-1} at full conversion. Additionally, the SEC traces obtained from the copolymerizations of HPCA and styrene (10:1 mol/mol) are included in Figure 3.11. Each evolution of the SEC traces throughout the polymerization time exhibits a clear and uniform shift of the polymer signal and a significant decrease in the intensity of the signal related to the monomer. As noted above (in the context of the RDRP of UMA), such a uniform shift is a key feature of a controlled polymerization featuring living characteristics. As a clear proof for the latter, a chain extension experiment is performed via the NMP technique: Figure 3.12 demonstrates that polyHPCA macromolecules (SG1-capped and radicals) are able to polymerize additionally added *n*-butyl acrylate, thereby resulting in a copolymer.

➔

Figure 3.11 Exemplary SEC traces acquired during the NMP of HPCA and styrene.
A M_n of 5000 g·mol^{-1} **(upper part)**, 35000 g·mol^{-1} **(middle part)**, and 70000 g·mol^{-1} **(lower part)** is targeted by employing 23 eq. (or 157 eq. or 366 eq., respectively) HPCA and 10 eq. (or 29 eq. or 67 eq.) styrene with MAMA-SG1 (1 eq.) as the NMP agent and a slight excess of the controlling agent SG1 (0.085 eq.) at 110°C in DMAc solution (2:1 w/w). The dispersities of the polymer ($Đ$ > 1.5 in the middle and lower part) are stated in the legend jointly with the related polymerization time. Despite the fact that some dispersities feature values clearly above $Đ$ = 1.5, a clear and uniform shift of the polymer signal can be observed. The elevated dispersities may be associated with the evaluation of the SEC traces employing poly(styrene) MHKS in lack of pHPCA specific MHKS parameters. The traces in the upper part are normalized to their peak maximum, which is initially the monomer signal close to 28 min retention time and towards the end of the polymerization the polymer signal close to 24 min retention time, whereas the traces in the middle and lower part are normalized to their polymer peak (around 22 min retention time) in order to emphasize the decreasing monomer content. Reprinted from ref. 200 with permission of The Royal Society of Chemistry.

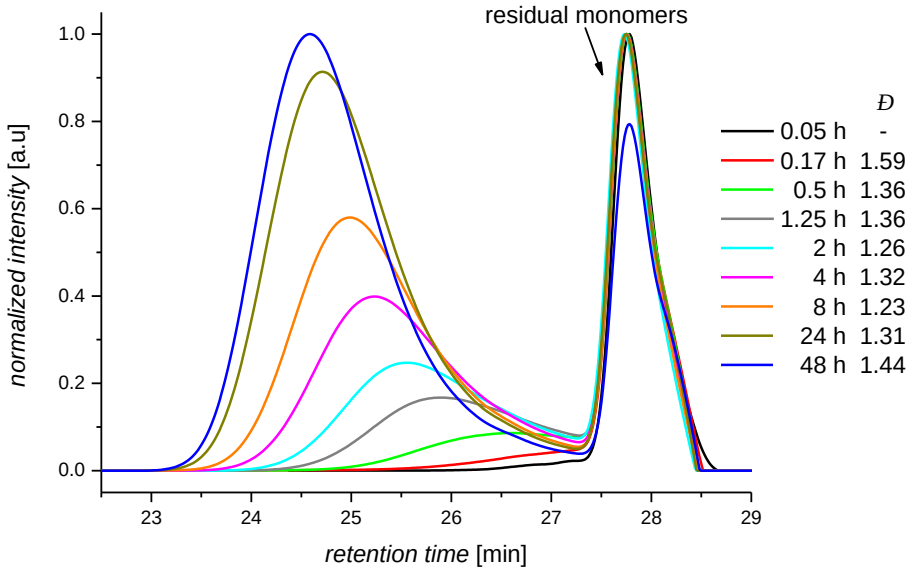
residual monomers
normalized intensity [a.u]
retention time [min]
Đ
0.05 h -
0.17 h 1.59
0.5 h 1.36
1.25 h 1.36
2 h 1.26
4 h 1.32
8 h 1.23
24 h 1.31
48 h 1.44

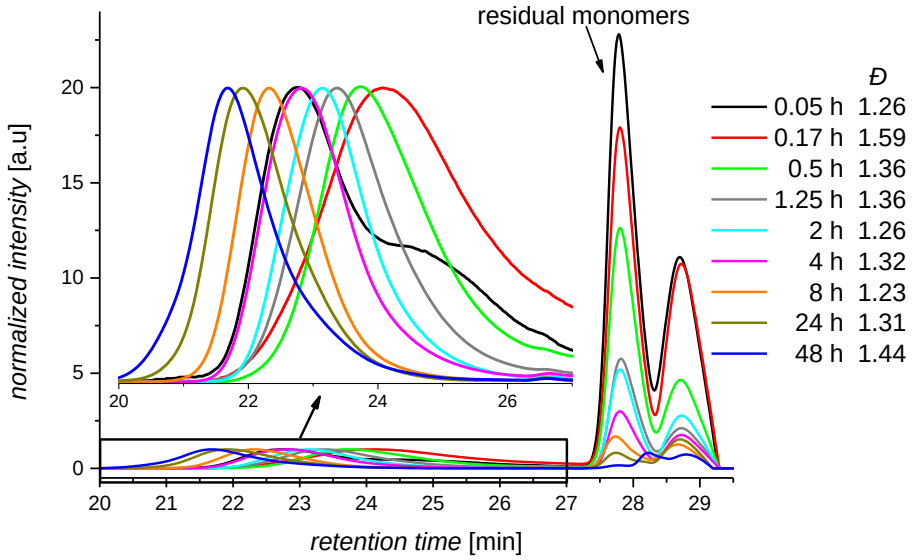
residual monomers
normalized intensity [a.u]
retention time [min]
Đ
0.05 h 1.26
0.17 h 1.59
0.5 h 1.36
1.25 h 1.36
2 h 1.26
4 h 1.32
8 h 1.23
24 h 1.31
48 h 1.44

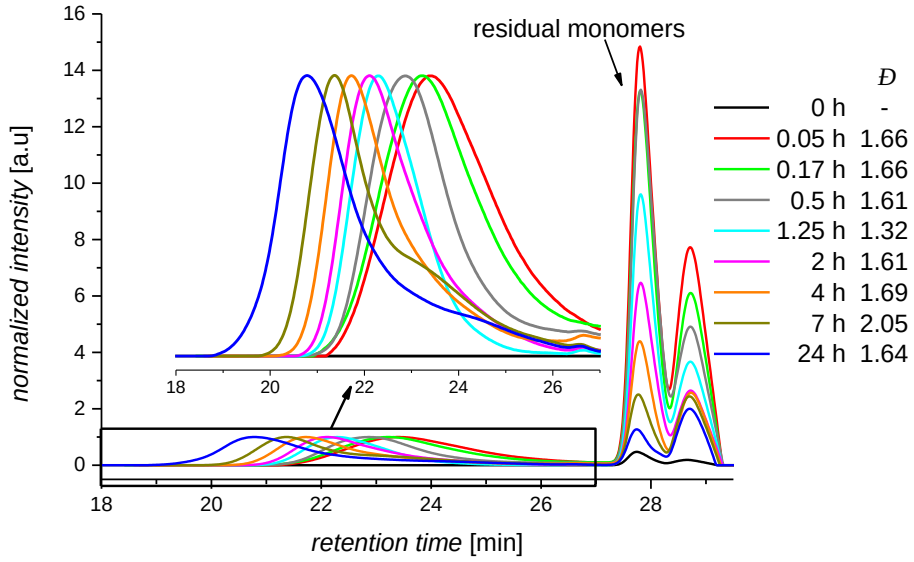
residual monomers
normalized intensity [a.u]
retention time [min]
Đ
0 h -
0.05 h 1.66
0.17 h 1.66
0.5 h 1.61
1.25 h 1.32
2 h 1.61
4 h 1.69
7 h 2.05
24 h 1.64

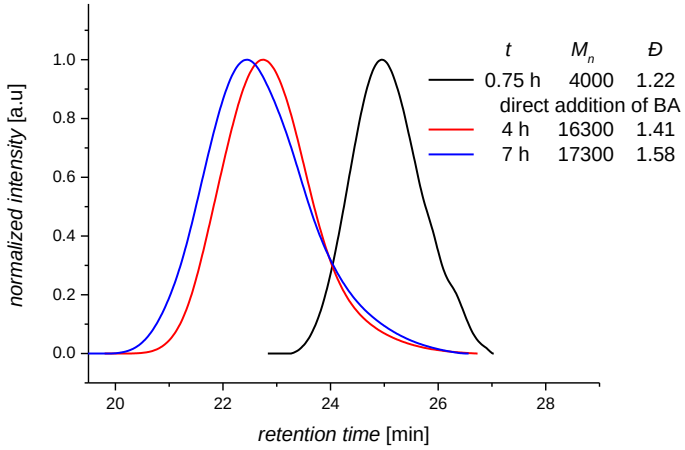

Figure 3.12 Exemplary SEC traces acquired in the chain extension experiment of HPCA with butyl acrylate (BA).
HPCA (50 eq., M_n^{theo} = 9900 g·mol^{-1}) was polymerized with MAMA-SG1 (1 eq.) and a slight excess of SG1 at 110°C in DMAc solution (2:1 w/w). After 45 min reaction time a HPCA polymer featuring a M_n = 4000 g·mol^{-1} and a dispersity of $Đ$ = 1.2 was obtained. BA was added directly as additional monomer in order to produce a copolymer via NMP featuring a M_n = 16300 g·mol^{-1} and a dispersity of $Đ$ = 1.4 after 4 h reaction time, which is exceeding the initial M_n^{theo} at full conversion of 9900 g·mol^{-1}. Reprinted from ref. 200 with permission of The Royal Society of Chemistry.

3.5 Conclusions

The Arrhenius parameters of HPCA and UMA were successfully determined for a wide temperature range via PLP-SEC-MALLS. By comparing the obtained propagation rate coefficients of HPCA with the literature known data for the structurally similar monomers PhCPA and HCPA, a trend of k_p is observed with regards to the ester side chain: The more sterically demanding the ester side chain, the higher the corresponding propagation rate coefficient. The observed trend is similar to trends reported for linear alkyl (meth)acrylates, yet is significantly more pronounced. In lack of structurally similar heteroatom-containing methacrylates, the propagation rate coefficient of UMA is compared to hydroxyl functional as well as linear, branched, and cyclic alkyl methacrylates. UMA features distinctly higher k_p values at all temperatures than the cyclic and branched alkyl methacrylates, which are yet clearly below the value of HEMA, but comparable to the one of HPMA. Solely based on the

determined k_p value, UMA would correspond to a linear methacrylate with more than 20 carbon atoms in its ester side chain.

In addition, the free-radical polymerization behavior of both monomers was studied via in-situ NMR experiments at elevated temperatures (i.e., 70°C). The recorded conversion vs. time evolutions were employed to determine the apparent polymerization rate coefficient and the radical concentration (typically in the range of 10^{-7} – 10^{-8} mol·L^{-1}). Furthermore, estimates of the average termination rate coefficient, $\overline{k_t}$, were calculated. The average $\overline{k_t}$ values for UMA as well as for HPCA are close to 10^6 L·mol^{-1}·s^{-1}, respectively, for the given experimental conditions and are reflecting the relatively high viscosity of the reaction solution.

In order to achieve a thorough description of the polymerization behavior of both monomers, RDRP experiments (RAFT polymerization and NMP) were performed. Employing UMA as the monomer, linear evolutions of M_n with conversion were observed in NMP and RAFT polymerization, with dispersity values close to 1.35 and 1.2, respectively, as well as uniform shifts of the polymer distribution up to a targeted molar mass of 5000 g·mol^{-1} and 35000 g·mol^{-1}. Furthermore, RAFT and NMP experiments were successfully carried out with HPCA, resulting in a linear evolution of M_n vs. conversion (for RAFT via in-situ NMR and SEC-RI), successful chain extension experiments (RAFT and NMP) as well as uniform shifts of the polymer distribution up to a targeted molar mass varying between 5000 g·mol^{-1} and 70000 g·mol^{-1} for HPCA homo-polymerizations and copolymerizations with styrene (in NMP).

4 Experimental Section

In the subsequent chapter the materials employed in the current thesis are collated along with a brief outline of the applied analysis and characterization methods.

4.1 Materials

2,2-Dimethoxy-2-phenylacetophenone (DMPA, Aldrich, 99%), 4-methyl hydroquinone (MeHQ, Aldrich, 99%), hydroquinone (HQ, Fluka, ≥ 99%), tetrahydrofuran (THF, HPLC grade, not stabilized), *N*,*N*-dimethylacetamide (DMAc, Sigma Aldrich, ≥ 99.9%), butyl acetate (BuAc, Acros, 99%), 2-(dodecylthiocarbonothioylthio)propionic acid (DoPAT, Sigma-Aldrich, 97%), and 2-cyanopropan-2-yl benzodithioate (CPDB, Sigma-Aldrich, 97%,) were used as received.

Cumyl phenyldithioacetate (CPDA),[218] *N*-*tert*-butyl-*N*-[1-diethylphosphono-(2,2-dimethylpropyl)] nitroxide (SG1 or DEPN),[5] and 2-methyl-2-[*N*-*tert*-butyl-*N*-(1-diethoxyphos-phoryl-2,2-dimethylpropyl)aminoxy]propionic acid (MAMA-SG1 or MAMA-DEPN)[219] were synthesized according to previously published procedures.

Stearyl acrylate (SA, C14 / C16 / C18 / C20 = 0.0112 / 0.4834 / 0.4510 / 0.0076, > 95%, < 20 ppm MeHQ), behenyl acrylate (BeA, C16 / C18 / C20 / C22 = 0.0027 / 0.453 / 0.1169 / 0.4275, 98%, < 70 ppm MeHQ), stearyl methacrylate (SMA, C16 / C18 = 0.3 / 0.7, < 20 ppm MeHQ), behenyl methacrylate (BeMA, C16 / C18 / C20 / C22 = 0.0027 / 0.453 / 0.1169 / 0.4275, 98%, < 70 ppm MeHQ), 2-propylheptyl methacrylate (PHMA, isomeric mixture with following ester groups: 2-propylheptyl / 2-propyl-4-methylhexyl / 2-propyl-5-methylhexyl / 2-*iso*-propylheptyl = 0.93 / 0.029 / 0.039 / 0.02, < 20 ppm MeHQ), tridecyl methacrylate (TDA-MA, isomeric mixture, isoindex 2.6, < 20 ppm MeHQ), tridecyl methacrylate (TDN-

MA, isomeric mixture, isoindex 2.2, < 20 ppm MeHQ), heptadecyl methacrylate (C17MA, isomeric mixture, isoindex 3.1, < 20 ppm MeHQ), 2-propylheptyl acrylate (PHA, isomeric mixture with following ester groups: 2-propylheptyl / 2-propyl-4-methylhexyl / 2-propyl-5-methylhexyl / 2-*iso*-propylheptyl = 0.93 / 0.029 / 0.039 / 0.02, < 30 ppm MeHQ), *iso*-nonyl acrylate (INA-A, isomeric mixture, isoindex 1.3, < 20 ppm MeHQ), tridecyl acrylate (TDA-A, isomeric mixture, isoindex 3.1, < 20 ppm MeHQ), tridecyl acrylate (TDN-A, isomeric mixture, isoindex 2.1, < 20 ppm MeHQ), heptadecyl acrylate (C17A, isomeric mixture, isoindex 3.1, < 20 ppm MeHQ), henicosyl acrylate (C21A, isomeric mixture, isoindex 4.2, < 20 ppm MeHQ), hydroxyl-*iso*-propylcarbamate acrylate (HPCA, isomeric mixture, < 20 ppm MeHQ), and ureidoethyl methacrylate (UMA, < 40 ppm MeHQ) were used as received from BASF.

Azobis(2-methylpropionitrile) (AIBN, Acros, 98%) was re-crystallized in ethanol prior to use. Styrene (Acros, 99%), methyl acrylate (VWR, 99%), and *n*-butyl acrylate (Acros, > 99%) were passed over basic alumina in order to remove the stabilizer.

4.2 Pulsed Laser Polymerization Experiments

The herein employed experimental PLP setup and basic procedures were previously established in our group.[177, 186, 220] The stock monomer solutions containing varying concentrations of photoinitiator (and solvent) are transferred into sample vials (approx. 0.5 mL), sealed with rubber septa and purged with nitrogen for approx. 2 min in order to remove oxygen. The sample is equilibrated to the desired temperature at which the PLP experiment is performed by placing it for 2-5 min into a stainless steel sample holder, which is brought to temperature by a thermostat (VWR 1196D). Polymerization is initiated by laser pulsing at constant repetition rates of up to 500 Hz employing a Coherent Xantos XS-500 (compact version of the ExciStar EXS-500) operated at the XeF line at 351 nm wavelength. The laser beam is redirected and concentrated via an optical setup to hit the sample vial from the

bottom. The energy of the beam is typically adjusted to 2 mJ·pulse^{-1}. The temperature is measured directly at the sample and in none of the numerous PLP samples a relevant temperature increase throughout or after the polymerization process was observed. After polymerization, MeHQ dissolved in solvent (THF or DMAc) is added and the samples are filtered and analyzed directly via SEC, since most of the monomers do not evaporate (as they feature relatively high boiling points or they are solids). Possible influence of the conversion on the resulting propagation rate coefficient values is assessed by variation of the pulse repetition number (between 30 and up to 15000 pulse repetitions) and found to be negligible in the applied range of pulse repetitions. Every individual PLP distribution is tested for consistency in terms of the appearance of at least L_2 and the resulting ratio of $k_{p,1}/k_{p,2}$. In several cases (especially for the linear methacrylates) up to 5 inflection points are observable. Only samples that showed a ratio of $k_{p,1}/k_{p,2}$ within 0.95 and 1.2 are admitted to the final Arrhenius data set (if not otherwise stated) and the majority of the $k_{p,1}/k_{p,2}$ ratios are between 1.03 and 1.12. The individual $k_{p,1}/k_{p,2}$ ratios for each sample are collated, e.g., in Table S1 in the Appendix A.

Additionally to the PLP setup at the KIT (Karlsruhe), the experimental setup at the Polymer Institute of the Slovak Academy of Sciences (SAS, Bratislava) was employed for the investigation of the monomers described in Chapter 3. At the SAS a Coherent ExciStar XS-500 laser, also operating at the XeF line of 351 nm and providing laser pulse repetitions rates of up to 500 Hz, was employed. The general sample preparation procedure is the same as employed at the KIT. The laser beam, which is adjusted to an energy of close to 2 mJ·pulse^{-1}, is directed to hit the sample solution (approx. 1 mL in QS 110 cuvette of 10 mm path length, Hellma-Worldwide) horizontally. Temperature equilibration is achieved using a thermostat (Julabo ED) and monitored for several samples directly in the reaction solution during the PLP experiment. Again, no significant temperature increase was observed under the applied PLP conditions.

4.3 Fractionation of Polymer Samples via SEC

Fractionation is performed with non-stabilized THF as the eluent on a PSS system consisting of an Agilent Technologies G1310A iso pump, G1329A ALS autosampler, G1316A TCC column oven, SDV high speed column 5 µm linear M 20×50 mm (or a preparative column SDV linear M 20×300 mm, to which the values in brackets refer to in the following), and an Advantec CHF122SC fraction collector controlled via a UDC810 from WinGPC 7 software. An initial sample concentration of 20 $g \cdot L^{-1}$ (or approx. 100 $g \cdot L^{-1}$, if possible) is chosen and approx. 1 mg of polymer (equal to 50 µL injection volume) (or approx. 90 mg, equal to 900 µL injection volume) is injected into the SEC column. The broadly distributed polymer is separated into fractions of 20 s elution time intervals in order to obtain the narrowly distributed polymer samples (flow rate: 1 $mL \cdot min^{-1}$) (or 15 s; flow rate: 5 $mL \cdot min^{-1}$). In approx. 250 (or 10) repetitive injections a polymer sample of 3 mg to 20 mg accumulates for each fraction. THF is allowed to evaporate and the polymer samples are subsequently prepared for analysis via triple detection SEC.

4.4 Characterization

4.4.1 Size-Exclusion Chromatography (SEC) in THF

SEC measurements are performed on a PL-SEC 50 Plus Integrated System, comprising an autosampler, a PLgel 5 µm bead-size guard column (50 × 7.5 mm) followed by one PLgel 5 µm Mixed E column (300 × 7.5 mm), three PLgel 5 µm Mixed C columns (300 × 7.5 mm), and a differential refractive index (RI) detector using THF as the eluent at 35°C with a flow rate of 1 $mL \cdot min^{-1}$. The SEC system is calibrated using linear poly(styrene) standards ranging from 474 to 2.5×10^6 $g \cdot mol^{-1}$ (PSS – Polymer Standards Service, Mainz / Germany).[143-145] All SEC calculations are carried out applying a universal calibration by using the specific Mark-Houwink-Kuhn-Sakurada (MHKS) parameters (collated in Table 2.1) for the corresponding

polymer, which were determined during the current study. The MHKS parameters employed for poly(styrene) are $K = 14.1 \cdot 10^{-3}$ cm^{-3}·g^{-1} and $\alpha = 0.7$. The obtained M_n (V_e) are subsequently smoothed to remove noise from the RI detector signal and the derivatives are determined using Origin software.[221]

4.4.2 Size-Exclusion Chromatography (SEC) in DMAc

SEC measurements of the polymer samples obtained in the RDRP experiments are performed on a PL-SEC 50 Plus Integrated System, comprising an autosampler, a PLgel 5 µm bead-size guard column (50 × 7.5 mm) followed by three PLgel 5 µm Mixed C column (300 × 7.5 mm), and a differential refractive index (RI) detector using *N*,*N*-dimethylacetamide (DMAc) containing 0.3 wt% LiBr as the eluent at 50°C with a flow rate of 1 mL·min^{-1}. The SEC system is calibrated using linear poly(styrene) standards ranging from 474 to 2.5×10^6 g·mol^{-1} and linear poly(methyl methacrylate) standards ranging from 700 to 2·10^6 g·mol^{-1} (PSS, see above).[9-11] SEC calculations are carried out applying an effective calibration by using the Mark-Houwink-Kuhn-Sakurada (MHKS) parameters for poly(styrene) ($K = 14.1 \cdot 10^{-3}$ cm^3·g^{-1} and $\alpha = 0.7$).[12] No absolute molar mass information was available for the RDRP samples (cf. Chapter 3.4), since the MHKS parameters of polyUMA and polyHPCA are not available. In contrast to the PLP samples, the RDRP samples do not contain high molar mass polymer chains, which would allow for a valid extrapolation to the low molar mass range via MALLS detector analysis.

4.4.3 Triple Detector Size-Exclusion Chromatography in THF

The triple detection chromatographic setup employed for the determination of MHKS parameters consists of a modular system (Polymer Standard Service, PSS, Mainz/Agilent 1200 series) incorporating an ETA2010 viscosimeter (WGE Dr. Bures) and a light-scattering unit (PSS SLD7000/BI-M w A, Brookhaven Instruments). Sample separation is achieved via two linear columns (PSS SDV- Lux-10^3 Å and 10^5 Å , 5 µm) with THF as the eluent at 35°C

with a flow rate of 1 mL·min^{-1}. The system is calibrated using poly(styrene) standards (PSS, see above). The refractive index increments d*n*/d*c*, where *n* is the refractive index and *c* is the polymer concentration, is determined for each individual sample via their precisely known concentrations. The refractive index increments, d*n*/d*c*, employed for the calculation of the absolute molecular weights, are determined via averaging of the d*n*/d*c* values of representative SEC samples and are provided in Table 2.1. The MALLS detector signal determines M_W of the analyzed polymer sample and the intrinsic viscosity [η] is derived from the viscosimeter signal. The data from the viscosimeter are directly processed without applying any smoothing procedure as the scattering in the residual plots was sufficiently low throughout the entire study. Exemplary triple SEC chromatograms (RI, MALLS as well as viscosimeter detector signals) of the narrowly distributed polymer samples are depicted in Figure S19 to Figure S22 in the Appendix A.

4.4.4 Size-Exclusion Chromatography (SEC) in DMAc – Determination of Absolute Molar Masses

Absolute SEC analysis of the molar mass distributions was performed at the Polymer Institute of the Slovak Academy of Sciences (SAS) in Bratislava with the eluent *N*,*N*-dimethylacetamide (DMAc) containing 0.1 wt% LiBr on a Polymer Standards Service (PSS, Mainz / Germany) column setup consisting of an 8 × 50 mm PSS GRAM 10 µm guard column and three 8 × 300 mm PSS GRAM 10 µm columns with pore sizes of 100, 1000, and 3000 Å placed in a column heater set to 45°C. The flow rate of 0.8 mL·min^{-1} is controlled by using toluene as the flow rate marker in a Waters SEC system (degasser, autosampler 717 with loop volume 100 µL, 515 pump, column heater). A direct calibration of the SEC columns was not possible due to the non-availability of narrowly distributed polymer calibration standards. A universal calibration was as well not possible due to the non-availability of the specific MHKS parameters of the polymers of interest. Therefore, the use

of MALLS-RI detection was required. A MALLS absolute detector PSS SLD7000 (PSS, Mainz / Germany) in conjunction with a Waters 2410 DRI detector provided absolute molar masses.[8] The values of the refractive index increment, d*n*/d*c*, were determined on a DnDc2010 (PSS, Mainz, Germany) differential refractometer to be 0.084 and 0.068 $mL \cdot g^{-1}$ for polyUMA and polyHPCA, respectively. These numbers are measured at a wavelength of 620 nm and are assumed to be the same as for 633 nm, which is the wavelength employed by the MALLS detector. A narrowly distributed poly(styrene) calibration standard of 67500 $g \cdot mol^{-1}$ molecular mass (PSS, Mainz, Germany) is used as the isotropic scatterer. Effective calibration is achieved using poly(styrene) standards, each of narrow molecular mass distribution, for the range from 376 to 2.3×10^6 $g \cdot mol^{-1}$ (PSS, Mainz, Germany). PSS WinGPC7.2.1 is used for data acquisition and evaluation. The MALLS detector signal was sufficient to allow a precise molar mass distribution analysis for all samples currently incorporated into the Arrhenius plots.

4.4.5 Density Measurements

The temperature dependent densities of the solutions are determined with an Anton Paar DMA 5000 M density meter with a precision of $1 \cdot 10^{-2}$°C and $5 \cdot 10^{-6}$ $g \cdot cm^{-3}$. Methyl hydroquinone (MeHQ) is added in replacement of 2,2-dimethoxy-2-phenylacetophenone (DMPA) to prevent the solutions from polymerizing inside the density measurement device.

4.4.6 NMR Spectroscopy

NMR measurements are conducted on a Bruker AM250 spectroscope at 250 MHz and a Bruker AM400 spectroscope at 400 MHz for hydrogen nuclei for conversion determination and for structure verification. At the Institute of Chemistry of the Faculty of Natural Sciences, Comenius University in Bratislava, the in-situ NMR measurements are conducted on a Varian VNMRS 600 MHz. Samples are dissolved in DMSO-d_6 using residual solvent peaks for shift correction.

Furthermore, conversion vs. time evolutions are recorded for the free-radical polymerization of both heteroatom containing monomers employing AIBN as the initiator. Thus, in-situ NMR measurements of monomer solutions (0.2 $mol \cdot L^{-1}$; 1 $mol \cdot L^{-1}$; 2 $mol \cdot L^{-1}$) in DMSO-d_6 containing 12 $mmol \cdot L^{-1}$ AIBN are carried out with a heatable sample head at 70°C and spectra are recorded every 20 and 40 seconds, respectively. The necessary shimming and lock to the NMR tube is performed with an identical NMR tube containing the pure monomer in the NMR solvent without initiator. After the preparation of the NMR experiment the NMR tubes are exchanged so that the first spectrum of the polymerization could already be recorded after 20 or 40 s instead of after several minutes, which are necessary for the shimming and lock. Monitoring the continuous decay of the resonances associated with the vinylic protons (i.e., at δ = 5.95 ppm for HPCA and at δ = 5.65 ppm for UMA), normalized in each spectrum to resonances associated with protons of the ester side chain (i.e., the tertiary proton in HPCA at δ = 4.85 ppm and the CH_2 group in the side chain in UMA at δ = 3.95 ppm) provides the conversion vs. time evolutions.

4.5 Standard Procedures Applied in RDRP Techniques

As presented in Chapter 3.4, the M_n data of batch polymerizations determined via SEC-RI can be correlated with the conversion values obtained via ^{1}H-NMR experiments at elevated temperatures. Therefore, a stock solution containing solvent, monomer, controlling agent, and initiator is filtered and portioned in a number of SEC sample vials after removal of the oxygen by standard freeze-pump-thaw techniques (up to 4 cycles). The SEC vials are subsequently placed into a metal heating block (60°C for RAFT polymerization experiments for both monomers, as well as 90 and 110°C for NMP of UMA and HPCA, respectively) with magnetic stirring during polymerization. After pre-set time intervals the polymerization in the SEC vial is stopped by addition of solvent containing inhibitor (methyl hydroquinone, MeHQ) and the mixture is subsequently analyzed via SEC-RI without further purification. A

similar polymerization solution containing deuterated solvent with the same concentrations of initiator, controlling agent, and monomer is prepared and degassed directly in the NMR tube for the RAFT polymerization of HPCA. The conversion values are determined via integration of the resonances associated with the vinylic protons in the repetitive measured NMR spectra (every 100 s) at the same temperature as for the above described batch polymerizations, i.e., 60°C.

5 Outlook

The capabilities of the PLP-SEC method for acrylates are currently limited due to the non-availability of UV-laser set-ups with a pulse frequency (significantly) above 500 Hz, which is limiting the temperature range accessible for investigation at 60°C (sometimes 70°C). Recently 1000 Hz lasers became commercially available at 351 nm, which however is not sufficient to significantly expand the accessible temperature range.[193] Another possible approach to tackle the major challenge of investigating acrylates at elevated temperatures might be to establish new types of photoinitiators in the PLP-SEC method which initiate the polymerization under infrared light, for which already significantly higher pulse repetition rates are available (exceeding 10 kHz at 1064 nm wavelength). Such infrared photoinitiators are not yet wide spread, though their principal applicability in the FRP process is already proven.[222-224] However, photoinitiators featuring an absorption maximum in the infrared light might bear further experimental challenges which have to be overcome, since they might promote undesired background polymerization during sample preparation prior to the PLP experiment.

Furthermore, the variety of monomers for which precise kinetic rate coefficients are available has to be extended. To date only a few (meth)acrylates with heteroatom containing monomers are reported. Currently, a series of methacrylates containing amine functionalities as well as poly(ethylene glycol) substituents (MPEG-MA) in their ester side chains are studied in our laboratories. It will be interesting to establish if the MPEG-MAs display a comparable increase of the propagation rate coefficient with increasing ester side chain length as the linear alkyl (meth)acrylates and if such an increase will level off at a certain chain length or if propagation becomes even faster. In addition, the systematic investigation via the PLP-SEC

method of sugar containing monomers or monomers which consist of cyclic structures and do not only contain them in their ester side chains (such as γ-methyl-α-methylene-γ-butyrolactone)[225] are up to date not yet reported. An in-depth understanding of the effects of hydrogen bonding, solvent influences, and the related suppression of transfer to polymer reactions might also be accessible via the PLP-SEC method.[194, 196, 208, 226-228] As noted in Chapter 1.2, a chain length dependence of the propagation rate coefficient was often suggested, however it was up to date not possible to experimentally clearly prove or disprove it.

In summary, the PLP-SEC method, which was developed almost 4 decades ago and which has demonstrated its advantages in the last 20 years, still bears a major potential in answering basic and cutting edge questions associated with the mechanism of the FRP process.

REFERENCES

[1] Nikitin, A. N.; Hutchinson, R. A.; Buback, M.; Hesse, P. *Macromolecules* **2007,** *40*, 8631-8641.

[2] Haehnel, A. P.; Fleischmann, S.; Hesse, P.; Hungenberg, K.-D.; Barner-Kowollik, C. *Macromol. React. Eng.* **2013,** *7*, 8-23.

[3] Zhong, M.; Matyjaszewski, K. *Macromolecules* **2011,** *44*, 2668-2677.

[4] Coote, M. L.; Barner-Kowollik, C. *Aust. J. Chem.* **2006,** *59*, 712-718.

[5] Hlalele, L.; Klumperman, B. *Macromolecules* **2011,** *44*, 6683-6690.

[6] Jenkins, A. D.; Jones, R. G.; Moad, G. *Pure Appl. Chem.* **2010,** *82*, 483-491.

[7] Flory, P. J. *Principles of Polymer Chemistry*. Cornell Univ. Press,: Ithaca, New York, **1953**.

[8] Odian, G. *Principles of Polymerization*. 4th ed.; Wiley-Interscience: Hoboken, New Jersey, **2004**.

[9] Heuts, J. P. A.; Russell, G. T. *Eur. Polym. J.* **2006,** *42*, 3-20.

[10] Heuts, J. P. A.; Gilbert, R. G.; Radom, L. *Macromolecules* **1995,** *28*, 8771-8781.

[11] Junkers, T.; Barner-Kowollik, C. *J. Polym. Sci., Part A: Polym. Chem.* **2008,** *46*, 7585-7605.

[12] Scott, G. E.; Senogles, E. *Journal of Macromolecular Science: Part A - Chemistry* **1970,** *4*, 1105-1117.

[13] Scott, G. E.; Senogles, E. *Journal of Macromolecular Science, Part C* **1973,** *9*, 49-69.

[14] Scott, G. E.; Senogles, E. *Journal of Macromolecular Science: Part A - Chemistry* **1974,** *8*, 753-773.

[15] Barner-Kowollik, C.; Junkers, T. *J. Polym. Sci., Part A: Polym. Chem.* **2011,** *49*, 1293-1297.

[16] Peck, A. N. F.; Hutchinson, R. A. *Macromolecules* **2004,** *37*, 5944-5951.

[17] Bennet, F.; Rölle, T.; Fäcke, T.; Weiser, M.-S.; Bruder, F.-K.; Barner-Kowollik, C.; Junkers, T. *Macromol. Chem. Phys.* **2013,** *214*, 236-245.

[18] Vandenbergh, J.; Junkers, T. *Macromolecules* **2012,** *45*, 6850-6856.

[19] Feldermann, A.; Coote, M. L.; Stenzel, M. H.; Davis, T. P.; Barner-Kowollik, C. *J. Am. Chem. Soc.* **2004,** *126*, 15915-15923.

[20] Barth, J.; Buback, M.; Russell, G. T.; Smolne, S. *Macromol. Chem. Phys.* **2011,** *212*, 1366-1378.

[21] Johnston-Hall, G.; Theis, A.; Monteiro, M. J.; Davis, T. P.; Stenzel, M. H.; Barner-Kowollik, C. *Macromol. Chem. Phys.* **2005,** *206*, 2047-2053.

[22] Theis, A.; Feldermann, A.; Charton, N.; Davis, T. P.; Stenzel, M. H.; Barner-Kowollik, C. *Polymer* **2005,** *46*, 6797-6809.

[23] Theis, A.; Feldermann, A.; Charton, N.; Stenzel, M. H.; Davis, T. P.; Barner-Kowollik, C. *Macromolecules* **2005,** *38*, 2595-2605.

[24] Barner-Kowollik, C.; Russell, G. T. *Prog. Polym. Sci.* **2009,** *34*, 1211-1259.

[25] Junkers, T.; Theis, A.; Buback, M.; Davis, T. P.; Stenzel, M. H.; Vana, P.; Barner-Kowollik, C. *Macromolecules* **2005,** *38*, 9497-9508.

[26] Lechner, M. D.; Gehrke, K.; Nordmeier, E. H. *Makromolekulare Chemie*. 5. ed.; Birkhäuser Verlag: Basel, **2014**.

[27] Vana, P.; Davis, T. P.; Barner-Kowollik, C. *Macromol. Rapid Commun.* **2002,** *23*, 952-956.

[28] Buback, M.; Junkers, T.; Vana, P. *Macromol. Rapid Commun.* **2005,** *26*, 796-802.

[29] Johnston-Hall, G.; Barner-Kowollik, C.; Monteiro, M. J. *Macromol. Theory Simul.* **2008,** *17*, 460-469.

[30] Theis, A.; Davis, T. P.; Stenzel, M. H.; Barner-Kowollik, C. *Macromolecules* **2005,** *38*, 10323-10327.
[31] Theis, A.; Davis, T. P.; Stenzel, M. H.; Barner-Kowollik, C. *Polymer* **2006,** *47*, 999-1010.
[32] Buback, M.; Hesse, P.; Junkers, T.; Theis, T.; Vana, P. *Aust. J. Chem.* **2007,** *60*, 779-787.
[33] Johnston-Hall, G.; Stenzel, M. H.; Davis, T. P.; Barner-Kowollik, C.; Monteiro, M. J. *Macromolecules* **2007,** *40*, 2730-2736.
[34] Szwarc, M. *Nature* **1956,** *178*, 1168-1169.
[35] Moad, G.; Rizzardo, E.; Thang, S. H. *Aust. J. Chem.* **2005,** *58*, 379-410.
[36] Barner-Kowollik, C. *Handbook of RAFT Polymerization*. Wiley-VCH: Weinheim, **2008**.
[37] Nicolas, J.; Guillaneuf, Y.; Lefay, C.; Bertin, D.; Gigmes, D.; Charleux, B. *Prog. Polym. Sci.* **2013,** *38*, 63-235.
[38] Rosen, B. M.; Percec, V. *Chemical Reviews* **2009,** *109*, 5069-5119.
[39] Matyjaszewski, K.; Xia, J. H. *Chemical Reviews* **2001,** *101*, 2921-2990.
[40] Matyjaszewski, K. *Macromolecules* **2012,** *45*, 4015-4039.
[41] Quirk, R. P.; Lee, B. *Polym. Int.* **1992,** *27*, 359-367.
[42] Matyjaszewski, K.; Müller, A. H. E. *Controlled and Living Polymerizations: From Mechanisms to Applications* Wiley-VCH: Weinheim, **2009**; Vol. 634.
[43] Otsu, T.; Yoshida, M.; Tazaki, T. *Makromol. Chem-Rapid* **1982,** *3*, 133-140.
[44] Hawker, C. J.; Bosman, A. W.; Harth, E. *Chemical Reviews* **2001,** *101*, 3661-3688.
[45] Iovu, M. C.; Craley, C. R.; Jeffries-El, M.; Krankowski, A. B.; Zhang, R.; Kowalewski, T.; McCullough, R. D. *Macromolecules* **2007,** *40*, 4733-4735.
[46] Tang, W.; Fukuda, T.; Matyjaszewski, K. *Macromolecules* **2006,** *39*, 4332-4337.
[47] Vinas, J.; Chagneux, N.; Gigmes, D.; Trimaille, T.; Favier, A.; Bertin, D. *Polymer* **2008,** *49*, 3639-3647.
[48] Vandenbergh, J.; Junkers, T. *Macromolecules* **2013,** *46*, 3324-3331.
[49] Benoit, D.; Grimaldi, S.; Finet, J. P.; Tordo, P.; Fontanille, M.; Gnanou, Y. Controlled/Living Free-Radical Polymerization of Styrene and *n*-Butyl Acrylate in the Presence of a Novel Asymmetric Nitroxyl Radical. In *Controlled Radical Polymerization*, American Chemical Society: **1998**; Vol. 685, pp 225-235.
[50] Fischer, H. *J. Polym. Sci., Part A: Polym. Chem.* **1999,** *37*, 1885-1901.
[51] Chiefari, J.; Chong, Y. K.; Ercole, F.; Krstina, J.; Jeffery, J.; Le, T. P. T.; Mayadunne, R. T. A.; Meijs, G. F.; Moad, C. L.; Moad, G.; Rizzardo, E.; Thang, S. H. *Macromolecules* **1998,** *31*, 5559-5562.
[52] Corpart, P.; Michelet, D.; Zard, S. Z.; Biadatti, T. *PCT Int. Appl. WO 9858974 A1* **1998**.
[53] Destarac, M.; Bzducha, W.; Taton, D.; Gauthier-Gillaizeau, I.; Zard, S. Z. *Macromol. Rapid Commun.* **2002,** *23*, 1049-1054.
[54] Barner-Kowollik, C.; Buback, M.; Charleux, B.; Coote, M. L.; Drache, M.; Fukuda, T.; Goto, A.; Klumperman, B.; Lowe, A. B.; McLeary, J. B.; Moad, G.; Monteiro, M. J.; Sanderson, R. D.; Tonge, M. P.; Vana, P. *J. Polym. Sci., Part A: Polym. Chem.* **2006,** *44*, 5809-5831.
[55] Junkers, T.; Delaittre, G.; Chapman, R.; Günzler, F.; Chernikova, E.; Barner-Kowollik, C. *Macromol. Rapid Commun.* **2012,** *33*, 984-990.
[56] Moad, G.; Rizzardo, E.; Thang, S. H. *Aust. J. Chem.* **2009,** *62*, 1402-1472.
[57] Altintas, O.; Riazi, K.; Lee, R.; Lin, C. Y.; Coote, M. L.; Wilhelm, M.; Barner-Kowollik, C. *Macromolecules* **2013,** *46*, 8079-8091.
[58] Teodorescu, M.; Gaynor, S. G.; Matyjaszewski, K. *Macromolecules* **2000,** *33*, 2335-2339.

[59] Zhang, L.; Cheng, Z.; Tang, F.; Li, Q.; Zhu, X. *Macromol. Chem. Phys.* **2008,** *209*, 1705-1713.
[60] Camerano, J. A.; Rodrigues, A.-S.; Rominger, F.; Wadepohl, H.; Gade, L. H. *J. Organomet. Chem.* **2011,** *696*, 1425-1431.
[61] Kotani, Y.; Kamigaito, M.; Sawamoto, M. *Macromolecules* **1999,** *32*, 2420-2424.
[62] Moineau, G.; Granel, C.; Dubois, P.; Jérôme, R.; Teyssié, P. *Macromolecules* **1998,** *31*, 542-544.
[63] Uegaki, H.; Kotani, Y.; Kamigaito, M.; Sawamoto, M. *Macromolecules* **1998,** *31*, 6756-6761.
[64] Ando, T.; Kato, M.; Kamigaito, M.; Sawamoto, M. *Macromolecules* **1996,** *29*, 1070-1072.
[65] Simal, F.; Demonceau, A.; Noels, A. F. *Angewandte Chemie International Edition* **1999,** *38*, 538-540.
[66] del Río, I.; van Koten, G.; Lutz, M.; Spek, A. L. *Organometallics* **2000,** *19*, 361-364.
[67] Haddleton, D. M.; Limer, A. *Prog. React. Kinet. Mech.* **2004,** *29*, 187-241.
[68] Levere, M. E.; Nguyen, N. H.; Leng, X.; Percec, V. *Polym. Chem.* **2013,** *4*, 1635-1647.
[69] Levere, M. E.; Nguyen, N. H.; Sun, H.-J.; Percec, V. *Polym. Chem.* **2013,** *4*, 686-694.
[70] Nguyen, N. H.; Leng, X.; Percec, V. *Polym. Chem.* **2013,** *4*, 2760-2766.
[71] Nguyen, N. H.; Sun, H.-J.; Levere, M. E.; Fleischmann, S.; Percec, V. *Polym. Chem.* **2013,** *4*, 1328-1332.
[72] Konkolewicz, D.; Wang, Y.; Zhong, M.; Krys, P.; Isse, A. A.; Gennaro, A.; Matyjaszewski, K. *Macromolecules* **2013,** *46*, 8749-8772.
[73] Konkolewicz, D.; Krys, P.; Góis, J. R.; Mendonça, P. V.; Zhong, M.; Wang, Y.; Gennaro, A.; Isse, A. A.; Fantin, M.; Matyjaszewski, K. *Macromolecules* **2014,** *47*, 560-570.
[74] Kato, M.; Kamigaito, M.; Sawamoto, M.; Higashimura, T. *Macromolecules* **1995,** *28*, 1721-1723.
[75] Wang, J.-S.; Matyjaszewski, K. *J. Am. Chem. Soc.* **1995,** *117*, 5614-5615.
[76] Percec, V.; Barboiu, B. *Macromolecules* **1995,** *28*, 7970-7972.
[77] Monteiro, M. J.; Guliashvili, T.; Percec, V. *J. Polym. Sci., Part A: Polym. Chem.* **2007,** *45*, 1835-1847.
[78] Wang, J.-S.; Matyjaszewski, K. *Macromolecules* **1995,** *28*, 7901-7910.
[79] Matyjaszewski, K.; Göbelt, B.; Paik, H.-j.; Horwitz, C. P. *Macromolecules* **2001,** *34*, 430-440.
[80] Rosen, B. M.; Jiang, X.; Wilson, C. J.; Nguyen, N. H.; Monteiro, M. J.; Percec, V. *Journal of Polymer Science Part a-Polymer Chemistry* **2009,** *47*, 5606-5628.
[81] Lligadas, G.; Rosen, B. M.; Monteiro, M. J.; Percec, V. *Macromolecules* **2008,** *41*, 8360-8364.
[82] Sumerlin, B. S.; Tsarevsky, N. V.; Louche, G.; Lee, R. Y.; Matyjaszewski, K. *Macromolecules* **2005,** *38*, 7540-7545.
[83] Chatterjee, D. P.; Chatterjee, U.; Mandal, B. M. *J. Polym. Sci., Part A: Polym. Chem.* **2004,** *42*, 4132-4142.
[84] Nguyen, N. H.; Rosen, B. M.; Jiang, X.; Fleischmann, S.; Percec, V. *J. Polym. Sci., Part A: Polym. Chem.* **2009,** *47*, 5577-5590.
[85] Jiang, X.; Fleischmann, S.; Nguyen, N. H.; Rosen, B. M.; Percec, V. *J. Polym. Sci., Part A: Polym. Chem.* **2009,** *47*, 5591-5605.
[86] Asandei, A. D.; Percec, V. *J. Polym. Sci., Part A: Polym. Chem.* **2001,** *39*, 3392-3418.
[87] Percec, V.; Popov, A. V.; Ramirez-Castillo, E.; Monteiro, M.; Barboiu, B.; Weichold, O.; Asandei, A. D.; Mitchell, C. M. *J. Am. Chem. Soc.* **2002,** *124*, 4940-4941.

[88] Coelho, J. F. J.; Silva, A. M. F. P.; Popov, A. V.; Percec, V.; Abreu, M. V.; Gonçalves, P. M. O. F.; Gil, M. H. *J. Polym. Sci., Part A: Polym. Chem.* **2006,** *44*, 3001-3008.
[89] Whittaker, M. R.; Urbani, C. N.; Monteiro, M. J. *J. Polym. Sci., Part A: Polym. Chem.* **2008,** *46*, 6346-6357.
[90] Rosen, B. M.; Percec, V. *J. Polym. Sci., Part A: Polym. Chem.* **2008,** *46*, 5663-5697.
[91] Fleischmann, S.; Percec, V. *J. Polym. Sci., Part A: Polym. Chem.* **2010,** *48*, 4884-4888.
[92] Turan, E.; Caykara, T. *J. Polym. Sci., Part A: Polym. Chem.* **2010,** *48*, 5842-5847.
[93] Lligadas, G.; Percec, V. *J. Polym. Sci., Part A: Polym. Chem.* **2008,** *46*, 2745-2754.
[94] Lligadas, G.; Rosen, B. M.; Bell, C. A.; Monteiro, M. J.; Percec, V. *Macromolecules* **2008,** *41*, 8365-8371.
[95] Lligadas, G.; Percec, V. *J. Polym. Sci., Part A: Polym. Chem.* **2008,** *46*, 6880-6895.
[96] Fleischmann, S.; Percec, V. *J. Polym. Sci., Part A: Polym. Chem.* **2010,** *48*, 4889-4893.
[97] Tang, W.; Matyjaszewski, K. *Macromolecules* **2007,** *40*, 1858-1863.
[98] Kwak, Y.; Matyjaszewski, K. *Macromolecules* **2008,** *41*, 6627-6635.
[99] Egorov, A.; Matyukhova, S.; Anisimov, A. *Russ. J. Gen. Chem.* **2005,** *75*, 1131-1135.
[100] Egorov, A. M.; Matyukhova, S. A.; Anisimov, A. V. *Int. J. Chem. Kinet.* **2005,** *37*, 296-305.
[101] Egorov, A. M.; Matyukhova, S. A. *Int. J. Chem. Kinet.* **2007,** *39*, 547-555.
[102] Nguyen, N. H.; Rosen, B. M.; Percec, V. *J. Polym. Sci., Part A: Polym. Chem.* **2011,** *49*, 1235-1247.
[103] Isse, A. A.; Gennaro, A.; Lin, C. Y.; Hodgson, J. L.; Coote, M. L.; Guliashvili, T. *J. Am. Chem. Soc.* **2011,** *133*, 6254-6264.
[104] Rosen, B. M.; Percec, V. *J. Polym. Sci., Part A: Polym. Chem.* **2007,** *45*, 4950-4964.
[105] Bell, C. A.; Whittaker, M. R.; Gahan, L. R.; Monteiro, M. J. *Journal of Polymer Science Part a-Polymer Chemistry* **2008,** *46*, 146-154.
[106] Nguyen, N. H.; Jiang, X.; Fleischmann, S.; Rosen, B. M.; Percec, V. *J. Polym. Sci., Part A: Polym. Chem.* **2009,** *47*, 5629-5638.
[107] Nguyen, N. H.; Rosen, B. M.; Lligadas, G.; Percec, V. *Macromolecules* **2009,** *42*, 2379-2386.
[108] Nguyen, N. H.; Percec, V. *J. Polym. Sci., Part A: Polym. Chem.* **2010,** *48*, 5109-5119.
[109] Levere, M. E.; Willoughby, I.; O'Donohue, S.; Wright, P. M.; Grice, A. J.; Fidge, C.; Remzi Becer, C.; Haddleton, D. M. *J. Polym. Sci., Part A: Polym. Chem.* **2011,** *49*, 1753-1763.
[110] Caretti, I.; Dervaux, B.; Du Prez, F. E.; Van Doorslaer, S. *J. Polym. Sci., Part A: Polym. Chem.* **2010,** *48*, 1493-1501.
[111] Tang, W.; Matyjaszewski, K. *Macromol. Theory Simul.* **2008,** *17*, 359-375.
[112] D'hooge, D. R.; Reyniers, M.-F. o.; Stadler, F. J.; Dervaux, B.; Bailly, C.; Du Prez, F. E.; Marin, G. B. *Macromolecules* **2010,** *43*, 8766-8781.
[113] Aleksandrov, A. P.; Vladimir, N. G.; Kitaĭ, M. S.; Smirnova, I. M.; Sokolov, V. V. *Sov. J. Quantum Electron.* **1977,** *7*, 547-550.
[114] Olaj, O. F.; Bitai, I.; Hinkelmann, F. *Makromol. Chem.* **1987,** *188*, 1689-1702.
[115] Kornherr, A.; Olaj, O. F.; Schnöll-Bitai, I.; Zifferer, G. *Macromol. Theory Simul.* **2003,** *12*, 332-338.
[116] Schnöll-Bitai, I.; Olaj, O. F. *Makromol. Chem.* **1990,** *191*, 2491-2499.
[117] Beuermann, S.; Buback, M. *Prog. Polym. Sci.* **2002,** *27*, 191-254.
[118] van Herk, A. M. *Macromol. Rapid Commun.* **2009,** *30*, 1964-1968.
[119] Buback, M.; Gilbert, R. G.; Russell, G. T.; Hill, D. J. T.; Moad, G.; O'Driscoll, K. F.; Shen, J.; Winnik, M. A. *J. Polym. Sci., Part A: Polym. Chem.* **1992,** *30*, 851-863.

[120] Buback, M.; Garcia-Rubio, L. H.; Gilbert, R. G.; Napper, D. H.; Guillot, J.; Hamielec, A. E.; Hill, D.; O'Driscoll, K. F.; Olaj, O. F.; Shen, J.; Solomon, D.; Moad, G.; Stickler, M.; Tirrell, M.; Winnik, M. A. *Journal of Polymer Science Part C: Polymer Letters* **1988,** *26*, 293-297.
[121] Asua, J. M.; Beuermann, S.; Buback, M.; Castignolles, P.; Charleux, B.; Gilbert, R. G.; Hutchinson, R. A.; Leiza, J. R.; Nikitin, A. N.; Vairon, J.-P.; van Herk, A. M. *Macromol. Chem. Phys.* **2004,** *205*, 2151-2160.
[122] Beuermann, S.; Buback, M.; El Rezzi, V.; Jürgens, M.; Nelke, D. *Macromol. Chem. Phys.* **2004,** *205*, 876-883.
[123] Buback, M. *Macromol. Symp.* **2009,** *275–276*, 90-101.
[124] Dervaux, B.; Junkers, T.; Schneider-Baumann, M.; Du Prez, F. E.; Barner-Kowollik, C. *J. Polym. Sci., Part A: Polym. Chem.* **2009,** *47*, 6641-6654.
[125] Beuermann, S.; Buback, M.; Davis, T. P.; García, N.; Gilbert, R. G.; Hutchinson, R. A.; Kajiwara, A.; Kamachi, M.; Lacík, I.; Russell, G. T. *Macromol. Chem. Phys.* **2003,** *204*, 1338-1350.
[126] Beuermann, S.; Buback, M.; Davis, T. P.; Gilbert, R. G.; Hutchinson, R. A.; Kajiwara, A.; Klumperman, B.; Russell, G. T. *Macromol. Chem. Phys.* **2000,** *201*, 1355-1364.
[127] Beuermann, S.; Buback, M.; Davis, T. P.; Gilbert, R. G.; Hutchinson, R. A.; Olaj, O. F.; Russell, G. T.; Schweer, J.; van Herk, A. M. *Macromol. Chem. Phys.* **1997,** *198*, 1545-1560.
[128] Buback, M.; Gilbert, R. G.; Hutchinson, R. A.; Klumperman, B.; Kuchta, F.-D.; Manders, B. G.; O'Driscoll, K. F.; Russell, G. T.; Schweer, J. *Macromol. Chem. Phys.* **1995,** *196*, 3267-3280.
[129] Beuermann, S. *Pure Appl. Chem.* **2003,** *75*, 1091-1096.
[130] Brandrup, J.; Immergut, E. H.; Grulke, E. A.; Abe, A.; Bloch, D. R. *Polymer Handbook (4th Edition)*. John Wiley & Sons: Weinheim, **1999**.
[131] Voll, D.; Neshchadin, D.; Hiltebrandt, K.; Gescheidt, G.; Barner-Kowollik, C. *Macromolecules* **2012,** *45*, 5850-5858.
[132] Szablan, Z.; Junkers, T.; Koo, S. P. S.; Lovestead, T. M.; Davis, T. P.; Stenzel, M. H.; Barner-Kowollik, C. *Macromolecules* **2007,** *40*, 6820-6833.
[133] Buback, M.; Kuelpmann, A. *Macromol. Chem. Phys.* **2003,** *204*, 632-637.
[134] Haehnel, A. P.; Schneider-Baumann, M.; Hiltebrandt, K. U.; Misske, A. M.; Barner-Kowollik, C. *Macromolecules* **2013,** *46*, 15-28.
[135] Siegmann, R.; Jeličić, A.; Beuermann, S. *Macromol. Chem. Phys.* **2010,** *211*, 546-562.
[136] Lacík, I.; Beuermann, S.; Buback, M. *Macromolecules* **2003,** *36*, 9355-9363.
[137] Beuermann, S.; Buback, M.; Hesse, P.; Kukučková, S.; Lacık, I. *Macromol. Symp.* **2007,** *248*, 23-32.
[138] Beuermann, S.; Buback, M.; Schmaltz, C. *Macromolecules* **1998,** *31*, 8069-8074.
[139] Beuermann, S.; Buback, M.; Schmaltz, C.; Kuchta, F. D. *Macromol. Chem. Phys.* **1998,** *199*, 1209-1216.
[140] Coote, M. L.; Davis, T. P. *Journal of Polymer Science Part B: Polymer Physics* **1999,** *37*, 2557-2570.
[141] Xu, Z.; Hadjichristidis, N.; Fetters, L. J. *Macromolecules* **1984,** *17*, 2303-2306.
[142] Gaborieau, M.; Nicolas, J.; Save, M.; Charleux, B.; Vairon, J.-P.; Gilbert, R. G.; Castignolles, P. *Journal of Chromatography A* **2008,** *1190*, 215-223.
[143] Penzel, E.; Goetz, N. *Angew. Makromol. Chem.* **1990,** *178*, 191-200.
[144] Xu, Z.; Song, M.; Hadjichristidis, N.; Fetters, L. J. *Macromolecules* **1981,** *14*, 1591-1594.
[145] Stickler, M.; Panke, D.; Wunderlich, W. *Makromol. Chem.* **1987,** *188*, 2651-2664.
[146] Grubisic, Z.; Rempp, P.; Benoit, H. *Journal of Polymer Science Part B: Polymer Letters* **1967,** *5*, 753-759.

[147] Wild, L.; Guliana, R. *Journal of Polymer Science Part A-2: Polymer Physics* **1967,** *5*, 1087-1101.
[148] Jackson, C.; Chen, Y.-J.; Mays, J. W. *J. Appl. Polym. Sci.* **1996,** *61*, 865-874.
[149] Temyanko, E.; Russo, P. S.; Ricks, H. *Macromolecules* **2000,** *34*, 582-586.
[150] Ahmad, N. M.; Charleux, B.; Farcet, C.; Ferguson, C. J.; Gaynor, S. G.; Hawkett, B. S.; Heatley, F.; Klumperman, B.; Konkolewicz, D.; Lovell, P. A.; Matyjaszewski, K.; Venkatesh, R. *Macromol. Rapid Commun.* **2009,** *30*, 2002-2021.
[151] van Herk, A. M.; Dröge, T. *Macromol. Theory Simul.* **1997,** *6*, 1263-1276.
[152] van Herk, A. M.; van den Brand, H.; Berg, I. *Contour V2.0.2*, **2012**.
[153] Stach, M.; Lacík, I.; Kasák, P.; Chorvát, D. J.; Saunders, A. J.; Santanakrishnan, S.; Hutchinson, R. A. *Macromol. Chem. Phys.* **2010,** *211*, 580-593.
[154] Stach, M.; Lacík, I.; Kasák, P.; Chorvát, D.; Saunders, A. J.; Santanakrishnan, S.; Hutchinson, R. A. *Macromol. Chem. Phys.* **2010,** *211*, 580-593.
[155] Stach, M.; Lacík, I.; Chorvát, D. J.; Buback, M.; Hesse, P.; Hutchinson, R. A.; Tang, L. *Macromolecules* **2008,** *41*, 5174-5185.
[156] Seabrook, S. A.; Tonge, M. P.; Gilbert, R. G. *J. Polym. Sci., Part A: Polym. Chem.* **2005,** *43*, 1357-1368.
[157] Ganachaud, F.; Balic, R.; Monteiro, M. J.; Gilbert, R. G. *Macromolecules* **2000,** *33*, 8589-8596.
[158] Buback, M.; Hesse, P.; Lacík, I. *Macromol. Rapid Commun.* **2007,** *28*, 2049-2054.
[159] Beuermann, S.; Buback, M.; Hesse, P.; Lacík, I. *Macromolecules* **2005,** *39*, 184-193.
[160] Kuchta, F.-D.; van Herk, A. M.; German, A. L. *Macromolecules* **2000,** *33*, 3641-3649.
[161] Beuermann, S.; Buback, M.; Hesse, P.; Kukučková, S.; Lacík, I. *Macromol. Symp.* **2007,** *248*, 41-49.
[162] Vladimir, F. G.; Bune, E. V.; Eduard, N. T. *Russ. Chem. Rev.* **1994,** *63*, 507.
[163] Lacík, I.; Beuermann, S.; Buback, M. *Macromolecules* **2001,** *34*, 6224-6228.
[164] Beuermann, S.; Buback, M.; Hesse, P.; Kuchta, F.-D.; Lacík, I.; Herk, A. M. v. *Pure Appl. Chem.* **2007,** *79*, 1463-1469.
[165] Lacík, I.; Učňová, L.; Kukučková, S.; Buback, M.; Hesse, P.; Beuermann, S. *Macromolecules* **2009,** *42*, 7753-7761.
[166] Lacík, I.; Beuermann, S.; Buback, M. *Macromol. Chem. Phys.* **2004,** *205*, 1080-1087.
[167] Stach, M.; Lacík, I.; Chorvát, D. a. J.; Buback, M.; Hesse, P.; Hutchinson, R. A.; Tang, L. *Macromolecules* **2008,** *41*, 5174-5185.
[168] Beuermann, S.; Buback, M.; Hesse, P.; Hutchinson, R. A.; Kukučková, S.; Lacík, I. *Macromolecules* **2008,** *41*, 3513-3520.
[169] Buback, M.; Hesse, P.; Hutchinson, R. A.; Kasák, P.; Lacík, I.; Stach, M.; Utz, I. *Ind. Eng. Chem. Res.* **2008,** *47*, 8197-8204.
[170] Buback, M.; Hippler, H.; Schweer, J.; Vögele, H.-P. *Makromol. Chem-Rapid* **1986,** *7*, 261-265.
[171] Buback, M.; Kowollik, C. *Macromolecules* **1998,** *31*, 3211-3215.
[172] de Kock, J. B. L.; Klumperman, B.; van Herk, A. M.; German, A. L. *Macromolecules* **1997,** *30*, 6743-6753.
[173] Buback, M.; Müller, E.; Russell, G. T. *J. Polym. Sci., Part A: Polym. Chem.* **2006,** *110*, 3222-3230.
[174] Barth, J.; Buback, M.; Barner-Kowollik, C.; Junkers, T.; Russell, G. T. *J. Polym. Sci., Part A: Polym. Chem.* **2012,** *50*, 4740-4748.
[175] Barth, J.; Meiser, W.; Buback, M. *Macromolecules* **2012,** *45*, 1339-1345.
[176] Barth, J.; Buback, M.; Hesse, P.; Sergeeva, T. *Macromolecules* **2010,** *43*, 4023-4031.
[177] Barner-Kowollik, C.; Günzler, F.; Junkers, T. *Macromolecules* **2008,** *41*, 8971-8973.
[178] Hutchinson, R. A.; Beuermann, S.; Paquet, D. A.; McMinn, J. H. *Macromolecules* **1997,** *30*, 3490-3493.

[179] Zammit, M. D.; Coote, M. L.; Davis, T. P.; Willett, G. D. *Macromolecules* **1998,** *31*, 955-963.
[180] Barner-Kowollik, C.; Beuermann, S.; Buback, M.; Castignolles, P.; Charleux, B.; Coote, M. L.; Hutchinson, R. A.; Junkers, T.; Lacik, I.; Russell, G.; Stach, M.; van Herk, A. *Polym. Chem.* **2014,** *5*, 204-212.
[181] Willemse, R. X. E.; van Herk, A. M. *Macromol. Chem. Phys.* **2010,** *211*, 539-545.
[182] Buback, M.; Kurz, C. H.; Schmaltz, C. *Macromol. Chem. Phys.* **1998,** *199*, 1721-1727.
[183] Haehnel, A. P.; Schneider-Baumann, M.; Arens, L.; Misske, A. M.; Fleischhaker, F.; Barner-Kowollik, C. *Macromolecules* **2014,** *47*, 3483-3496.
[184] Roberts, G. E.; Davis, T. P.; Heuts, J. P. A.; Ball, G. E. *Macromolecules* **2002,** *35*, 9954-9963.
[185] Pascal, P.; Winnik, M. A.; Napper, D. H.; Gilbert, R. G. *Makromol. Chem-Rapid* **1993,** *14*, 213-215.
[186] Junkers, T.; Schneider-Baumann, M.; Koo, S. S. P.; Castignolles, P.; Barner-Kowollik, C. *Macromolecules* **2010,** *43*, 10427-10434.
[187] Fleischhaker, F.; Haehnel, A. P.; Misske, A. M.; Blanchot, M.; Haremza, S.; Barner-Kowollik, C. *Macromol. Chem. Phys.* **2014,** *215*, 1192-1200.
[188] Sato, E.; Emoto, T.; Zetterlund, P. B.; Yamada, B. *Macromol. Chem. Phys.* **2004,** *205*, 1829-1839.
[189] Castignolles, P. *Macromol. Rapid Commun.* **2009,** *30*, 1995-2001.
[190] García, N.; Tiemblo, P.; Guzmán, J. *Macromolecules* **2007,** *40*, 4802-4808.
[191] Nikitin, A. N.; Castignolles, P.; Charleux, B.; Vairon, J.-P. *Macromol. Rapid Commun.* **2003,** *24*, 778-782.
[192] *Coherent homepage*, supplier for LASER systems, **2013, viewed 26.04.2014** https://www.coherent.com/
[193] *GAM LASER, Inc. homepage*, supplier for LASER systems, **2014, viewed 26.04.2014** http://www.gamlaser.com/
[194] Liang, K.; Hutchinson, R. A. *Macromol. Rapid Commun.* **2011,** *32*, 1090-1095.
[195] Lin, C. Y.; Izgorodina, E. I.; Coote, M. L. *Macromolecules* **2009,** *43*, 553-560.
[196] Thickett, S. C.; Gilbert, R. G. *Polymer* **2004,** *45*, 6993-6999.
[197] Beuermann, S. *Macromol. Rapid Commun.* **2009,** *30*, 1066-1088.
[198] Isa, D.; Benjamin, B. N.; Ching Yeh, L.; Michelle, L. C. The Mechanism of Stereoregulation in Free-Radical Polymerization of Bulky Methacrylates. In *Progress in Controlled Radical Polymerization: Mechanisms and Techniques*, American Chemical Society: **2012**; Vol. 1100, pp 15-32.
[199] Steinfeld, J. I.; Francisco, J. S.; Hase, W. L. e. *Chemical Kinetics and Dynamics*. 2 ed.; Prentice Hall: Upper Saddle River, New Jersey, **1998**.
[200] Haehnel, A. P.; Stach, M.; Chovancova, A.; Rueb, J. M.; Delaittre, G.; Misske, A. M.; Lacík, I.; Barner-Kowollik, C. *Polym. Chem.* **2014,** *5*, 862-873.
[201] Qiu, X.-P.; Winnik, F. M. *Macromol. Rapid Commun.* **2006,** *27*, 1648-1653.
[202] Deletre, M.; Levesque, G. *Macromolecules* **1990,** *23*, 4733-4741.
[203] Thomas, D. B.; Sumerlin, B. S.; Lowe, A. B.; McCormick, C. L. *Macromolecules* **2003,** *36*, 1436-1439.
[204] Barner-Kowollik, C.; Bennet, F.; Schneider-Baumann, M.; Voll, D.; Rölle, T.; Facke, T.; Weiser, M.-S.; Bruder, F.-K.; Junkers, T. *Polym. Chem.* **2010,** *1*, 470-479.
[205] Buback, M.; Kurz, C. H. *Macromol. Chem. Phys.* **1998,** *199*, 2301-2310.
[206] Hutchinson, R. A.; Beuermann, S.; Paquet, D. A.; McMinn, J. H.; Jackson, C. *Macromolecules* **1998,** *31*, 1542-1547.
[207] Polarity Index. http://macro.lsu.edu/howto/solvents/Polarity%20index.htm.
[208] Beuermann, S.; Nelke, D. *Macromol. Chem. Phys.* **2003,** *204*, 460-470.

[209] Santanakrishnan, S.; Tang, L.; Hutchinson, R. A.; Stach, M.; Lacík, I.; Schrooten, J.; Hesse, P.; Buback, M. *Macromol. React. Eng.* **2010,** *4*, 499-509.
[210] Charton, N.; Feldermann, A.; Theis, A.; Stenzel, M. H.; Davis, T. P.; Barner-Kowollik, C. *J. Polym. Sci., Part A: Polym. Chem.* **2004,** *42*, 5170-5179.
[211] Moad, G.; Rizzardo, E.; Solomon, D. H.; Johns, S. R.; Willing, R. I. *Makromol. Chem-Rapid* **1984,** *5*, 793-798.
[212] Sicherheitsdatenblatt / Safety Information Sheet for *N*,*N*-dimethyl acetamide (DMAc). http://www.carlroth.de/jsp/de-de/sdpdf/3617.PDF.
[213] Gestis Stoffdatenbank. http://www.dguv.de/ifa/de/gestis/stoffdb/index.jsp.
[214] Buback, M.; Kuchta, F.-D. *Macromol. Chem. Phys.* **1997,** *198*, 1455-1480.
[215] Ganachaud, F.; Monteiro, M. J.; Gilbert, R. G.; Dourges, M.-A.; Thang, S. H.; Rizzardo, E. *Macromolecules* **2000,** *33*, 6738-6745.
[216] Delaittre, G.; Save, M.; Gaborieau, M.; Castignolles, P.; Rieger, J.; Charleux, B. *Polym. Chem.* **2012,** *3*, 1526-1538.
[217] Charleux, B.; Nicolas, J.; Guerret, O. *Macromolecules* **2005,** *38*, 5485-5492.
[218] Barner-Kowollik, C.; Quinn, J. F.; Nguyen, T. L. U.; Heuts, J. P. A.; Davis, T. P. *Macromolecules* **2001,** *34*, 7849-7857.
[219] Harrisson, S.; Couvreur, P.; Nicolas, J. *Polym. Chem.* **2011,** *2*, 1859-1865.
[220] Junkers, T.; Koo, S. P. S.; Barner-Kowollik, C. *Polym. Chem.* **2010,** *1*, 438-441.
[221] Corporation, O. *OriginPro 9.0G*, 9.0G; OriginLab Corporation: Northampton, MA 01060, USA, **2014**.
[222] Belfield, K. D.; Ren, X.; Van Stryland, E. W.; Hagan, D. J.; Dubikovsky, V.; Miesak, E. J. *J. Am. Chem. Soc.* **2000,** *122*, 1217-1218.
[223] Soppera, O.; Turck, C.; Lougnot, D. J. *Opt. Lett.* **2009,** *34*, 461-463.
[224] Li, B.; Zhang, S.; Tang, L.; Zhou, Q. *Polym J* **2001,** *33*, 263-269.
[225] Cockburn, R. A.; Siegmann, R.; Payne, K. A.; Beuermann, S.; McKenna, T. F. L.; Hutchinson, R. A. *Biomacromolecules* **2011,** *12*, 2319-2326.
[226] Jansen Johan, F. G. A.; Dias Aylvin, A.; Dorschu, M.; Coussens, B. Effect of Preorganization Due to Hydrogen Bonding on the Rate of Photoinitiated Acrylate Polymerization. In *Photoinitiated Polymerization*, American Chemical Society: **2003**; Vol. 847, pp 127-139.
[227] Jeličić, A.; Köhler, F.; Winter, A.; Beuermann, S. *J. Polym. Sci., Part A: Polym. Chem.* **2010,** *48*, 3188-3199.
[228] Liang, K.; Rooney, T. R.; Hutchinson, R. A. *Ind. Eng. Chem. Res.* **2013**, doi: 10.1021/ie4027549.
[229] Rudolph, J.; Ulonska, A.; Papp, R.; Paciello, R.; Breitscheidel, B.; Faller, K. C17 Alcohol Mixture. WO/2009/124979, **2009**.

APPENDIX A: CHAPTER 2: ALKYL (METH)ACRYLATES[f]

Exemplary molecular weight distributions (MWD) at 4 different temperatures obtained by SEC analysis, followed by tables with the specific conditions of the PLP-SEC samples, are provided for each monomer and solvent condition (i.e., bulk and 1 M solution in BuAc). For each solution the temperature dependent density curves are highlighted. Furthermore, tables collating all data points employed for the determination of the MHKS parameters together with exemplary triple detector SEC traces of the samples are depicted. Three possible structures of the isomeric heptadecyl alcohol (employed in the synthesis of C17A and C17MA) are highlighted exemplary for all branched alkyl ester side chains of the current study, which were derived via the oligomerization of *n*-butene (or propene) with subsequent hydroformylation and reduction to the corresponding alcohol. The calculation of the isoindex is illustrated by an exemplary ^{1}H-NMR spectrum of TDN-MA. Finally, DSC traces highlighting the newly reported glass transition temperatures of several polymers are provided.

[f] Parts of this chapter, including all Figures and Schemes, were reproduced with permission from Haehnel, A. P.; Schneider-Baumann, M.; Hiltebrandt, K. U.; Misske, A. M.; Barner-Kowollik, C. *Macromolecules* **2013**, *46*, 15-28. and Haehnel, A. P.; Schneider-Baumann, M.; Arens, L.; Misske, A. M.; Fleischhaker, F. Y.; Barner-Kowollik, C. *Macromolecules* **2014,** DOI: 10.1021/ma500304f. Copyright (2014) American Chemical Society.

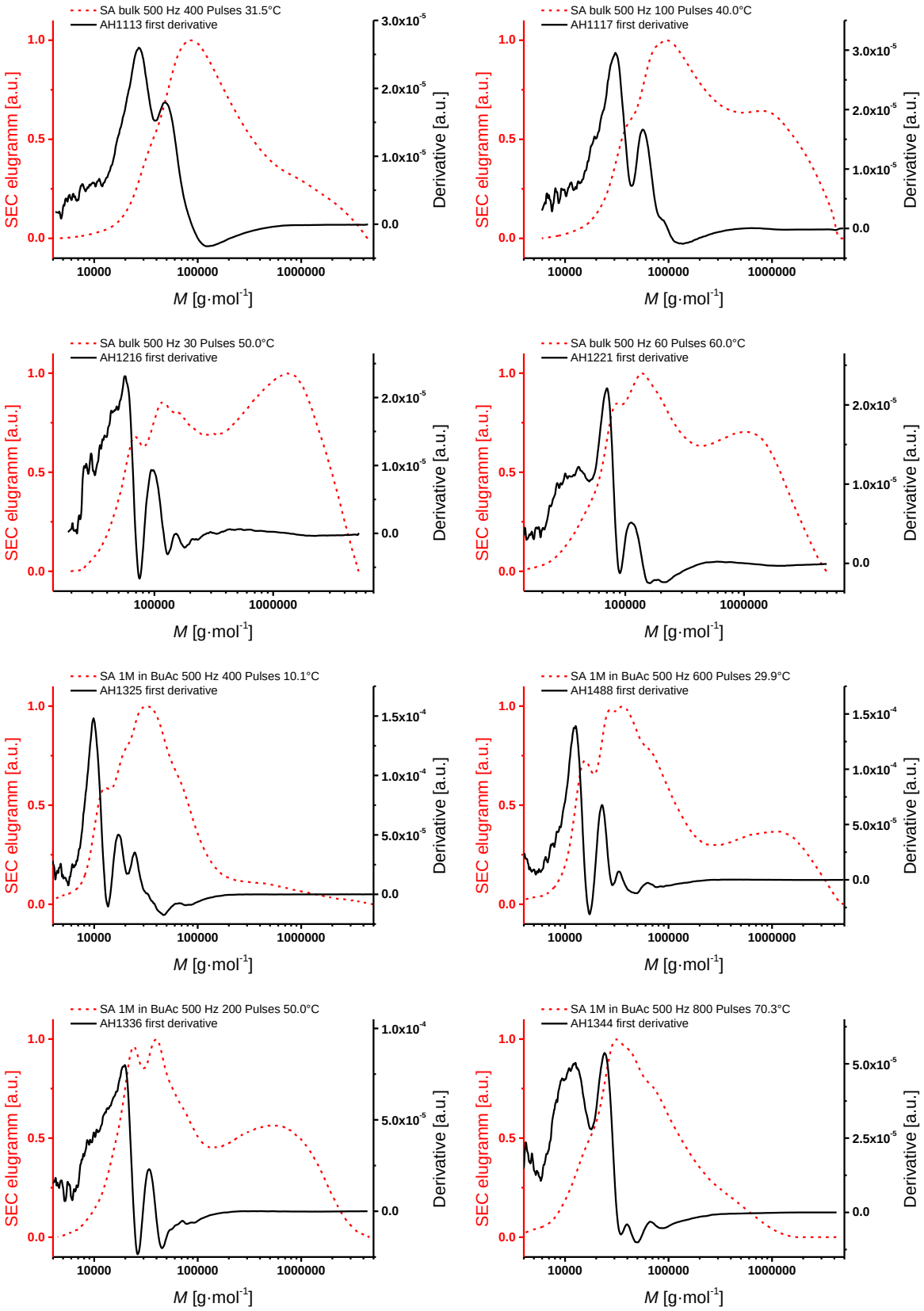

Figure S1 Exemplary molecular weight distributions (red dotted lines) and their first derivative (solid black lines) of SA in bulk (**upper four diagrams**) and in 1 molar solution in BuAc (**lower four diagrams**). The sample specific conditions are displayed in the diagrams and also collated in Table S1 for bulk and in Table S2 for 1 molar solution in BuAc. The typical PLP structure is observed for all samples.

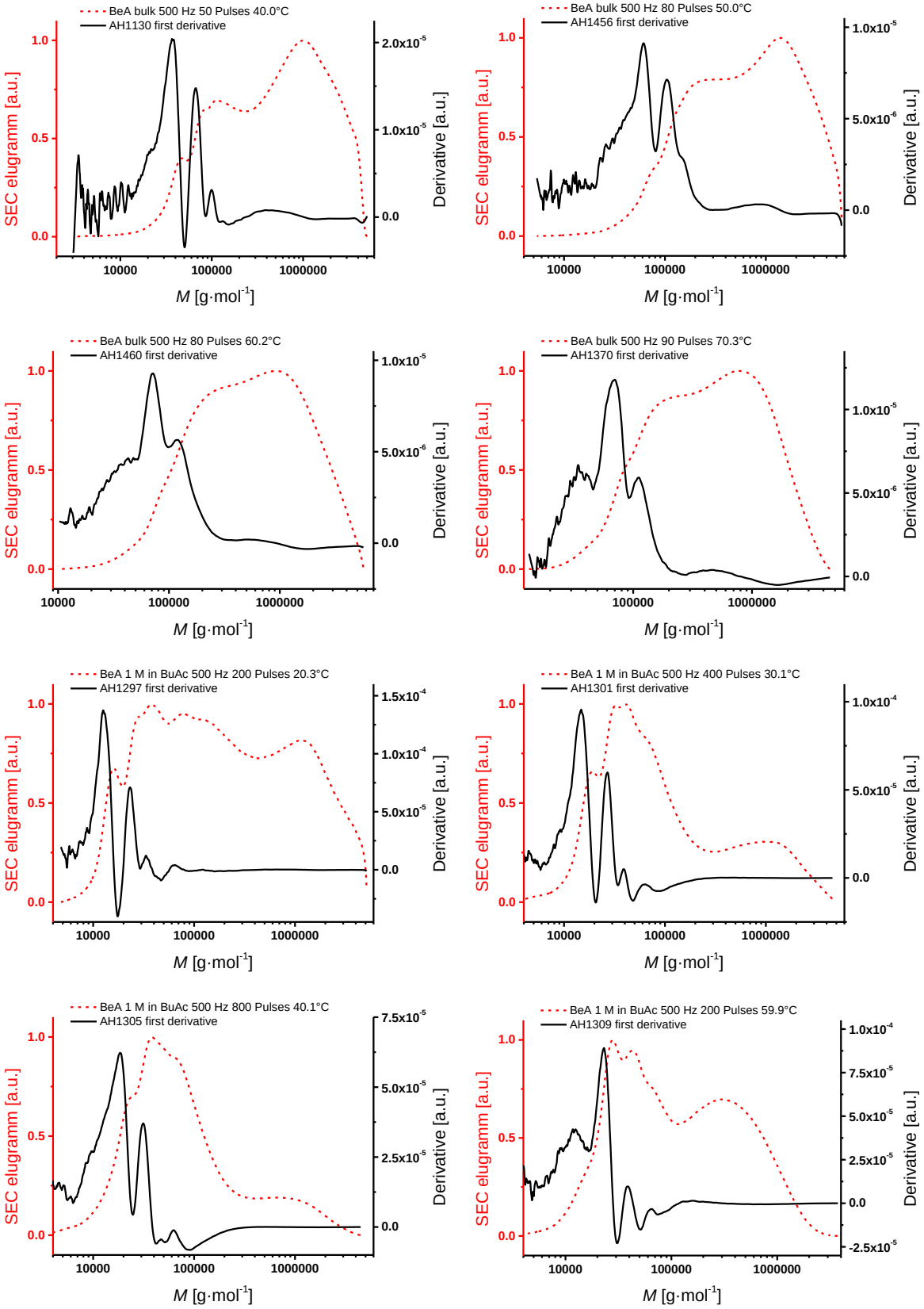

Figure S2 Exemplary molecular weight distributions (red dotted lines) and their first derivative (solid black lines) of BeA in bulk (**upper four diagrams**) and in 1 molar solution in BuAc (**lower four diagrams**). The sample specific conditions are displayed in the diagrams and also collated in Table S3 for bulk and in Table S4 for 1 molar solution in BuAc. The typical PLP structure is observed for all samples.

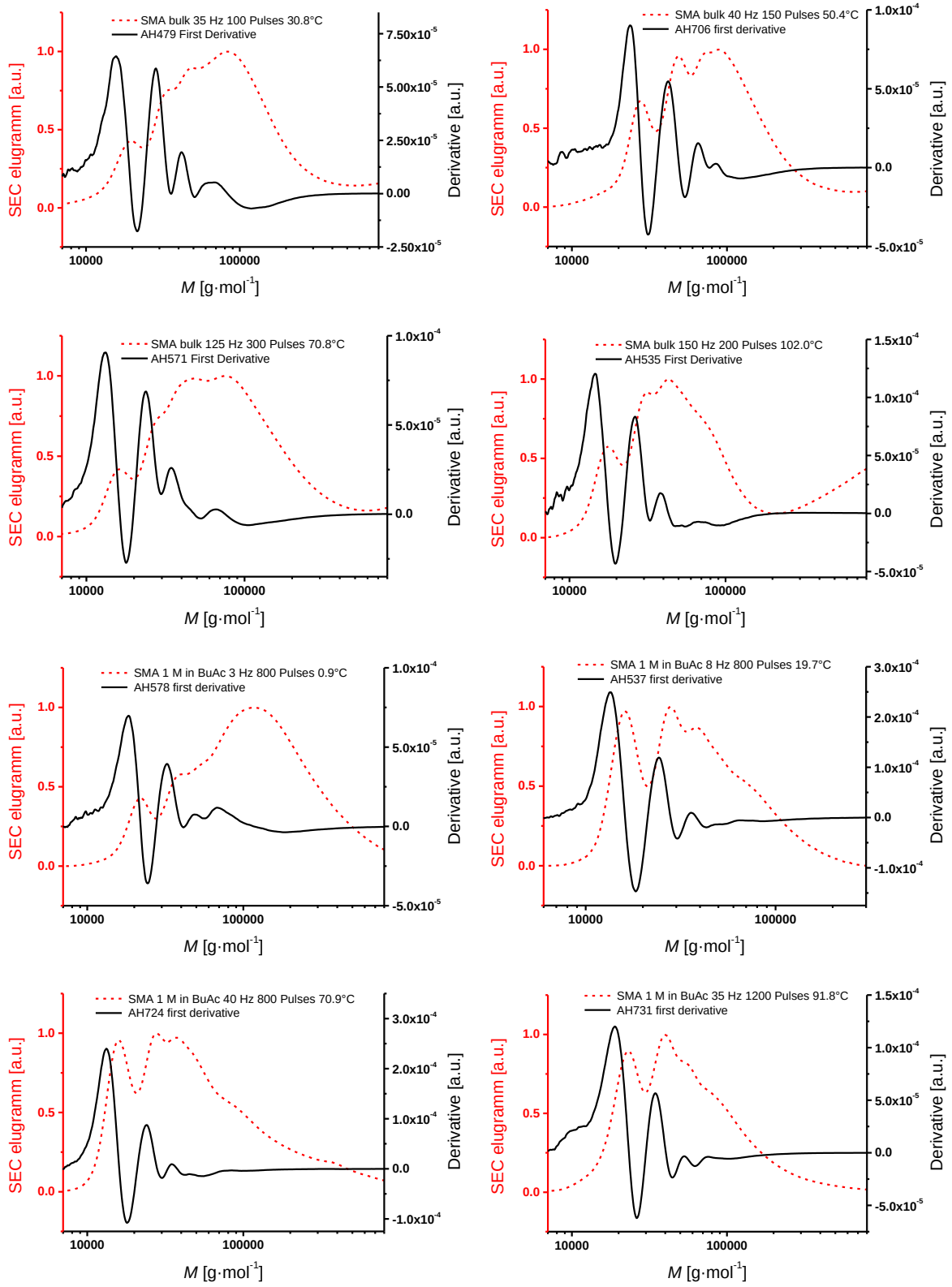

Figure S3 Exemplary molecular weight distributions (red dotted lines) and their first derivative (solid black lines) of SMA in bulk (**upper four diagrams**) and in 1 molar solution in BuAc (**lower four diagrams**). The sample specific conditions are displayed in the diagrams and also collated in Table S5 for bulk and in Table S6 for 1 molar solution in BuAc The typical PLP structure is observed for all samples.

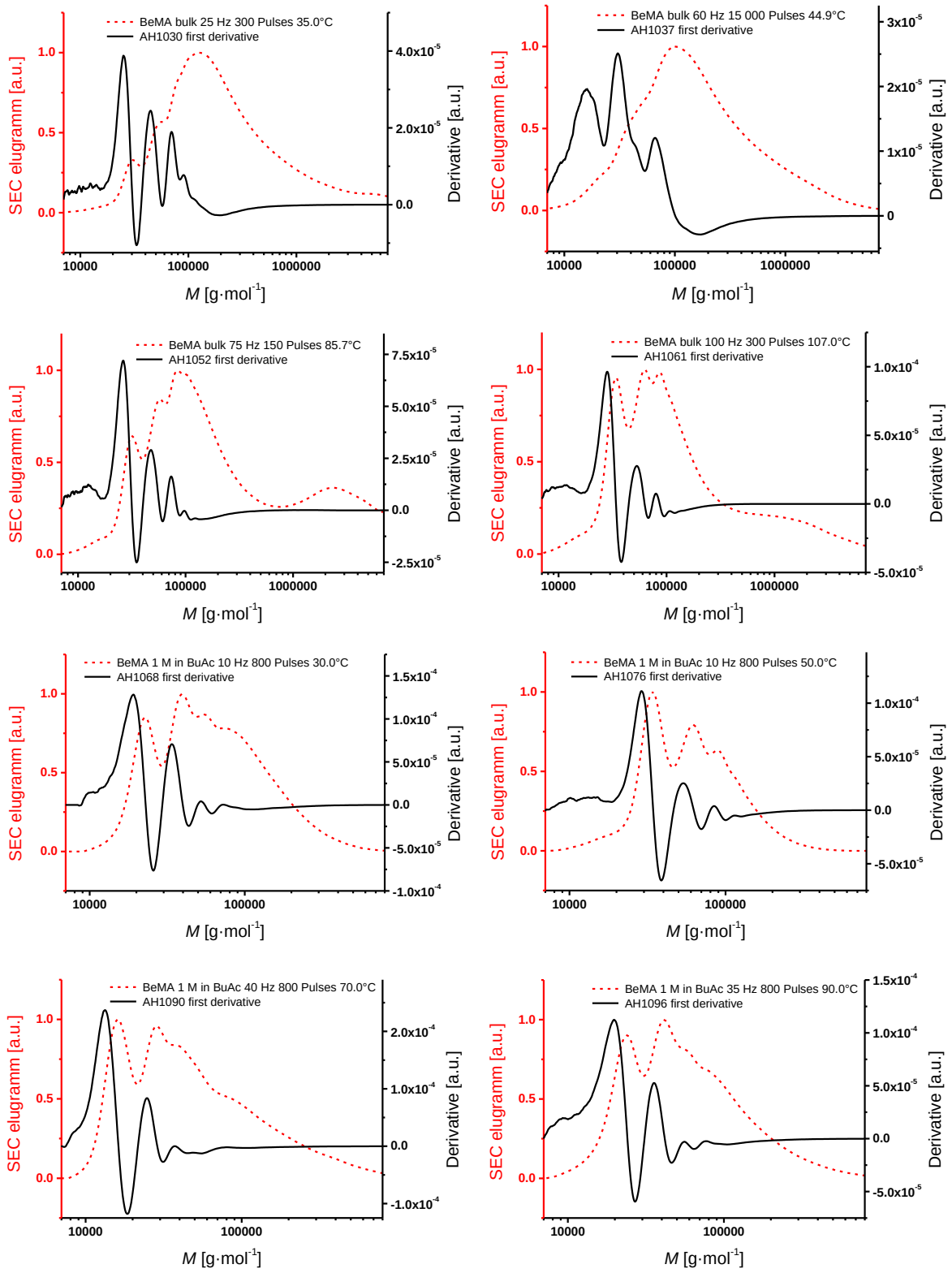

Figure S4 Exemplary molecular weight distributions (red dotted lines) and their first derivative (solid black lines) of BeMA in bulk (**upper four diagrams**) and in 1 molar solution in BuAc (**lower four diagrams**). The sample specific conditions are displayed in the diagrams and also collated in Table S7 for bulk and in Table S8 for 1 molar solution in BuAc. The typical PLP structure is observed for all samples.

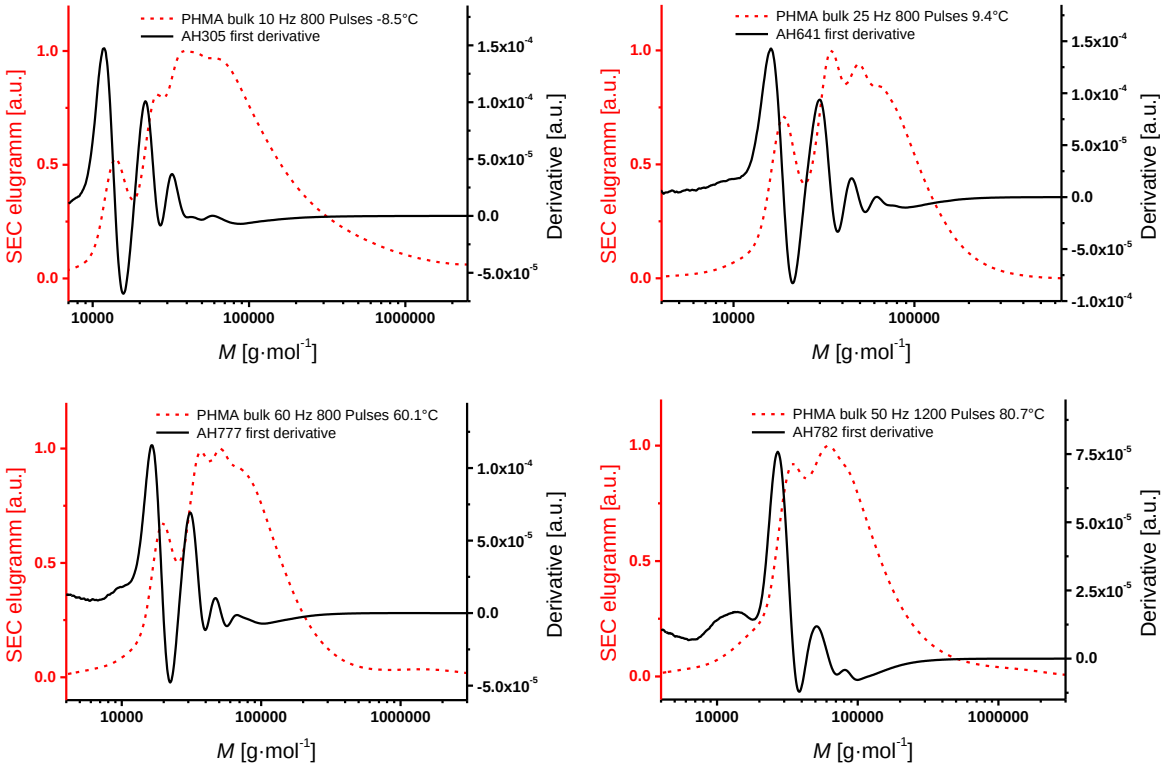

Figure S5 Exemplary molecular weight distributions (red dotted lines) and their first derivative (solid black lines) of PHMA. The sample specific conditions are displayed in the diagrams and also collated in Table S9 for PHMA. The typical PLP structure is observed for all samples.

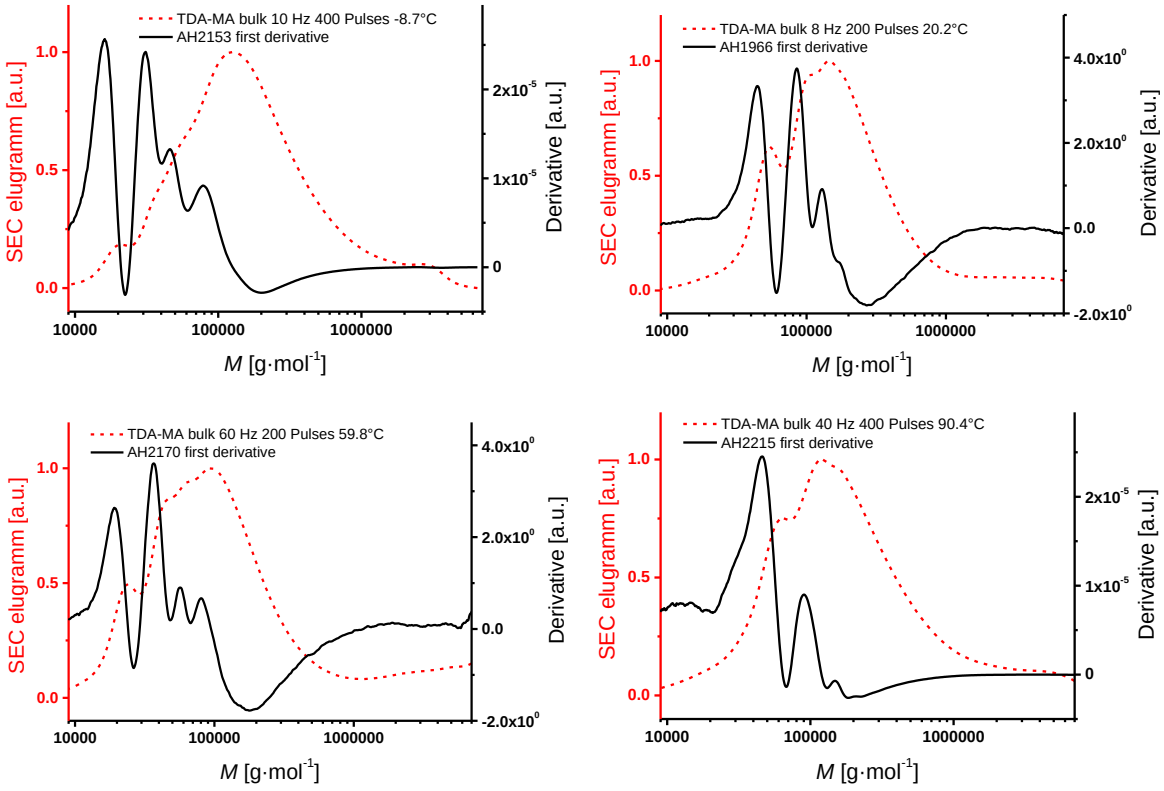

Figure S6 Exemplary molecular weight distributions (red dotted lines) and their first derivative (solid black lines) of TDA-MA in bulk. The sample specific conditions are displayed in the diagrams and also collated in Table S10 for bulk. The typical PLP structure is observed for all samples.

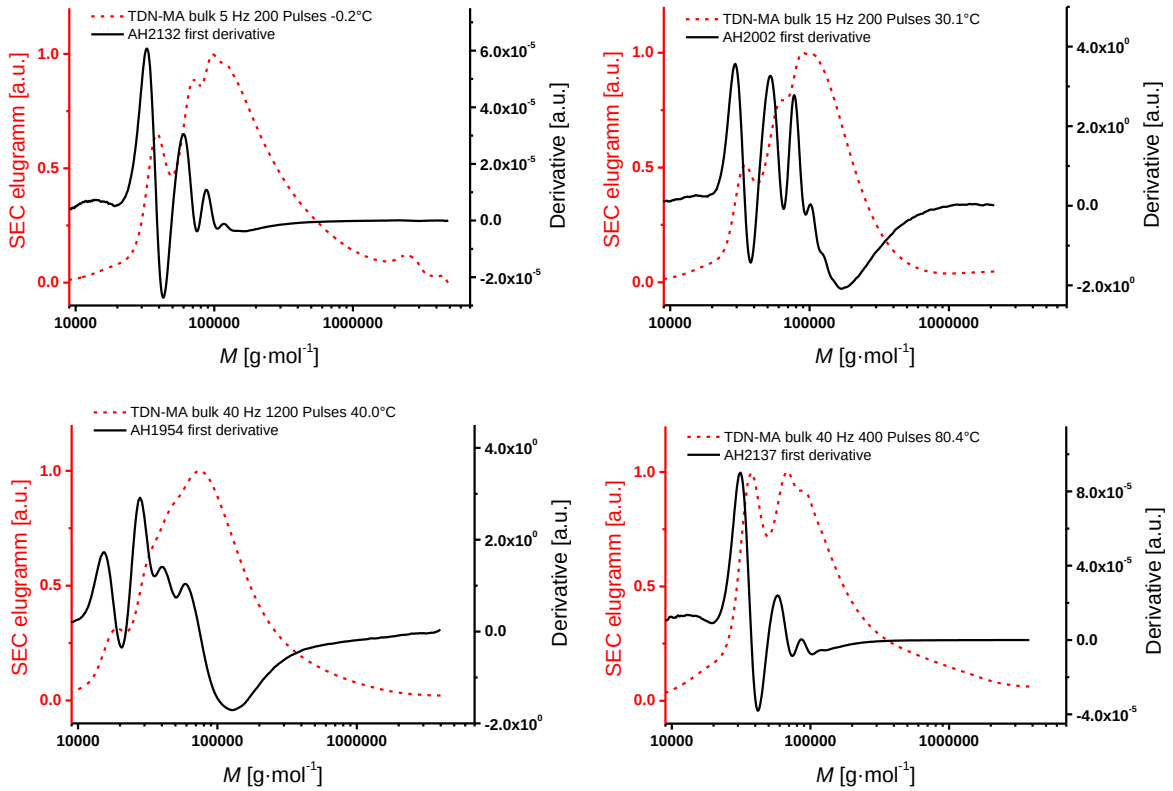

Figure S7 Exemplary molecular weight distributions (red dotted lines) and their first derivative (solid black lines) of TDN-MA in bulk. The sample specific conditions are displayed in the diagrams and also collated in Table S11 for bulk. The typical PLP structure is observed for all samples.

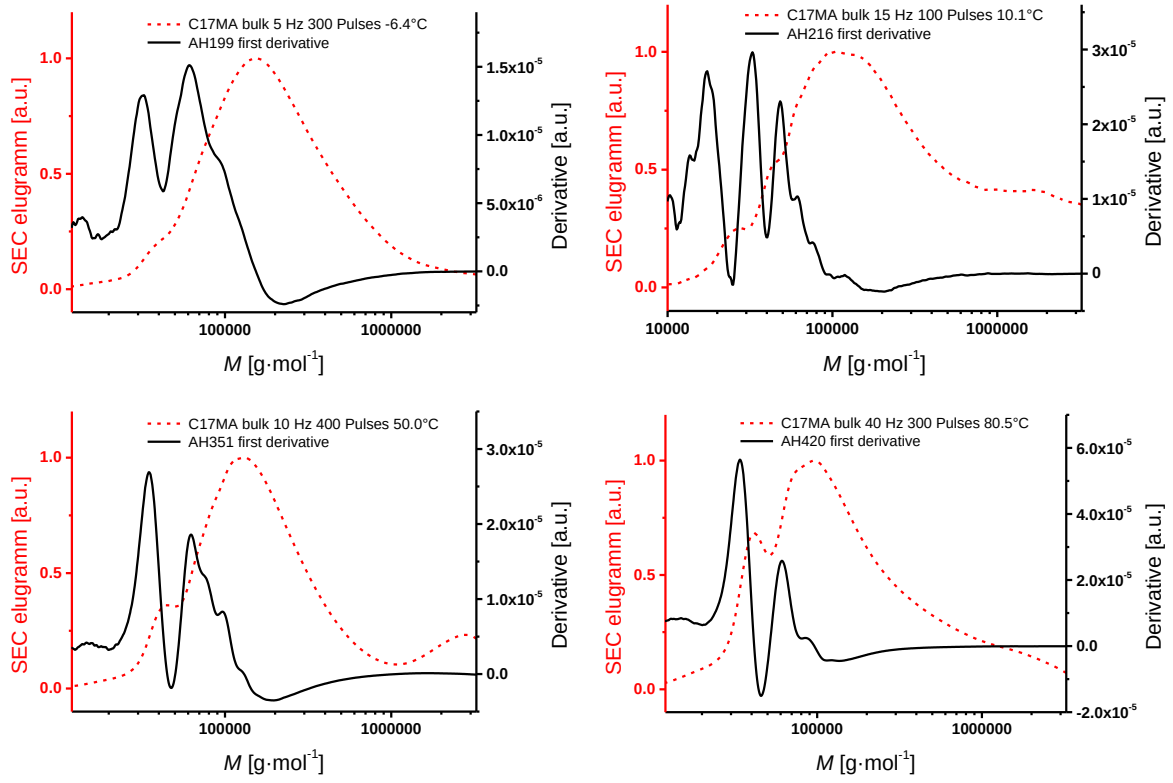

Figure S8 Exemplary molecular weight distributions (red dotted lines) and their first derivative (solid black lines) of C17MA. The sample specific conditions are displayed in the diagrams and also collated in Table S12 for C17MA. The typical PLP structure is observed for all samples.

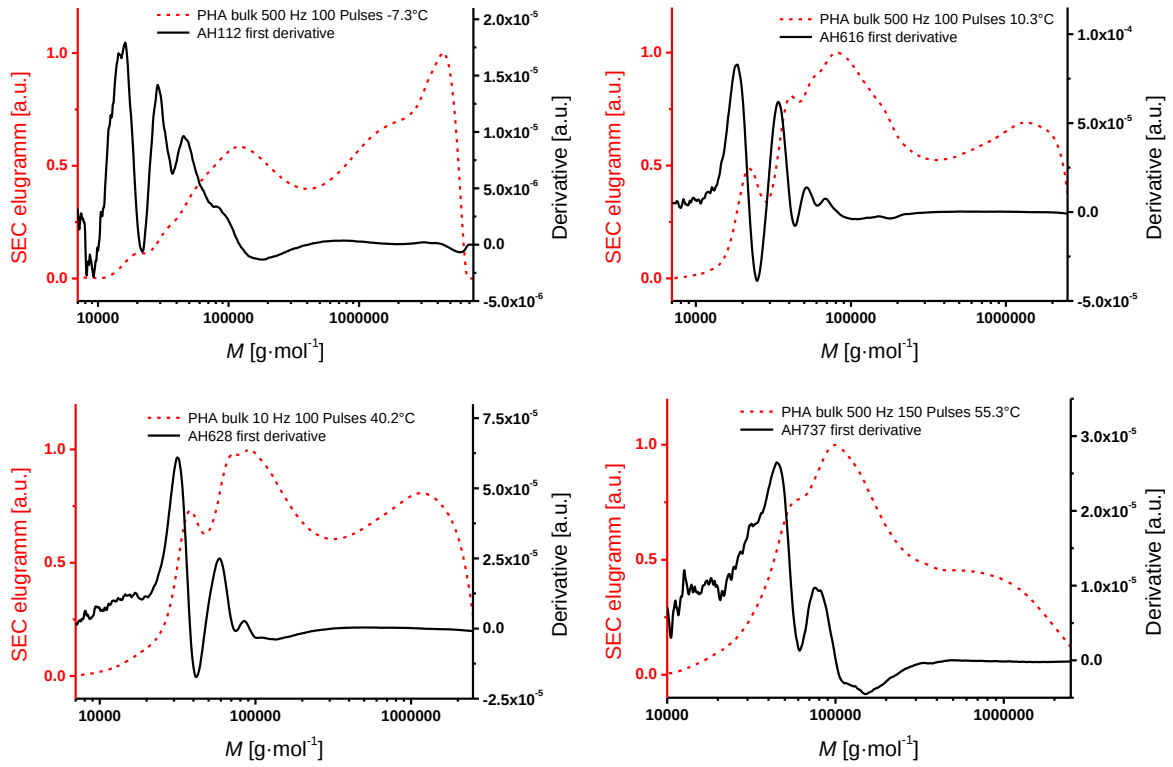

Figure S9 Exemplary molecular weight distributions (red dotted lines) and their first derivative (solid black lines) of PHA in bulk. The sample specific conditions are displayed in the diagrams and also collated in Table S13 for PHA. The typical PLP structure is observed for all samples.

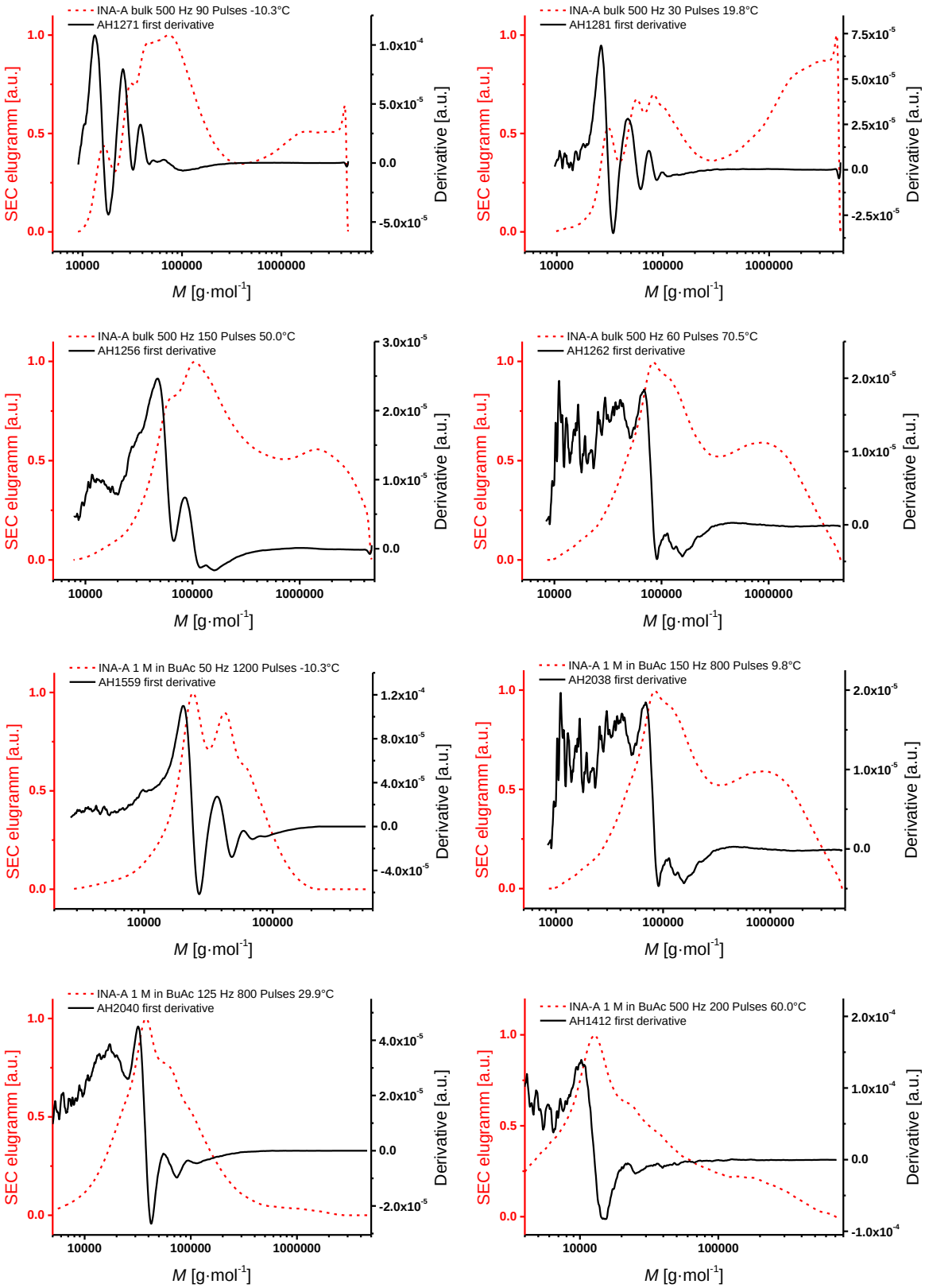

Figure S10 Exemplary molecular weight distributions (red dotted lines) and their first derivative (solid black lines) of INA-A in bulk (**upper four diagrams**) and in 1 molar solution in BuAc (**lower four diagrams**). The sample specific conditions are displayed in the diagrams and also collated in Table S14 for bulk and in Table S15 for 1 molar solution in BuAc. The typical PLP structure is observed for all samples.

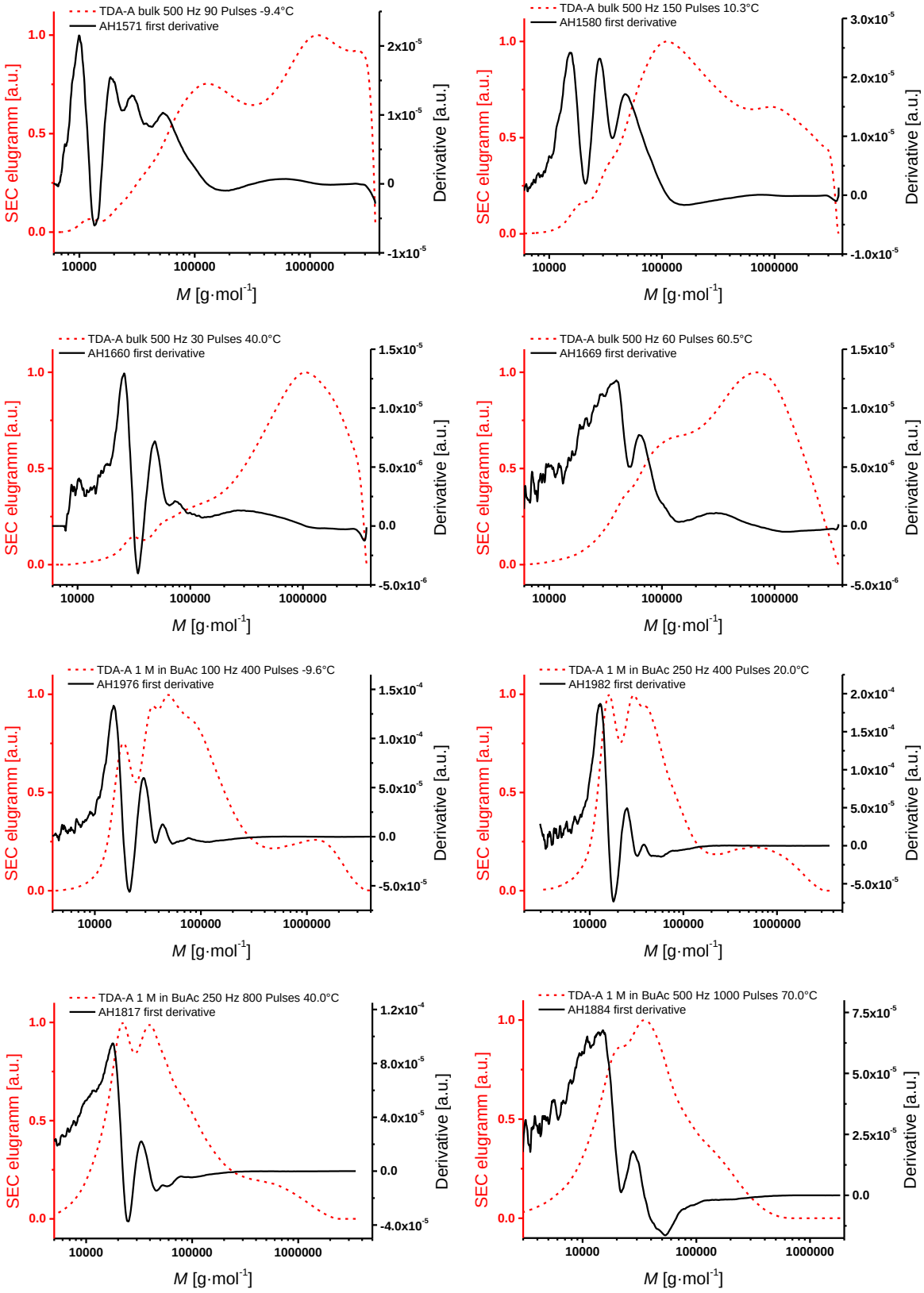

Figure S11 Exemplary molecular weight distributions (red dotted lines) and their first derivative (solid black lines) of TDA-A in bulk (**upper four diagrams**) and in 1 molar solution in BuAc (**lower four diagrams**). The sample specific conditions are displayed in the diagrams and also collated in Table S16 for bulk and in Table S17 for 1 molar solution in BuAc. The typical PLP structure is observed for all samples.

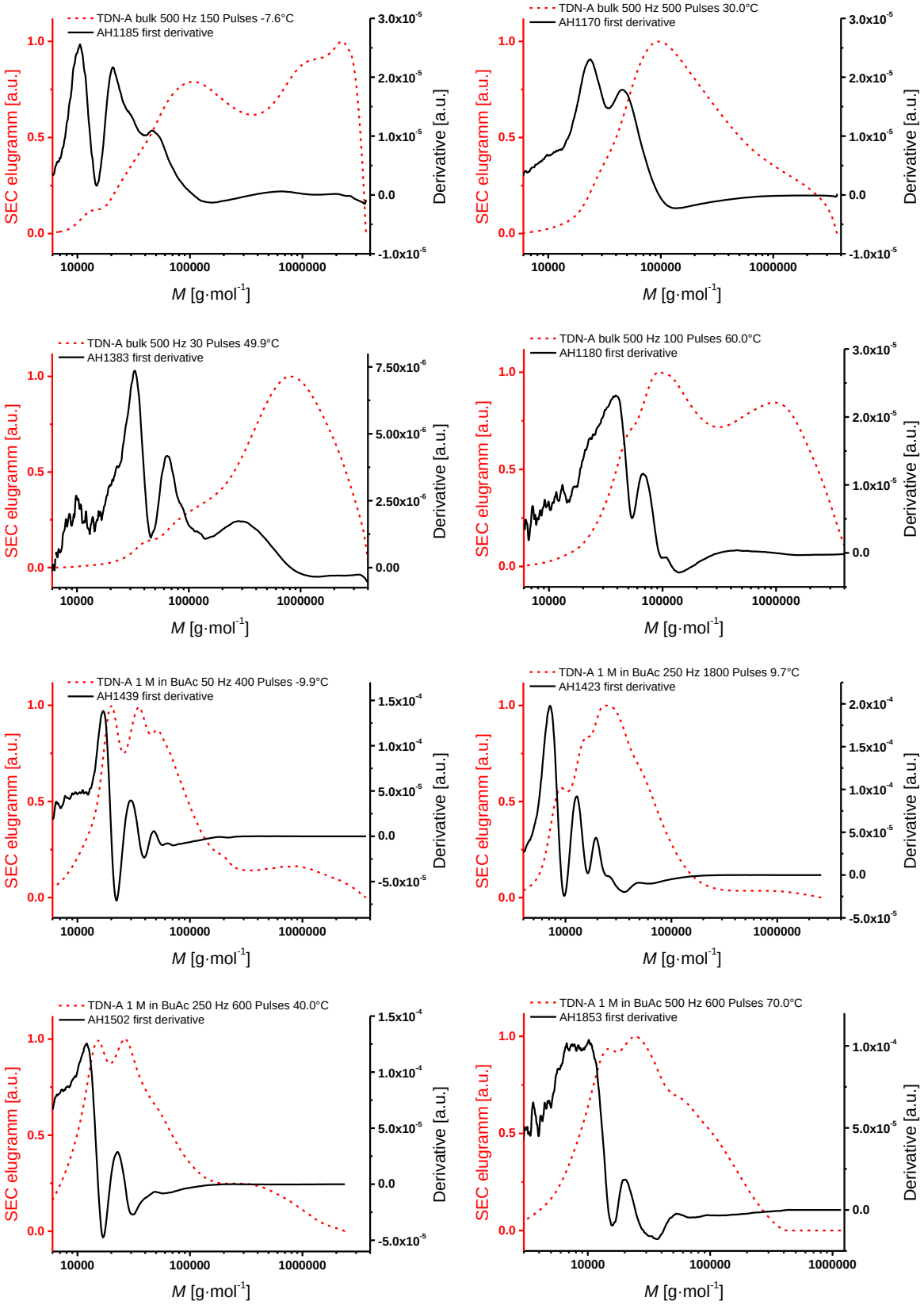

Figure S12 Exemplary molecular weight distributions (red dotted lines) and their first derivative (solid black lines) of TDN-A in bulk (**upper four diagrams**) and in 1 molar solution in BuAc (**lower four diagrams**). The sample specific conditions are displayed in the diagrams and also collated in Table S18 for bulk and in Table S19 for 1 molar solution in BuAc. The typical PLP structure is observed for all samples.

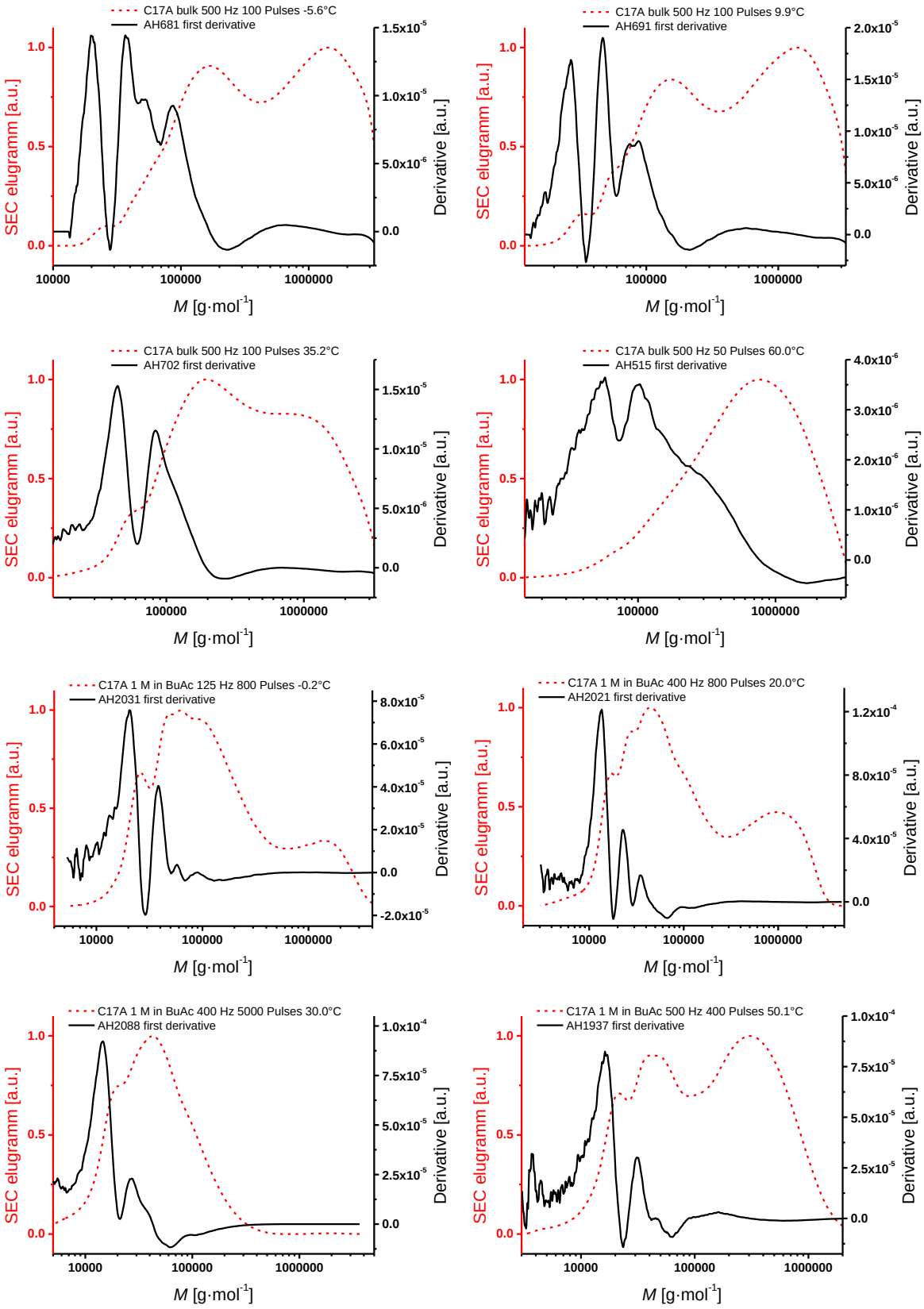

Figure S13 Exemplary molecular weight distributions (red dotted lines) and their first derivative (solid black lines) of C17A in bulk (**upper four diagrams**) and in 1 molar solution in BuAc (**lower four diagrams**). The sample specific conditions are displayed in the diagrams and also collated in Table S20 for C17A and in Table S21 and in 1 molar solution in BuAc. The typical PLP structure is observed for all samples.

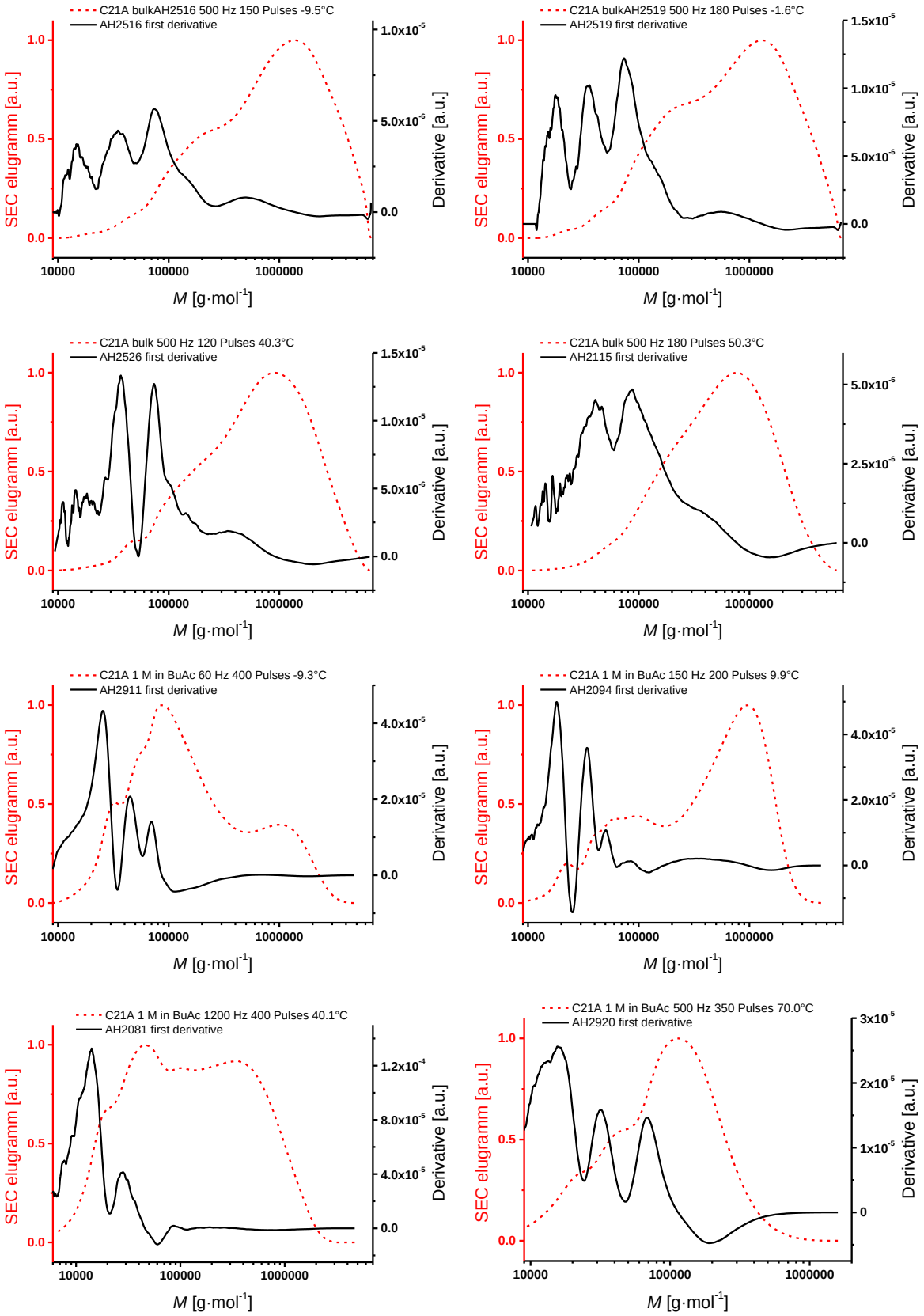

Figure S14 Exemplary molecular weight distributions (red dotted lines) and their first derivative (solid black lines) of C21A in bulk (**upper four diagrams**) and in 1 molar solution in BuAc (**lower four diagrams**). The sample specific conditions are displayed in the diagrams and also collated in Table S22 for bulk and in Table S23 for 1 molar solution in BuAc. The typical PLP structure is observed for all samples.

Sample	f	n	θ	T^{-1}	$\ln(k_{p1})$	k_{p1}/k_{p2}	M_1	M_2	c_M	k_{p1}	k_{p2}
	Hz	–	°C	10^{-3} K^{-1}	–	–	g·mol^{-1}		mol·L^{-1}	mol·L^{-1} s^{-1}	
AH1111	500	50	31.3	3.285	10.0625	1.098	40500	73500	2.477	23448	21359
AH1113	500	400	31.5	3.282	10.0409	1.100	39500	71500	2.476	22946	20857
AH1112	500	100	31.6	3.281	10.0806	1.092	41000	75000	2.476	23875	21869
AH1114	500	200	31.7	3.280	10.0113	1.068	38000	71500	2.476	22276	20861
AH1117	500	100	40.0	3.193	10.1786	1.089	45000	82500	2.459	26335	24185
AH1212	500	30	40.0	3.193	10.2306	1.105	47500	85500	2.460	27740	25101
AH1214	500	90	40.0	3.193	10.2432	1.109	48000	86500	2.460	28092	25336
AH1118	500	200	40.0	3.193	10.1882	1.103	45500	82000	2.459	26589	24100
AH1120	500	100	50.0	3.095	10.3638	1.136	53500	94500	2.438	31690	27894
AH1216	500	30	50.0	3.095	10.4396	1.183	58000	97500	2.439	34188	28894
AH1294	500	45	50.0	3.095	10.4534	1.195	58500	98000	2.439	34661	29012
AH1217	500	60	50.0	3.095	10.4820	1.200	60500	100500	2.439	35667	29722
AH1295	500	45	60.2	3.000	10.5916	1.194	66500	111500	2.418	39799	33325
AH1220	500	30	60.2	3.000	10.6241	1.224	69000	112500	2.418	41112	33594
AH1221	500	60	60.0	3.002	10.6454	1.236	70500	114000	2.418	42000	33976
AH1223	500	150	60.2	3.000	10.6442	1.267	70500	111000	2.418	41947	33116

Table S1 Detailed PLP sample conditions, absolute molecular weights of the first two inflection points, and the resulting propagation rate coefficients of the monomer SA in bulk.

Sample	f	n	θ	T^{-1}	$\ln(k_{p1})$	k_{p1}/k_{p2}	M_1	M_2	c_M	k_{p1}	k_{p2}
	Hz	–	°C	10^{-3} K^{-1}	–	–	g·mol^{-1}		mol·L^{-1}	mol·L^{-1} s^{-1}	
AH1325	500	400	10.1	3.530	9.5420	1.145	9900	17300	1.025	13933	12174
AH1324	500	200	10.1	3.530	9.5521	1.190	10000	17000	1.025	14074	11822
AH1326	500	800	10.2	3.529	9.5621	1.168	10000	17500	1.025	14216	12175
AH1328	500	400	19.9	3.412	9.7019	1.106	11500	21000	1.015	16349	14786
AH1327	500	200	20.1	3.410	9.6934	1.096	11500	21000	1.015	16211	14789
AH1329	500	800	20.2	3.409	9.7195	1.093	11500	21500	1.015	16639	15217
AH1487	500	300	29.7	3.302	9.8941	1.119	12500	22500	0.925	19813	17707
AH1488	500	600	29.9	3.300	9.8864	1.105	12500	23000	0.925	19661	17789
AH1331	500	400	30.2	3.297	9.8581	1.104	13500	24000	1.004	19113	17316
AH1493	500	300	40.1	3.192	10.0376	1.082	14500	27000	0.915	22871	21136
AH1494	500	600	40.1	3.192	10.0237	1.079	14500	26500	0.915	22555	20899
AH1333	500	200	40.2	3.191	10.0535	1.115	16000	28500	0.993	23236	20840
AH1338	500	800	49.9	3.095	10.2752	1.161	20000	34000	0.985	29005	24976
AH1337	500	400	49.9	3.095	10.2853	1.173	20000	34000	0.985	29298	24976
AH1336	500	200	50.0	3.095	10.3052	1.172	20500	35000	0.985	29887	25492
AH1339	500	200	60.0	3.002	10.4272	1.178	23000	38500	0.974	33764	28655
AH1340	500	400	60.0	3.002	10.4446	1.181	23000	39500	0.974	34357	29100
AH1341	500	800	60.0	3.002	10.4272	1.200	23000	38000	0.974	33764	28137
AH1343	500	400	70.3	2.912	10.5103	1.201	24500	41000	0.963	36691	30551
AH1344	500	800	70.3	2.912	10.5021	1.215	24500	40000	0.963	36391	29952
AH1342	500	200	70.4	2.911	10.5543	1.228	25500	41500	0.963	38342	31228

Table S2 Detailed PLP sample conditions, absolute molecular weights of the first two inflection points, and the resulting propagation rate coefficients of the monomer SA in 1 M solution in BuAc.

Sample	f	n	θ	T^{-1}	$\ln(k_{p1})$	k_{p1}/k_{p2}	M_1	M_2	c_M	k_{p1}	k_{p2}
	Hz	–	°C	10^{-3} K^{-1}	–	–	g·mol^{-1}		mol·L^{-1}	mol·L^{-1} s^{-1}	
AH1130	500	50	40.0	3.193	10.3517	1.119	53429	95483	2.302	31311	27978
AH1131	500	100	40.0	3.193	10.3357	1.121	52578	93786	2.302	30812	27480
AH1132	500	200	40.0	3.193	10.3000	1.142	50734	88835	2.302	29731	26030
AH1234	500	90	40.2	3.191	10.2896	1.136	50200	88400	2.302	29426	25909
AH1453	500	40	45.0	3.143	10.4242	1.129	57300	101500	2.297	33663	29815
AH1454	500	80	45.0	3.143	10.4785	1.167	60500	103700	2.297	35543	30461
AH1355	500	150	45.1	3.142	10.2879	1.209	50000	82700	2.297	29375	24293
AH1456	500	80	50.0	3.095	10.5039	1.175	61800	105200	2.287	36458	31030
AH1475	500	40	50.0	3.095	10.4283	1.146	57300	100000	2.287	33803	29497
AH1236	500	30	50.1	3.094	10.4576	1.184	58900	99500	2.283	34810	29402
AH1290	500	45	50.2	3.093	10.5025	1.182	61600	104200	2.283	36408	30793
AH1479	500	60	54.8	3.049	10.5160	1.202	62300	103700	2.278	36900	30710
AH1358	500	90	55.1	3.046	10.4412	1.147	57800	100800	2.278	34240	29857
AH1357	500	60	55.1	3.046	10.4918	1.188	60800	102400	2.278	36018	30331
AH1360	500	30	60.0	3.002	10.5409	1.173	63600	108400	2.268	37831	32239
AH1459	500	40	60.1	3.001	10.6706	1.190	72400	121700	2.268	43072	36201
AH1460	500	80	60.2	3.000	10.6610	1.206	71700	118900	2.268	42659	35371
AH1461	500	40	65.3	2.955	10.7748	1.259	80000	127100	2.258	47802	37972
AH1365	500	60	65.4	2.954	10.6225	1.233	68700	111400	2.258	41050	33282
AH1366	500	90	65.4	2.954	10.6049	1.266	67500	106600	2.258	40333	31848
AH1464	500	80	70.2	2.912	10.8049	1.263	82100	130000	2.249	49259	38999
AH1368	500	30	70.2	2.912	10.6804	1.278	72500	113500	2.249	43496	34047
AH1370	500	90	70.3	2.912	10.6554	1.267	70700	111600	2.249	42420	33480
AH1463	500	40	70.3	2.912	10.8408	1.193	85100	142700	2.249	51064	42813

Table S3 Detailed PLP sample conditions, absolute molecular weights of the first two inflection points, and the resulting propagation rate coefficients of the monomer BeA in bulk.

Sample	f	n	θ	T^{-1}	$\ln(k_{p1})$	k_{p1}/k_{p2}	M_1	M_2	c_M	k_{p1}	k_{p2}
	Hz	–	°C	10^{-3} K^{-1}	–	–	g·mol^{-1}		mol·L^{-1}	mol·L^{-1} s^{-1}	
AH1298	500	400	19.9	3.412	9.7962	1.128	13200	23400	0.991	17965	15924
AH1297	500	200	20.3	3.408	9.7658	1.094	12800	23400	0.991	17428	15930
AH1299	500	800	20.3	3.408	9.7890	1.096	13100	23900	0.991	17837	16271
AH1202	500	100	30.1	3.298	9.9427	1.076	14900	27700	0.967	20799	19334
AH1206	500	1200	30.2	3.297	9.9627	1.090	15200	27900	0.966	21220	19475
AH1301	500	400	30.1	3.298	9.9344	1.115	15000	26900	0.981	20628	18496
AH1211	500	1200	40.2	3.191	10.1855	1.175	18800	32000	0.957	26517	22567
AH1303	500	200	40.0	3.193	10.1434	1.162	18300	31500	0.971	25423	21880
AH1305	500	800	40.1	3.192	10.1651	1.191	18700	31400	0.971	25981	21813
AH1306	500	200	50.1	3.094	10.3104	1.182	21400	36200	0.961	30042	25409
AH1307	500	400	50.1	3.094	10.3197	1.197	21600	36100	0.961	30323	25339
AH1308	500	800	50.1	3.094	10.3150	1.208	21500	35600	0.961	30183	24988
AH1309	500	200	59.9	3.003	10.3971	1.194	23100	38700	0.951	32763	27444
AH1310	500	400	60.2	3.000	10.4145	1.199	23500	39200	0.951	33341	27808
AH1311	500	800	60.3	2.999	10.4189	1.216	23600	38800	0.951	33486	27527

Table S4 Detailed PLP sample conditions, absolute molecular weights of the first two inflection points, and the resulting propagation rate coefficients of the monomer BeA in 1 M solution in BuAc.

Sample	f	n	θ	T^{-1}	$\ln(k_{p1})$	k_{p1}/k_{p2}	M_1	M_2	c_M	k_{p1}	k_{p2}
	Hz	–	°C	10^{-3} K^{-1}	–	–	g·mol^{-1}		mol·L^{-1}	mol·L^{-1} s^{-1}	
AH479	35	100	30.8	3.290	6.4627	1.101	15700	28600	2.602	641	582
AH558	25	150	31.7	3.280	6.4778	1.152	22300	38800	2.600	651	565
AH562	30	150	40.0	3.193	6.6809	1.153	22600	39300	2.582	797	691
AH565	50	300	40.2	3.191	6.7670	1.105	14800	26800	2.581	869	786
AH569	75	300	50.3	3.092	7.0944	1.103	13600	24600	2.559	1205	1093
AH706	40	150	50.4	3.091	7.0272	1.139	23800	41800	2.559	1127	990
AH708	50	150	60.3	2.999	7.2795	1.138	24300	42700	2.538	1450	1274
AH711	100	300	60.7	2.995	7.4072	1.104	13800	25000	2.537	1648	1493
AH438	75	300	70.2	2.912	7.4388	1.171	18800	32100	2.513	1701	1452
AH571	125	300	70.8	2.907	7.5921	1.107	13200	23800	2.515	1982	1790
AH443	150	300	80.2	2.830	7.7991	1.120	13400	23900	2.492	2439	2178
AH439	75	150	80.5	2.828	7.6465	1.153	23000	39800	2.491	2093	1815
AH485	100	150	90.8	2.748	7.9142	1.155	22300	38700	2.472	2736	2368
AH489	200	150	91.4	2.743	8.0562	1.116	12900	23100	2.471	3153	2826
AH531	100	150	102.0	2.666	8.0790	1.132	26100	46100	2.448	3226	2849
AH535	200	150	102.0	2.666	8.1922	1.111	14600	26300	2.448	3613	3252

Table S5 Detailed PLP sample conditions, absolute molecular weights of the first two inflection points, and the resulting propagation rate coefficients of the monomer SMA in bulk.

Sample	f	n	θ	T^{-1}	$\ln(k_{p1})$	k_{p1}/k_{p2}	M_1	M_2	c_M	k_{p1}	k_{p2}
	Hz	–	°C	10^{-3} K^{-1}	–	–	g·mol^{-1}		mol·L^{-1}	mol·L^{-1} s^{-1}	
AH581	7	1200	0.8	3.650	5.3802	1.174	10000	17100	0.979	217	185
AH578	3	800	0.9	3.649	5.1523	1.136	18600	32800	0.978	173	152
AH713	10	1200	10.1	3.530	5.8302	1.164	11700	20100	1.041	340	292
AH582	5	800	11.1	3.518	5.4448	1.113	14800	26600	0.968	232	208
AH715	15	1200	18.7	3.426	6.1737	1.191	10900	18300	1.032	480	403
AH537	8	800	19.7	3.415	5.8093	1.103	13600	24600	0.987	333	302
AH327	10	800	29.9	3.300	6.1504	1.111	15500	28000	1.003	469	422
AH543	15	800	30.5	3.293	6.2135	1.122	10700	19100	0.976	499	445
AH545	10	800	39.9	3.194	6.3176	1.126	17700	31400	0.966	554	492
AH547	20	800	40.2	3.191	6.5301	1.143	10900	19100	0.966	685	600
AH333	10	800	50.0	3.095	6.5896	1.145	23600	41200	0.982	727	635
AH335	30	800	50.0	3.095	6.8911	1.195	10600	17800	0.982	983	823
AH550	15	1200	60.4	2.998	6.8605	1.149	19800	34600	0.945	954	830
AH551	30	800	60.4	2.998	7.0374	1.134	11800	20900	0.945	1138	1004
AH555	30	800	70.7	2.908	7.1776	1.109	13500	24300	0.935	1310	1181
AH724	40	800	70.9	2.907	7.4088	1.108	13300	24000	0.976	1650	1489
AH727	30	1200	80.9	2.824	7.4566	1.089	18400	33800	0.966	1731	1590
AH728	50	800	81.2	2.822	7.6204	1.097	13000	23700	0.965	2039	1859
AH731	35	1200	91.8	2.740	7.6550	1.108	19000	34300	0.954	2111	1906
AH732	70	800	91.6	2.742	7.8800	1.144	11900	20800	0.954	2644	2311

Table S6 Detailed PLP sample conditions, absolute molecular weights of the first two inflection points, and the resulting propagation rate coefficients of the monomer SMA in 1molar solution in BuAc.

Sample	f	n	θ	T^{-1}	$\ln(k_{p1})$	k_{p1}/k_{p2}	M_1	M_2	c_M	k_{p1}	k_{p2}
	Hz	–	°C	10^{-3} K^{-1}	–	–	g·mol^{-1}		mol·L^{-1}	mol·L^{-1} s^{-1}	
AH1030	25	300	35.0	3.245	6.6085	1.131	25300	44800	2.336	741	655
AH1031	50	150	35.0	3.245	6.7210	1.111	14200	25500	2.336	830	747
AH1033	30	150	44.8	3.145	6.8505	1.107	26700	48200	2.316	944	853
AH1035	50	150	44.9	3.144	6.9496	1.111	17000	31800	2.316	1043	939
AH1037	60	15000	44.9	3.144	7.0425	1.047	16200	30900	2.316	1144	1093
AH1041	40	300	55.2	3.046	7.1241	1.117	26100	46700	2.299	1242	1111
AH1043	80	300	55.2	3.046	7.2333	1.095	14600	26600	2.299	1385	1264
AH1044	50	150	65.9	2.949	7.3711	1.104	26500	48000	2.277	1589	1440
AH1047	100	300	66.3	2.946	7.5043	1.099	15100	27500	2.277	1816	1653
AH1048	75	150	75.4	2.869	7.6510	1.141	23200	40600	2.258	2103	1843
AH1051	150	300	75.4	2.869	7.7634	1.097	13000	23600	2.258	2353	2146
AH1052	75	150	85.7	2.787	7.7943	1.104	26500	48000	2.237	2427	2198
AH1054	150	150	86.0	2.784	7.9212	1.103	15000	27200	2.237	2755	2497
AH1056	100	150	96.2	2.707	8.0248	1.132	24800	43800	2.216	3056	2699
AH1059	200	300	96.2	2.707	8.1467	1.100	14000	25400	2.216	3452	3138
AH1061	100	300	107.0	2.631	8.1805	1.065	28600	53600	2.188	3571	3351
AH1062	200	150	107.0	2.631	8.2740	1.098	15700	28600	2.188	3921	3571

Table S7 Detailed PLP sample conditions, absolute molecular weights of the first two inflection points, and the resulting propagation rate coefficients of the monomer BeMA in bulk.

Sample	f	n	θ	T^{-1}	$\ln(k_{p1})$	k_{p1}/k_{p2}	M_1	M_2	c_M	k_{p1}	k_{p2}
	Hz	–	°C	10^{-3} K^{-1}	–	–	g·mol^{-1}		mol·L^{-1}	mol·L^{-1} s^{-1}	
AH1064	8	800	19.5	3.417	5.9243	1.109	17300	31200	1.012	374	337
AH1066	15	800	19.4	3.418	6.1702	1.146	11800	20600	1.012	478	417
AH1068	10	800	30.0	3.299	6.2623	1.129	19200	34000	1.001	524	464
AH1071	15	1200	30.3	3.295	6.3523	1.111	14000	25200	1.001	574	516
AH1072	10	800	40.0	3.193	6.5041	1.131	24200	42800	0.991	668	591
AH1074	20	800	40.0	3.193	6.6571	1.115	14100	25300	0.991	778	698
AH1076	10	800	50.0	3.095	6.7023	1.090	29200	53600	0.980	814	747
AH1078	30	800	50.0	3.095	6.9917	1.130	13000	23000	0.980	1088	962
AH1080	15	800	60.0	3.002	7.0022	1.118	26000	46500	0.970	1099	983
AH1082	30	800	60.0	3.002	7.1183	1.106	14600	26400	0.970	1234	1116
AH1084	20	800	70.0	2.914	7.2485	1.120	23800	42500	0.926	1406	1255
AH1090	40	800	70.0	2.914	7.3597	1.077	13300	24700	0.926	1571	1459
AH1093	30	1200	80.2	2.830	7.4707	1.110	19600	35300	0.915	1756	1581
AH1094	50	800	80.3	2.829	7.5711	1.088	13000	23900	0.915	1941	1784
AH1096	35	800	90.0	2.754	7.6507	1.115	19900	35700	0.906	2102	1886
AH1098	70	800	90.0	2.754	7.8380	1.086	12000	22100	0.906	2535	2335
AH1100	45	800	100.0	2.680	7.8182	1.074	18100	33700	0.896	2485	2314
AH1102	90	800	100.0	2.680	8.0313	1.103	11200	20300	0.896	3076	2788

Table S8 Detailed PLP sample conditions, absolute molecular weights of the first two inflection points, and the resulting propagation rate coefficients of the monomer BeMA in 1molar solution in BuAc.

Sample	f	n	θ	T^{-1}	$\ln(k_{p1})$	k_{p1}/k_{p2}	M_1	M_2	c_M	k_{p1}	k_{p2}
	Hz	–	°C	10^{-3} K^{-1}	–	–	g·mol^{-1}		mol·L^{-1}	mol·L^{-1} s^{-1}	
AH307	30	800	-8.8	3.783	5.1204	1.070	5000	9400	3.964	167	156
AH305	10	800	-8.5	3.779	4.8900	1.085	11900	22000	3.963	133	123
AH637	20	800	-0.1	3.662	5.3481	1.133	9400	16500	3.933	210	185
AH635	10	800	0.0	3.661	5.2054	1.072	16200	30300	3.933	182	170
AH641	25	800	9.4	3.539	5.6389	1.112	9900	17800	3.900	281	253
AH639	12	800	9.9	3.533	5.5083	1.091	18100	33200	3.898	247	226
AH645	30	800	19.4	3.418	5.9217	1.079	10900	20100	3.865	373	346
AH643	15	800	19.8	3.414	5.8167	1.097	19600	35700	3.863	336	306
AH311	30	800	30.0	3.299	6.1508	1.081	13500	25000	3.828	469	434
AH313	50	800	30.1	3.298	6.4335	1.096	10800	19700	3.827	622	568
AH647	30	800	39.6	3.197	6.3748	1.082	16800	31000	3.794	587	542
AH650	60	1200	40.3	3.190	6.5615	1.098	10100	18400	3.791	707	644
AH651	30	800	50.2	3.093	6.6880	1.123	22700	40500	3.757	803	715
AH653	60	800	50.3	3.092	6.8557	1.069	13400	25100	3.756	949	888
AH777	60	800	60.1	3.001	7.0748	1.071	16600	31000	3.726	1182	1103
AH776	30	1200	60.2	3.000	6.9009	1.026	27900	54400	3.726	993	968
AH779	40	800	69.9	2.915	7.2014	1.096	28000	51100	3.692	1341	1224
AH780	80	800	70.5	2.910	7.3292	1.067	15900	29800	3.690	1524	1428
AH783	100	800	80.3	2.829	7.5298	1.066	15400	28900	3.655	1863	1748
AH782	50	1200	80.7	2.826	7.3985	1.061	27000	50900	3.654	1634	1540

Table S9 Detailed PLP sample conditions, absolute molecular weights of the first two inflection points, and the resulting propagation rate coefficients of the monomer PHMA in bulk.

Sample	f	n	θ	T^{-1}	$\ln(k_{p1})$	k_{p1}/k_{p2}	M_1	M_2	c_M	k_{p1}	k_{p2}
	Hz	–	°C	10^{-3} K^{-1}	–	–	g·mol^{-1}		mol·L^{-1}	mol·L^{-1} s^{-1}	
AH2150	5	200	-9.7	3.796	5.0626	1.120	28769	51369	3.392	158	141
AH2151	5	400	-9.0	3.786	5.0692	1.100	29000	52500	3.390	159	145
AH2152	10	200	-8.8	3.783	5.1400	1.024	15500	30500	3.389	171	167
AH2153	10	400	-8.7	3.781	5.1723	1.028	16000	31000	3.389	176	172
AH2154	5	200	-0.4	3.666	5.3027	1.017	36500	71500	3.365	201	197
AH2155	5	400	-0.4	3.666	5.2782	1.019	35500	69500	3.365	196	192
AH2157	10	400	-0.4	3.666	5.4399	1.069	21000	39000	3.365	230	216
AH2156	10	200	-0.4	3.666	5.4233	1.071	20500	38000	3.365	227	212
AH1963	5	400	9.7	3.535	5.5941	1.058	48000	91000	3.337	269	254
AH1962	5	200	9.8	3.534	5.6125	1.044	49000	94000	3.336	274	262
AH1964	10	200	9.8	3.534	5.7414	1.102	28000	50500	3.336	312	283
AH1965	10	400	10.0	3.532	5.7601	1.099	28500	51500	3.336	317	289
AH1969	15	400	19.9	3.412	6.1044	1.105	26500	48000	3.308	448	405
AH1968	15	200	19.9	3.412	6.0979	1.106	26500	47500	3.308	445	402
AH1966	8	200	20.2	3.409	5.9843	1.037	44000	85000	3.307	397	383
AH1967	8	400	20.2	3.409	5.9883	1.052	44000	84000	3.307	399	379
AH1887	20	1200	29.5	3.304	6.3550	1.083	25500	46500	3.276	575	531
AH1888	40	800	29.6	3.303	6.4330	1.025	13500	26500	3.276	622	607
AH1972	25	200	30.0	3.299	6.3904	1.040	21000	40500	3.279	596	573
AH1971	12	400	30.2	3.297	6.3146	1.029	40500	79000	3.279	553	537
AH2158	20	200	40.0	3.193	6.6003	1.073	32000	60000	3.251	735	685
AH2163	40	2000	40.2	3.191	6.6718	1.024	17000	33500	3.251	790	772
AH2161	40	200	40.2	3.191	6.6913	1.038	17500	34000	3.251	805	776
AH2159	20	400	40.2	3.191	6.6167	1.059	32500	61500	3.251	747	706
AH1893	30	1200	49.8	3.096	6.8946	1.028	28500	55500	3.218	987	960
AH1895	60	1200	49.9	3.095	6.9389	0.991	15000	30000	3.218	1032	1041
AH2167	50	400	50.0	3.095	6.9422	1.037	18000	34500	3.223	1035	998
AH2164	25	200	50.0	3.095	6.9059	1.039	34500	66500	3.223	998	960
AH2169	30	400	59.8	3.003	7.1416	1.025	36000	70500	3.195	1263	1232
AH2170	60	200	59.8	3.003	7.1888	1.033	19000	36500	3.195	1325	1282
AH2171	60	400	59.8	3.003	7.2243	1.045	19500	37500	3.195	1372	1313
AH2168	30	200	60.0	3.002	7.1658	1.024	37000	72500	3.194	1294	1264
AH2206	30	200	70.1	2.913	7.2960	1.011	42000	82500	3.166	1474	1459
AH2209	60	400	70.1	2.913	7.4740	1.068	25000	46500	3.166	1762	1650
AH2207	30	400	70.2	2.912	7.3294	1.023	43000	84500	3.166	1525	1491
AH2208	60	200	70.2	2.912	7.4879	1.070	25500	47500	3.166	1786	1669
AH2210	35	200	80.0	2.832	7.6088	1.034	48500	94000	3.138	2016	1949
AH2212	70	200	80.2	2.830	7.7364	1.096	27500	50500	3.137	2290	2090
AH2211	35	400	80.2	2.830	7.6236	1.115	49000	88500	3.137	2046	1835
AH2213	70	400	80.3	2.829	7.7490	1.094	28000	51000	3.137	2319	2120
AH2214	40	200	90.4	2.751	7.7950	0.958	50500	106000	3.108	2428	2535
AH2215	40	400	90.4	2.751	7.7144	1.020	46500	91500	3.108	2240	2195
AH2216	80	200	90.4	2.751	7.8979	1.089	28000	51500	3.108	2692	2471
AH2217	80	400	90.5	2.750	7.8729	1.085	27500	50500	3.108	2625	2420

Table S10 Detailed PLP sample conditions, absolute molecular weights of the first two inflection points, and the resulting propagation rate coefficients of the monomer TDA-MA in bulk.

Sample	f	n	θ	T^{-1}	$\ln(k_{p1})$	k_{p1}/k_{p2}	M_1	M_2	c_M	k_{p1}	k_{p2}
	Hz	–	°C	10^{-3} K^{-1}	–	–	g·mol^{-1}		mol·L^{-1}	mol·L^{-1} s^{-1}	
AH2128	5	200	-10.9	3.813	4.8849	1.146	23738	41439	3.343	132	115
AH2129	5	400	-10.0	3.800	4.9095	1.154	24500	42000	3.340	136	118
AH2130	10	200	-9.8	3.797	5.0893	1.088	14500	26500	3.339	162	149
AH2131	10	400	-9.7	3.796	5.0993	1.088	14500	27000	3.339	164	151
AH2135	10	400	-0.7	3.670	5.3186	1.101	18000	33000	3.313	204	185
AH2133	5	400	-0.6	3.669	5.2311	1.087	33500	61000	3.313	187	172
AH2134	10	200	-0.6	3.669	5.3266	1.100	18500	33500	3.313	206	187
AH2132	5	200	-0.2	3.664	5.2229	1.086	33000	60500	3.312	185	171
AH1994	8	200	9.8	3.534	5.5747	1.125	29000	52000	3.294	264	234
AH1995	8	400	10.1	3.530	5.5553	1.121	28500	51000	3.294	259	231
AH1996	15	200	10.1	3.530	5.6729	1.091	17000	31500	3.294	291	267
AH1997	15	400	10.6	3.524	5.6734	1.101	17000	31000	3.292	291	264
AH2001	25	400	19.7	3.415	6.0477	10.296	15000	3000	3.266	423	41
AH2000	25	200	19.8	3.414	6.0380	1.093	14500	27000	3.265	419	383
AH1998	12	200	20.0	3.411	5.9290	1.146	27500	48000	3.265	376	328
AH1999	12	400	20.2	3.409	5.9395	1.148	27500	48500	3.264	380	331
AH2002	15	200	30.1	3.298	6.2263	1.118	29500	52500	3.235	506	452
AH2005	30	400	30.1	3.298	6.3410	1.105	16500	29500	3.235	567	513
AH2144	15	2000	31.9	3.278	6.2020	1.077	28500	53000	3.218	494	458
AH2146	30	2000	32.1	3.276	6.3809	1.073	17000	31500	3.218	590	551
AH1953	40	800	39.9	3.194	6.5559	1.080	15000	28000	3.204	703	651
AH1955	60	800	39.9	3.194	6.6747	1.095	11500	20500	3.204	792	723
AH1952	20	1200	40.0	3.193	6.4637	1.129	27500	49000	3.204	641	568
AH1954	40	1200	40.0	3.193	6.5655	1.101	15500	27500	3.204	710	645
AH2006	25	200	50.0	3.095	6.7601	1.115	29500	53000	3.177	863	774
AH2007	25	400	50.0	3.095	6.7745	1.119	30000	53500	3.177	875	782
AH2008	50	200	50.0	3.095	6.8699	1.085	16500	30500	3.177	963	888
AH2009	50	400	50.0	3.095	6.8699	1.095	16500	30000	3.177	963	879
AH1958	30	1200	59.8	3.003	6.9078	1.064	28000	53000	3.146	1000	940
AH1957	30	800	60.0	3.002	6.9475	1.110	29500	53000	3.146	1041	938
AH1959	60	800	60.1	3.001	7.0623	1.095	16500	30000	3.146	1167	1066
AH1960	60	1200	60.1	3.001	7.0535	1.112	16500	29500	3.146	1157	1041
AH2011	35	400	70.3	2.912	7.2460	1.082	33500	62000	3.118	1403	1296
AH2010	35	200	70.4	2.911	7.1852	1.079	31500	58500	3.118	1320	1224
AH2012	70	200	70.4	2.911	7.3488	1.099	18500	34000	3.118	1554	1415
AH2013	70	400	70.4	2.911	7.3565	1.098	18500	34000	3.118	1566	1426
AH2138	80	200	80.3	2.829	7.4874	1.081	18500	34000	3.078	1785	1651
AH2139	80	400	80.3	2.829	7.5768	1.105	20000	36500	3.078	1952	1768
AH2136	40	200	80.4	2.828	7.4540	1.076	35500	66500	3.078	1727	1605
AH2137	40	400	80.4	2.828	7.3273	1.071	31500	58500	3.078	1521	1420
AH2140	45	200	90.3	2.751	7.5489	1.068	34500	64500	3.049	1899	1777
AH2142	90	200	90.3	2.751	7.7181	1.112	20500	37000	3.049	2249	2023
AH2141	45	400	90.5	2.750	7.6201	1.086	37000	68500	3.048	2039	1877
AH2143	90	400	90.5	2.750	7.7183	1.107	20500	37000	3.048	2249	2031

Table S11 Detailed PLP sample conditions, absolute molecular weights of the first two inflection points, and the resulting propagation rate coefficients of the monomer TDN-MA in bulk.

Sample	f	n	θ	T^{-1}	$\ln(k_{p1})$	k_{p1}/k_{p2}	M_1	M_2	c_M	k_{p1}	k_{p2}
	Hz	–	°C	10^{-3} K^{-1}	–	–	g·mol^{-1}		mol·L^{-1}	mol·L^{-1} s^{-1}	
AH201	15	300	-6.6	3.752	5.4519	1.028	13900	27000	2.756	233	227
AH199	5	300	-6.4	3.749	5.1861	1.020	32000	62700	2.755	179	175
AH206	15	600	0.8	3.650	5.6331	1.040	16600	31900	2.739	280	269
AH205	5	300	0.9	3.649	5.3744	1.040	38400	73700	2.739	216	207
AH211	5	200	9.9	3.533	5.6596	1.165	50700	86900	2.719	287	246
AH216	15	100	10.1	3.530	5.8589	1.087	20600	37900	2.718	350	322
AH218	10	700	20.0	3.411	5.9962	1.106	35200	63600	2.696	402	363
AH403	20	400	20.1	3.410	5.9307	1.117	16500	29500	2.693	376	337
AH407	40	400	30.0	3.299	6.3582	1.126	12500	22200	2.671	577	513
AH187	15	200	30.3	3.295	6.3254	1.129	32300	57200	2.674	559	495
AH347	20	200	40.0	3.193	6.5585	1.160	30400	52400	2.654	705	608
AH195	50	200	40.1	3.192	6.7743	1.119	15100	26900	2.652	875	782
AH408	40	250	49.9	3.095	6.8339	1.137	19800	34800	2.627	929	817
AH351	20	200	50.0	3.095	6.7232	1.125	35500	63100	2.632	831	739
AH411	30	500	60.1	3.001	6.9041	1.045	28100	53700	2.605	996	953
AH414	50	250	60.1	3.001	7.0480	1.132	19500	34400	2.605	1151	1016
AH417	40	500	70.3	2.912	7.2483	1.087	29500	54200	2.582	1406	1293
AH418	70	300	70.3	2.912	7.3570	1.114	18800	33700	2.582	1567	1407
AH420	40	300	80.5	2.828	7.4116	1.109	34400	62000	2.560	1655	1493
AH422	70	300	80.5	2.828	7.5605	1.157	22800	39400	2.560	1921	1660

Table S12 Detailed PLP sample conditions, absolute molecular weights of the first two inflection points, and the resulting propagation rate coefficients of the monomer C17MA in bulk.

Sample	f	n	θ	T^{-1}	$\ln(k_{p1})$	k_{p1}/k_{p2}	M_1	M_2	c_M	k_{p1}	k_{p2}
	Hz	–	°C	10^{-3} K^{-1}	–	–	g·mol^{-1}		mol·L^{-1}	mol·L^{-1} s^{-1}	
AH111	500	150	-7.3	3.762	8.7628	1.091	11400	20900	4.199	6392	5861
AH112	500	100	-7.3	3.762	8.7083	1.076	10800	20100	4.199	6053	5626
AH114	500	150	0.8	3.650	8.9330	1.014	13400	26500	4.179	7578	7472
AH115	500	100	0.1	3.660	8.9145	1.033	13200	25600	4.181	7439	7200
AH616	500	100	10.3	3.528	9.2835	1.079	18600	34500	4.076	10759	9970
AH617	500	150	10.3	3.528	9.2705	1.076	18400	34200	4.076	10620	9867
AH618	500	50	19.1	3.422	9.4489	1.110	21900	39400	4.055	12694	11436
AH619	500	100	19.6	3.416	9.5076	1.107	23200	41900	4.054	13462	12163
AH622	500	100	30.2	3.297	9.6487	1.101	26500	48200	4.029	15502	14074
AH623	500	150	30.3	3.295	9.6666	1.100	27000	49100	4.029	15782	14352
AH625	500	100	35.3	3.242	9.7583	1.079	29500	54700	4.017	17297	16024
AH626	500	150	35.3	3.242	9.7663	1.072	29700	55500	4.017	17437	16267
AH628	500	100	40.2	3.191	9.8388	1.076	31900	59300	4.006	18748	17425
AH629	500	150	40.2	3.191	9.8610	1.079	32600	60500	4.006	19168	17772
AH631	500	100	45.3	3.140	9.9446	1.102	35300	64100	3.994	20840	18904
AH632	500	150	45.3	3.140	9.9208	1.093	34500	63200	3.994	20348	18625
AH633	500	50	50.1	3.094	10.0030	1.095	37400	68200	3.982	22094	20177
AH734	500	150	50.2	3.093	10.1394	1.122	42800	76300	3.980	25322	22571
AH735	500	50	55.1	3.046	10.1835	1.115	44600	80000	3.969	26464	23734
AH737	500	150	55.3	3.045	10.1926	1.163	45000	77400	3.968	26704	22966
AH739	500	100	60.4	2.998	10.2725	1.193	48600	81500	3.956	28927	24255

Table S13 Detailed PLP sample conditions, absolute molecular weights of the first two inflection points, and the resulting propagation rate coefficients of the monomer PHA in bulk.

Sample	f	n	θ	T^{-1}	$\ln(k_{p1})$	k_{p1}/k_{p2}	M_1	M_2	c_M	k_{p1}	k_{p2}
	Hz	–	°C	10^{-3} K^{-1}	–	–	g·mol^{-1}		mol·L^{-1}	mol·L^{-1} s^{-1}	
AH1269	500	30	-10.3	3.804	8.8313	1.047	12399	23686	4.567	6845	6538
AH1270	500	60	-10.3	3.804	8.8520	1.046	12500	24000	4.567	6988	6681
AH1271	500	90	-10.3	3.804	8.9118	1.043	13500	26000	4.567	7419	7110
AH1272	500	150	-10.3	3.804	8.9118	1.049	13500	25500	4.567	7419	7075
AH1273	500	30	0.1	3.660	9.0898	1.037	16000	30500	4.524	8865	8549
AH1274	500	60	0.1	3.660	9.1531	1.068	17000	31500	4.524	9443	8838
AH1275	500	90	0.1	3.660	9.1531	1.047	17000	32500	4.524	9443	9018
AH1276	500	150	0.1	3.660	9.1683	1.046	17000	33000	4.524	9588	9162
AH1277	500	30	10.0	3.532	9.3813	1.058	21000	40000	4.483	11864	11210
AH1278	500	60	9.9	3.533	9.4055	1.088	21500	39500	4.483	12155	11173
AH1279	500	90	10.0	3.532	9.4293	1.079	22000	41000	4.483	12447	11538
AH1280	500	150	9.9	3.533	9.4580	1.169	23000	39000	4.483	12811	10955
AH1281	500	30	19.8	3.414	9.6150	1.106	26500	47500	4.442	14988	13550
AH1282	500	60	20.1	3.410	9.6632	1.084	27500	51000	4.441	15727	14507
AH1283	500	90	19.8	3.414	9.6675	1.112	28000	50000	4.442	15796	14210
AH1284	500	150	20.2	3.409	9.6909	1.074	28500	53000	4.441	16170	15058
AH1285	500	30	30.1	3.298	9.7662	1.062	30500	57500	4.400	17434	16420
AH1286	500	60	30.1	3.298	9.8556	1.063	33500	62500	4.400	19065	17936
AH1287	500	90	30.1	3.298	9.8556	1.048	33500	63500	4.400	19065	18194
AH1288	500	150	30.1	3.298	9.8672	1.045	33500	64500	4.400	19288	18453
AH1249	500	30	40.1	3.192	10.0394	1.046	39500	75500	4.358	22912	21911
AH1250	500	60	40.0	3.193	10.0491	1.063	40000	75000	4.359	23134	21760
AH1251	500	90	40.1	3.192	10.0620	1.066	40500	76000	4.358	23436	21986
AH1252	500	150	40.0	3.193	10.0809	1.086	41500	76000	4.359	23882	21983
AH1253	500	30	50.1	3.094	10.1973	1.090	46000	84500	4.317	26831	24606
AH1254	500	60	50.1	3.094	10.2332	1.127	47500	84500	4.317	27812	24681
AH1255	500	90	50.0	3.095	10.2412	1.140	48000	84500	4.317	28036	24603
AH1256	500	150	50.0	3.095	10.2385	1.118	48000	85500	4.317	27960	25017
AH1257	500	30	60.3	2.999	10.4851	1.237	60500	98000	4.275	35779	28914
AH1258	500	60	60.3	2.999	10.4830	1.241	60500	97500	4.275	35703	28762
AH1259	500	90	60.1	3.001	10.4807	1.297	60500	93000	4.275	35620	27465
AH1260	500	150	60.4	2.998	10.4873	1.275	61000	95500	4.274	35859	28119
AH1261	500	30	70.5	2.910	10.6152	1.295	68500	105500	4.232	40748	31466
AH1262	500	60	70.5	2.910	10.6338	1.217	69500	114500	4.232	41516	34111
AH1263	500	90	70.4	2.911	10.6169	1.285	68500	106500	4.233	40821	31769
AH1264	500	150	70.3	2.912	10.6093	1.256	68000	108500	4.233	40509	32265

Table S14 Detailed PLP sample conditions, absolute molecular weights of the first two inflection points, and the resulting propagation rate coefficients of the monomer INA-A in bulk.

Sample	f	n	θ	T^{-1}	$\ln(k_{p1})$	k_{p1}/k_{p2}	M_1	M_2	c_M	k_{p1}	k_{p2}
	Hz	–	°C	10^{-3} K^{-1}	–	–	g·mol^{-1}		mol·L^{-1}	mol·L^{-1} s^{-1}	
AH1557	50	400	-10.4	3.806	8.4610	1.085	19797	36501	1.056	4727	4358
AH1558	50	800	-10.3	3.804	8.5060	1.092	20500	38000	1.056	4944	4528
AH1559	50	1200	-10.3	3.804	8.4870	1.090	20500	37500	1.056	4851	4451
AH1560	100	400	-10.2	3.803	8.5639	1.046	11000	21000	1.056	5239	5007
AH1561	100	800	-10.2	3.803	8.5873	1.052	11000	21500	1.056	5363	5099
AH1562	100	1200	-10.1	3.802	8.5989	1.051	11500	21500	1.056	5426	5162
AH1563	50	400	-0.3	3.665	8.7502	1.110	26000	47000	1.044	6312	5685
AH1564	50	800	-0.2	3.664	8.7700	1.085	26500	49000	1.044	6438	5935
AH1567	100	800	-0.2	3.664	8.8342	1.056	14000	27000	1.044	6865	6500
AH1565	50	1200	-0.1	3.662	8.7603	1.088	26500	48500	1.044	6376	5858
AH1566	100	400	-0.1	3.662	8.8343	1.046	14000	27000	1.044	6866	6564
AH1568	100	1200	-0.1	3.662	8.8434	1.056	14500	27000	1.044	6928	6564
AH2038	150	800	9.8	3.534	9.2252	1.034	14000	26500	1.028	10150	9819
AH1466	125	2000	9.9	3.533	9.0766	1.056	14000	27000	1.024	8748	8283
AH2039	150	1200	9.9	3.533	9.2180	1.030	13500	26500	1.028	10077	9783
AH2036	75	800	10.0	3.532	9.1502	1.123	25500	45500	1.028	9416	8386
AH2037	75	1200	10.2	3.529	9.1582	1.129	26000	45500	1.028	9492	8406
AH1465	125	1000	10.2	3.529	9.0950	1.065	14500	27000	1.024	8911	8366
AH1471	125	3000	19.6	3.416	9.2704	1.072	17000	32000	1.013	10619	9903
AH1472	250	1000	19.6	3.416	9.4345	1.087	10000	18500	1.013	12513	11507
AH1473	250	2000	19.6	3.416	9.4345	1.080	10000	18500	1.013	12513	11588
AH1474	250	3000	19.8	3.414	9.4347	1.095	10000	18500	1.013	12516	11429
AH1469	125	1000	20.0	3.411	9.3155	1.045	18000	34000	1.013	11109	10632
AH1470	125	2000	20.2	3.409	9.2936	1.062	17500	33000	1.013	10869	10232
AH2040	125	800	29.9	3.300	9.6515	1.130	25000	44000	1.006	15546	13759
AH2041	125	1200	30.1	3.298	9.6638	1.138	25000	44000	1.005	15737	13825
AH2042	250	800	30.2	3.297	9.7144	1.023	13000	26000	1.005	16554	16178
AH2043	250	1200	30.2	3.297	9.7068	1.008	13000	26000	1.005	16429	16304
AH2044	200	800	40.0	3.193	9.8181	1.025	18000	35500	0.994	18364	17907
AH2045	200	1200	40.0	3.193	9.8236	1.034	18000	35000	0.994	18465	17856
AH2046	400	800	40.0	3.193	9.9856	1.059	10500	20000	0.994	21712	20494
AH2047	400	1200	40.0	3.193	9.9762	1.050	10500	20000	0.994	21509	20494
AH2048	200	800	50.0	3.095	10.1283	1.146	24500	42500	0.983	25042	21861
AH2049	200	1200	50.0	3.095	10.1160	1.150	24000	42000	0.983	24734	21502
AH2050	400	800	50.0	3.095	10.1526	0.992	12500	25000	0.983	25658	25863
AH2051	400	1200	50.0	3.095	10.1526	0.996	12500	25000	0.983	25658	25761
AH1409	500	200	50.0	3.095	10.0844	1.092	9500	17500	1.004	23966	21938
AH1410	500	400	50.0	3.095	10.0567	1.079	9500	17000	1.004	23312	21612
AH1411	500	800	50.0	3.095	10.0567	1.071	9500	17500	1.004	23312	21775
AH1412	500	200	60.0	3.002	10.1996	0.967	10500	22000	0.992	26892	27800
AH1414	500	800	60.0	3.002	10.1747	0.997	10500	20500	0.992	26231	26317
AH1413	500	400	60.1	3.001	10.1873	0.997	10500	21000	0.992	26565	26649
AH2056	500	800	70.1	2.913	10.5127	1.026	14000	27500	0.960	36778	35859
AH2057	500	1200	70.1	2.913	10.5198	1.011	14000	28000	0.960	37041	36647
AH1417	500	800	70.2	2.912	10.3054	0.950	11500	24500	0.980	29893	31470

Table S15 Detailed PLP sample conditions, absolute molecular weights of the first two inflection points, and the resulting propagation rate coefficients of the monomer INA-A in 1 M solution in BuAc.

Sample	f	n	θ	T^{-1}	$\ln(k_{p1})$	k_{p1}/k_{p2}	M_1	M_2	c_M	k_{p1}	k_{p2}
	Hz	–	°C	10^{-3} K^{-1}	–	–	g·mol^{-1}		mol·L^{-1}	mol·L^{-1} s^{-1}	
AH1569	500	30	-9.5	3.793	8.9008	1.075	13273	24703	3.555	7338	6828
AH1570	500	60	-9.5	3.793	8.8782	1.051	13000	24500	3.555	7174	6828
AH1571	500	90	-9.4	3.791	8.9230	1.054	13500	25500	3.555	7502	7117
AH1574	500	60	-0.1	3.662	9.1195	1.054	16500	31000	3.527	9132	8665
AH1575	500	90	-0.3	3.665	9.1373	1.068	16500	31000	3.527	9295	8705
AH1576	500	150	-0.1	3.662	9.1978	1.040	17500	34000	3.527	9876	9494
AH1577	500	30	9.7	3.535	9.3894	1.100	21500	38500	3.497	11961	10871
AH1578	500	60	9.6	3.537	9.4032	1.086	21500	39500	3.498	12127	11164
AH1579	500	90	9.7	3.535	9.4304	1.096	22000	40500	3.497	12462	11374
AH1580	500	150	10.3	3.528	9.4639	1.096	23000	42000	3.496	12886	11757
AH1652	500	30	20.4	3.407	9.5846	1.092	25500	47000	3.460	14539	13318
AH1653	500	60	19.9	3.412	9.6128	1.106	26500	47500	3.461	14955	13523
AH1654	500	90	20.3	3.408	9.6131	1.076	26500	49000	3.460	14960	13909
AH1655	500	150	20.5	3.405	9.6736	1.068	28000	52500	3.460	15892	14886
AH1656	500	30	30.0	3.299	9.8067	1.061	31500	59500	3.431	18154	17104
AH1657	500	60	30.0	3.299	9.8253	1.040	32500	62000	3.431	18495	17788
AH1658	500	90	30.0	3.299	9.8615	1.045	33500	64000	3.431	19177	18344
AH1659	500	150	29.9	3.300	9.8569	1.024	33500	65000	3.431	19090	18642
AH1660	500	30	40.0	3.193	10.0072	1.065	38500	72000	3.401	22186	20836
AH1661	500	60	40.1	3.192	10.0189	1.073	39000	72500	3.401	22446	20924
AH1662	500	90	40.0	3.193	10.0111	1.051	38500	73500	3.401	22272	21182
AH1663	500	150	40.0	3.193	10.0226	1.049	39000	74500	3.401	22530	21484
AH1664	500	30	50.1	3.094	10.1638	1.059	44500	84000	3.371	25947	24509
AH1665	500	60	50.1	3.094	10.1771	1.050	45000	86000	3.371	26295	25032
AH1666	500	90	50.1	3.094	10.1903	1.076	45500	85000	3.371	26642	24771
AH1667	500	150	50.0	3.095	10.1366	1.074	43500	80500	3.371	25250	23505
AH1668	500	30	59.9	3.003	10.3641	1.117	54000	96500	3.342	31701	28376
AH1669	500	60	60.5	2.997	10.4722	1.250	60000	96000	3.340	35319	28259
AH1670	500	90	60.3	2.999	10.4157	1.252	56500	90500	3.340	33381	26669
AH1672	500	30	70.0	2.914	10.5913	1.271	67000	105500	3.311	39789	31300
AH1673	500	60	70.1	2.913	10.6113	1.342	68500	102000	3.311	40590	30237

Table S16 Detailed PLP sample conditions, absolute molecular weights of the first two inflection points, and the resulting propagation rate coefficients of the monomer TDA-A in bulk.

Sample	f	n	θ	T^{-1}	$\ln(k_{p1})$	k_{p1}/k_{p2}	M_1	M_2	c_M	k_{p1}	k_{p2}
	Hz	–	°C	10^{-3} K^{-1}	–	–	g·mol^{-1}		mol·L^{-1}	mol·L^{-1} s^{-1}	
AH1974	60	400	-10.0	3.800	8.5336	1.075	22474	41822	1.043	5083	4729
AH1975	60	800	-9.8	3.797	8.5534	1.069	23000	43000	1.043	5185	4848
AH1976	100	400	-9.6	3.794	8.6635	1.053	15500	29000	1.042	5788	5499
AH1977	100	800	-9.3	3.790	8.6443	1.037	15000	29000	1.042	5678	5472
AH1864	80	400	-0.4	3.666	8.7521	1.073	21000	39000	1.036	6324	5893
AH1865	80	800	-0.3	3.665	8.7593	1.081	21000	39000	1.036	6370	5894
AH1978	150	400	0.0	3.661	8.9559	1.042	13500	26000	1.032	7753	7440
AH1979	150	800	0.0	3.661	8.9449	1.049	13500	25500	1.032	7669	7312
AH1798	100	400	9.9	3.533	9.1213	1.093	23500	43500	1.017	9148	8372
AH1980	200	400	10.0	3.532	9.1981	1.045	13000	24500	1.021	9878	9454
AH1981	200	800	10.0	3.532	9.1981	1.020	13000	25000	1.021	9878	9683
AH1799	100	800	10.3	3.528	9.1280	1.107	24000	43000	1.016	9210	8318
AH1982	250	400	20.0	3.411	9.4548	1.038	13000	25500	1.010	12770	12307
AH1804	125	400	20.3	3.408	9.3743	1.113	24000	43500	1.005	11782	10584
AH1806	125	1200	20.3	3.408	9.3866	1.123	24500	43500	1.005	11927	10620
AH1983	250	800	20.4	3.407	9.4665	1.031	13500	25500	1.010	12920	12529
AH1984	350	400	30.1	3.298	9.7322	1.068	12000	23000	0.999	16851	15783
AH1985	350	800	30.1	3.298	9.7077	1.063	12000	22500	0.999	16443	15476
AH1810	250	400	30.3	3.295	9.6364	1.047	15500	29500	0.994	15313	14630
AH1811	250	800	30.3	3.295	9.6740	1.045	16000	31000	0.994	15899	15218
AH1816	250	400	40.0	3.193	9.8303	1.060	18500	35000	0.984	18589	17537
AH1817	250	800	40.0	3.193	9.8061	1.090	18000	33500	0.984	18145	16645
AH1986	400	400	40.1	3.192	9.9240	1.032	13000	25000	0.988	20415	19774
AH1987	400	800	40.2	3.191	9.9241	1.039	13000	24500	0.988	20417	19658
AH1988	400	400	50.1	3.094	10.1048	1.048	15000	29000	0.977	24460	23346
AH1878	500	1000	49.8	3.096	10.0788	1.035	12000	23000	0.985	23831	23022
AH1879	500	1500	49.8	3.096	10.1033	1.041	12000	23500	0.985	24423	23467
AH1989	400	800	50.2	3.093	10.0951	1.022	15000	29500	0.977	24224	23708
AH1880	500	500	59.9	3.003	10.2503	1.024	14000	27500	0.973	28292	27637
AH1881	500	1000	59.9	3.003	10.2609	1.029	14000	27500	0.973	28591	27788
AH1990	400	400	60.1	3.001	10.2180	1.052	17000	32000	0.966	27393	26032
AH1991	400	800	60.1	3.001	10.2355	1.066	17000	32000	0.966	27876	26153
AH1883	500	500	70.0	2.914	10.3719	1.090	15500	28500	0.962	31950	29324
AH1884	500	1000	70.0	2.914	10.3528	1.047	15500	29500	0.962	31344	29932
AH1992	400	400	70.3	2.912	10.4289	0.879	20500	46500	0.955	33823	38479
AH1993	400	800	70.3	2.912	10.4143	0.883	20000	46000	0.955	33334	37742

Table S17 Detailed PLP sample conditions, absolute molecular weights of the first two inflection points, and the resulting propagation rate coefficients of the monomer TDA-A in 1 M solution in BuAc.

Sample	f	n	θ	T^{-1}	$\ln(k_{p1})$	k_{p1}/k_{p2}	M_1	M_2	c_M	k_{p1}	k_{p2}
	Hz	–	°C	10^{-3} K^{-1}	–	–	g·mol^{-1}		mol·L^{-1}	mol·L^{-1} s^{-1}	
AH1182	500	30	-8.4	3.778	9.0608	1.055	15472	29331	3.531	8611	8162
AH1183	500	60	-8.3	3.776	9.0804	1.065	16000	29500	3.531	8782	8246
AH1184	500	90	-7.9	3.770	9.1186	1.074	16500	30500	3.530	9124	8498
AH1185	500	150	-7.6	3.766	9.1281	1.043	16500	31500	3.529	9211	8831
AH1189	500	150	0.7	3.652	9.3415	1.047	20500	39000	3.504	11402	10889
AH1187	500	60	0.7	3.652	9.2880	1.070	19500	36000	3.504	10808	10101
AH1188	500	90	0.7	3.652	9.3190	1.077	20000	37000	3.504	11147	10350
AH1192	500	90	10.0	3.532	9.5621	1.106	25000	45500	3.476	14215	12849
AH1191	500	60	10.1	3.530	9.5441	1.123	24500	44000	3.476	13962	12435
AH1193	500	150	10.3	3.528	9.6089	1.119	26500	47000	3.475	14897	13309
AH1162	500	100	18.5	3.429	9.8013	1.136	31500	56000	3.452	18057	15898
AH1163	500	200	18.6	3.428	9.7967	1.054	31500	60000	3.451	17974	17060
AH1164	500	500	18.8	3.425	9.8607	1.110	33500	60500	3.451	19162	17270
AH1161	500	50	18.8	3.425	9.7485	1.121	30000	53500	3.451	17129	15279
AH1169	500	200	30.0	3.299	10.0060	1.040	38500	74000	3.417	22159	21313
AH1168	500	100	30.0	3.299	9.9906	1.052	38000	72000	3.417	21820	20732
AH1167	500	50	30.0	3.299	9.9749	1.059	37500	70500	3.417	21479	20274
AH1170	500	500	30.0	3.299	9.9467	1.065	36500	68000	3.417	20884	19609
AH1172	500	100	40.0	3.193	10.1303	1.043	43000	83000	3.388	25092	24051
AH1171	500	50	40.0	3.193	10.1571	1.089	44500	81500	3.388	25774	23675
AH1173	500	200	40.0	3.193	10.2087	1.089	47000	86000	3.388	27137	24926
AH1381	500	100	40.0	3.193	10.1450	1.027	44000	85500	3.395	25464	24789
AH1382	500	100	40.0	3.193	10.1040	1.046	42000	81000	3.395	24441	23374
AH1383	500	30	49.9	3.095	10.2849	1.050	50000	95500	3.365	29286	27896
AH1176	500	100	50.0	3.095	10.2987	1.121	50500	90500	3.358	29694	26492
AH1175	500	50	50.0	3.095	10.3130	1.125	51500	91500	3.358	30122	26785
AH1384	500	60	50.0	3.095	10.2583	1.086	49000	90000	3.365	28519	26267
AH1180	500	100	60.0	3.002	10.4765	1.192	60000	101000	3.328	35474	29771
AH1179	500	50	60.0	3.002	10.5145	1.200	62500	104000	3.328	36847	30699

Table S18 Detailed PLP sample conditions, absolute molecular weights of the first two inflection points, and the resulting propagation rate coefficients of the monomer TDN-A in bulk.

Sample	f	n	θ	T^{-1}	$\ln(k_{p1})$	k_{p1}/k_{p2}	M_1	M_2	c_M	k_{p1}	k_{p2}
	Hz	–	°C	10^{-3} K^{-1}	–	–	g·mol^{-1}		mol·L^{-1}	mol·L^{-1} s^{-1}	
AH1439	50	400	-9.9	3.799	8.5044	1.145	26193	45748	1.043	4936	4311
AH1440	50	800	-9.5	3.793	8.5218	1.184	26500	45000	1.042	5023	4243
AH1443	100	800	-9.5	3.793	8.6414	1.073	15000	28000	1.042	5661	5277
AH1444	100	1200	-9.4	3.791	8.6517	1.072	15000	28500	1.042	5720	5334
AH1445	50	400	-0.2	3.664	8.6917	1.072	31500	58500	1.032	5953	5552
AH1447	50	1200	-0.1	3.662	8.7013	1.067	31500	59000	1.032	6011	5636
AH1450	100	1200	-0.1	3.662	8.8359	1.088	18000	33000	1.032	6877	6322
AH1448	100	400	-0.1	3.662	8.8190	1.089	18000	32500	1.032	6761	6209
AH1423	250	1800	9.7	3.535	9.3115	1.147	11500	20000	1.020	11065	9645
AH1421	250	600	10.0	3.532	9.2846	1.125	11000	20000	1.020	10771	9576
AH1549	100	800	10.1	3.530	9.1500	1.148	24000	42000	1.012	9414	8197
AH1548	100	400	10.3	3.528	9.1314	1.135	24000	42000	1.012	9241	8142
AH1428	250	1200	19.6	3.416	9.4938	1.085	13500	25000	1.009	13278	12240
AH1427	250	600	20.1	3.410	9.4831	1.073	13500	25000	1.009	13136	12247
AH1554	100	400	19.7	3.415	9.3559	1.156	29500	51000	1.002	11566	10009
AH1429	250	1800	20.3	3.408	9.4946	1.085	13500	25000	1.009	13288	12249
AH1736	175	600	30.1	3.298	9.6262	1.139	22500	39000	1.012	15156	13301
AH1737	175	1200	30.1	3.298	9.6194	1.149	22000	38500	1.012	15054	13100
AH1434	250	800	30.2	3.297	9.6796	1.080	16000	30000	0.998	15989	14811
AH1433	250	400	30.2	3.297	9.6511	1.081	16000	29000	0.998	15539	14371
AH1504	250	1800	40.0	3.193	9.7516	1.082	18500	34000	1.050	17182	15882
AH1502	250	600	40.0	3.193	9.7841	1.084	19000	35000	1.050	17749	16367
AH1503	250	1200	40.0	3.193	9.7599	1.091	18500	34000	1.050	17324	15882
AH1744	350	600	50.0	3.095	10.0790	1.102	17000	31000	0.990	23838	21632
AH1745	350	1200	50.0	3.095	10.0611	1.104	17000	30500	0.990	23415	21218
AH1747	500	1200	50.1	3.094	10.2069	1.059	13500	25500	0.989	27088	25567
AH1746	500	600	50.1	3.094	10.1726	1.061	13000	25000	0.989	26175	24674
AH1845	350	600	60.0	3.002	10.1399	1.041	18000	34500	0.972	25333	24326
AH1847	500	600	60.0	3.002	10.3504	1.039	15500	30000	0.972	31271	30093
AH1848	500	1200	60.0	3.002	10.3891	1.086	16000	29500	0.972	32503	29943
AH1853	500	600	70.0	2.914	10.4376	1.078	16500	31000	0.961	34120	31656
AH1854	500	1200	70.0	2.914	10.4192	1.084	16500	30000	0.961	33498	30895

Table S19 Detailed PLP sample conditions, absolute molecular weights of the first two inflection points, and the resulting propagation rate coefficients of the monomer TDN-A in 1 M solution in BuAc.

Sample	f	n	θ	T^{-1}	$\ln(k_{p1})$	k_{p1}/k_{p2}	M_1	M_2	c_M	k_{p1}	k_{p2}
	Hz	–	°C	10^{-3} K^{-1}	–	–	g·mol^{-1}		mol·L^{-1}	mol·L^{-1} s^{-1}	
AH491	500	150	-8.4	3.777	9.1946	1.078	17700	32800	2.891	9844	9133
AH681	500	100	-5.6	3.738	9.3647	1.083	20500	37800	2.827	11669	10779
AH686	500	200	-0.1	3.662	9.4540	1.068	22300	41700	2.814	12759	11942
AH494	500	100	1.1	3.646	9.3004	1.026	19500	38000	2.869	10942	10667
AH690	500	200	5.0	3.595	9.6022	1.083	25800	47600	2.803	14797	13667
AH689	500	100	5.2	3.593	9.5567	1.102	24600	44700	2.802	14139	12832
AH498	500	100	9.5	3.538	9.8324	1.105	33000	59700	2.849	18627	16862
AH691	500	100	9.9	3.533	9.6376	1.129	26600	47100	2.791	15330	13582
AH694	500	200	14.4	3.478	9.8263	1.170	32000	54700	2.781	18515	15829
AH693	500	100	14.5	3.476	9.7740	1.158	30300	52400	2.781	17570	15177
AH501	500	100	19.8	3.414	10.0334	1.132	40000	70600	2.825	22776	20115
AH502	500	150	20.0	3.411	10.0497	1.096	40600	74100	2.825	23150	21122
AH697	500	100	25.6	3.347	9.9646	1.114	36400	65300	2.756	21260	19077
AH698	500	200	26.3	3.339	9.8564	0.931	32600	70100	2.754	19080	20494
AH699	500	100	30.1	3.298	9.9992	1.054	37500	71200	2.745	22008	20888
AH505	500	150	30.1	3.298	10.2662	1.041	50000	96100	2.801	28744	27622
AH597	500	100	35.1	3.244	10.1015	1.081	41100	76000	2.714	24380	22550
AH702	500	200	35.2	3.243	10.1740	1.060	44500	84000	2.734	26214	24741
AH507	500	50	40.1	3.192	10.4016	1.054	56800	107700	2.778	32912	31212
AH509	500	150	40.1	3.192	10.3032	0.938	51500	109700	2.778	29827	31808
AH599	500	50	44.6	3.147	10.2525	1.110	47400	85400	2.693	28354	25546
AH601	500	150	45.3	3.140	10.2932	1.110	49400	88900	2.691	29531	26609
AH511	500	50	50.0	3.095	10.4836	1.017	61100	120200	2.755	35726	35127
AH512	500	100	50.2	3.093	10.4463	1.095	58900	107500	2.754	34416	31432
AH602	500	50	54.5	3.052	10.3916	1.125	54000	96100	2.670	32585	28976
AH603	500	100	55.1	3.046	10.4128	1.126	55200	98000	2.669	33282	29566
AH515	500	50	60.0	3.002	10.6998	1.091	75200	137900	2.731	44347	40634
AH517	500	100	60.3	2.999	10.7376	1.171	78100	133400	2.731	46054	39344

Table S20 Detailed PLP sample conditions, absolute molecular weights of the first two inflection points, and the resulting propagation rate coefficients of the monomer C17A in bulk.

Sample	f	n	θ	T^{-1}	$\ln(k_{p1})$	k_{p1}/k_{p2}	M_1	M_2	c_M	k_{p1}	k_{p2}
	Hz	–	°C	10^{-3} K^{-1}	–	–	g·mol^{-1}		mol·L^{-1}	mol·L^{-1} s^{-1}	
AH2082	100	400	-11.8	3.826	8.7337	1.098	20200	36800	1.048	6209	5656
AH2083	100	800	-11.2	3.818	8.7064	1.083	19500	36000	1.045	6042	5579
AH2084	200	400	-10.8	3.812	8.9581	1.167	12500	21500	1.044	7771	6661
AH2085	200	800	-10.6	3.809	8.9663	1.149	12500	22000	1.044	7834	6816
AH2030	125	400	-0.5	3.668	8.9999	1.075	21000	38500	1.033	8102	7537
AH2031	125	800	-0.2	3.664	9.0050	1.077	21000	39000	1.033	8144	7559
AH2032	250	400	-0.1	3.662	9.2387	1.138	13000	23000	1.033	10288	9041
AH2033	250	800	0.0	3.661	9.2312	1.139	13000	23000	1.033	10211	8964
AH2014	150	400	10.2	3.529	9.2915	1.093	23000	42000	1.024	10846	9926
AH2015	150	800	10.2	3.529	9.2784	1.084	22500	42000	1.024	10704	9879
AH2016	300	400	10.2	3.529	9.4954	1.160	14000	24500	1.024	13298	11459
AH2017	300	800	10.3	3.528	9.4955	1.151	14000	24500	1.024	13299	11554
AH2018	200	400	19.8	3.414	9.5264	1.072	21500	40500	1.014	13717	12797
AH2020	400	400	19.9	3.412	9.7571	1.167	13500	23500	1.014	17276	14799
AH2021	400	800	20.0	3.411	9.7572	1.177	13500	23000	1.014	17277	14673
AH2019	200	800	20.1	3.410	9.5221	1.086	21500	39500	1.014	13658	12578
AH2088	400	5000	30.0	3.299	9.8612	1.092	15000	27500	1.001	19172	17564
AH1927	200	400	30.1	3.298	9.6696	1.106	24500	44500	1.001	15830	14317
AH1928	200	800	30.1	3.298	9.6737	1.115	24500	44500	1.001	15894	14253
AH1929	400	400	30.1	3.298	9.8681	1.107	15000	27000	1.001	19304	17438
AH1931	250	400	40.0	3.193	9.8660	1.097	23500	43000	0.990	19265	17558
AH1932	250	800	40.0	3.193	9.8744	1.101	24000	43500	0.990	19428	17639
AH1933	450	400	40.0	3.193	10.0420	1.072	15500	29500	0.990	22972	21435
AH1934	450	800	40.0	3.193	10.0356	1.080	15500	29000	0.990	22825	21143
AH1938	500	800	50.0	3.095	10.2078	1.051	16500	31500	0.980	27115	25800
AH2034	300	400	50.1	3.094	10.1245	1.129	25500	45000	0.980	24947	22087
AH2035	300	800	50.1	3.094	10.1205	1.125	25000	45000	0.980	24848	22087
AH1937	500	400	50.1	3.094	10.2260	1.060	17000	31500	0.980	27611	26049
AH2024	500	400	60.2	3.000	10.3888	1.057	19500	37000	0.971	32493	30752
AH2025	500	800	60.2	3.000	10.3785	1.057	19500	36500	0.971	32161	30421
AH2028	500	400	70.0	2.914	10.4097	1.042	20000	38000	0.961	33180	31839
AH2029	500	800	70.0	2.914	10.4297	1.069	20000	38000	0.961	33850	31672

Table S21 Detailed PLP sample conditions, absolute molecular weights of the first two inflection points, and the resulting propagation rate coefficients of the monomer C17A in 1 M solution in BuAc.

Sample	f	n	θ	T^{-1}	$\ln(k_{p1})$	k_{p1}/k_{p2}	M_1	M_2	c_M	k_{p1}	k_{p2}
	Hz	–	°C	10^{-3} K^{-1}	–	–	g·mol^{-1}		mol·L^{-1}	mol·L^{-1} s^{-1}	
AH2515	500	120	-9.5	3.793	9.0098	0.840	14703	35017	2.451	8182	9744
AH2516	500	150	-9.5	3.793	9.0441	0.853	15000	35500	2.451	8469	9933
AH2517	500	180	-9.0	3.786	9.1099	0.902	16000	36000	2.450	9044	10032
AH2518	500	120	-1.6	3.683	9.1770	1.016	17500	34000	2.435	9672	9519
AH2519	500	180	-1.6	3.683	9.2254	1.021	18000	35500	2.435	10152	9947
AH2242	500	150	0.9	3.649	9.2451	1.011	18500	36500	2.433	10354	10243
AH2108	500	150	9.7	3.535	9.4374	1.050	22000	42500	2.416	12549	11946
AH2521	500	180	10.3	3.528	9.4541	1.088	22500	41500	2.413	12760	11723
AH2520	500	120	10.8	3.522	9.4392	1.068	22000	41500	2.412	12572	11776
AH2524	500	180	19.0	3.423	9.7309	1.137	29500	52000	2.396	16830	14799
AH2522	500	120	19.3	3.419	9.7078	1.129	29000	51000	2.395	16446	14561
AH2523	500	150	19.8	3.414	9.7373	1.122	29500	53000	2.395	16938	15098
AH2111	500	150	30.1	3.298	9.8164	1.119	32000	57000	2.377	18332	16376
AH2112	500	180	30.1	3.298	9.7949	1.049	31500	59500	2.377	17941	17104
AH2110	500	120	30.2	3.297	9.8165	1.154	32000	55500	2.377	18334	15891
AH2526	500	120	40.3	3.190	9.9875	1.006	37500	74500	2.355	21754	21622
AH2527	500	150	40.3	3.190	10.0231	1.040	39000	75000	2.355	22541	21671
AH2528	500	180	40.3	3.190	10.0187	1.006	39000	77000	2.355	22443	22307
AH2113	500	120	50.2	3.093	10.1298	1.008	43000	85500	2.339	25080	24879
AH2114	500	150	50.2	3.093	10.2022	1.057	46000	87500	2.339	26961	25519
AH2115	500	180	50.3	3.092	10.1299	0.990	43000	87000	2.338	25082	25324

Table S22 Detailed PLP sample conditions, absolute molecular weights of the first two inflection points, and the resulting propagation rate coefficients of the monomer C21A in bulk.

Sample	f	n	θ	T^{-1}	$\ln(k_{p1})$	k_{p1}/k_{p2}	M_1	M_2	c_M	k_{p1}	k_{p2}
	Hz	–	°C	10^{-3} K^{-1}	–	–	g·mol^{-1}		mol·L^{-1}	mol·L^{-1} s^{-1}	
AH2910	60	300	-9.3	3.790	8.3121	1.137	25700	45200	1.033	4073	3582
AH2911	60	400	-9.3	3.790	8.3160	1.144	26000	45000	1.033	4089	3574
AH2912	100	200	-9.2	3.789	8.3979	1.077	17000	31000	1.033	4438	4121
AH2914	100	400	-9.1	3.787	8.4098	1.076	17000	31500	1.033	4491	4174
AH2175	100	400	0.0	3.661	8.6554	1.048	21500	41000	1.024	5741	5480
AH2173	50	400	0.0	3.661	8.5316	1.066	38000	71500	1.024	5072	4760
AH2172	50	200	0.1	3.660	8.5227	1.041	37500	72500	1.024	5028	4828
AH2174	100	200	0.1	3.660	8.6475	1.057	21500	40500	1.024	5696	5390
AH2095	150	400	9.7	3.535	8.9069	1.072	18000	34000	1.005	7383	6888
AH2094	150	200	9.9	3.533	8.9165	1.071	18500	34000	1.004	7454	6958
AH2093	75	400	9.9	3.533	8.8173	1.161	33000	57000	1.004	6750	5813
AH2092	75	200	10.0	3.532	8.8276	1.146	33500	58500	1.004	6820	5952
AH2072	100	1200	19.5	3.417	9.0323	1.182	31000	52500	1.008	8369	7081
AH2071	100	800	19.6	3.416	9.0434	1.165	31500	53500	1.008	8462	7265
AH2074	175	800	20.0	3.411	9.1221	1.078	19500	36000	1.008	9156	8496
AH2073	175	400	20.6	3.404	9.1315	1.062	19500	36500	1.007	9242	8703
AH2099	250	400	30.0	3.299	9.3899	1.081	17500	32000	0.984	11967	11069
AH2098	250	200	30.0	3.299	9.3997	1.086	17500	32000	0.984	12085	11128
AH2915	125	300	30.0	3.299	9.2567	0.971	30500	63000	0.993	10474	10783
AH2096	125	200	30.1	3.298	9.3066	1.184	32000	53500	0.984	11011	9301
AH2076	200	400	39.8	3.195	9.5655	1.155	26000	44500	0.987	14264	12349
AH2077	200	800	40.0	3.193	9.5723	1.181	26000	44000	0.987	14361	12164
AH2081	400	1200	40.1	3.192	9.6603	1.012	14000	28000	0.987	15682	15493
AH2079	400	400	40.1	3.192	9.6959	1.055	14500	28000	0.987	16251	15399
AH2102	400	200	50.0	3.095	9.8503	1.072	17000	31500	0.964	18965	17694
AH2103	400	400	50.0	3.095	9.8297	1.050	16500	31500	0.964	18577	17694
AH2179	500	400	50.3	3.092	9.8981	1.071	14000	26500	0.973	19893	18577
AH2176	350	200	50.4	3.091	9.7960	1.035	18500	35500	0.973	17962	17352
AH2183	500	400	60.0	3.002	10.0541	1.028	16500	32000	0.963	23252	22629
AH2180	350	200	60.0	3.002	9.9695	1.070	21500	40500	0.963	21365	19973
AH2181	350	400	60.1	3.001	9.8519	1.039	19000	37000	0.963	18994	18289
AH2182	500	200	60.2	3.000	10.0333	0.990	16000	32500	0.963	22772	22996
AH2917	500	150	69.9	2.915	10.1176	1.048	17500	33000	0.952	24775	23629
AH2918	500	250	70.0	2.914	10.0943	1.040	17000	32500	0.952	24205	23274
AH2919	500	300	70.0	2.914	10.0884	1.024	17000	33000	0.952	24062	23489
AH2920	500	350	70.0	2.914	10.0520	1.006	16000	32000	0.952	23202	23059

Table S23 Detailed PLP sample conditions, absolute molecular weights of the first two inflection points, and the resulting propagation rate coefficients of the monomer C21A in 1 M solution in BuAc.

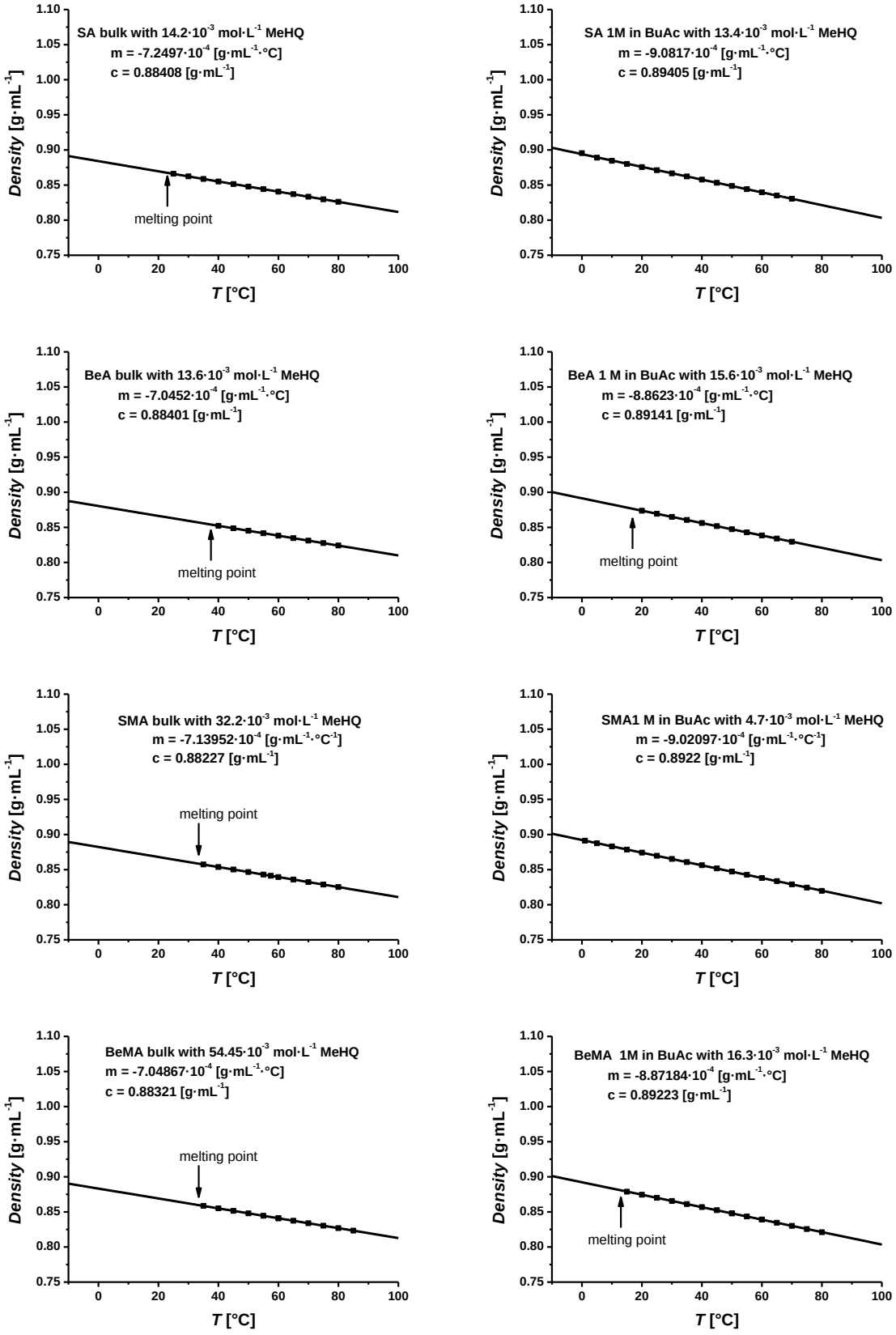

Figure S15 Temperature dependent densities for the monomers SA, BeA, SMA, and BeMA as well as their 1 molar solution in BuAc. Methyl hydroquinone (MeHQ) was added in replacement of 2,2-dimethoxy-2-phenylacetophenone (DMPA) to prevent the solutions from polymerization inside the density measurement device. The temperature dependent densities are summarized in Table 2.1.

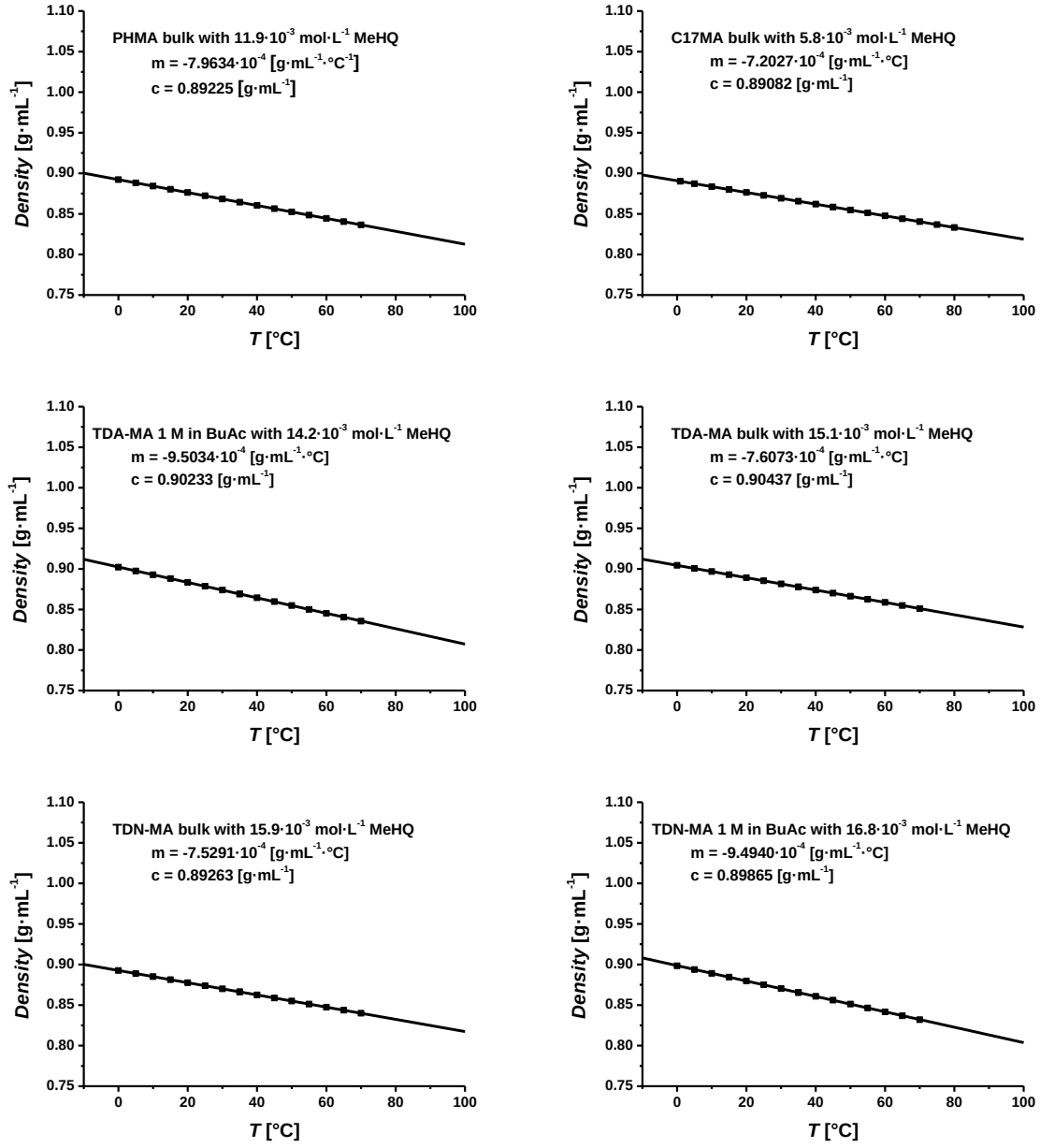

Figure S16 Temperature dependent densities for the studied monomers PHMA, C17MA, TDA-MA, and TDN-MA as well as the 1 molar solutions in BuAc of the latter both monomers. Methyl hydroquinone (MeHQ) was added in replacement of 2,2-dimethoxy-2-phenylacetophenone (DMPA) to prevent the solutions from polymerization inside the density measurement device. The temperature dependent densities are summarized in Table 2.1.

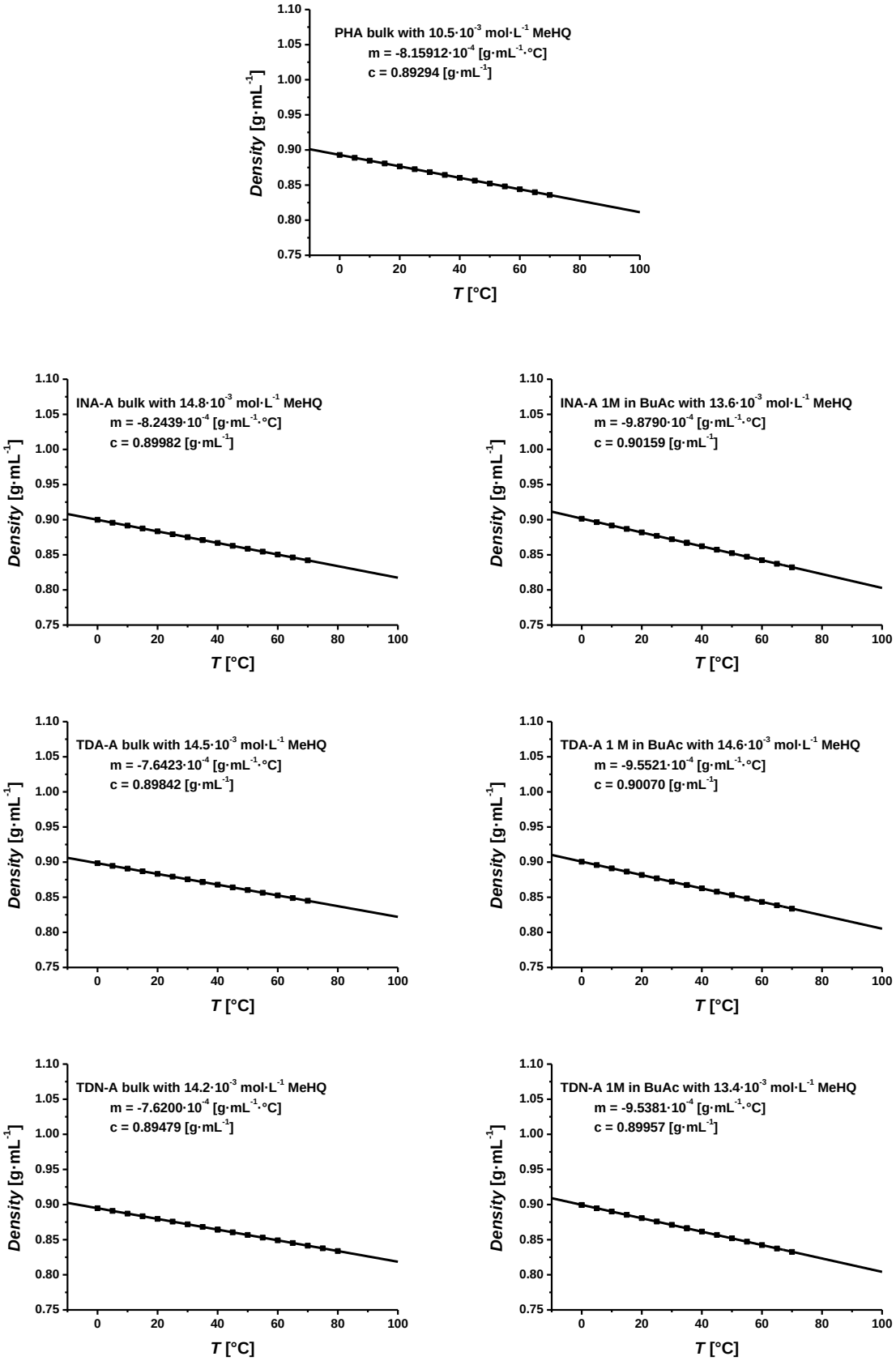

Figure S17 Temperature dependent densities for the studied monomers PHA, INA-A, TDA-A, and TDN-A as well as the 1 molar solutions in BuAc of each of them (except PHA). Methyl hydroquinone (MeHQ) was added in replacement of 2,2-dimethoxy-2-phenylacetophenone (DMPA) to prevent the solutions from polymerization inside the density measurement device. The temperature dependent densities are summarized in Table 2.1.

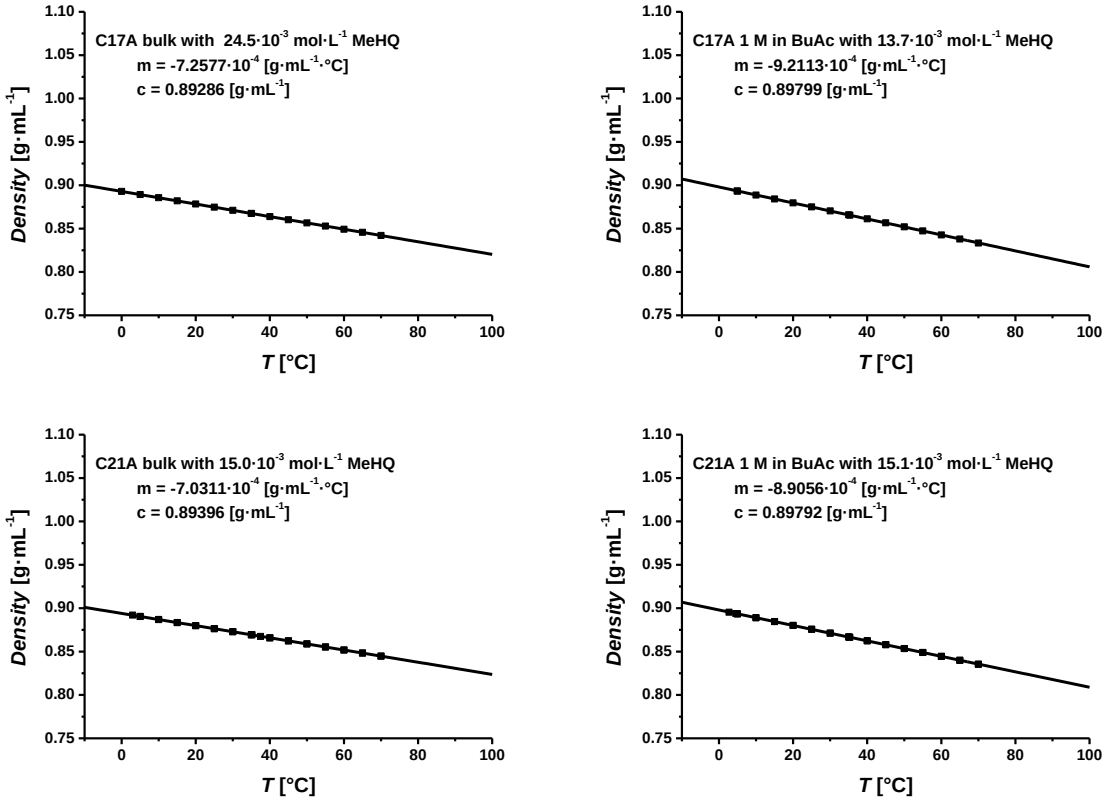

Figure S18 Temperature dependent densities for the studied monomers C17A and C12A as well as the 1 molar lsolutions in BuAc of each of them. Methyl hydroquinone (MeHQ) was added in replacement of 2,2-dimethoxy-2-phenylacetophenone (DMPA) to prevent the solutions from polymerization inside the density measurement device. The temperature dependent densities are summarized in Table 2.1.

SA		BeA		SMA		BeMA	
M_1 g·mol^{-1}	$[\eta]$ ml·g^{-1}	M_1 g·mol^{-1}	$[\eta]$ ml·g^{-1}	M_1 g·mol^{-1}	$[\eta]$ ml·g^{-1}	M_1 g·mol^{-1}	$[\eta]$ ml·g^{-1}
2175310	224.48	1956120	194.37	420760	43.51	3196530	177.94
1193450	130.13	1615260	192.24	415271	44.81	3285380	177.74
1074590	116.13	1778240	194.91	298414	33.65	2146160	127.27
944101	130.31	1296910	149.85	265614	36.00	2038310	136.55
914949	129.92	1257110	147.92	173082	29.40	1232840	86.28
725060	84.62	846209	110.73	176468	28.05	1248200	95.88
643355	91.10	838992	111.90	127826	20.04	481277	51.22
428613	70.80	596068	79.47	129280	19.98	502077	45.15
424658	72.03	559844	77.31	84883	16.19	311452	34.20
311442	51.52	382762	63.86	90591	16.75	320904	34.42
318078	46.52	375078	61.31	56633	12.81	206987	25.80
298745	49.26	257069	48.49	53393	12.85	216550	25.03
185020	40.42	254757	48.94	38965	11.18	126705	21.64
190432	34.89	180801	37.39	37796	9.95	125656	20.47
127895	27.43	180474	36.23	21207	6.98	82377	15.85
125143	27.86	137162	31.75	22259	7.05	80551	17.17
82915	19.77	101875	25.47			49876	13.36
90668	20.08					54358	13.60
70197	17.92					34538	10.55
58629	17.59					32617	11.07
43377	15.08					20008	8.94
39402	13.41					24501	9.32
38879	12.23					14702	7.47
						14946	6.36

Table S24 Weight average molecular weight, M_W, and related intrinsic viscosity, $[\eta]$, data employed for the determination of the MHKS parameters of SA, BeA, SMA, and BeMA. The M_W and $[\eta]$ were determined via the MALLS detector as well as the viscosimeter of the triple SEC set-up.

PHMA		TDA-MA		TDN-MA		C17MA		PHA	
M_1 g·mol^{-1}	$[\eta]$ ml·g^{-1}	M_1 g·mol^{-1}	$[\eta]$ ml·g^{-1}	M_1 g·mol^{-1}	$[\eta]$ ml·g^{-1}	M_1 g·mol^{-1}	$[\eta]$ ml·g^{-1}	M_1 g·mol^{-1}	$[\eta]$ ml·g^{-1}
917986	110.89	5398470	203.28	2751640	333.22	1860680	123.56	3196530	177.94
601755	86.19	6225020	236.26	2156180	301.14	1046820	83.68	2241190	288.36
584072	84.23	3735140	177.71	2127500	226.03	1124960	80.15	2332610	277.97
417877	62.08	4664100	183.18	2077250	223.64	740137	70.82	1415320	218.1
419889	60.88	2347640	127.97	1245260	149.88	748385	68.94	1472620	211.05
282858	45.41	2698400	129.34	1255720	150.58	522746	50.54	912463	156.35
304783	42.46	2224050	131.53	1221030	151.97	495502	54.04	930324	152.79
192146	33.49	2489380	130.74	1252280	148.21	344849	39.28	587693	113.36
189405	33.71	1290480	86.84	633235	104.7	330983	38.29	601895	113.13
129326	25.45	1527160	81.06	670779	96.47	257439	27.38	400524	82.6
132866	25.06	1398080	81.47	608376	101.19	254872	27.87	416109	78.21
88424	20.25	968582	83.65	648782	94.37	172381	22.34	275266	62.2
95817	20.45	848321	56.23	366442	70.73	156313	23.65	265763	60.45
47179	14.44	827733	58.86	368562	70.25	112315	18.31	189829	41.89
68006	18.59	812149	59.92	253176	49.34	116869	18.51	190774	40.29
47746	14.09	820197	59.42	248728	51.66	74856	13.13	127922	34.2
42907	13.46	485982	46.61	174136	38.52	85458	13.02	130556	35.39
32563	11.91	495072	44.19	177944	37.8	50251	10.48	104454	26.75
31499	10.4	311045	34.04	126269	32.49	51679	10.54	102663	27.99
		328323	34.20	130412	29.6			62919	21.95
		220691	27.25	95622	29.04			62757	19.54
		209022	28.78	96575	24.95			43143	16.68
		158399	24.58	79548	20.49			44191	16.64
		159986	21.35	78679	21.77				
		123182	19.05	62511	17.67				
		122208	20.22	68005	17.79				
		87412	16.14	57683	14.86				
		90802	15.45	53860	14.22				
		68022	13.34						
		69488	13.46						
		60011	13.22						
		55997	12.66						
		53818	10.90						
		53781	11.81						

Table S25 Weight average molecular weight, M_W, and related intrinsic viscosity, $[\eta]$, data employed for the determination of the MHKS parameters of PHMA, TDA-MA, TDN-MA, C17MA, and PHA. The M_W and $[\eta]$ were determined via the MALLS detector as well as the viscosimeter of the triple SEC set-up.

INA-A		TDA-A		TDN-A		C17A		C21A	
M_1 g·mol^{-1}	$[\eta]$ ml·g^{-1}	M_1 g·mol^{-1}	$[\eta]$ ml·g^{-1}	M_1 g·mol^{-1}	$[\eta]$ ml·g^{-1}	M_1 g·mol^{-1}	$[\eta]$ ml·g^{-1}	M_1 g·mol^{-1}	$[\eta]$ ml·g^{-1}
6605000	493.86	5709230	331.35	4710600	457.70	3141210	230.05	5391910	299.10
7388550	550.20	4366190	318.36	3331960	341.66	3162980	229.54	3882500	268.24
6723520	559.79	4485410	310.28	2578230	219.93	2384870	175.09	3647940	265.46
2999910	328.94	3035560	254.39	2110260	251.90	2272960	178.89	3553210	263.67
3097450	332.67	3065490	242.38	2101920	251.53	1601770	142.68	2633410	208.63
3073240	331.33	2499950	196.99	1443620	186.82	1615360	145.11	3005770	196.06
1441130	194.40	2451950	204.05	1116390	124.56	1153750	116.04	2793020	207.05
1462000	201.86	1911360	171.55	991151	132.39	1118750	115.39	3050460	197.76
1471960	200.80	1953820	176.54	773624	88.73	824059	92.38	2310530	168.93
947111	140.48	1253380	133.50	658032	96.35	784855	91.30	2395930	174.29
975983	147.32	1234680	137.91	445384	72.06	602561	64.81	2226470	169.46
939614	142.05	801417	81.27	436466	74.37	639773	65.85	2366990	170.46
578807	102.62	707887	94.99	240928	52.29	451774	49.59	1872660	148.17
598606	101.13	175435	32.71	252159	46.31	438230	52.10	1965330	152.78
585848	105.67	168442	33.54	256855	47.84	360878	42.32	1885640	148.08
351994	80.12	519215	71.05	193109	40.90	345812	41.04	1982960	147.28
389364	74.43	543010	71.26	177387	36.53	264632	32.11	1616660	125.82
379368	76.05	90741	21.74	172783	36.76	241880	30.13	1554690	127.51
255801	58.81	92725	20.62	111141	20.57	166412	25.77	1301120	111.31
267610	56.76	481798	67.17	125892	26.79	187979	26.75	1372070	102.53
261431	58.70	471009	64.58	43090	13.73	123214	22.52	1036650	88.65
93918	31.84	52021	15.55	119229	27.65			1028460	89.08
118786	31.95	2876350	283.13	89508	20.41			652323	77.22
121081	32.81	318820	45.16	84202	18.23			767016	71.07
136098	34.79			85274	22.15			471339	55.37
140639	31.55			61001	14.59			557204	57.63
136942	34.76			43269	11.60			367321	51.56
137320	35.37			60768	15.49			380908	50.81
67649	27.81							283993	41.64
90071	23.73							273751	40.37
67966	24.49							243442	33.53
90671	24.36							249613	36.81
61256	19.54							270157	32.81
64068	20.15							256187	35.36
49393	16.41							330525	43.94
46562	16.18							321309	38.77
33439	12.92								
35221	12.83								

Table S26 Weight average molecular weight, M_W, and related intrinsic viscosity, $[\eta]$, data employed for the determination of the MHKS parameters of INA-A, TDA-A, TDN-A, C17A, and C21A. The M_W and $[\eta]$ were determined via the MALLS detector as well as the viscosimeter of the triple SEC set-up.

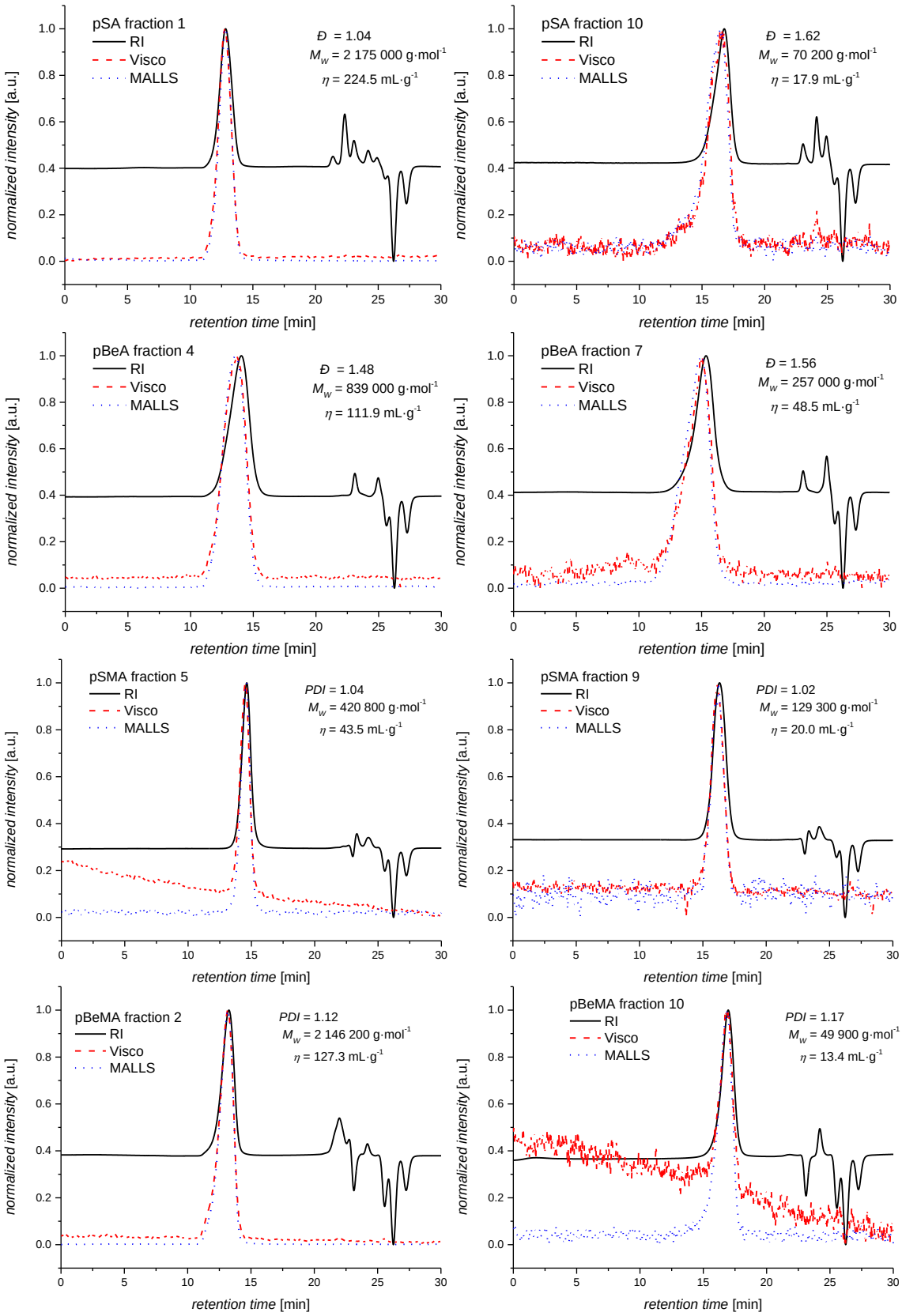

Figure S19 Exemplary triple detector SEC traces: refractive index (RI, black solid line), viscosimeter (Visco, red dashed line) and MALLS detector signal (MALLS at 90°, blue dotted line) of pSA, pBeA, pSMA, and pBeMA. The entire set of samples incorporated into the MHKS determination is collated in Table S24. All samples feature a sufficiently low signal to noise ratio in each detector signal.

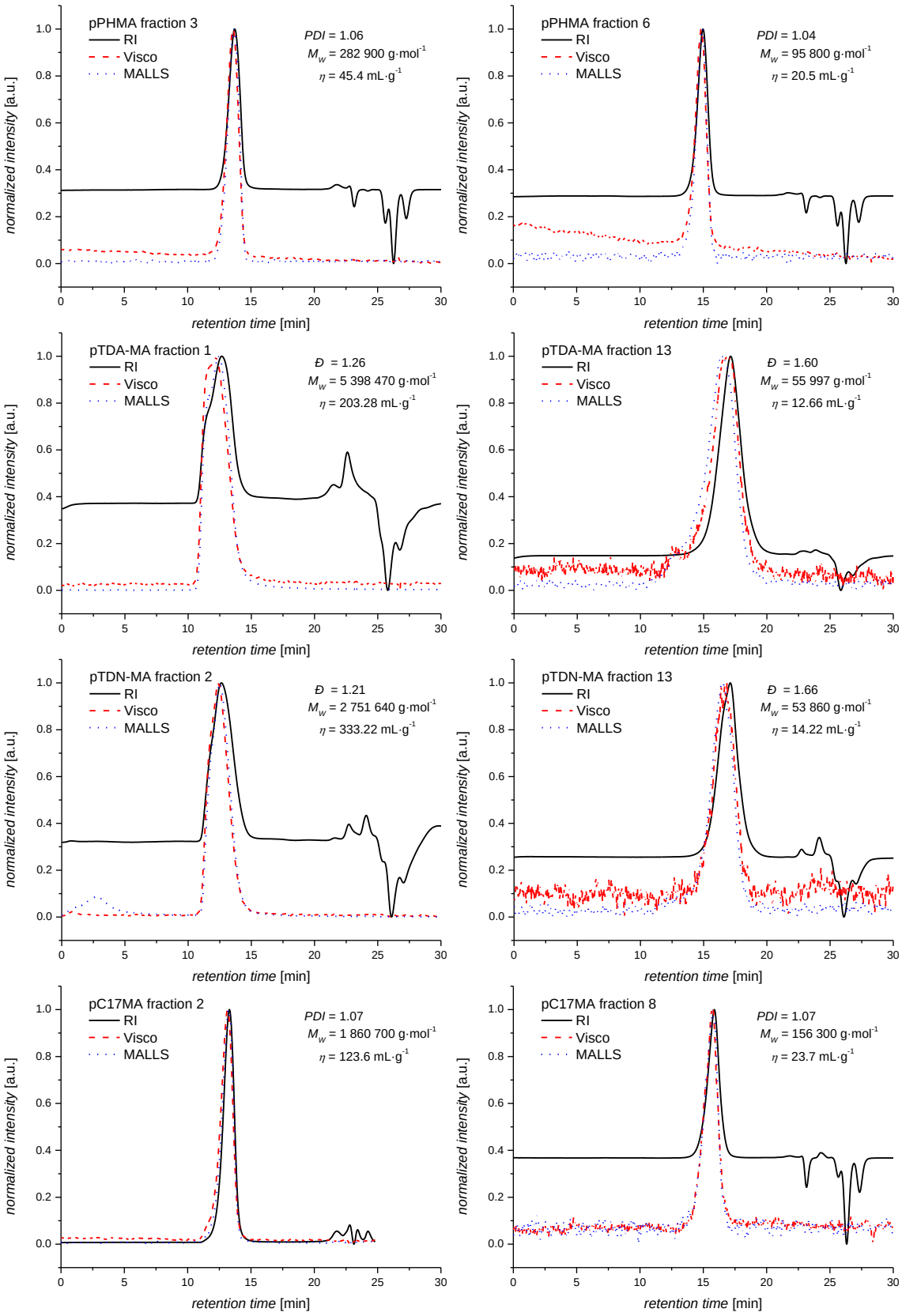

Figure S20 Exemplary triple detector SEC traces: refractive index (RI, black solid line), viscosimeter (Visco, red dashed line) and MALLS detector signal (MALLS at 90°, blue dotted line) of pPHMA, pTDA-MA, pTDN-MA, and pC17MA. The entire set of samples incorporated into the MHKS determination is collated in Table S25. All samples feature a sufficiently low signal to noise ratio in each detector signal.

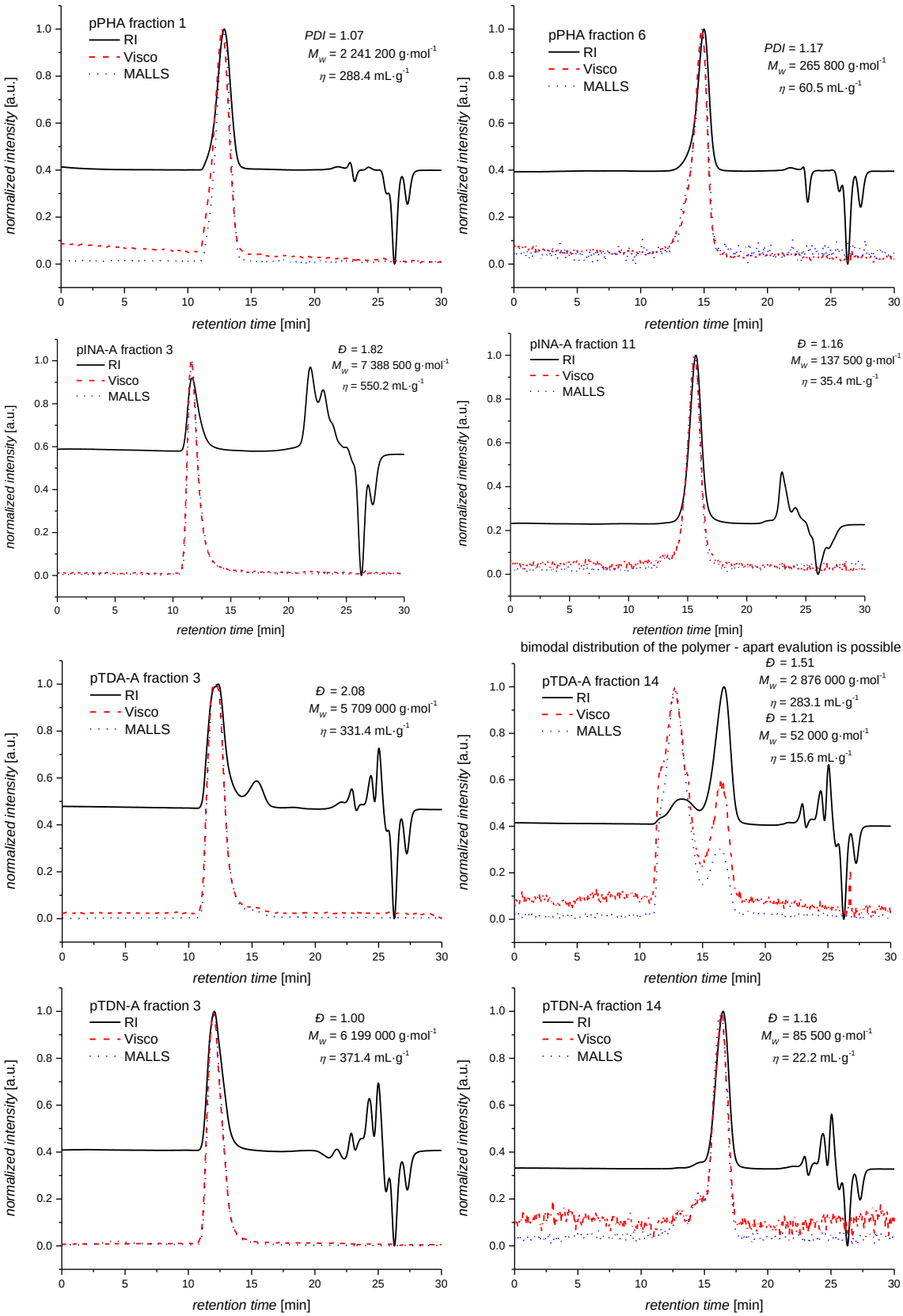

Figure S21 Exemplary triple detector SEC traces: refractive index (RI, black solid line), viscosimeter (Visco, red dashed line) and MALLS detector signal (MALLS at 90°, blue dotted line) of pPHA, pINA-A, pTDA-A, and pTDN-A. The entire set of samples incorporated into the MHKS determination is collated in Table S25 for PHA and Table S26 for the other monomers. All samples feature a sufficiently low signal to noise ratio in each detector signal.

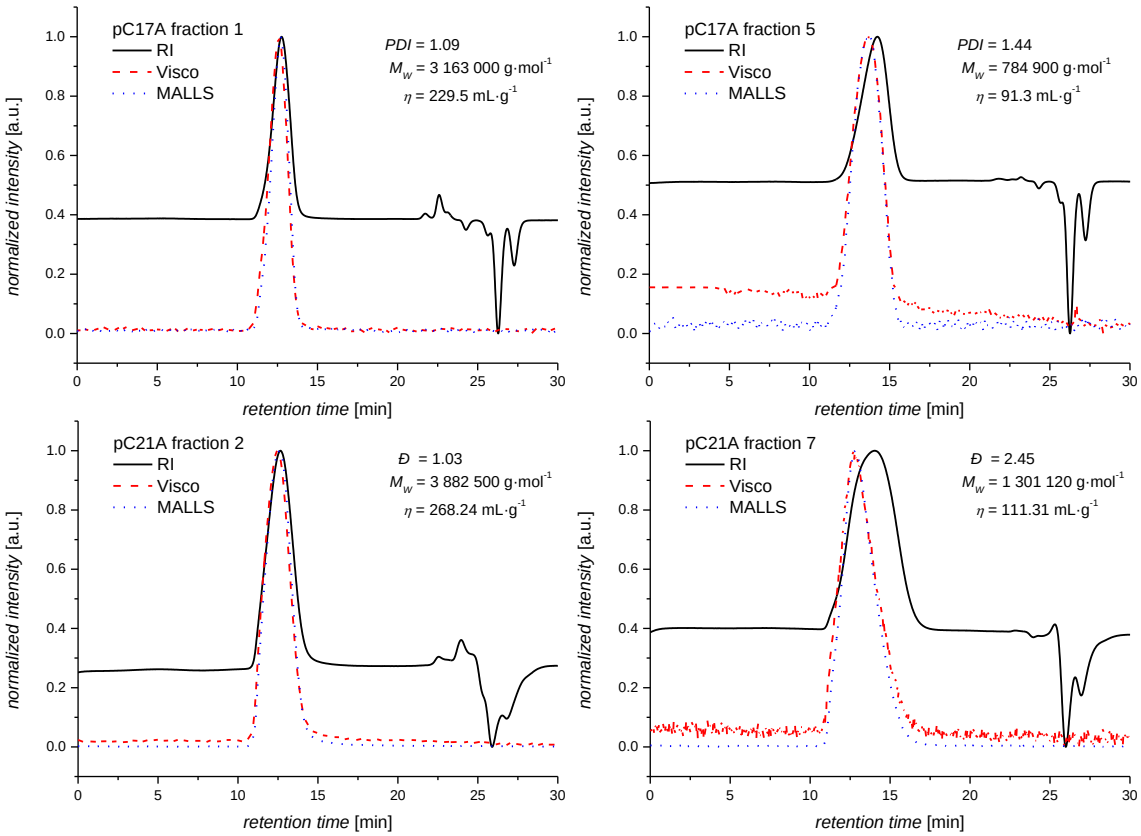

Figure S22 Exemplary triple detector SEC traces: refractive index (RI, black solid line), viscosimeter (Visco, red dashed line) and MALLS detector signal (MALLS at 90°, blue dotted line) of pC17A and pC21A. The entire set of samples incorporated into the MHKS determination is collated in Table S26. All samples feature a sufficiently low signal to noise ratio in each detector signal.

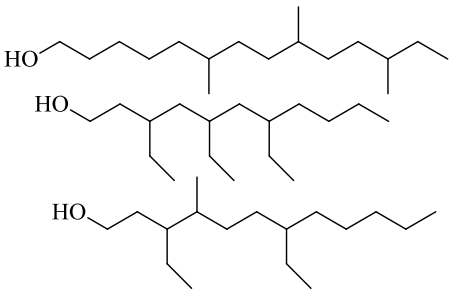

Scheme S1 Three possible structures of the highly branched heptadecyl alcohol employed in the synthesis of the heptadecyl methacrylate and acrylate.

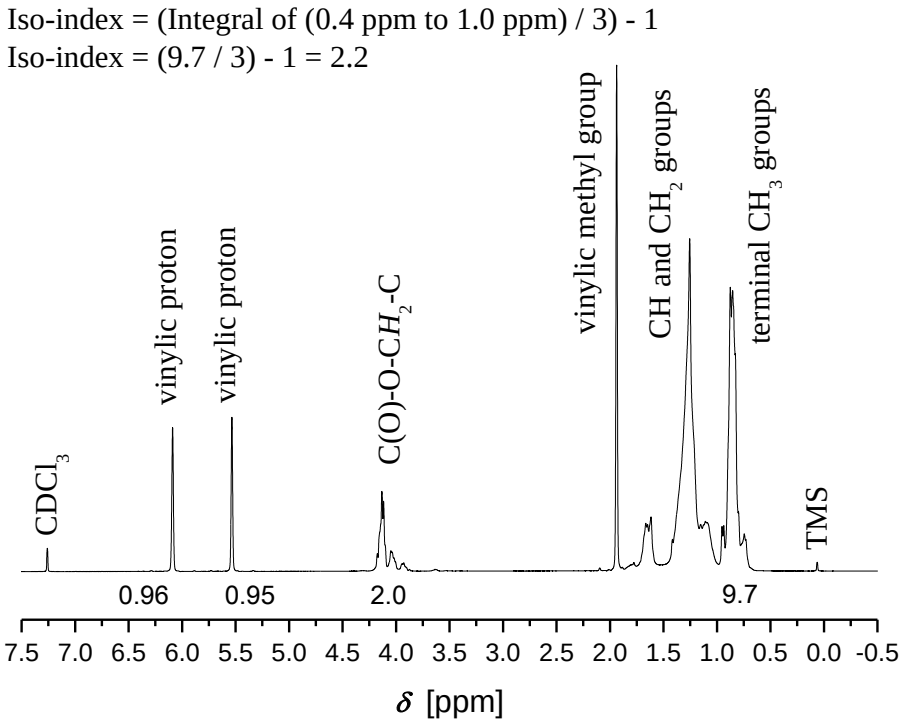

Figure S23 Exemplary ^{1}H-NMR of TDN-MA for the determination of the isoindex.[229] The integrals corresponding to the CH_2 protons next to the ester functionality are normalized to unity. The isoindex is calculated from the integral value of the terminal CH_3 protons via the stated equation.

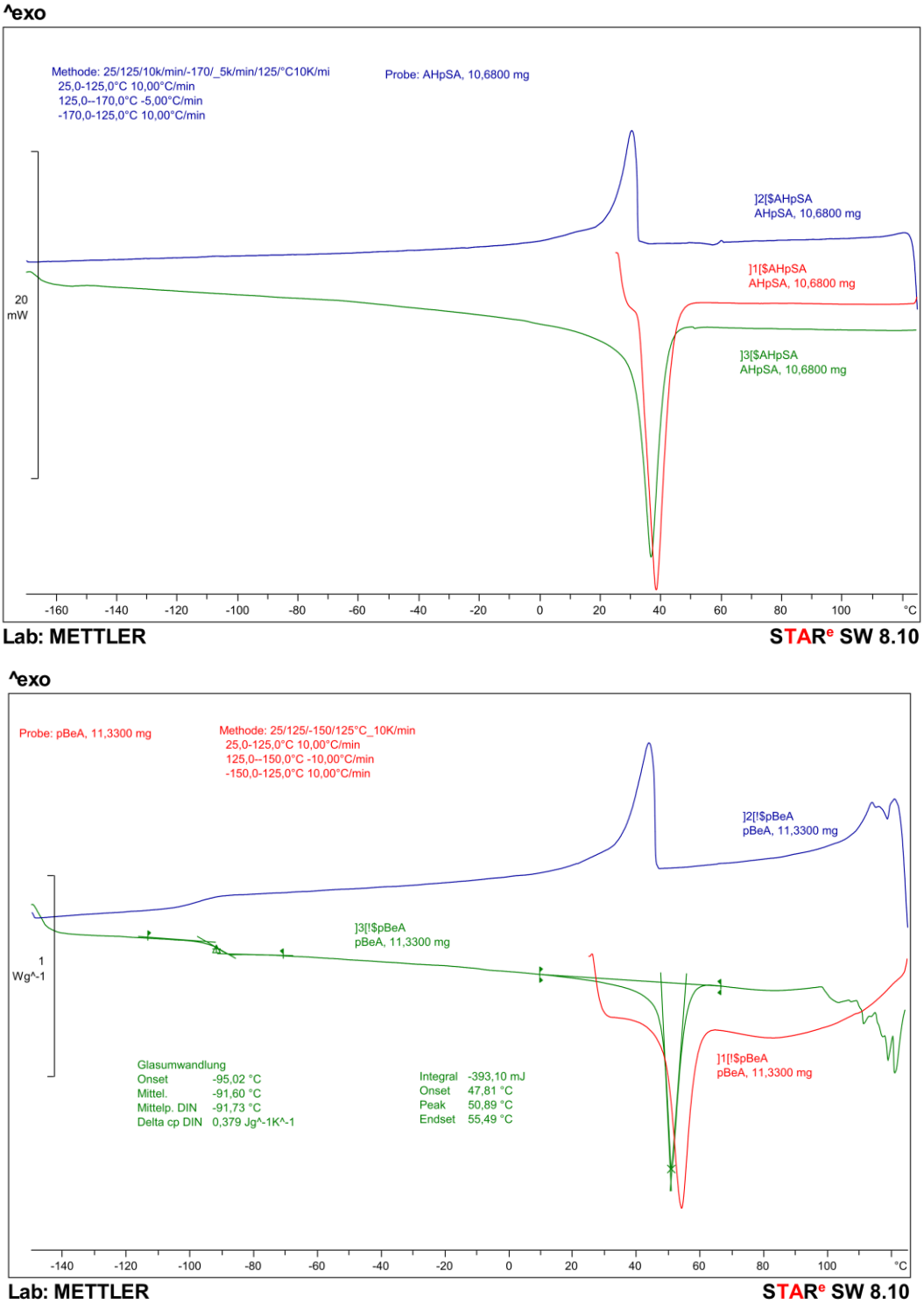

Figure S24 Differential scanning calorimetry of pSA (**upper part**) and pBeA (**lower part**). No glass transition is detectable in the temperature range between -150°C and 125°C for pSA. In the case of pBeA additionally to the glass transition a melting point is observed. The observed melting point and glass transition temperatures are provided in Table 2.1.

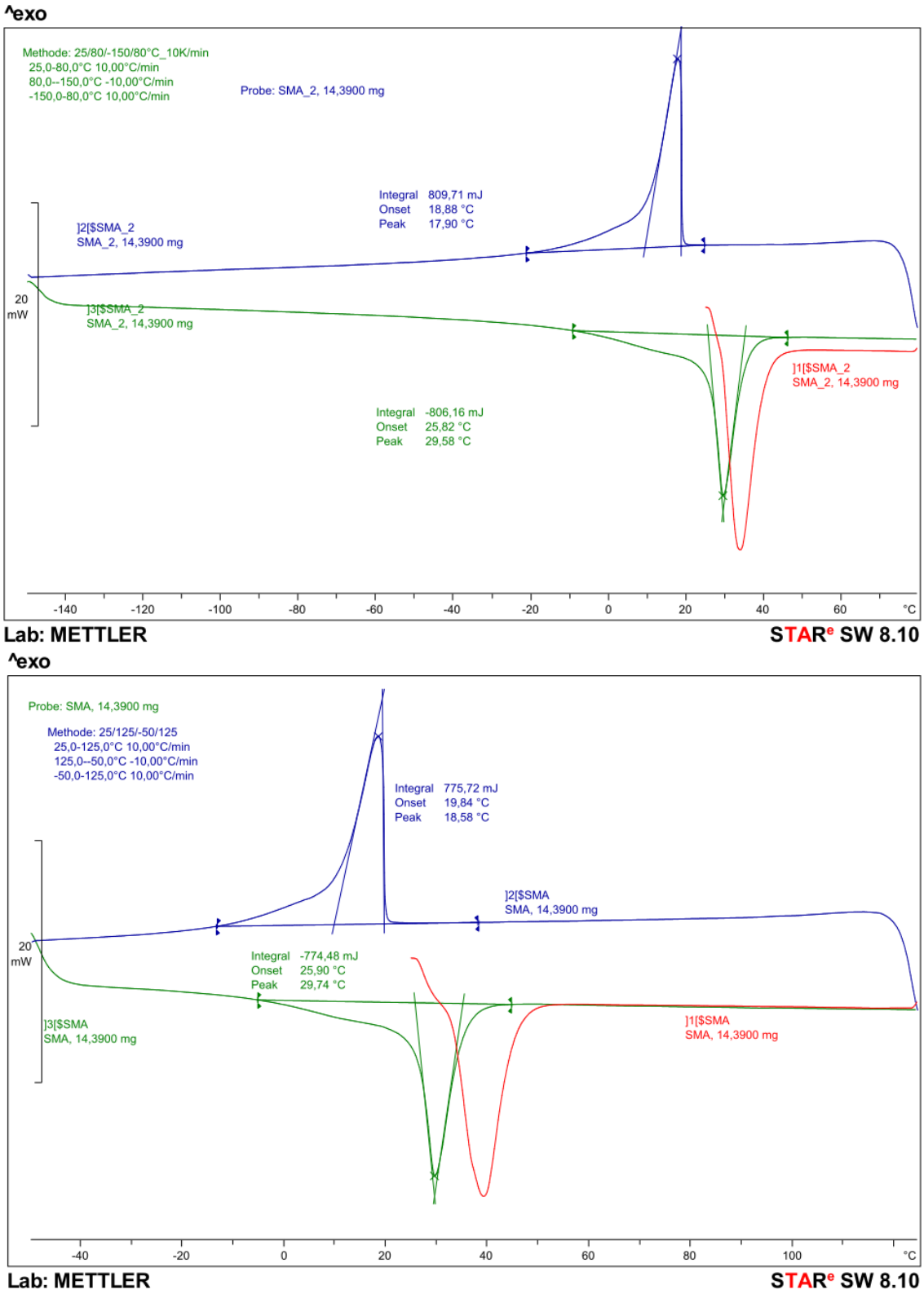

Figure S25 Differential scanning calorimetry of pSMA. No glass transition temperature is detectable in the temperature range between -150°C and 125°C. The observed melting point is provided in Table 2.1.

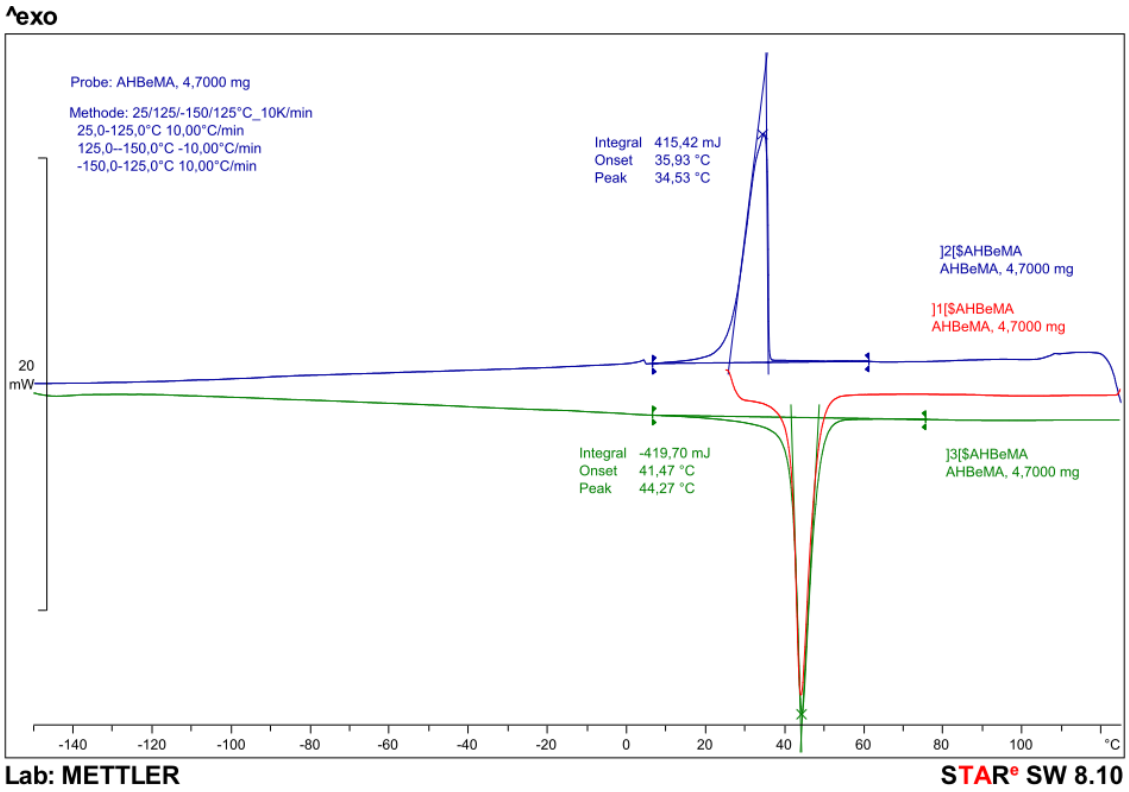

Figure S26 Differential scanning calorimetry of pBeMA. No glass transition temperature is detectable in the temperature range between -150°C and 125°C. The observed melting point is provided in Table 2.1.

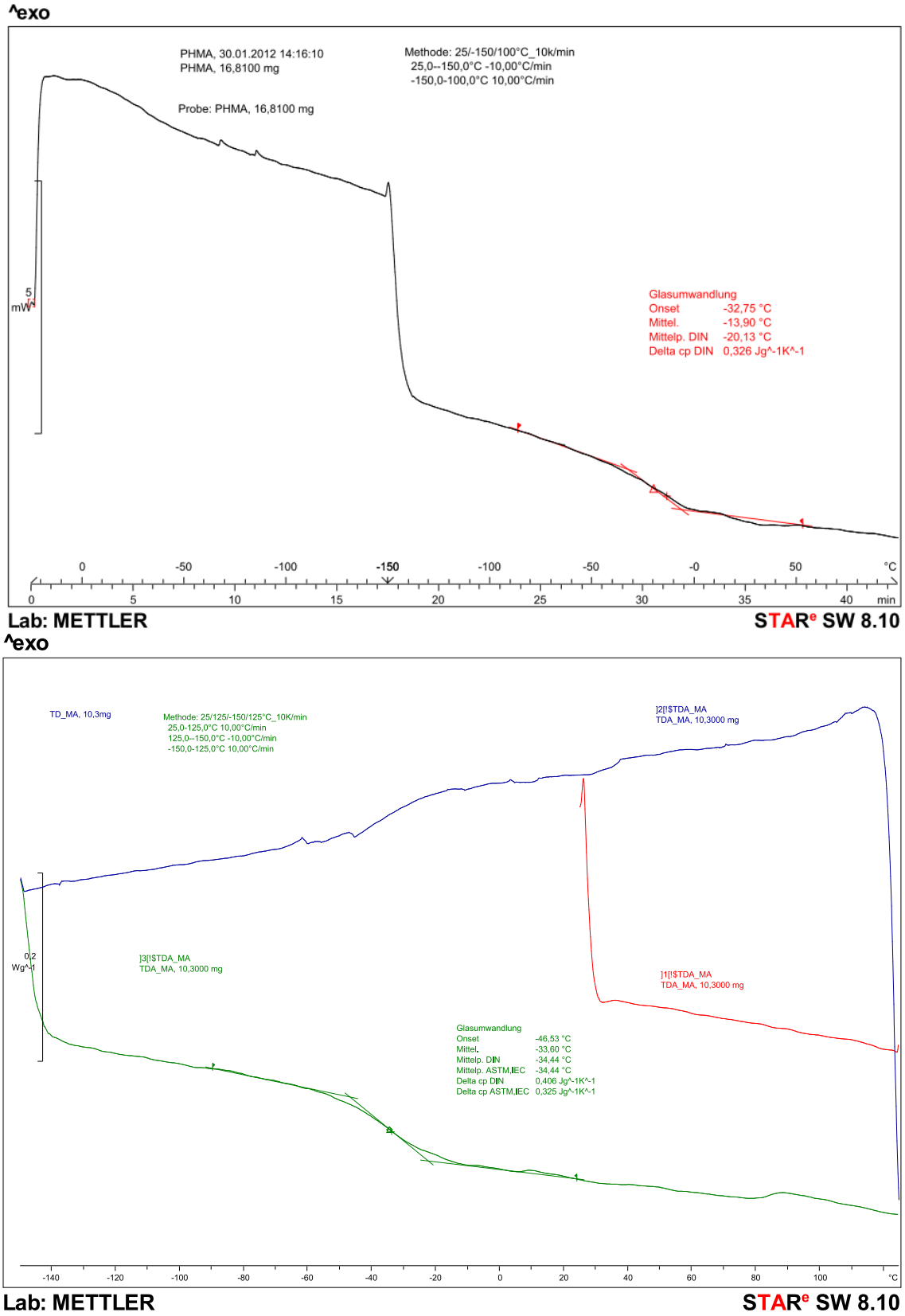

Figure S27 Differential scanning calorimetry of pPHMA (**upper part**) and pTDA-MA (**lower part**). The glass transition temperatures are summarized in Table 2.1. The glass transition effect of PHMA is relatively less pronounced, however the handling experiences (brittle/hard below 20°C, chewy/sticky above 20°C) underpin the measured effect.

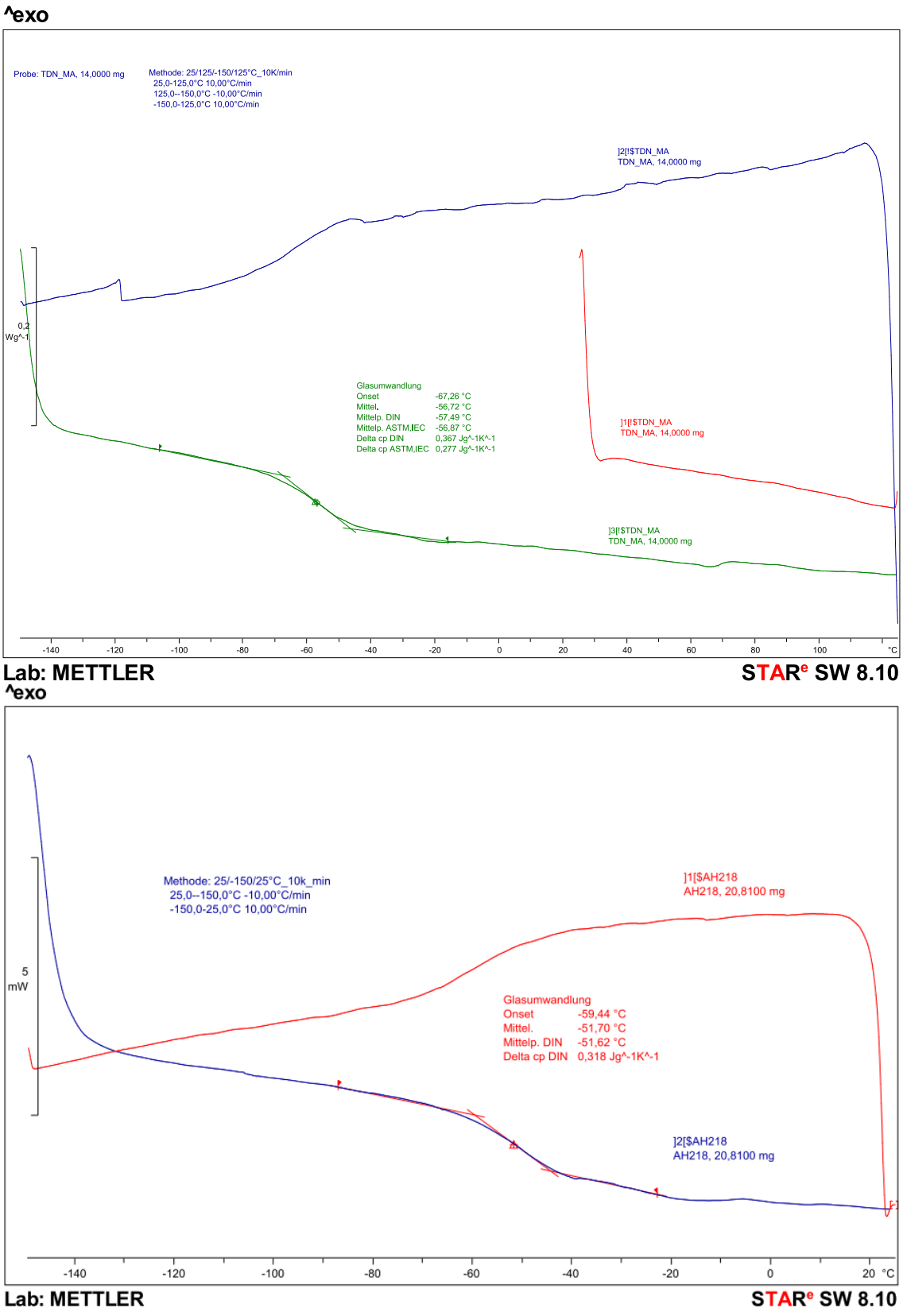

Figure S28 Differential scanning calorimetry of pTDN-MA (**upper part**) and pC17MA (**lower part**). The glass transition temperatures are summarized in Table 2.1.

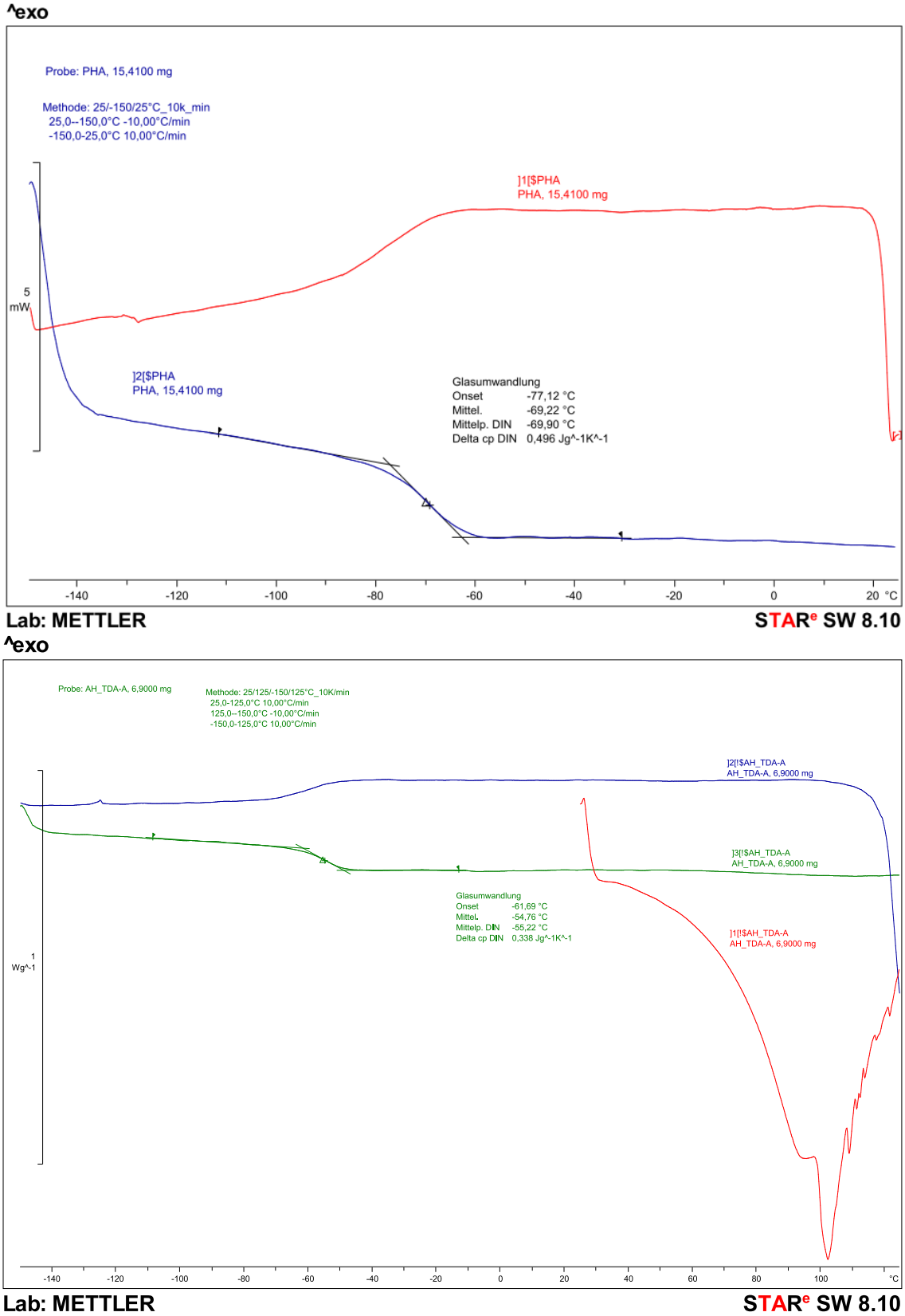

Figure S29 Differential scanning calorimetry of pPHA (**upper part**) and pTDA-A (**lower part**). The glass transition temperatures are summarized in Table 2.1.

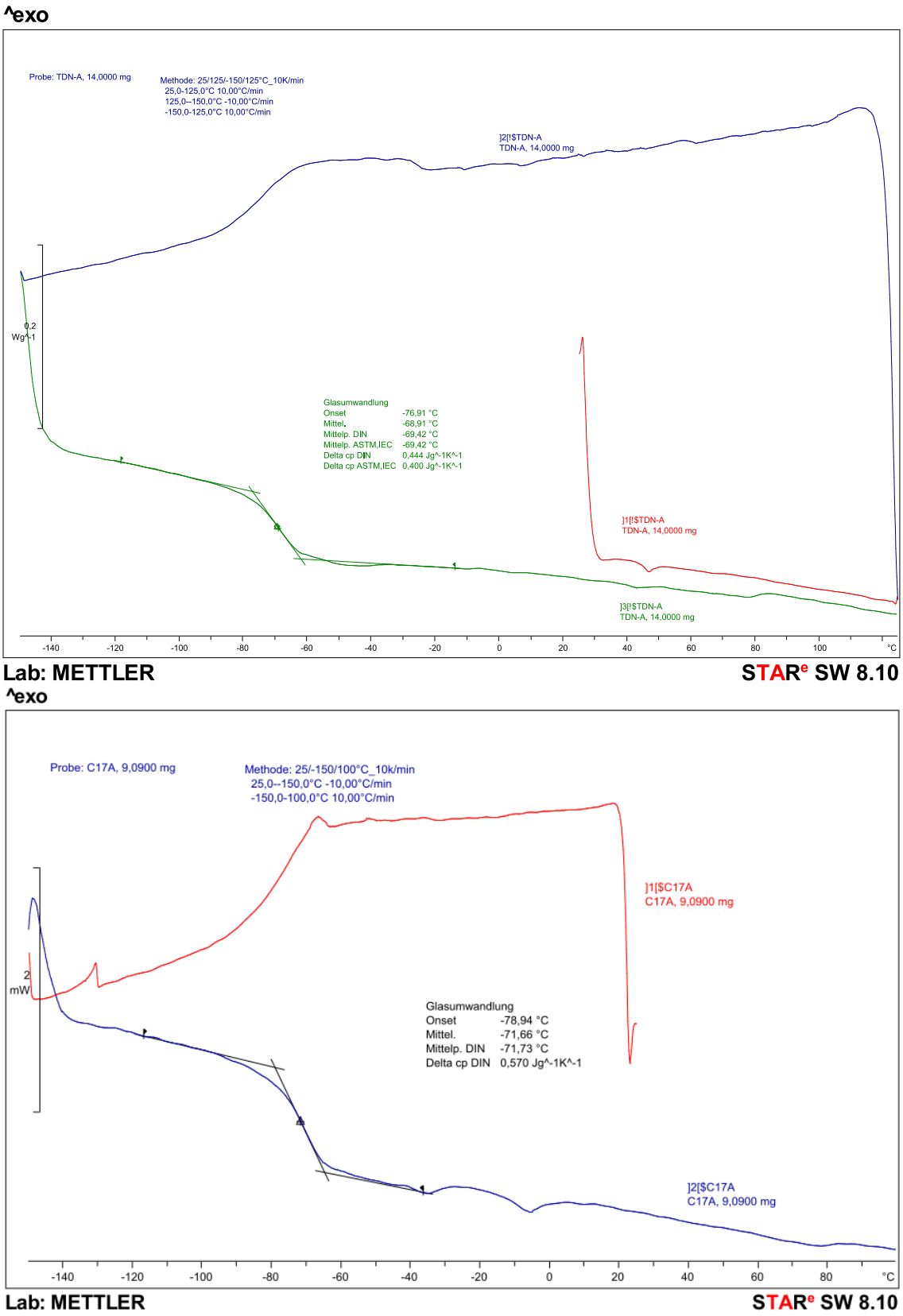

Figure S30 Differential scanning calorimetry of pTDN-A (**upper part**) and pC17A (**lower part**). The glass transition temperatures are summarized in Table 2.1.

APPENDIX B: CHAPTER 3: HETEROATOM CONTAINING (METH)-ACRYLIC MONOMERS[g]

For the PLP-SEC experiments exemplary SEC chromatograms are shown for both heteroatom containing monomers (i.e., UMA and HPCA) at 4 different temperatures as well as tables with the exact PLP sample conditions. Furthermore, the temperature dependent density curves for both monomers and the DSC curves are provided and the results are summarized in Table 3.1. Concomitantly, the ^{1}H-NMR spectrum of pure HPCA, employed to determine the isomeric composition, is depicted.

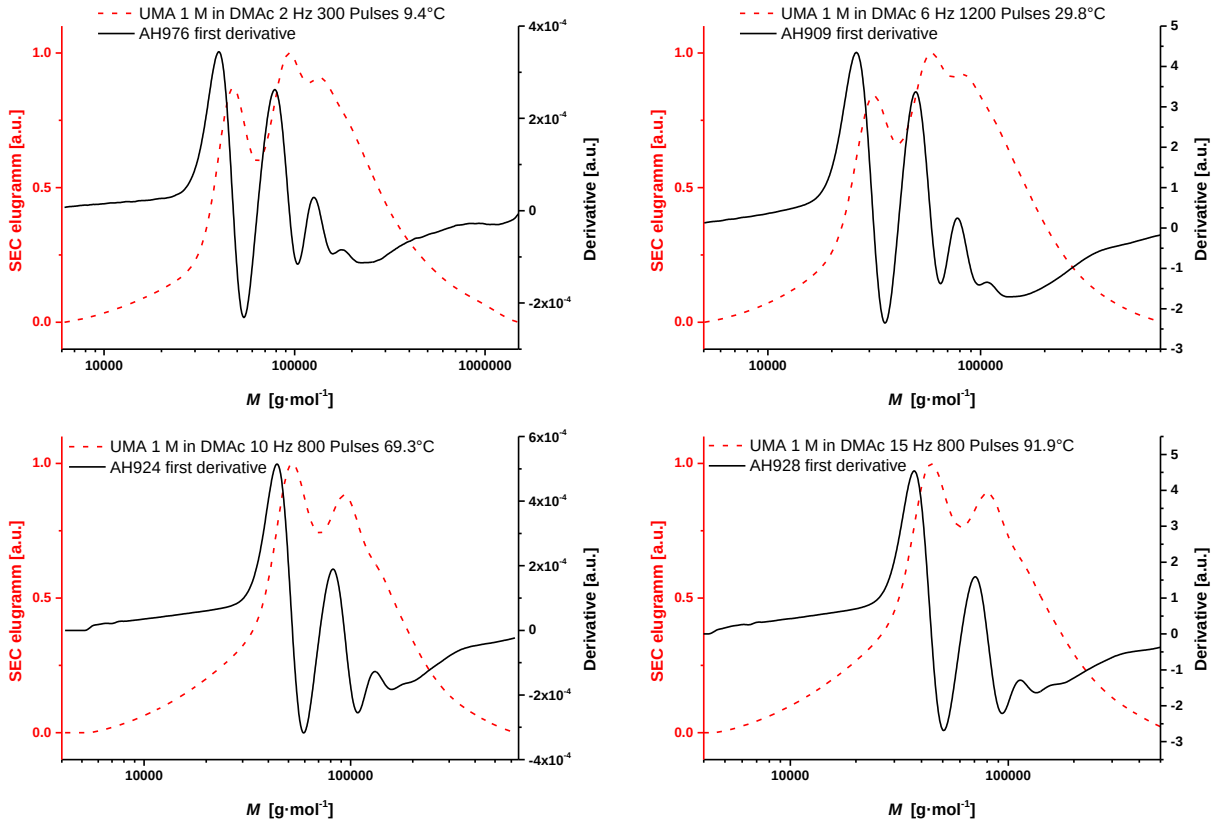

Figure S31 Exemplary molar mass distributions (red dashed lines) and their first derivative (solid black lines) for PLP experiments of UMA in 1 M solution in *N*,*N*-dimethylacetamide (DMAc). The sample-specific conditions are displayed in the diagrams and also collated in Table S27 for 1 M solution in DMAc. The typical PLP structure is observed for all samples.

[g] Haehnel, A. P.; Stach, M.; Chovancova, A.; Rueb, J. M.; Delaittre, G.; Misske, A. M.; Lacik, I.; Barner-Kowollik, C. Polym. Chem. 2014, 5, 862-873.[200] – Parts of this chapter, including all Figures and Schemes, are reproduced with permission of The Royal Society of Chemistry.

Sample	f	n	θ	T^{-1}	$\ln(k_{p1})$	k_{p1}/k_{p2}	M_1	M_2	c_M	k_{p1}	k_{p2}
	Hz	–	°C	10^{-3} K^{-1}	–	–	g·mol^{-1}	g·mol^{-1}	mol·L^{-1}	mol·L^{-1} s^{-1}	
AH1022	2	800	-10.7	3.810	5.2308	1.087	19409	35727	1.048	187	172
AH1021	1	1200	-10.4	3.810	5.0145	1.019	31261	61376	1.047	151	148
AH1021	1	1200	-10.4	3.810	5.1619	1.042	36224	69502	1.047	174	167
AH1023	2	1200	-10.0	3.800	5.1162	1.089	17298	31769	1.047	167	153
AH1024	1	800	1.1	3.650	5.4135	1.026	46132	89950	1.037	224	219
AH1025	1	1200	1.5	3.640	5.3677	1.007	44055	87498	1.037	214	213
AH1026	2	800	1.5	3.640	5.5589	1.050	26669	50816	1.037	260	247
AH1027	2	1200	1.5	3.640	5.4415	1.007	23714	47098	1.037	231	229
AH976	2	300	9.4	3.540	5.9654	1.016	40087	78886	1.038	390	383
AH977	4	300	9.4	3.540	6.1404	1.089	23878	43853	1.038	464	426
AH903	2	1200	12.1	3.510	6.0875	1.052	44771	85114	1.026	440	419
AH904	4	800	12.1	3.510	6.1014	1.040	22699	43652	1.026	446	429
AH905	4	1200	12.1	3.510	6.1659	1.062	24210	45604	1.026	476	449
AH898	2	800	12.2	3.500	6.0070	1.030	41305	80168	1.026	406	394
AH978	3	300	28.6	3.310	6.6708	0.991	53211	107399	1.021	789	796
AH979	6	300	28.7	3.310	6.8459	0.975	31696	65013	1.021	940	964
AH907	3	1200	29.6	3.300	6.5681	1.062	47534	89536	1.010	712	671
AH910	3	800	29.8	3.300	6.5989	1.047	49091	93756	1.012	734	701
AH908	6	800	29.8	3.300	6.6036	1.030	24660	47863	1.012	738	716
AH909	6	1200	29.8	3.300	6.6611	1.052	26122	49659	1.012	781	743
AH918	4	800	47.0	3.120	7.0692	1.019	57016	111944	0.979	1175	1154
AH919	4	1200	47.1	3.120	7.0509	1.009	55976	110917	0.979	1154	1143
AH920	8	800	47.2	3.120	7.1293	1.005	30269	60256	0.979	1248	1242
AH921	8	1200	47.3	3.120	6.9890	0.991	26303	53088	0.979	1085	1095
AH922	5	800	68.3	2.930	7.6546	1.138	80353	141254	0.960	2110	1855
AH923	5	1200	69.3	2.920	7.4967	0.995	68549	137721	0.960	1802	1810
AH924	10	800	69.3	2.920	7.7477	1.069	44055	82414	0.960	2316	2167
AH925	10	1200	69.3	2.920	7.6050	1.016	38194	75162	0.960	2008	1976
AH926	7	800	89.5	2.760	7.8287	1.019	66988	131522	0.942	2512	2466
AH927	7	1200	91.7	2.740	7.9205	1.064	73282	137721	0.940	2753	2587
AH928	15	800	91.9	2.740	8.0013	1.047	37068	70795	0.940	2985	2850
AH929	15	1200	92.0	2.740	8.0382	1.109	38459	69343	0.940	3097	2792

Table S27 Detailed PLP sample conditions, absolute molar masses of the first two inflection points, and the resulting propagation rate coefficients of HPCA polymerized in 1 M solution in DMAc.

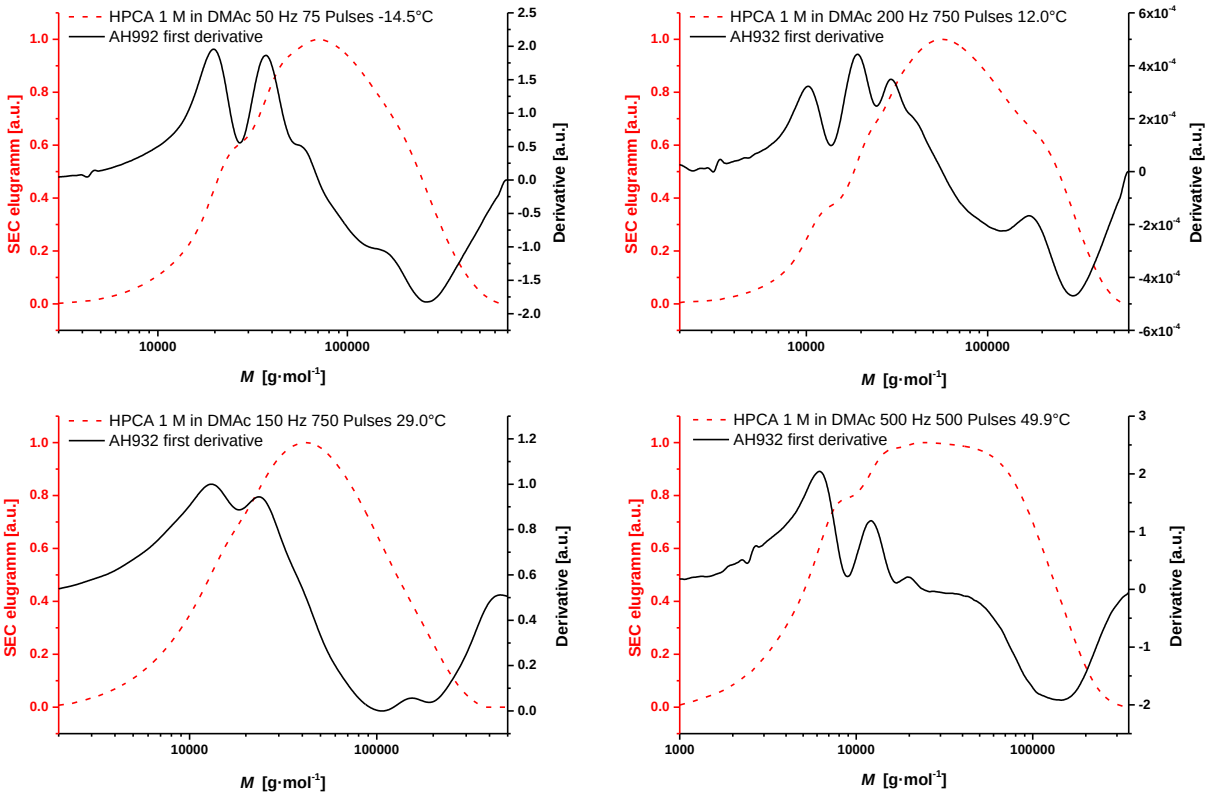

Figure S32 Exemplary molar mass distributions (red dashed lines) and their first derivative (solid black lines) for PLP experiments of HPCA in 1 M solution in *N*,*N*-dimethylacetamide (DMAc). The sample-specific conditions are displayed in the diagrams and also collated in Table S28 for 1 M solution in DMAc. The typical PLP structure is observed for all samples.

Sample	f	n	θ	T^{-1}	$\ln(k_{p1})$	k_{p1}/k_{p2}	M_1	M_2	c_M	k_{p1}	k_{p2}
	Hz	–	°C	10^{-3} K^{-1}	–	–	g·mol^{-1}	g·mol^{-1}	mol·L^{-1}	mol·L^{-1} s^{-1}	
AH992	50	750	-14.5	3.866	8.5863	1.062	19634	36983	1.058	5358	5046
AH993	50	1500	-13.8	3.856	8.2945	1.094	14655	26792	1.057	4002	3658
AH994	75	750	-11.8	3.826	8.5843	1.026	13032	25410	1.056	5347	5213
AH997	50	1500	-8.0	3.771	8.7027	1.077	21928	40738	1.052	6019	5591
AH997	50	1500	-8.0	3.771	8.5231	1.005	18323	36475	1.052	5030	5006
AH1000	100	750	-7.5	3.764	8.8373	1.079	12331	22856	1.034	6886	6382
AH1006	100	750	-0.3	3.665	8.8393	1.035	12274	23714	1.027	6900	6665
AH1004	75	750	0.1	3.660	8.7961	1.038	15668	30200	1.027	6608	6369
AH1002	50	750	0.3	3.657	8.9618	1.130	27733	49091	1.027	7800	6903
AH934	100	750	11.5	3.513	9.1653	1.072	17140	31989	1.035	9559	8921
AH932	200	750	12.0	3.507	8.9563	0.989	6950	14060	1.035	7756	7846
AH932	200	750	12.0	3.507	9.3362	1.069	10162	19011	1.035	11341	10608
AH982	250	750	28.8	3.312	9.7425	1.114	11858	21281	1.005	17025	15278
AH983	250	1500	28.8	3.312	9.6112	1.099	10399	18923	1.005	14931	13585
AH980	150	750	29.0	3.310	9.3308	1.117	13092	23442	1.005	11281	10100
AH1010	400	750	49.7	3.097	9.9526	1.057	8933	16904	0.982	21006	19875
AH1013	500	500	49.9	3.095	9.8121	1.021	6209	12162	0.982	18253	17878
AH1011	400	1000	50.0	3.095	9.7594	0.984	7362	14962	0.982	17317	17597

Table S28 Detailed PLP sample conditions, absolute molar masses of the first two inflection points, and the resulting propagation rate coefficients of HPCA polymerized in 1 M solution in DMAc.

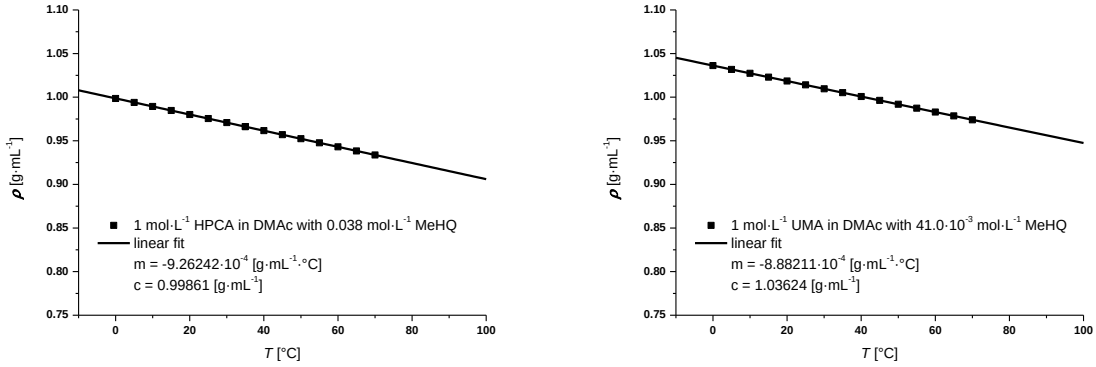

Figure S33 Temperature dependent densities for the 1 M solutions of the HPCA **(left hand part)** and UMA **(right hand part)** in *N*,*N*-dimethylacetamide. Methyl hydroquinone (MeHQ) was added in replacement of 2,2-dimethoxy-2-phenylacetophenone (DMPA) to prevent the solutions from polymerization inside the density measurement device. The temperature dependent densities are summarized in Table 3.1.

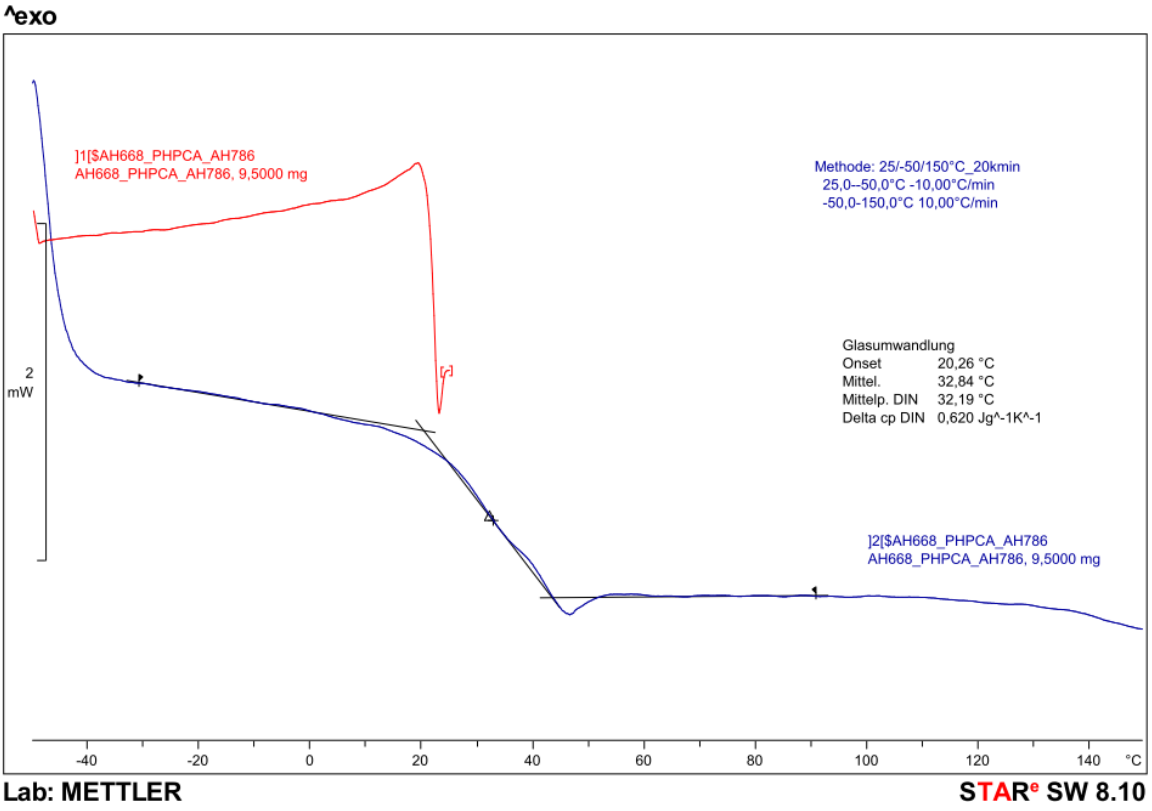

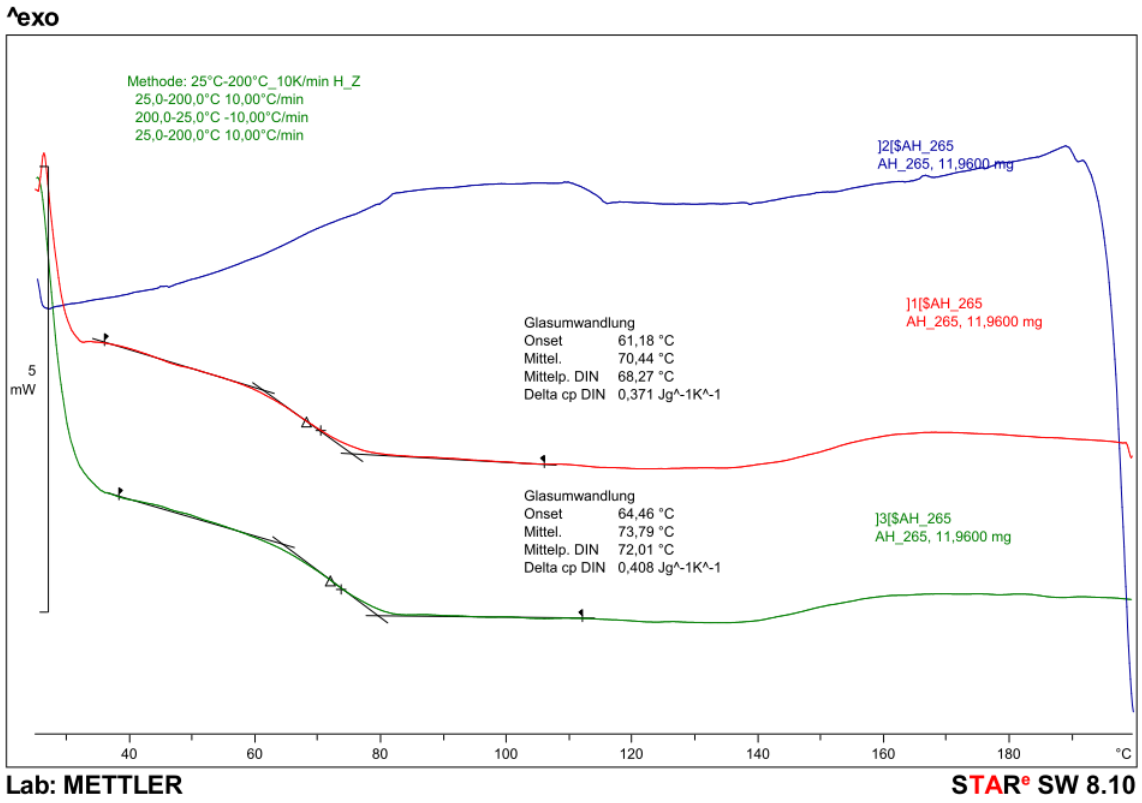

Figure S34 Differential scanning calorimetry of pHPCA (**upper part**) and pUMA (**lower part**). The glass transition temperatures are indicated in Table 3.1.

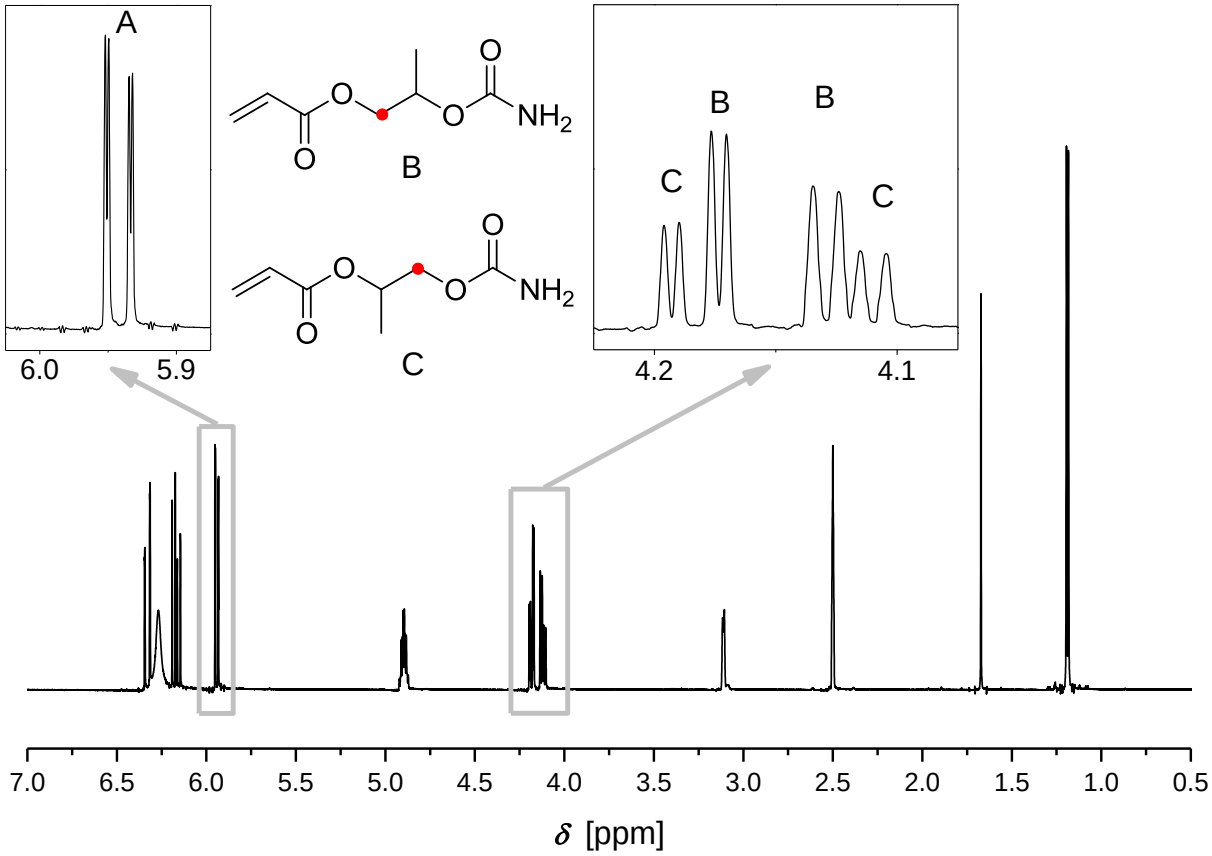

Figure S35 ^{1}H-NMR of HPCA. The integral of the vinylic proton (δ = 5.94 ppm) is set to unity. The ratio of the integrals corresponding to the signals labeled B and C is B : C = 2 : 1. B and C are a doublet of doublets associated with the CH_2 group (marked with a red dot) in alpha position of the ester and carbamate functionalities, respectively. Consequently, the upper structure labeled with B is the dominant isomer in HPCA.

EIGENSTÄNDIGKEITSERKLÄRUNG

Hiermit erkläre ich, dass ich diese Arbeit, die ich in der Zeit zwischen Juni 2011 und Juni 2014 im Rahmen der Betreuung von Prof. Dr. Christopher Barner-Kowollik ausgeführt habe, selbstständig verfasst habe und dabei keine anderen als die angegebenen Quellen und Hilfsmittel verwendet habe. Darüber hinaus erkläre ich, dass ich mich zurzeit in keinem weiteren laufenden Promotionsverfahren befinde und auch keine früheren Promotionsversuche unternommen habe.

.....

Alexander Peter Hähnel

Karlsruhe, 29. Mai 2014

CURRICULUM VITAE

Name	Alexander Peter Hähnel
Date and Place of Birth	28th of April 1987 in Bruchsal (Germany)
Nationality	German

Education

Since 6/2011	**Doctorate in Chemistry** KIT – Karlsruher Institut für Technologie, Lehrstuhl für Präparative Makromolekulare Chemie (Prof. Dr. Christopher Barner-Kowollik) Topic: „Industrially Relevant Monomers: From Fundamental Kinetics to Application in Controlled Polymerization“
7/2012	**Research stay** at the Slovak Academy of Sciences (SAS) in Bratislava / Slovakia in the group of Prof. Igor Lacík
10/2006 – 4/2011	**Diploma in Chemistry** TU Karlsruhe / KIT – Karlsruher Institut für Technologie specialization: inorganic chemistry, diploma thesis in polymer chemistry: „Kinetics and Modeling of Single Electron Transfer – Living Radical Polymerization“
9/1998 – 7/2006	**Abitur** (High School Certificate) Privatgymnasium St. Paulusheim, Bruchsal, focus areas: chemistry / biology

Awards and Scholarships

8/2013	**Polymer Chemistry Poster Prize** at the **APME 2013** IUPAC 10th International Conference on Advanced Polymers via Macromolecular Engineering in Durham (UK)
2/2008 – 5/2011	**Scholarship** of the Deutsche Studentenförderung in der Begabtenförderung der **Konrad-Adenauer-Stiftung e.V.**
6/2006	**Awards in the context of the Abitur** in physics of the Deutsche Physikalische Gesellschaft (DPG) and in biology of the Verband Deutscher Biologen (VDbiol)

Conference Contributions und Abstracts

2	*Precision Kinetic Data for Precision Polymer Design: A Systematic Laser Polymerization Study* **Haehnel, A. P.**; Schneider-Baumann, M.; Stach, M.; Chovancová, A.; Hiltebrandt, K. U.; Rueb, J. M.; Arens, L.; Delaittre, G.; Fleischhaker, F. Y.; Misske, A. M.; Lacík, I.; Barner-Kowollik, C.; **APME 2013** – IUPAC 10th International Conference on Advanced Polymers via Macromolecular Engineering in Durham (UK); **August 2013, poster presentation.**
1	*Kinetics and Modeling of Single Electron Transfer – Living Radical Polymerization (SET–LRP)* Polymer Institute of the Slovak Academy of Sciences, **Bratislava**, Slovakia, **July 2011**, by Prof. Igor Lacík **invited lecture**.

LIST OF PUBLICATIONS

Refereed Journal Publications Contributing to the Current Thesis

1	*Global Trends for k_p? The Influence of Ester Side Chain Topography in Alkyl (Meth)Acrylates – Completing the Picture* **Haehnel, A. P.**; Schneider-Baumann, M.; Arens, L.; Misske, A. M.; Fleischhaker F. Y.; Barner-Kowollik, C. ***Macromolecules*** **2014**, DOI: 10.1021/ma500304f.
2	(*Meth)Acrylic Monomers with Heteroatom-Containing Ester Side Chains: A Systematic PLP-SEC and Polymerization Study* **Haehnel, A. P.**; Stach, M.; Chovancová, A.; Rueb, J. M.; Delaittre, G.; Misske, A. M.; Lacík, I.; Barner-Kowollik, C. ***Polymer Chemistry*** **2014**, *5*, 862-873.
3	*Global Trends for k_p? Expanding the Frontier of Ester Side Chain Topography in Acrylates and Methacrylates* **Haehnel, A. P.**; Schneider-Baumann, M.; Hiltebrandt, K. U.; Misske, A. M.; Barner-Kowollik, C. ***Macromolecules*** **2013**, *46*, 15-28.

Refereed Journal Publications Arising From Further Activities

4	*Glass Transition-, Melting- and Decomposition Temperatures of Tailored Polyacrylates and Polymethacrylates: General Trends and Structure-Property Relationships* Fleischhaker F.; **Haehnel, A. P.**; Misske, A. M.; Blanchot, M.; Haremza, S.; Barner-Kowollik, C. ***Macromolecular Chemistry and Physics*** **2014**, DOI: 10.1002/macp.201400062.
5	*Investigating Cu(0) Mediated Polymerizations: New Kinetic Insights Based on a Comparison of Kinetic Modeling with Experimental Data* **Haehnel, A. P.**; Fleischmann, S.; Hesse, P.; Hungenberg, K.-D.; Barner-Kowollik, C. ***Macromolecular Reaction Engineering*** **2013**, *7*, 8-23. ***highlighted in the promotional flyer „Macromolecular Journals" and granted with open access***
6	*Cyclic and polycyclic tellurium–tin and tellurium–lead compounds – synthesis, structures and thermal decomposition* Traut, S.; von Hänisch, C.; **Hähnel, A. P.**; Stahl, S. ***Chemical Communications*** **2012**, *48*, 6984-6986.
7	*Dichloro organosilicon bismuthanes as precursors for rare compounds with a bismuth–pnictogen or bismuth–tellurium bond* Traut, S.; **Hähnel, A. P.**; von Hänisch, C. ***Dalton Transactions*** **2011**, *40*, 1365-1371.

ACKNOWLEDGEMENTS

I am formost grateful to Prof. Dr. Barner-Kowollik for supervising my diploma and doctoral thesis, for continuous discussions, brain storming, and all your insights. Granting me the opportunity to work on these physicochemical topics – although against my initial wish to focus on organic synthesis – was a masterstroke for me. In fact, I enjoyed the projects a lot! Thank you for all the confidence you entrusted me with.

I am deeply grateful to Dr. Andrea Misske, Dr. Friederike Fleischhaker and Dr. Sylke Haremza (BASF SE, Ludwigshafen, Germany) for the excellent cooperation. Together with their teams, they facilitated the success of the current project with fruitful discussions and on-going support.

I am deeply thankful to Dr. Maria Schneider-Baumann. It was a huge chance for me to learn from someone who has not only such an immeasurable experience with SEC set-ups, but also has a very profound understanding of the related analyzing techniques. Thank you for your patience in measuring every sample I came up with.

I also wish to thank my office colleagues Thomas Tischer, Nicolas Zydziak, Astrid Hirschbiel, and Michael Kaupp for a very pleasant and entertaining atmosphere. I additionally thank Katrin Kockler, who will continue the current collaboration with BASF, Elena Frick, Dominik Voll and Johannes Willenbacher for proofreading of my thesis. Dr. Guillaume Delaittre is acknowledged for his help in achieving control over the heteroatom containing monomers and fruitful discussion on RDRP techniques. Kai Hiltebrandt, Lukas Arens, Jannick Rüb, Tobias Bantle, and Benjamin Wenn (University Hasselt, Belgium) are thanked for assisting me in my research as scientific visitor, “Vertiefer”, “HiWi“, or bachelor students. Without you, the herein gained insights (based on significantly more than 4000 PLP samples) would not have been accessible.

Of course, I also wish to thank the entire *macroarc* group for the helpful and great working atmosphere. Honestly, it was a pleasure to work with you guys!

I am much obliged to Dr. Marek Stach, Anna Chovancová as well as Prof. Dr. Igor Lacík. It was a great pleasure to work with them during my stay in Bratislava. I thank Marek for sharing his knowledge about the PLP-SEC method as well as on the experimental ruses of SEC. I thank Anna for the comfortable cooperation as well as warm welcome and Igor for the opportunity to work under his supervision and for sharing his insights into the kinetics of the aqueous systems. Without his support I would not have wrapped my head around this topic.

Special thanks go to Dr. Branislav Horváth (Institute of Chemistry of the Faculty of Natural Sciences Comenius University in Bratislava, Slovakia) for carrying out the in-situ NMR measurements at elevated temperatures of the FRP of the heteroatom containing monomers studied herein. Similarly, many thanks go to Kim Öhlenschläger with whom I attempted to apply a similar method to the alkyl (meth)acrylates. Unfortunately, chemistry was against us and did not reveal reasonable trends and insights. Nevertheless, I think we fought an honorable battle.

Furthermore, I am grateful to Helena Hörig (AK Wilhelm, KIT) for carrying out the DSC analysis of numerous samples.

A warm “Thank You” goes also to Prof. Dr. Thomas Junkers (University Hasselt, Belgium) for result-oriented discussions and his critical advice about the insights gained in the course of my thesis.

In addition, I thank my entire family for supporting, encouraging, and cheering me up.

When you stop doing things for fun you might as well be dead.

Ernest Hemingway